Performance Evaluation of Aqua-Pipe under Earthquake-Induced Ground Deformation

DRAFT

Interim Report

by

T. D. O'Rourke

J. E. Strait

N. Mottl

B. Berger

B. Wham

H. E. Stewart

D. Price

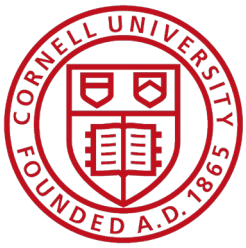

Cornell University

School of Civil and Environmental Engineering

Cornell University

Hollister Hall

Ithaca, NY 14853

September 2020

Acknowledgements

The authors recognize the excellent efforts of Cornell graduate, undergraduate, and other students who made these experiments successful. In particular, the contributions of Mia Stewart, Sarah Weinberg, Corbin Atkins, Quinton Hubbell, Andrew Greubel, Daniel Kusky, Afet Keskin, Loyan Hashi, Taylor Overton, Misha Dimmick, Emily Xu, and Elisabeth Sherman are acknowledged.

Table of Contents

List of Figures

List of Tables

Section 1
Introduction

1.1. Background

This report is submitted to Sanexen Environmental Services, Inc. (herein referred to as Sanexen). It presents the results of material property and full-scale testing to investigate the performance of Aqua-Pipe™, which is a commercial lining for water pipelines developed by Sanexen. Aqua-Pipe™ Cured-in-Place-Pipe (CIPP) is used to rehabilitate potable water pipelines as an alternative to pipeline removal and replacement. Sanexen is an environmental services contractor and consultant headquartered in Canada with a counterpart in the U.S., Sanexen Water.

As shown in, Figure 1.1, Aqua-Pipe™ is an epoxy resin-impregnated lining consisting of an inner and outer layer, or jacket, each composed of seamless, circular woven fabric. Each layer of woven fabric consists of polyethylene thermoplastic (PET) yarns in the longitudinal, or warp, direction and PET yarns in the circumferential, or weft, direction, as shown in the warp and weft schematic in Figure 1.2. The two jackets are impregnated with epoxy. The lining interior layer in contact with pipeline water is composed of a thermoplastic polyurethane (TPU) waterproof membrane.

Two types of Aqua-Pipe™ lining were tested: Aqua-Pipe™ Generation 1 (AP1) and Aqua-Pipe™ Generation 2 (AP2). The outside jacket of the AP2 lining is the same as that of the AP1 lining. Both the warp and weft directions of the outside jacket are composed of continuous PET yarns. For AP1 the inside and outside jackets are identical in composition with a simple plain weave fabric pattern. For AP2 the inside jacket in the weft direction is composed of PET and glass fibers intertwined into individual yarns which have the ability, upon loading, to irreversibly elongate.

The installation of AP1 results in a fold perpendicular to the circumference because the jackets are purposely chosen slightly oversized in diameter to ensure proper contact with the inner surface of the host pipeline once inflated onto it. Figure 1.3 shows the two layers of AP1 fabric before being impregnated with epoxy and cured in place. Figure 1.4 shows the AP1 lining after curing inside of an existing pipeline, where a limited-sized fold can be observed. The fold is virtually absent after the installation of AP2.

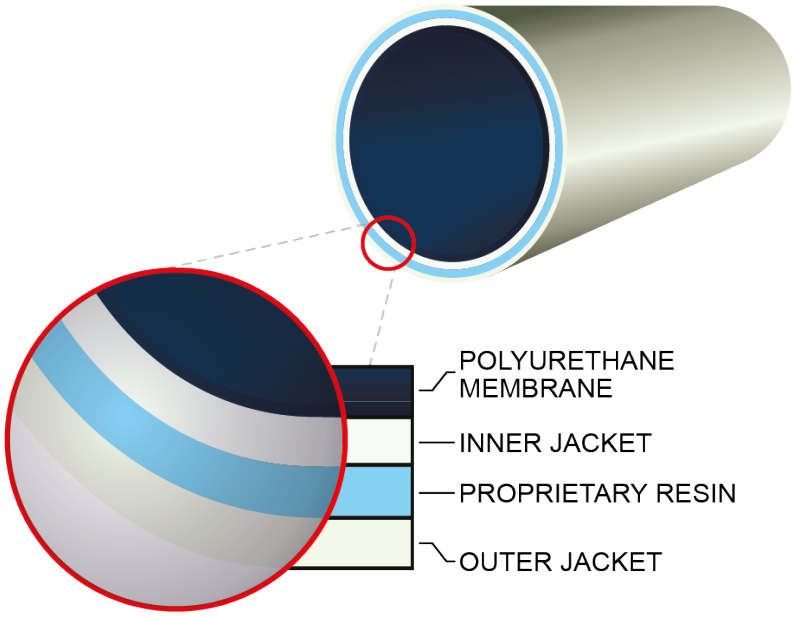

Figure 1.1. Aqua-Pipe™ Lining Components

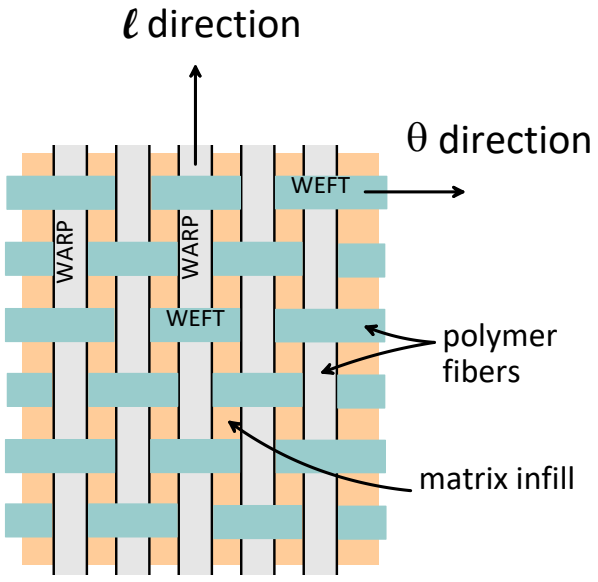

Figure 1.2. Schematic of Warp and Weft Yarn Pattern

Figure 1.3. Aqua-Pipe™ Generation 1 (AP1) Woven Fabric Lining before Curing

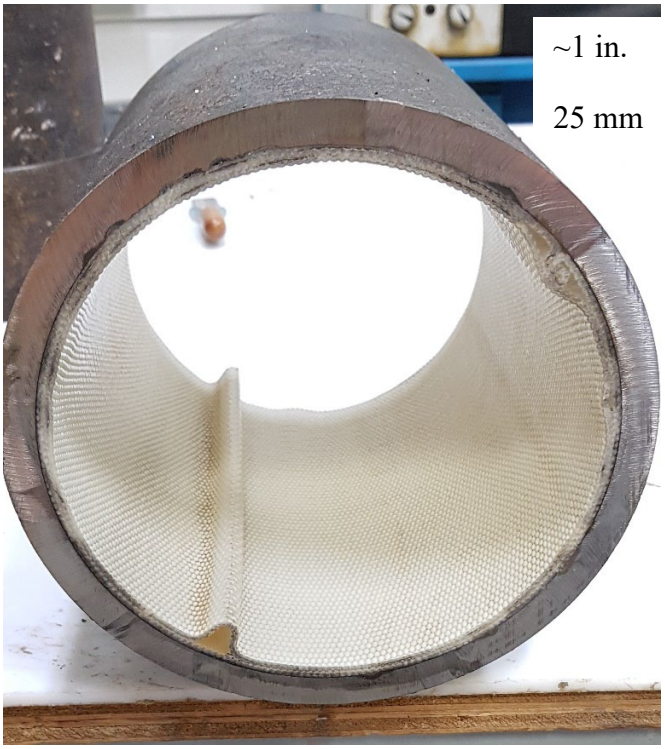

Figure 1.4. Aqua-Pipe™ Generation 1 (AP1) Woven Fabric Lining after Curing

Both AP1 and AP2 are installed by excavating access pits in excess of 1,000 ft (305 m) apart and pulling the lining through the pipeline between each access pit. The installation process begins by cleaning the pipe in-place. Then the lining infused with epoxy is pulled into place. Hot water is run through the pipeline, curing the epoxy resin. Finally, a robot reinstates service connections from within the pipeline, after which the lining is pressure-tested.

The AP2 lining was introduced by Sanexen while the tests summarized in this report were in progress. The report therefore contains the large-scale testing results for both the AP1 and AP2 linings. The large-scale tests and results, which are discussed herein, were performed with 6-in. (152-mm) nominal diameter pipelines, constructed of either cast iron (CI) or cementless ductile iron (DI). The fault rupture test, performed as part of this research, was conducted with a jointed 6-in. (152-mm) diameter cementless DI pipeline lined with AP2.

1.2. Report Organization

The report is organized into 10 sections. Section 1 provides report organization and introductory information on Sanexen and Aqua-Pipe™. Section 2 provides stress versus strain properties of the Aqua-Pipe™ lining determined through tensile testing. Section 3 provides a summary of force versus displacement relationships determined through direct tension testing. Section 4 provides a description of special friction tests. The friction tests were performed to explore the relationship between axial resistance to movement between pipe and lining and the internal lining pressure. Section 5 provides the results of direct shear tests and an estimate of the coefficient of friction between lining and the host pipe. Section 6 contains the results of axial compression tests performed on full-scale test specimens from the field that were lined with AP1 by Sanexen. Section 7 summarizes the results of three 4-point bending tests, including pipeline joints lined with AP1 and AP2. Section 8 provides the results of direct tension tests, in the form of axial force vs displacement tests, of pipelines lined with both AP1 and AP2. Section 9 gives the results of the fault rupture test that was performed with a DI pipeline reinforced with AP2. Section 10 summarizes the test results and discusses key findings.

Section 2
Tensile Coupon Tests

2.1. Introduction

This section of the report describes the uniaxial tensile coupon testing and results for the AP1 and AP2 linings in the warp and weft directions. The warp and weft directions pertain to the longitudinal and circumferential directions, respectively. AP1 tensile coupon specimens were cut and machined from flat cured lining sections and tested in accordance with ASTM–D3039 2017 (ASTM, 2017) for the specimens in the warp direction. In in the weft direction they were cut and machined from flat cured lining sections and tested in accordance with ASTM-D638 2014 (ASTM, 2014).

2.2. Tensile Coupon Testing and Procedure

A Baldwin Hamilton 60 BTE Universal Testing Machine was used to apply the tensile loads to the AP1 specimens. The load frame was fitted with a pressure sensor to measure axial force. Tensile strain was measured using strain gages epoxied to the specimen surface. A laser extensometer was used to measure specimen elongation. Figure 2.1 is a photograph of an Aqua-Pipe™ specimen for the warp direction in the testing apparatus. The photograph shows axial and transverse gages on the test specimen as well as the laser extensometer strips that were used for measurements of extension with a laser beam.

Six tensile coupon specimens were tested. Three specimens were cut in the warp direction, and three specimens were cut in the weft direction. All six specimens were instrumented with axial and transverse strain gages. Schematics and dimensions of the specimens in the warp and weft directions are provided in Figure 2.2 and Figure 2.3, respectively. The thickness of the specimens was approximately 0.17 in. (4.3 mm) in the warp and weft directions. The gages were mounted in the center of the specimen. Such gages frequently debond at tensile strains of 2 to 4%. To provide supplemental measurements of strain beyond the 2 to 4% range, the laser extensometer was used to measure axial strain to failure. The extensometer provides for reliable assessment of strain at larger values than the strain gages, specifically those beyond the initiation of plastic deformation.

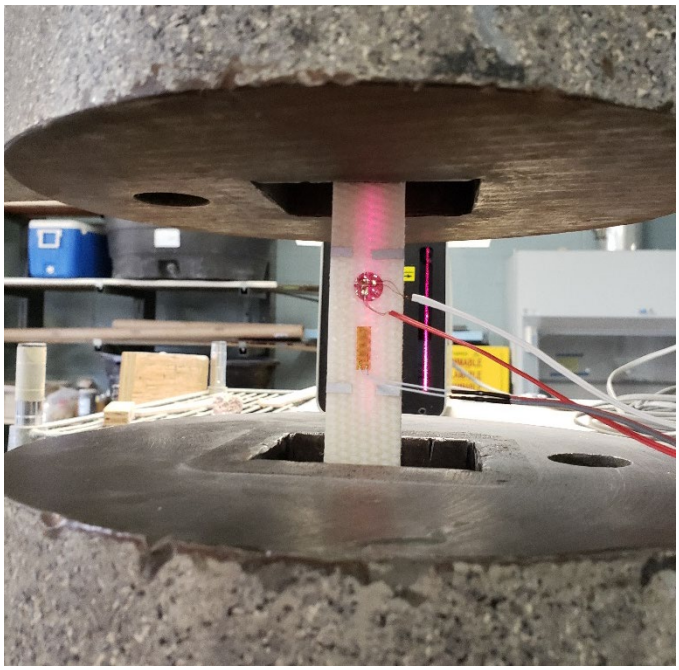

Figure 2.1. Tensile Coupon Test Setup with Aqua-Pipe™ Material

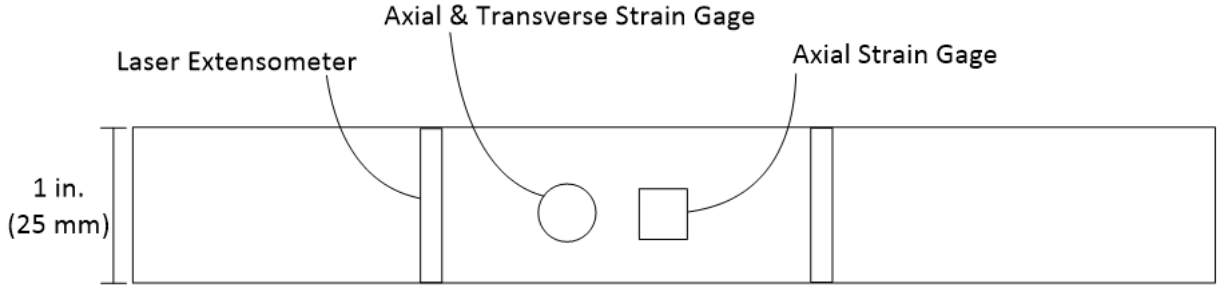

Figure 2.2. Schematic of Aqua-Pipe™ Tensile Coupon Specimen in the Warp Direction

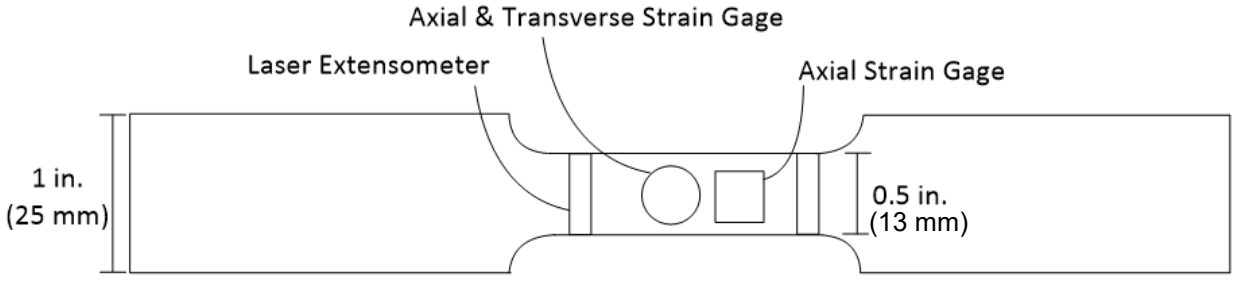

Figure 2.3. Schematic of Aqua-Pipe™ Tensile Coupon Specimen in the Weft Direction

2.3. Stress versus Strain Data (AP1)

The stress applied throughout the uniaxial tension test was computed by dividing the measured force by the original cross-sectional area of the tensile coupon. This strain generally is referred to as engineering strain. The uniaxial stress versus axial strain plots are shown in Figure 2.4 and Figure 2.5 for specimens in the warp and weft directions, respectively.

The results of the tensile coupon tests in each direction show good agreement. Each test was run until the woven fabric structure of the specimens tore apart, indicating failure. Axial stress versus strain data were used to determine the stress and strain at failure in each direction, as shown in Figure 2.4 and Figure 2.5 by the maximum measured stress. The average failure stress and strain for Specimens 1, 2, and 4 in the warp direction were 10.9 ksi and 15%, respectively, with standard deviations of 0.94 ksi and 1.2%. The average failure stress and strain for Specimens 3, 4, and 5 in the weft direction were 15.3 ksi and 11.1%, respectively, with standard deviations of 1.68 ksi and 1.6%. The ratio of the average stress at failure in the weft versus warp direction is 1.40, which is nearly identical to the ratio of stress at failure reported by the manufacturer.

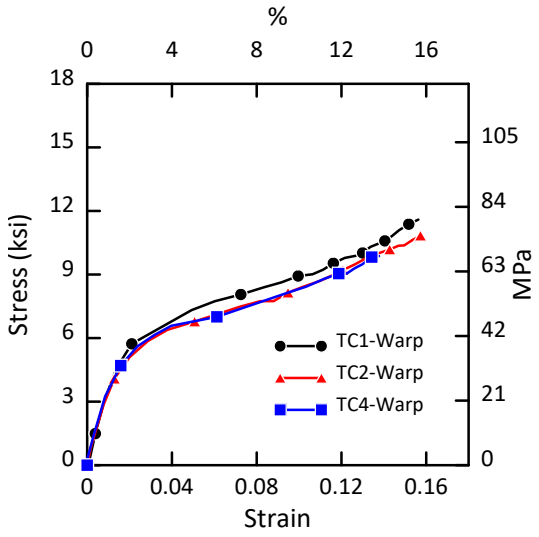

Figure 2.4. Stress versus Strain Plots to Failure for AP1 Specimens in the Warp Direction

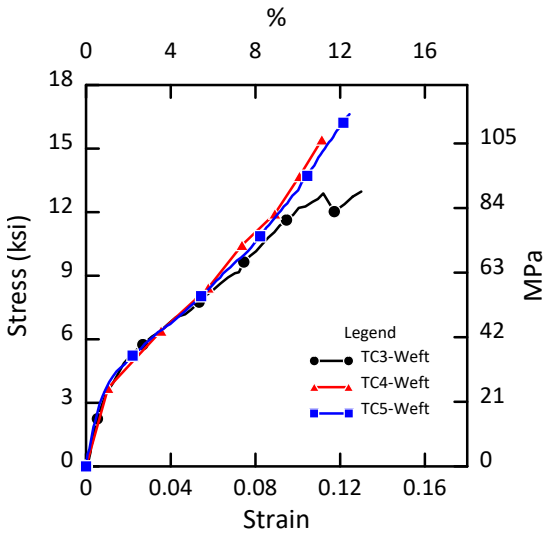

Figure 2.5. Stress versus Strain Plots to Failure for AP1 Specimens in the Weft Direction

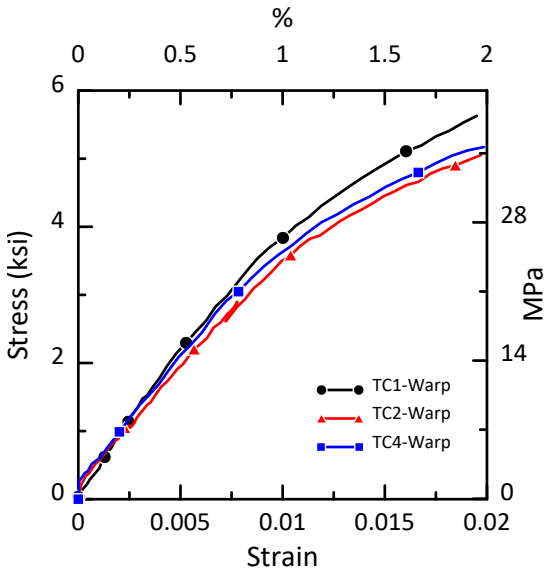

Figure 2.6. Expanded Stress versus Strain Plots for AP1 Specimens in the Warp Direction

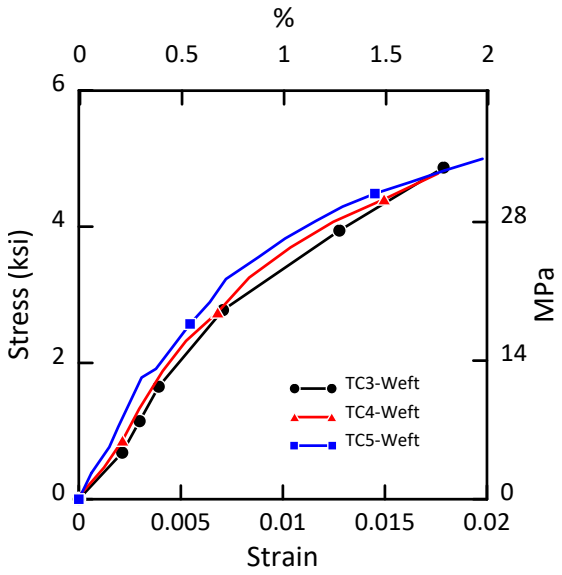

Figure 2.7. Expanded Stress versus Strain Plots for AP1 Specimens in the Weft Direction

Expanded views of the stress versus strain data are shown in Figure 2.6 and Figure 2.7 for the weft and warp directions, respectively. Young's modulus, E, was computed using the linear range of the stress versus strain plots. It was determined by performing linear regressions for stress versus strain from 0 to approximately 0.5% strain. The average Young's modulus for Specimens 1, 2, and 4 in the warp direction is 390 ksi (2.69 GPa) with a standard deviation of 60.7 ksi (0.42 GPa). The average Young's modulus for Specimens 3, 4, and 5 in the weft direction is 414 ksi (2.86 GPa) with a standard deviation of 29.0 ksi (0.20 GPa).

Poisson's ratio, ν, is the negative ratio of transverse strain to axial strain for uniaxial loading. Poisson's ratio was derived from the transverse versus axial strain plots. As shown in Figure 2.8 and Figure 2.9, the linear range in the warp direction of the transverse versus axial strain terminates at approximately 0.05 axial strain, beyond which axial strain accumulates at a faster rate than the transverse strain. The average Poisson's ratio for Specimens 1 and 4 in the warp direction is 0.23 with a standard deviation of 0.016. The average Poisson's ratio for Specimens 3, 4, and 5 in the weft direction is 0.25 with a standard deviation of 0.010.

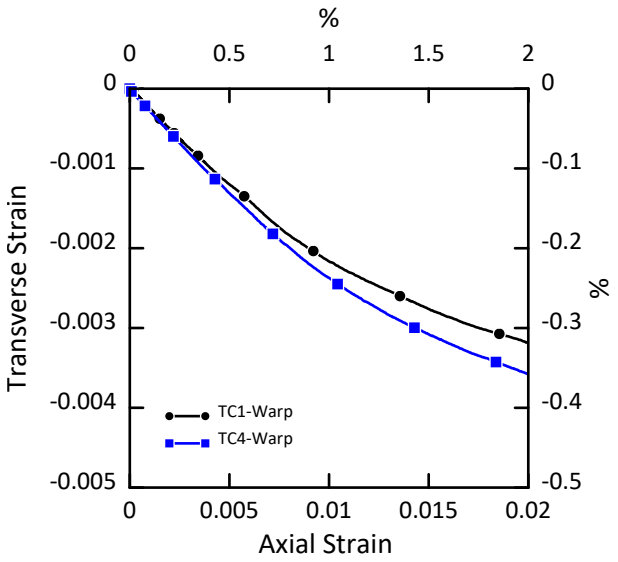

Figure 2.8. Transverse versus Axial Strain for Tensile Stress for AP1 Specimens in the Warp Direction

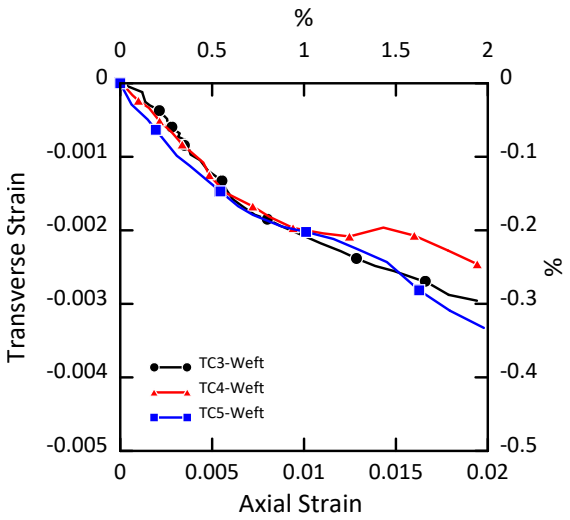

Figure 2.9. Transverse versus Axial Strain for Tensile Stress for AP1 Specimens in the Weft Direction

Table 2.1. Summary of AP1 Material Properties from Warp Tensile Coupons

		Specimen			Average	Standard Deviation
		1	2	4		
Young's Modulus, E	ksi (GPa)	459 (3.16)	344 (2.37)	368 (2.54)	390 (2.69)	60.7 (0.42)
Poisson's Ratio, ν		0.22	N/A^1	0.25	0.23	0.016
Ultimate Tensile Strength	ksi (MPa)	11.8 (81.7)	11.0 (75.7)	10.0 (68.8)	10.9 (75.2)	0.94 (6.5)
Ultimate Tensile Strain	%	16	15	14	15	1.2

1 – not available

Table 2.1 and Table 2.2 provide summaries of the Young's modulus, tensile stress and strain at failure, and Poisson's ratio in the warp and weft directions, respectively. A close examination of the plots in Figure 2.6, Figure 2.7, Figure 2.8 and Figure 2.9 shows a departure from linearity at a strain of between 0.5% and 1.0%. The Young's modulus and Poisson's ratio in both the warp and weft direction decreases at strains between 0.5% and 1.0%.

Table 2.2. Summary of AP1 Material Properties from Weft Tensile Coupons

		Specimen			Average	Standard Deviation
		3	4	5		
Young's Modulus, E	ksi	446	408	389	414	29.0
	(GPa)	(3.08)	(2.81)	(2.68)	(2.86)	(0.20)
Poisson's Ratio, ν		0.26	0.24	0.25	0.25	0.010
Ultimate Tensile Strength	ksi	13.4	16.0	16.6	15.3	1.68
	(MPa)	(92.6)	(110)	(115)	(106)	(11.6)
Ultimate Tensile Strain	%	9.3	11.5	12.5	11.1	1.6

2.4. Lining Stress versus Strain Response (AP1)

In Figure 2.10, the stress versus strain data for the warp and weft directions are plotted at the same scale. From zero to between 0.5% and 1.0% strain, the lining responds as a linear elastic solid. The Poisson's ratio is approximately 0.24 in both directions, and the difference in the Young's modulus is less than 7% lower in the warp than in the weft direction. In this range of tensile strain, the Young's modulus and Poisson's ratio are controlled principally by the epoxy.

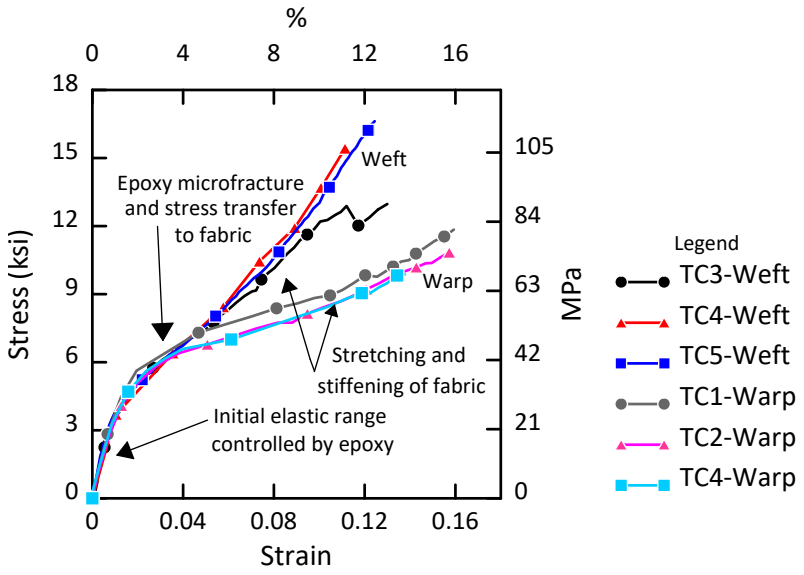

Figure 2.10. Stress versus Strain Plots for AP1 Specimens in the Warp and Weft Directions

As the strain approaches and exceeds 1.0%, micro-fractures develop in the epoxy, and stress is transferred increasingly from the epoxy matrix to the fabric. This stress transfer results in a reduction of modulus. Moreover, the fabric stretches more in the warp direction than in the weft direction, where the failure strain is smaller. As tensile strain exceeds approximately 5%, the fibers stretch and tighten, leading to increased modulus in both the warp and weft directions. The stiffness and strength in the weft direction exceed those in the warp direction due to the higher crimp in the latter direction.

2.5. AP2 Lining CDQC Test Results

Unused AP2 lining material was taken from the northern end of the fault rupture test specimen by Sanexen personnel after lining installation. Tensile coupon specimens in the warp and weft directions were cut, machined, and tested in accordance with ASTM-D638 2014 (ASTM, 2014) by the *Centre de Developpement des Composites du Quebec* [CDQC] (CDQC, 2019).

Because the great part of the load and deformation of the tensile coupon test specimens occurs in the inner and outer jackets and intervening epoxy layer, the thickness of the TPU is usually subtracted from the lining total thickness, which is then divided into the tensile force on the specimen. According to careful microscopic observations (magnification of 20-30X) of the lateral sections of the specimen, the TPU thickness varies typically between 0.024 and 0.032 in. (0.6 and 0.8 mm), although relatively small variants can occur above and below this range.

For the full-scale fault test the TPU thickness could not be measured accurately, whereas the total thickness of the AP2 lining in the full-scale test specimens could be measured with a caliper or scale. The total thickness therefore was used in the tensile coupon test together with the lining width to compute the cross-sectional area. It was divided into the measured tensile force to obtain the tensile stress in the warp and weft directions.

Table 2.3 and Table 2.4 summarize the maximum tensile stress, tensile strain at maximum stress, and secant modulus at 1% tensile strain in the warp and weft directions, respectively, obtained by CDCQ. All the test results from CDCQ were used in Table 2.3 and Table 2.4, including failure both inside and outside the test specimen section.

Table 2.3. Summary of Material Properties from AP2 Warp Tensile Coupons

		Specimen							Coeff. of
		1	2	3	4	5	6	Average	Variation
Maximum Tensile Stress	ksi	18.4	22.4	20.2	16.6	21.0	19.5	19.7	9.8%
	MPa	126.7	154.5	139.4	114.3	145.0	137.7	135.8	
Strain at Max Stress	%	22.1	23.2	23.0	21.7	22.6	22.7	22.6	2.5%
Secant Modulus at 1%	ksi	490	501	509	470	485	493	491	2.7%
	GPa	3.38	3.46	3.51	3.24	3.34	3.40	3.38	

Table 2.4. Summary of Material Properties from AP2 Weft Tensile Coupons

		Specimens						Coeff. of
		1	2	3	4	5	Average	Variation
Maximum Tensile Stress	ksi	11.4	10.8	10.4	10.3	9.6	10.5	6.3%
	MPa	78.8	74.5	71.4	71.3	66.4	72.5	
Strain at Max Stress	%	1.95	2.17	2.30	2.22	1.81	2.09	9.6%
Secant Modulus at 1%	ksi	857	763	715	702	801	767	8.3%
	GPa	5.91	5.26	4.93	4.84	5.52	5.29	

A statistical comparison was made among the test specimens. The coefficient of variation is the ratio of the standard deviation to the average maximum. When measurements are compared for failure both inside and outside with those just inside the test specimen section, the coefficient of variation was virtually the same for the tensile strain at maximum stress and was within 1% for the secant modulus at 1% in the warp direction. It was within 4.5% for the maximum tensile stress for the same direction. For the weft direction the coefficient of variation was within 1%, and the coefficient of variation was within 3.5% for the average strain at maximum stress as well as the secant modulus at 1%. Due the low coefficients of variation it was decided to report and plot the data for all tests.

Each of Table 2.3 and Table 2.4 lists the maximum tensile stress, tensile strain at maximum stress, and secant modulus at 1% tensile strain for all specimens tested, the average maximum values, and coefficients of variation. For the warp direction the average maximum tensile stress, tensile strain at maximum stress, and secant modulus at 1% tensile strain are 19.7 ksi (135.8 MPa), 22.6 %, and

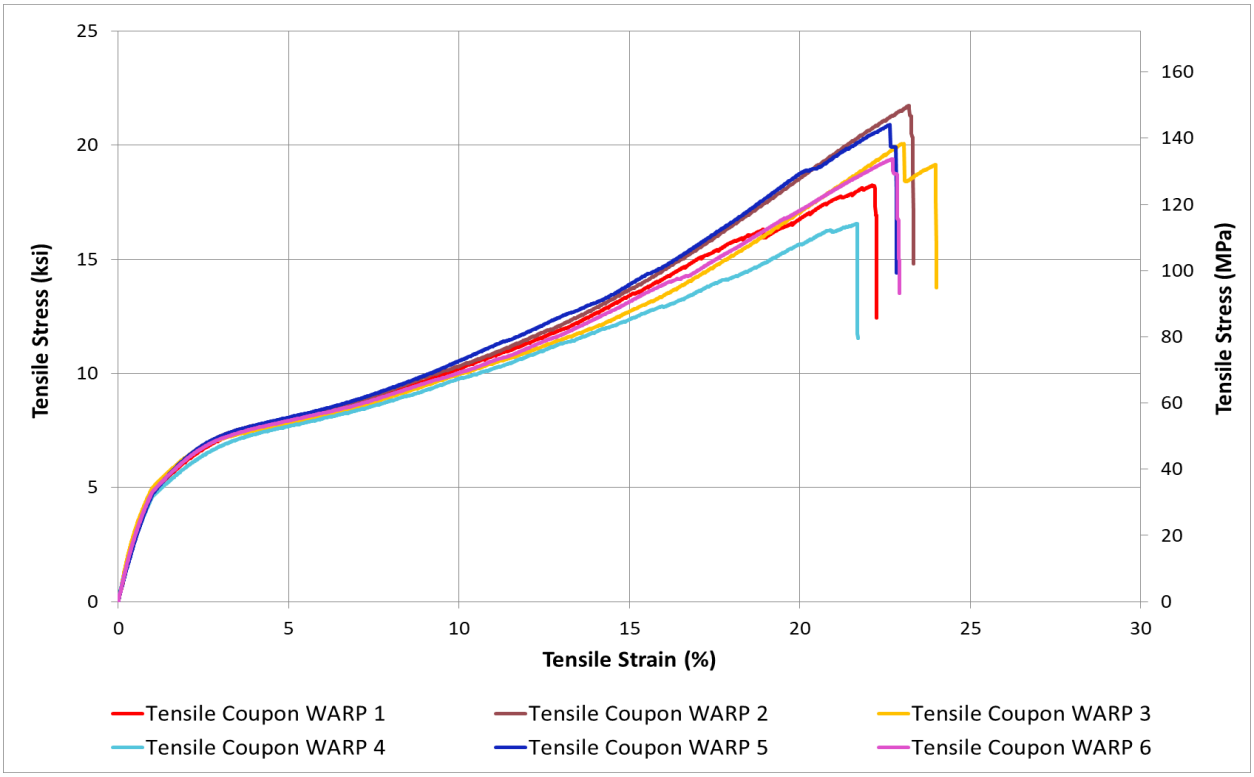

Figure 2.11 Tensile Stress vs Strain from CDCQ for the AP2 Warp Tensile Coupon Tests

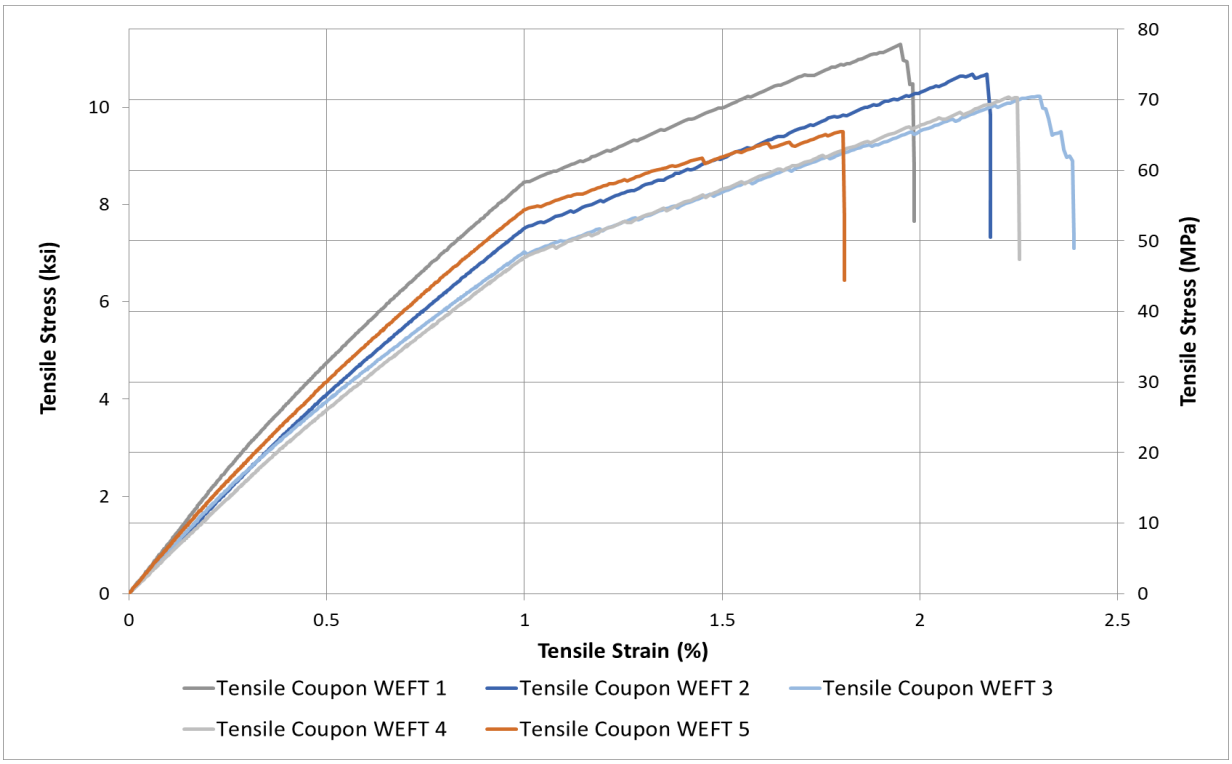

Figure 2.12 Tensile Stress vs Strain from CDCQ for the AP2 Weft Tensile Coupon Tests

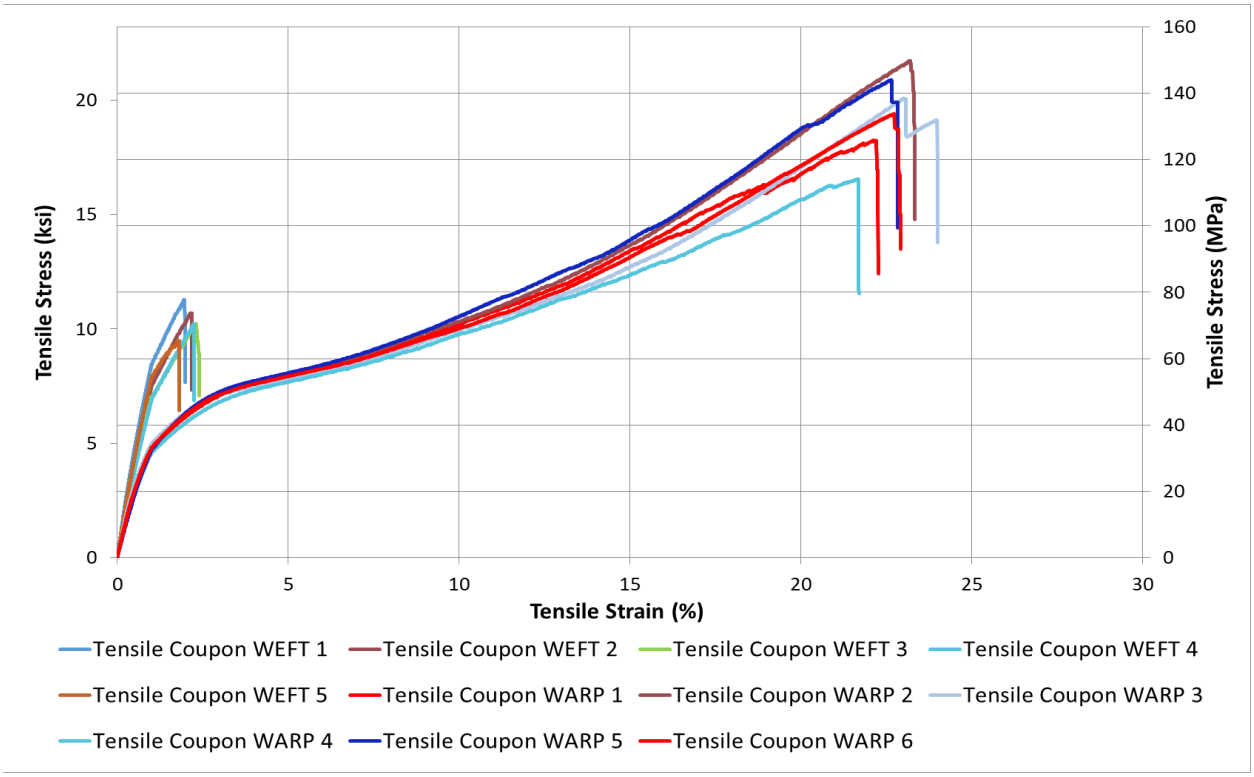

Figure 2.13 Tensile Stress vs Strain from CDCQ for AP2 Warp and Weft Tensile Coupon Tests

491 ksi (3.38 GPa), respectively. For the weft direction the average maximum tensile stress, tensile strain at maximum stress, and secant modulus at 1% tensile strain are 10.5 ksi (72.5 MPa), 22.6 %, and 767 ksi (5.29 GPa), respectively. There is modestly more variation in the weft results.

Figure 2.13 shows the tensile stress vs strain from CDCQ for all the specimens in the warp and weft directions. There is a significant difference in the maximum tensile strength and tensile strain at maximum stress for both directions. Like the AP1 specimens, there is marked departure from linearity for the AP2 specimens at tensile strains between 0.5 and 1.0%. The secant modulus in both the warp and weft directions of the AP2 specimens is larger than that in the same directions at the same strains for the AP1 specimens. At 0.5% strain, the secant modulus for AP2 is about 50% and 100% greater for AP1 in the warp and weft directions, respectively.

2.6. Summary of Tensile Coupon Test Results

Tensile coupon tests in the warp and weft directions were performed until the woven fabric tore apart, indicating failure. The average failure stress and strain for AP1 in the warp direction were 10.9 ksi and 15%, respectively, with standard deviations of 0.94 ksi and 1.2%. The average

failure stress and strain for AP1 in the weft direction were 15.3 ksi and 11.1%, respectively, with standard deviations of 1.68 ksi and 1.6%. Young's modulus, E, was computed using the linear range of the stress versus strain plots to approximately 0.5% strain. The average Young's modulus for AP1 in the warp direction is 390 ksi (2.69 GPa) with a standard deviation of 60.7 ksi (0.42 GPa). The average Young's modulus for AP1 in the weft direction is 414 ksi (2.86 GPa) with a standard deviation of 29.0 ksi (0.20 GPa).

From zero to between 0.5% and 1.0% strain, AP1 responds as a linear elastic solid. The Poisson's ratio is approximately 0.24 in both directions, and the difference in the Young's modulus is less than 7% lower in the warp than in the weft direction. In this range of tensile strain, the Young's modulus and Poisson's ratio are controlled principally by the epoxy.

Tensile coupon tests in the warp and weft directions of AP2 were performed by CDQC. For the warp direction the average maximum tensile stress, tensile strain at maximum stress, and secant modulus at 1% tensile strain are 19.7 ksi (135.8 MPa), 22.6 %, and 491 ksi (3.38 GPa), respectively. For the weft direction the average maximum tensile stress, tensile strain at maximum stress, and secant modulus at 1% tensile strain are 10.5 ksi (72.5 MPa), 22.6 %, and 767 ksi (5.29 GPa), respectively.

Like the AP1, there is marked departure from linearity for the AP2 specimens at tensile strains between 0.5 and 1.0%. The secant modulus in both the warp and weft directions of the AP2 specimens is larger than that in the same directions at the same strains for the AP1 specimens. At 0.5% strain, the secant modulus for AP2 is about 50% and 100% greater for AP1 in the warp and weft directions, respectively.

Section 3
Direct Tension Tests

3.1. Introduction

This section summarizes the results of direct tension tests on nominal 6 in. (152 mm) diameter pipe specimens with an AP1 lining. The direct tension tests were performed to evaluate the debonding characteristics between the AP1 lining and host pipe as well as determine the force versus displacement response of the lined pipe.

A summary of the full-scale direct tension tests performed as part of this investigation is provided in Table 3.1 that includes internal pressure, test pipe specimen length, sampling rate, and whether the pipe was new or old. Seven tests were performed and are labeled DT1 through DT7. The first four direct tension tests were performed on new ductile iron (DI) pipe that was procured directly from a local DI pipe supplier. The remaining tests were performed on older cast iron (CI) pipe that was excavated and removed from the field. All tests were loaded at a displacement rate of 1 in./min (25.4 mm/min).

3.2. Tension Test Setup

Figure 3.1 and Figure 3.2 show plan views of the axial tension test setup and equipment for large and small load frames. An actuator, load cell, and load frame were used to apply tensile load to the test specimen in each setup. The test specimens consisted of nominal 6 in. (152 mm) diameter DI and CI pipes lined with Aqua-Pipe that was installed by Sanexen. The specimen lengths were 8.5 ft (2.6 m) or 17 ft (5.2 m). Each specimen was fitted with end caps to allow for internal pressurization during loading. A photo of the test setup using the large load frame is shown in Figure 3.3, and a photo of the test setup using the small load frame is shown in Figure 3.4. Each test specimen consisted of two pipe sections of equal length on each side of a gap, representing a round crack.

In the small load frame setup, an actuator and load cell were installed at the south end of the load frame to apply and measure tensile force, respectively. The load cell had a capacity of 110 kips (489 kN) in the small and large load frame setups. In the large load frame setup, an actuator and load cell were installed at the north end of the load frame to apply and measure tensile force, respectively.

Table 3.1. Summary of Direct Tension Tests

Test	Pipe Condition	Length ft (m)	Pressure psi (kPa)	Sampling Rate Hz
Direct Tension 1 (DT1)	New DI	17 (5.2)	0	50
Direct Tension 2 (DT2)	New DI	8.5 (2.6)	0	20
Direct Tension 3 (DT3)	New DI	8.5 (2.6)	80 (551)	20
Direct Tension 4 (DT4)	New DI	17 (5.2)	0	2
Direct Tension 5 (DT5)	Field CI	8.5 (2.6)	80 (551)	2
Direct Tension 6 (DT6)	Field CI	8.5 (2.6)	80 (551)	25
Direct Tension 7 (DT7)	Field CI	16 (4.9)	80 (551)	50

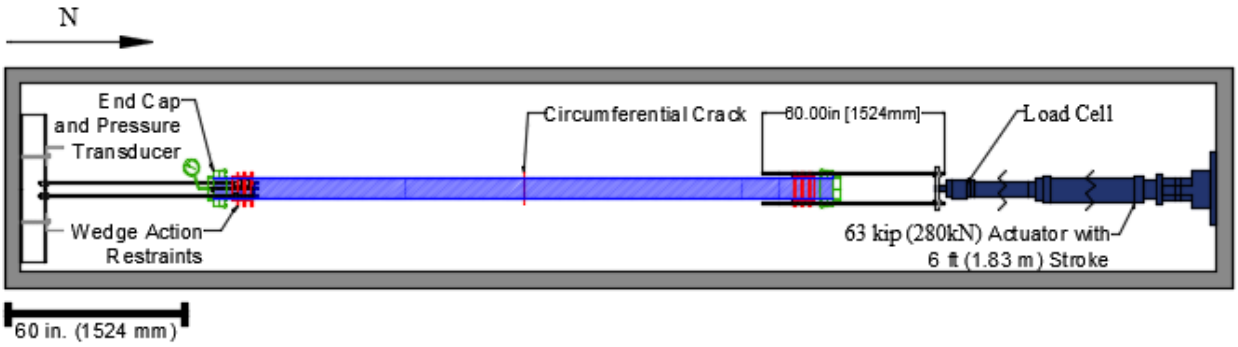

Figure 3.1. Plan View of a Direct Tension Test in the Large Load Frame

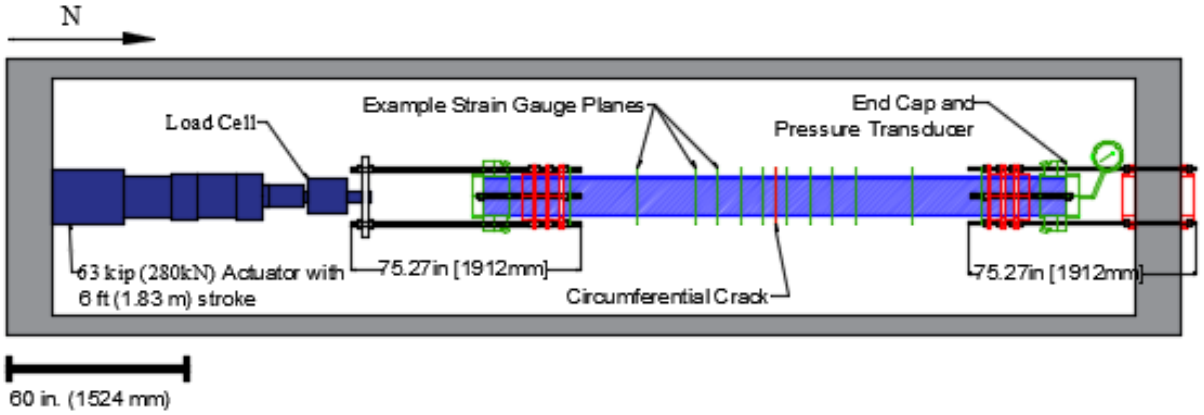

Figure 3.2. Plan View of a Direct Tension Test in the Small Load Frame

The actuator in DT1 had a tensile load capacity of 55 kips (245 kN) and stroke of 6 in. (150 mm). For DT2 through DT7, the actuator had a tensile load capacity of 63 kips (280 kN) and stroke

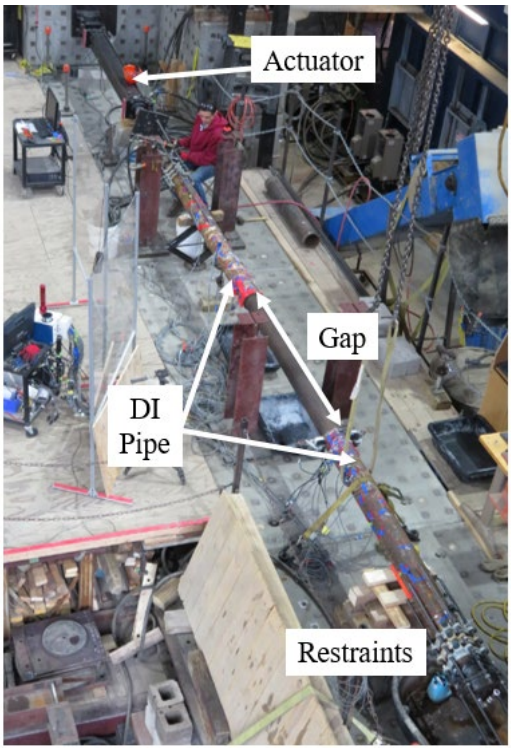

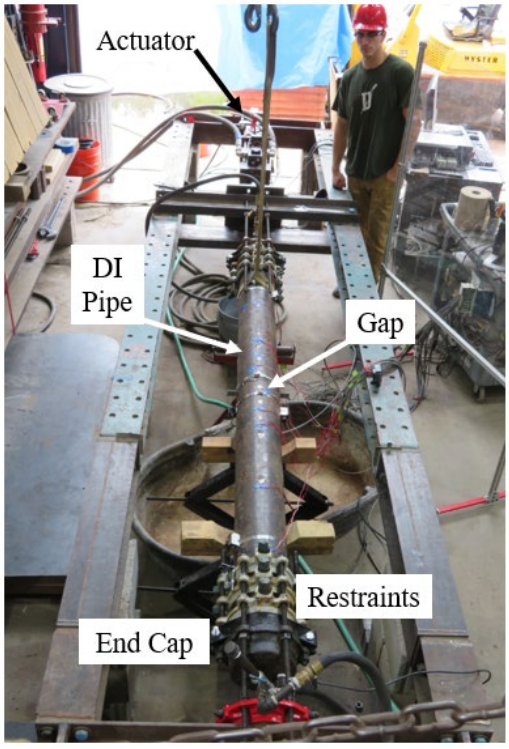

Figure 3.3. Large Load Frame (Facing North) Figure 3.4. Small Load Frame (Facing South)

of 6 ft (1.83 m). A series of three wedge action restraints were used at either end of each specimen to transfer load from the actuator and loading frame to the specimen. The three restraining collars acted as a grip for the pipes during axial load application.

Two electronic pressure transducers, located at the end cap and water source, measured internal water pressure during the test sequence when internal pressure was applied. String potentiometers (string pots) were attached to the specimen and restraints to measure axial displacements along the specimen.

Axial and circumferential strain gages were located on the exterior surface of the pipe specimen at varying distances from the gap at the center of the specimen. The gages were applied at the 12, 3, 6, and 9 o'clock positions around the pipe (crown, east springline, invert, and west springline, respectively). A detailed list of the instrumentation is provided for each test under Section 3.5.Instrumentation and Experimental Results.

3.3. Test Specimen Preparation

The test specimens for direct tension tests DT1, DT2, DT3, and DT4 were prepared by Sanexen using commercially available DI pipe without an internal cement lining. The installation procedure

was the same as used under field conditions, except that the interior pipe surface was not aged and thus did not require cleaning before placement of the lining. The DI pipe without cement mortar lining had a clean, new interior surface that mobilized the maximum interface friction between the host pipe and the Aqua-Pipe lining.

To prepare test specimens with interior surfaces representative of pipelines in the field, the test specimens for direct tension tests DT5, DT6, and DT7 were taken from CI pipelines, which had operated in the field for many years. These specimens were cleaned by Sanexen following their standard field installation procedures. The lining-pipe interface condition for DT5, DT6, and DT7 are more representative of field conditions than the pipes used in tests DT1 through DT4. The interface friction between the host pipe and Aqua-Pipe lining in the CI field samples was significantly lower than that of the pipe specimens with new interior DI surfaces for the first-time movement of the lining along the pipe. The characterization of the interface between DI and CI pipe and the lining before and after repeated loading is presented in Section 5 Direct Shear Tests.

Before lining a test specimen, a gap, approximately 0.25 in. (6 mm) wide, was located at the specimen center to replicate a round crack or gap between spigot and bell in an aging, deteriorated joint. It should be noted that that the roughness and chemical nature of the interior surface of a new DI pipe without a cement lining generates a higher resistance to axial pullout than the interior surface of an older CI pipe after cleaning.

3.4. Test Sequence

After the specimen was instrumented and centered in the test frame, the test sequence was initiated by starting the data acquisition system and laboratory hydraulic systems. The loading restraints at either end of the specimen were tightened to avoid end movement due to pressurization. The pipe was pressurized next with an internal water pressure of 80 psi (551 kPa). The tests were performed under displacement control using the servo-hydraulic actuator at the end of the test frame. The actuator was located at the south end for tests in the small load frame and at the north end in the large load frame.

During the application of axial load, the Aqua-Pipe lining separated itself, or debonded, from the DI host pipe starting at the centerline and then progressing towards the north and/or south ends. As the debonding front reached each strain gage station, there was a rapid reduction in strain in the DI pipe. As the Aqua-Pipe lining debonded in the north or south direction completely,

displacement was applied until the specimen was no longer capable of holding internal water pressure or until it reached the extent of the actuator range. The pipe on the debonded side of the specimen center was pulled from the lining in select tests.

3.5. Instrumentation and Experimental Results

The following subsections provide the instrumentation plan and key experimental results from the seven direct tension tests. The axial force versus crack opening, influence of internal pressure, geometric pipe effects, and debonding trends are described and compared in these sections.

3.1.1. DT1

As indicated in Table 3.1, DT1 was performed with a 17-ft (5.2 m)-long specimen in the large load frame. It was tested with zero internal pressure at a sampling rate of 50 Hz.

Figure 3.5 (a) and (d) show photographs of the DT1 test pipe. Figure 3.5 (a) shows the pipe at the beginning of the test. Strain gages on the crown of the pipe and a string pot along the eastern springline of the pipe can be seen in the photo. Figure 3.5 (b) and (c) show the pipe after the first and second 6 in. (152 mm) of actuator displacement, respectively. Figure 3.5 (d) shows the maximum 12 in. (305 mm) opening of the center crack near the end of the test. At 12 in. (305 mm) of crack opening, the loading frame geometric limits were met, and the specimen was unloaded.

Table 3.2 provides a list of the instrumentation used in DT1. The instrumentation for DT1 involved strain gages applied at 11 different locations both south and north of the gap. Longitudinal strain gages at the crown and invert were established at seven locations to 20 in. (508 mm) south and north of the gap. Circumferential strain gages at the crown and invert were positioned at 4 in. (102 mm) and 10 in. (254 mm) south and north of the center of the pipe. Only longitudinal gages at the crown were placed at distances greater than 20 in. (508 mm) from the pipe center. Horizontal string pots were located at eight different locations to measure the opening of the center gap as well as slip of the restraints.

Figure 3.6 shows the axial force versus gap, or crack, opening. As displacement was applied, the axial load increased rapidly so that the slope of the plot appears to be a vertical line. After approximately 1 in. (25 mm) of crack opening, the test was paused, causing the first cyclic loading in the figure. After resuming the test, multiple load and reload cycles were applied until a maximum gap opening of 12 in. (305 mm) was achieved. Six unloading and loading cycles are

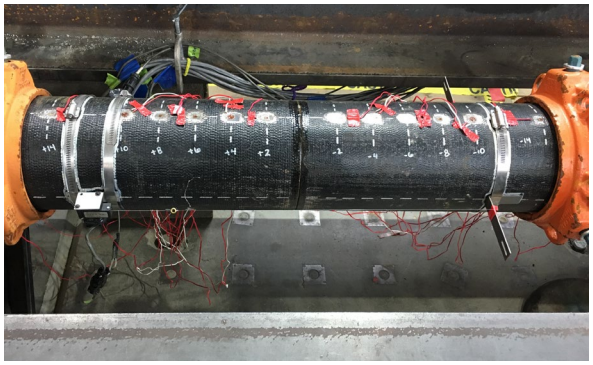

(a) View of DT1 Specimen in Load Frame Before Test Initiation

(b) View of Lining Exposed After First 6 in. (152 mm) of Actuator Displacement

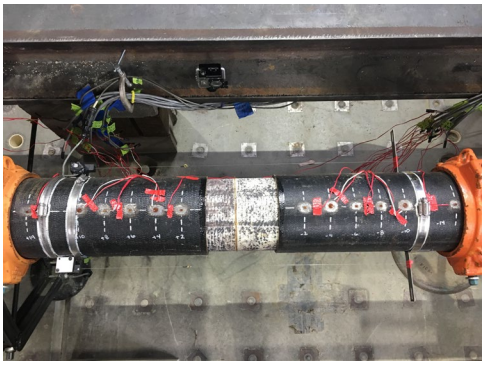

(c) View of Lining Exposed After Second 6 in. (152 mm) of Actuator Displacement

(d) View of Lining Exposed After Completion of Actuator Displacement

Figure 3.5. Photos of the Center Gap at Various Levels of Displacement during DT1

shown in the figure, which reflect multiple adjustments in the 6 in. (152 mm) stroke actuator to develop large axial displacement of the pipe relative to the lining.

The maximum axial force recorded varied between 26 kips (116 kN) and 29 kips (129 kN). This force represents the debonding capacity of the lining, which is the force required to propagate a Type II fracture between the lining and inside surface of the pipe (Argyrou et al, 2018). The maximum debonding force varied roughly ± 5% along the pipe specimen, with an average of approximately 27.5 kips (122 kN).

Additional insight with respect to the debonding characteristics of the lining can be obtained from the strain gage readings. Figure 3.7 shows plots of the crown and invert strains measured by longitudinal strain gages, 6C and 6I, at 6 in. (152 mm) north of the pipe specimen center.

Table 3.2. Instrumentation List for DT1

Location	Instrument Description	Local Instrument Name
66 in. South of Centerline	Crown, Axial Strain	-66C
54 in. South of Centerline		-54C
42 in. South of Centerline		-42C
30 in. South of Centerline		-30C
20 in. South of Centerline		-20C
	Invert, Axial Strain	-20I
14 in. South of Centerline	Crown, Axial Strain	-14C
	Invert, Axial Strain	-14I
10 in. South of Centerline	Crown, Axial Strain	-10C
	Crown, Circumferential Strain	-10CC
	Invert, Axial Strain	-10I
	Invert, Circumferential Strain	-10IC
8 in. South of Centerline	Crown, Axial Strain	-8C
	Invert, Axial Strain	-8I
6 in. South of Centerline	Crown, Axial Strain	-6C
	Invert, Axial Strain	-6I
4 in. South of Centerline	Crown, Axial Strain	-4C
	Crown, Circumferential Strain	-4CC
	Invert, Axial Strain	-4I
	Invert, Circumferential Strain	-4IC
2 in. South of Centerline	Crown, Axial Strain	-2C
	Invert, Axial Strain	-2I
2 in. North of Centerline	Crown, Axial Strain	2C
	Invert, Axial Strain	2I
4 in. North of Centerline	Crown, Axial Strain	4C
	Crown, Circumferential Strain	4CC
	Invert, Axial Strain	4I
	Invert, Circumferential Strain	4IC
6 in. North of Centerline	Crown, Axial Strain	6C
	Invert, Axial Strain	6I
8 in. North of Centerline	Crown, Axial Strain	8C
	Invert, Axial Strain	8I
10 in. North of Centerline	Crown, Axial Strain	10C
	Crown, Circumferential Strain	10CC
	Invert, Axial Strain	10I
	Invert, Circumferential Strain	10IC
14 in. North of Centerline	Crown, Axial Strain	14C
	Invert, Axial Strain	14I
20 in. North of Centerline	Crown, Axial Strain	20C
	Invert, Axial Strain	20I
30 in. North of Centerline	Crown, Axial Strain	30C
42 in. North of Centerline	Crown, Axial Strain	42C
Location	Instrument Description	Local Instrument Name

Table 3.2. Instrumentation List for DT1

54 in. North of Centerline	Crown, Axial Strain	54C
66 in. North of Centerline	Crown, Axial Strain	66C
Centerline	Horizontal String Pot	N-Pipe
		N-Liner
		S-Pipe
		S-Liner
		HSP_East
		HSP_West
Restraining Collars, North of Centerline		N_Slip
Restraining Collars, South of Centerline		S_Slip
Actuator, South of Centerline	Actuator Displacement	Act-Disp

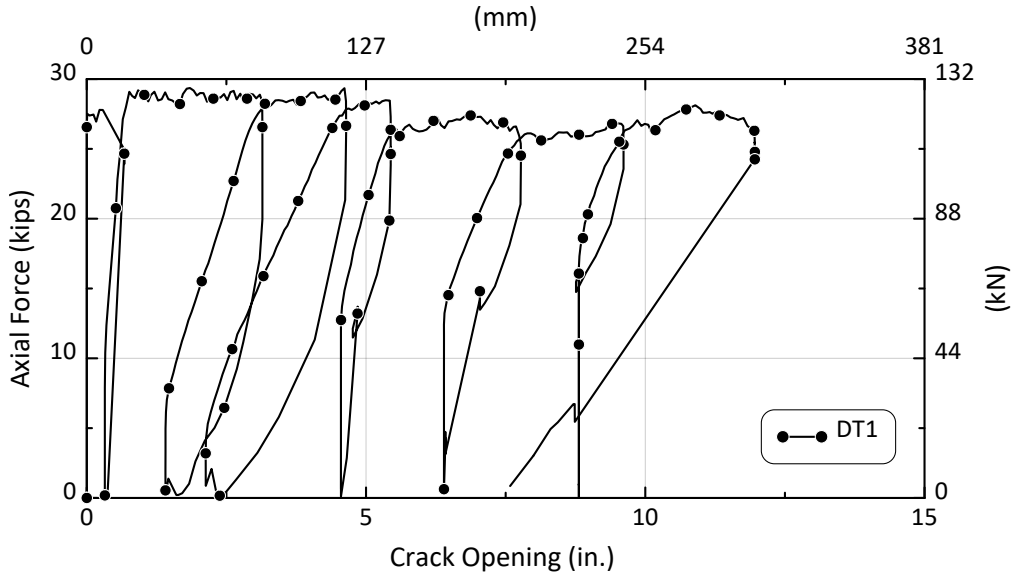

Figure 3.6. Axial Force versus Crack Opening for DT1

Each minimum reading indicates when debonding had fully propagated past the location of the gage. At approximately 1.7 in. (43 mm) of gap opening, the invert strain dropped to its minimum value, followed by the crown strain that dropped to its minimal value at 1.9 in. (48 mm) of gap opening. There is a lag of approximately 0.20 to 0.25 in. (5.1 to 6.4 mm) in crack opening between

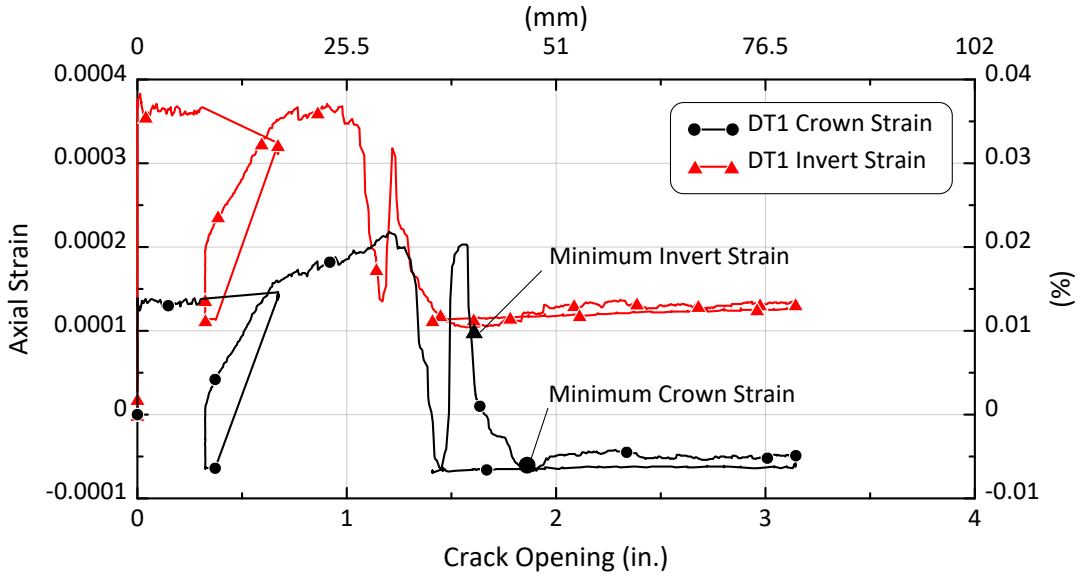

Figure 3.7. Longitudinal Strain at Strain Gage Station 6 versus Crack Opening for DT1 Specimen

the minimum readings. The same applies to the maximum strain readings (after which there is a perceptible decline). The maximum strain coincides with the crack opening at which debonding begins at the gage station.

3.1.2. DT2

As indicated in Table 3.1, DT2 was performed with an 8.5-ft (2.6 m)-long specimen in the small load frame. It was tested with no internal pressure at a sampling rate of 20 Hz. The test consisted of two stages. The first stage included the propagation of the debonding front along the pipe, and the second stage included pulling the DI pipe off the Aqua-Pipe lining.

Table 3.3 provides a list of the instrumentation used in DT2. The instrumentation for DT2 involved strain gages applied at 10 different locations both south and north of the gap at the center of the test pipe. Longitudinal strain gages at the crown and invert were established at six locations to 16 in. (406 mm) south and north of the gap. Longitudinal strain gages at the crown, invert, east springline, and west springline were positioned at 4 in. (102 mm) and 6 in. (152 mm) south and north of the center of the pipe.

Only longitudinal gages at the crown were placed at distances greater than 16 in. (406 mm) from the pipe center. Horizontal string pots were located at six different locations to measure opening of the center gap as well as any slip of the restraints.

Table 3.3. Instrumentation List for DT2

Location	Instrument Description	Local Instrument Name
40 in. South of Centerline	Crown, Axial Strain	-40C
30.5 in. South of Centerline		-30_5C
30 in. South of Centerline		-30C
16.5 in. South of Centerline		-16_5C
16 in. South of Centerline		-16C
	Invert, Axial Strain	-16I
8 in. South of Centerline	Crown, Axial Strain	-8C
	Invert, Axial Strain	-8I
6 in. South of Centerline	Crown, Axial Strain	-6C
	Invert, Axial Strain	-6I
	East, Axial Strain	-6E
	West, Axial Strain	-6W
4 in. South of Centerline	Crown, Axial Strain	-4C
	Invert, Axial Strain	-4I
	East, Axial Strain	-4E
	West, Axial Strain	-4W
3 in. South of Centerline	Crown, Axial Strain	-3C
	Invert, Axial Strain	-3I
2 in. South of Centerline	Crown, Axial Strain	-2C
	Invert, Axial Strain	-2I
2 in. North of Centerline	Crown, Axial Strain	2C
	Invert, Axial Strain	2I
3 in. North of Centerline	Crown, Axial Strain	3C
	Invert, Axial Strain	3I
4 in. North of Centerline	Crown, Axial Strain	4C
	Invert, Axial Strain	4I
	East, Axial Strain	4E
	West, Axial Strain	4W
6 in. North of Centerline	Crown, Axial Strain	6C
	Invert, Axial Strain	6I
	East, Axial Strain	6E
	West, Axial Strain	6W
8 in. North of Centerline	Crown, Axial Strain	8C
	Invert, Axial Strain	8I
16 in. North of Centerline	Crown, Axial Strain	16C
	Invert, Axial Strain	16I
16.5 in. North of Centerline	Crown, Axial Strain	16_5C
30 in. North of Centerline		30C
30.5 in. North of Centerline		30_5C
40 in. North of Centerline		40C
Centerline	Horizontal String Pot	N Pipe
		S Pipe
Location	Instrument Description	Local Instrument Name

Table 3.3. Instrumentation List for DT2

Centerline	Horizontal String Pot	HSP_East
		HSP_West
Restraining Collars, North of Centerline		N_Slip
Restraining Collars, South of Centerline		S_Slip
Actuator, South of Centerline	Actuator Displacement	SP_Act_Disp
Actuator, South of Centerline	Actuator Displacement	Act-Disp

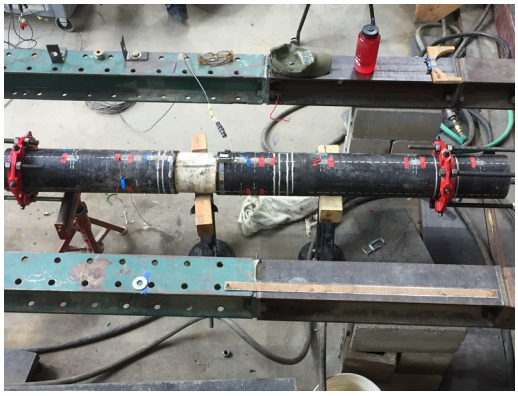

(a) View of DT2 Specimen in Load Frame

(b) View of Lining Exposed after DT2

Figure 3.8. Photos of the Center Gap at the End of DT2

Figure 3.8 (a) and (b) show photographs of the DT2 specimen after the lining fully debonded from the DI host pipe. Figure 3. (a) shows the specimen in the small load frame. A string pot on the crown of the crack opening and several strain gages are visible in Figure 3. (b).

The actuator displacement and crack opening versus time are shown in Figure 3.9. Actuator displacement is a direct measurement of the hydraulic piston movement. Crack opening represents the relative movement between the north and south pipe lengths. Only the south section of the pipe specimen debonded from the lining so the gap opening is equivalent to pipe movement along the south part of the lining. Crack opening was determined by averaging the displacements of the horizontal string pots, N-Pipe and S-Pipe, across the centerline. At approximately 1 minute, there was a slip of the retaining collars that resulted in an offset between the actuator displacement and gap opening. Further crack opening occurred in unison with the actuator displacement,

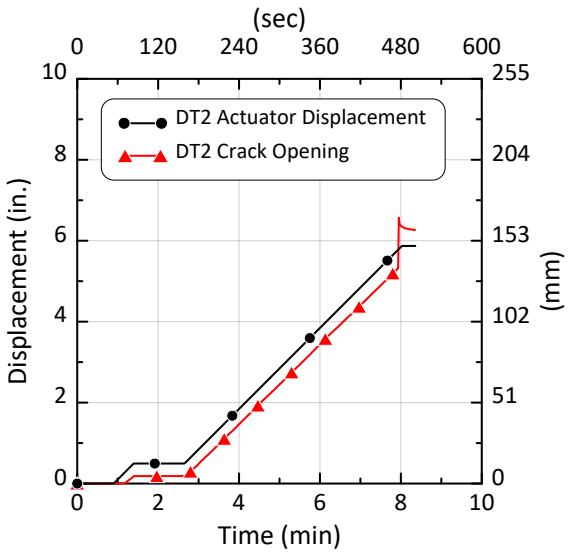

Figure 3.9. Actuator Displacement and Crack Opening versus Time for DT2 Specimen

indicating no further slip of the restraining collars and no significant axial deformation of the DI pipe.

As described previously, the test consisted of propagating the debonding front along the entire south pipe section, followed by pulling the debonded side of the DI pipe off the Aqua-Pipe lining. After the maximum range of the string pot was exceeded, further crack opening was based on the actuator displacements. Figure 3.10 shows the axial force versus crack opening until 12.5 in. (318 mm) of crack opening. Both the debonding/detachment and pull-off phases of the test are identified. A maximum force of approximately 27 kips (120 kN) was reached at a corresponding crack opening of 5.5 in. (140 mm). At that point, there was lining detachment from the south end of the pipe with a corresponding rapid decrease in axial load. The test was paused before the second phase of loading.

As explained with respect to DT1, the strain gage measurements show when the debonding front reaches each gage station. By correlating the string pot measurements of average gap opening in DT2 with debonding front propagation to gage stations at increasing distances from the specimen center, one can plot the debonding length as a function of gap opening as shown in Figure 3.11. As explained previously, the debonding occurred in the south pipe section so that the gap opening

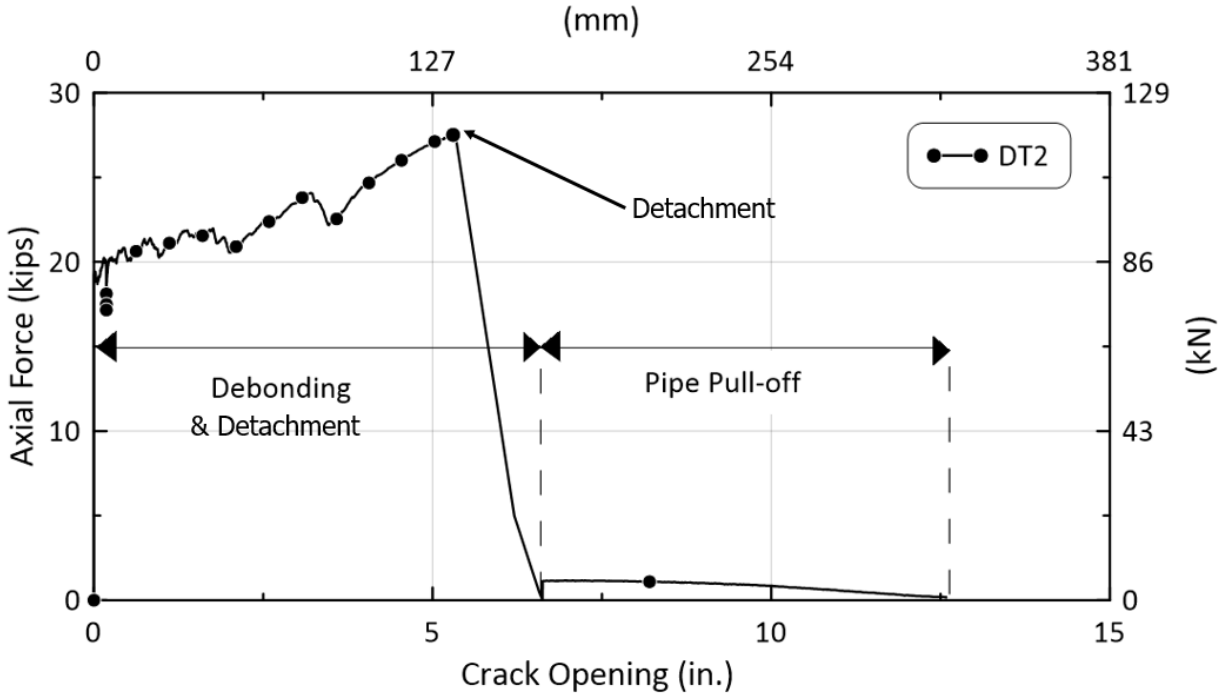

Figure 3.10. Axial Force versus Crack Opening for the DT2 Specimen

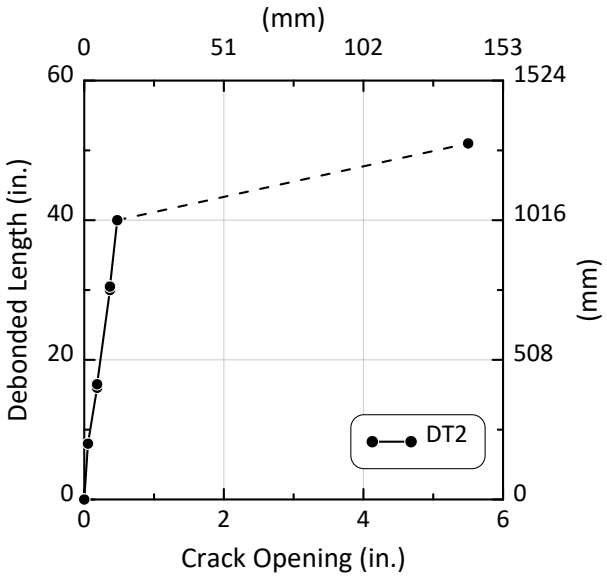

Figure 3.11. Location of Debonding Front
versus Crack Opening of the DT2 Specimen

is equivalent to the relative axial displacement between the initial center gap location and south section of pipe.

As shown in Figure 3.11, the debonding front propagated rapidly through the south section of pipe to 40 in. (1016 mm) at a crack opening of approximately 0.5 in. (13 mm); a ratio of roughly 80:1. All of the gap opening was in the southern direction. The increase in debonding length after 40 in. (1016 mm) is presented as a dashed line to indicate that there is uncertainty about the relationship between debonded length and crack opening from 40 to 51 in. (1016 to 1295 mm).

The second phase of the test consisted of pulling and pushing the DI pipe over the south section of the Aqua-Pipe lining. Figure 3.12 shows the first iteration of pulling the south section of pipe along the lining. The force increased to 1.5 kips (6.7 kN) rapidly and decreased to zero as the pipe moved towards the end of the lining. Figure 3.10 shows the axial force versus crack opening for the initial pipe pull-off, as well as two additional cycles of pushing and pulling the DI pipe along the lining. When the pipe was being pulled from the lining, it was in tension (positive force). The lining was in compression (negative force) while the pipe was pushed onto it. The axial force initially increased at the beginning of pipe pull off and decreased to zero. When the pipe was pushed back onto the lining, the force increased slowly from zero to the initial force necessary to pull the pipe off.

Figure 3.13 shows the average outside lining diameter plotted with respect to distance along the south side of the lining that was exposed after the south section of the pipe was pulled from the lining. The diameter is measured from the center of the specimen at zero to near the south end of the lining at 48 in. (1219 mm).

Because the lining was cast and cured inside the pipe, the outside diameter of the lining is the inside diameter of the pipe. As the pipe was pulled along the lining, the larger end of the pipe was pulled across a lining diameter that decreased until a minimum diameter at about 42 in. (1067 mm) south of the initial center gap. Because the end of the pipe was displaced past a lining diameter lower than that of the pipe, contact between the inside diameter of the pipe and outside diameter of the lining was lost with a corresponding loss of shear resistance between the two surfaces. This geometric condition resulted in the reduction of axial load with increasing pipe lining movement

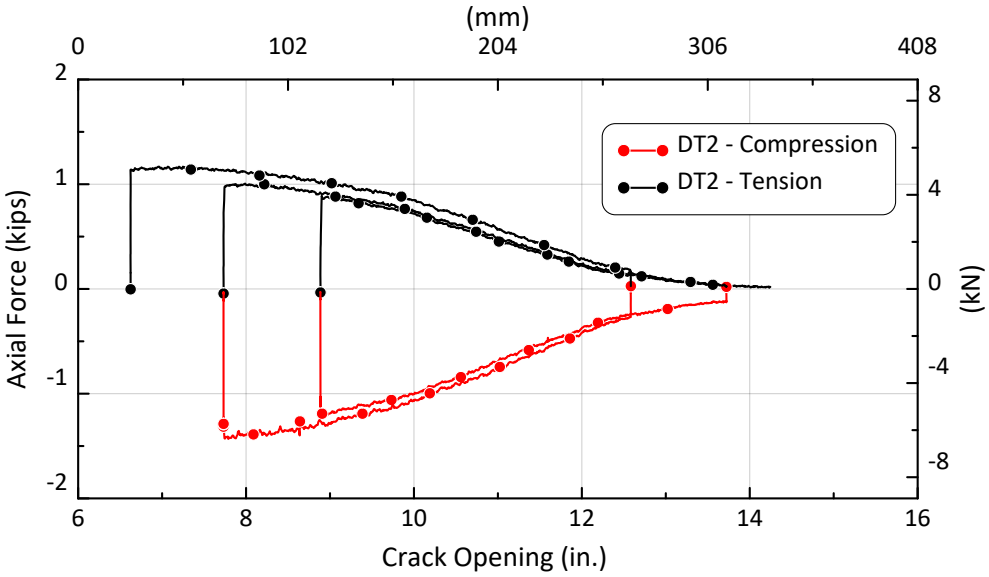

Figure 3.12. Axial Force versus Crack Opening during Pipe Pull-off for DT2

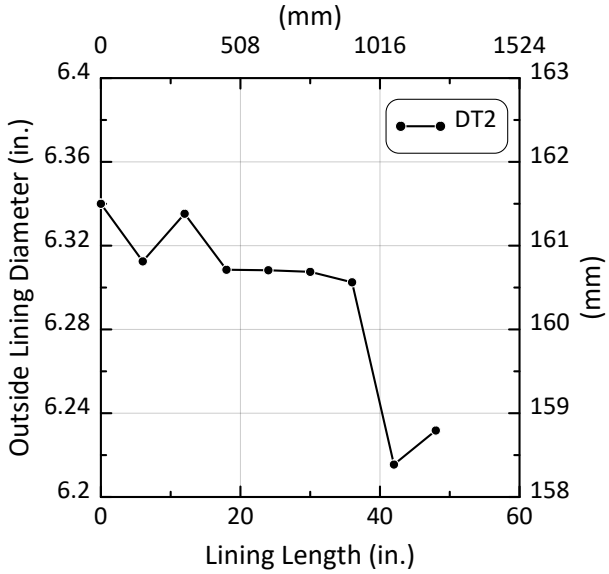

Figure 3.13. Average Outer Diameter of Lining along the South Section of the DT2 Specimen

under tension as well as an increasing axial load with increasing pipe/lining movement under compression.

3.1.3. DT3

As indicated in Table 3.1, DT3 was performed with an 8.5-ft (2.6 m)-long specimen in the small load frame. It was tested with 80 psi (551 kPa) internal pressure at a sampling rate of 20 Hz

Table 3.4 provides a list of the instrumentation used in DT3. The instrumentation for DT3 involved strain gages applied at 10 different locations both north and south of the crack at the center of the test pipe. Longitudinal strain gages at the crown and invert were established at six locations to 16 in. (406 mm) south and north of the gap. Longitudinal strain gages at the crown, invert, east springline, and west springline were positioned at 4 in. (102 mm) and 6 in. (152 mm) south and north of the center of the pipe. Only longitudinal gages at the crown were placed at distances greater than 16 in. (406 mm) from the pipe center. Horizontal string pots were located at four different locations to measure crack opening as well as any slip of the restraints. Pressure transducers were located at the end cap and water source to monitor the internal pressure.

Figure 3.14 (a) and (b) show photographs of the DT3 specimen before the start of the test and after the Aqua-Pipe lining failed. At approximately 2.0 in. (51 mm) of crack opening, the lining broke in tension rather than debonding along the length of the pipe. As the DI pipe was a new, clean specimen there was a relatively large amount of frictional resistance against debonding compared to the frictional resistance mobilized in field specimens.

Figure 3.15 shows the axial force versus crack opening. The force increased until a maximum force of approximately 30 kips (133 kN) was reached and the Aqua-Pipe lining failed at approximately 2 in. (51 mm) of crack opening. The stress at failure in DT3 was 10.7 ksi (74 MPa). This failure stress agrees with the findings of the tensile coupon tests, which show an average failure stress in the warp direction of 10.9 ksi (75 MPa).

3.1.4. DT4

As indicated in Table 3.1, DT4 was performed with a 17-ft (5.2 m)-long specimen in the large load frame. It was tested with no internal pressure at a sampling rate of 2 Hz. This specimen was later used in the friction tests described in Section 4 Friction Tests.

Similar to DT2, DT4 included two phases. The first phase consisted of propagating the debonding front along the entire north pipe section. The second phase consisted of pulling the debonded side of the DI pipe, which resulted from movement of the north pipe section relative to the lining. After

Table 3.4. Instrumentation List for DT3

Location	Instrument Description	Local Instrument Name
40 in. South of Centerline	Crown, Axial Strain	-40C
30.5 in. South of Centerline		-30_5C
30 in. South of Centerline		-30C
16.5 in. South of Centerline		-16_5C
16 in. South of Centerline		-16C
	Invert, Axial Strain	-16I
8 in. South of Centerline	Crown, Axial Strain	-8C
	Invert, Axial Strain	-8I
6 in. South of Centerline	Crown, Axial Strain	-6C
	Invert, Axial Strain	-6I
	East, Axial Strain	-6E
	West, Axial Strain	-6W
4 in. South of Centerline	Crown, Axial Strain	-4C
	Invert, Axial Strain	-4I
	East, Axial Strain	-4E
	West, Axial Strain	-4W
3 in. South of Centerline	Crown, Axial Strain	-3C
	Invert, Axial Strain	-3I
2 in. South of Centerline	Crown, Axial Strain	-2C
	Invert, Axial Strain	-2I
2 in. North of Centerline	Crown, Axial Strain	2C
	Invert, Axial Strain	2I
3 in. North of Centerline	Crown, Axial Strain	3C
	Invert, Axial Strain	3I
4 in. North of Centerline	Crown, Axial Strain	4C
	Invert, Axial Strain	4I
	East, Axial Strain	4E
	West, Axial Strain	4W
6 in. North of Centerline	Crown, Axial Strain	6C
	Invert, Axial Strain	6I
	East, Axial Strain	6E
	West, Axial Strain	6W
8 in. North of Centerline	Crown, Axial Strain	8C
	Invert, Axial Strain	8I
16 in. North of Centerline	Crown, Axial Strain	16C
	Invert, Axial Strain	16I
16.5 in. North of Centerline	Crown, Axial Strain	16_5C
30 in. North of Centerline		30C
30.5 in. North of Centerline		30_5C
40 in. North of Centerline		40C
Centerline	Horizontal String Pot	HSP_Crown
		HSP_Invert
Location	Instrument Description	Local Instrument Name

Table 3.4. Instrumentation List for DT3

Restraining Collars, North of Centerline	Horizontal String Pot	N_Slip
Restraining Collars, South of Centerline		S_Slip
South End Cap	Pressure Transducer	Pressure_End_cap
Water Source on Deck		Pressure_Deck
Actuator, South of Centerline	Actuator Displacement	Act-Disp

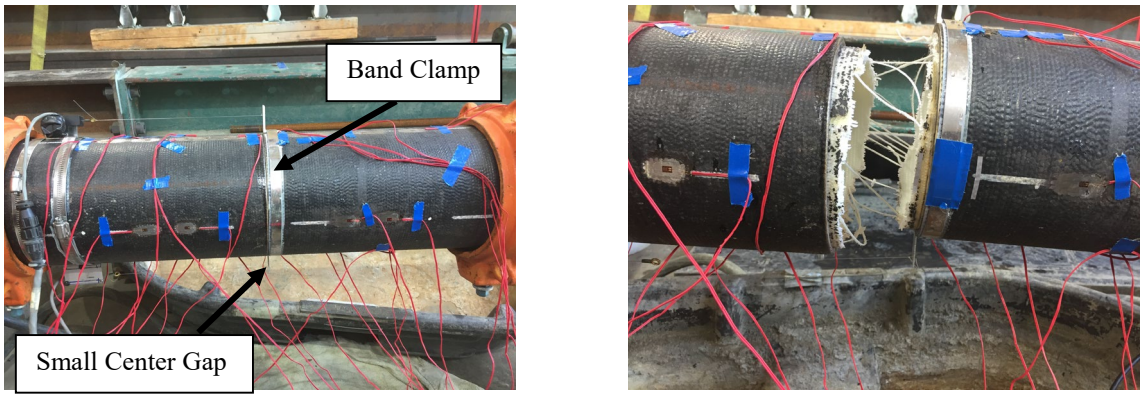

a) Full View of Specimen in Load Frame (b) View of Aqua-Pipe Failure

Figure 3.14. Photos of the Center Gap at the Beginning and End of DT3

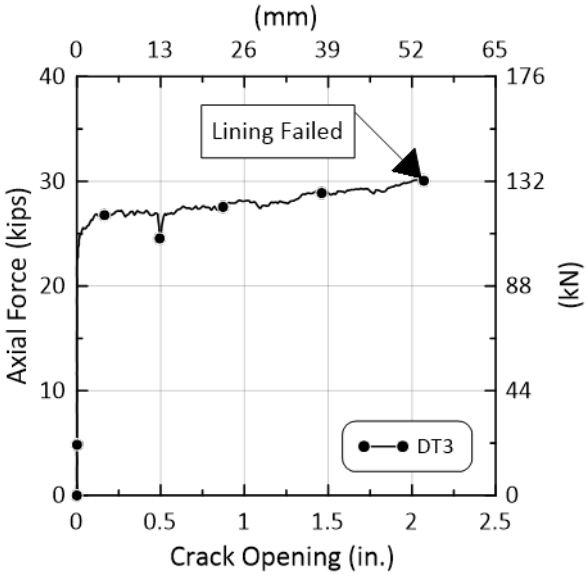

Figure 3.15. Axial Force versus Crack Opening for DT3

the maximum range of the string pot was exceeded, and further crack opening was measured by the actuator.

Table 3.5. Instrumentation List for DT4

Location	Instrument Description	Local Instrument Name
Centerline	Horizontal String Pot	Opening Disp
Restraining Collars, North of Centerline		North Slip
Restraining Collars, South of Centerline		South Slip
Actuator, South of Centerline	Actuator Displacement	LSA1-Disp

Table 3.5 provides a list of the instrumentation used in DT4. The instrumentation for DT4 involved horizontal string pots at three different locations to measure the opening of the center gap as well as any slip of the restraints. No strain data were recorded during DT4.

Figure 3.16 shows the axial force versus crack opening until 20 in. (508 mm) of movement. The gap opening was caused by displacement of the north pipe section relative to the lining. Thus, the gap opening is equivalent to the axial displacement of the north pipe.

The force increased rapidly followed by a relatively constant load until a peak load of 26.9 kips (120 kN). At about 12 in. (305 mm) of gap opening, the lining detached from the pipe south end, and the load dropped rapidly. With further crack opening the axial force began to increase.

Figure 3.17 shows the axial force versus crack opening until 103 in. (2616 mm) when the north pipe section was pulled completely from the lining. After the sudden drop in axial force at 12 in. (305 mm) of crack opening, the force increased steadily to a maximum force of 15.5 kips (69 kN) at about 48 in. (1219 mm) of crack opening. This increase in axial force was accompanied by a cyclic loading generated as the north section of the pipe was pulled along the lining. These cycles of axial force are shown in the force versus crack opening plot. The greatest difference between maximum and minimum load in a load cycle occurred when the maximum force of 15.5 kips (69 kN) was measured at 48 in. (1219 mm) of gap opening.

To understand the reason for the increase in cyclic as well as maximum axial force after debonding, the lining diameter was measured at various distances along the lining. Figure 3.18 shows the average outside lining diameter plotted with respect to distance along the north side of the lining that was exposed after the north section of the pipe was pulled from the lining. The diameter was

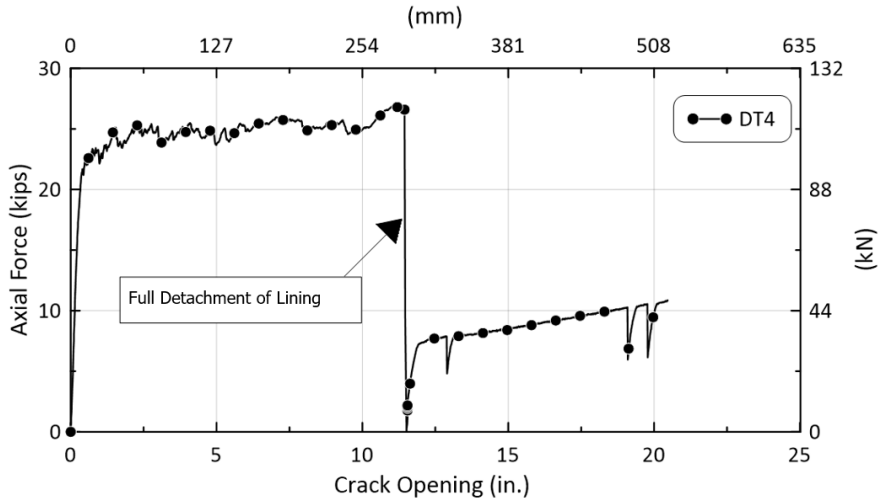

Figure 3.16. Axial Force versus Displacement for DT4 during Debonding

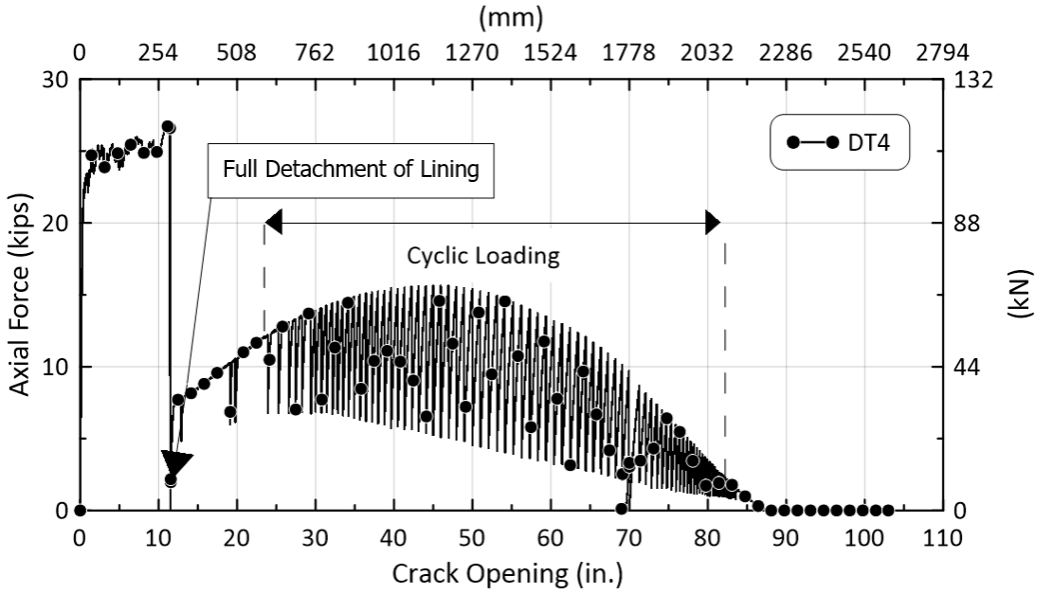

Figure 3.17. Axial Force versus Displacement for DT4 during the Full Test

measured from the center of the specimen at 0 in. to the north end of the lining at 104 in. (2642 mm).

Because the lining was cast and cured inside the pipe, the outside lining diameter is the inside pipe diameter. As the pipe was pulled along the lining, the low-diameter end of the pipe was pulled across a lining diameter that increased until a maximum at about 48 in. (1219 mm).

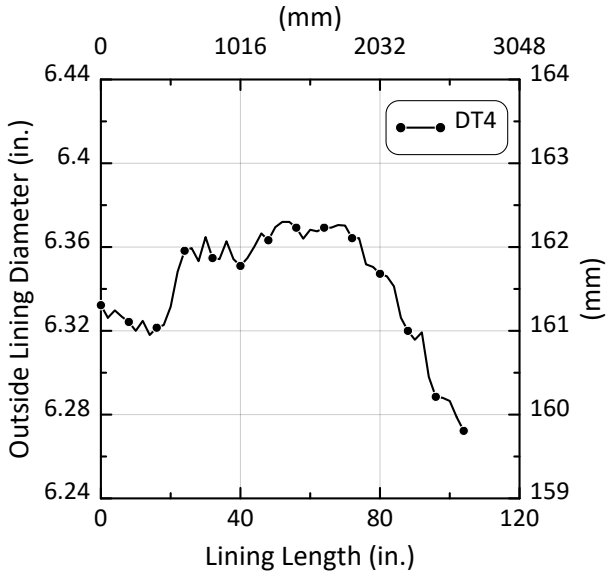

Figure 3.18. Average Outer Lining Diameter along the North Section of the DT4 Specimen

Pulling a smaller diameter pipe along an increasingly larger diameter lining generated an axial load in the pipe that peaked at the location of the maximum lining diameter. After a pipe displacement along the pipe length of roughly 70 in. (1778 mm), corresponding to an opening of 70 in. (1778 mm), the lining diameter decreased rapidly, corresponding to rapidly decreasing axial force. When the end of the pipe was pulled along the lining past a lining diameter lower than that of the pipe, the axial force was rapidly approaching zero.

As the smaller diameter pipe was pulled across an increasingly larger diameter lining, the axial load increased. Increased axial load in the lining was accompanied by a load-induced reduction in lining diameter that caused the lining to lurch forward with decreasing axial load until the lining diameter increased again and came in contact with the inside pipe diameter. Each axial load cycle was accompanied by a peak axial load and load-induced reduction in lining diameter as the lining lurched forward under constant pipe movement. As the lining lurched forward, it made firm contact with the pipe. Subsequent axial movement was accompanied by increased axial load until the next load cycle was initiated. During each cycle, there was an audible pop or boom as the lining lurched forward.

3.1.5. DT5

As indicated in Table 3.1, DT5 was performed with an 8.5-ft (2.6 m)-long specimen in the small load frame. It was initially tested with 80 psi (551 kPa) internal pressure at a sampling rate of 2 Hz. The testing protocol for DT5 was similar to that of DT4 and consisted of debonding, followed by pipe displacement along the debonded lining at zero internal pressure.

Table 3.6 provides a list of the instrumentation used in DT5. The instrumentation for DT5 involved strain gages applied at six different locations both south and north of the crack at the center of the test pipe. Longitudinal strain gages at the crown and invert were established at two locations at 2 in. (51 mm) and 6 in. (152 mm) south and north of the gap. Circumferential strain gages at the crown were positioned at 2 in. (51 mm) and 36 in. (914 mm) south and north of the center of the pipe. Only longitudinal gages at the crown were placed at the other distances. Horizontal string pots were located at four different locations to measure the crack opening as well as any slip of the restraints. Pressure transducers were installed at the end cap and the deck to measure the internal pressure during the test.

Figure 3.19. (a) and (b) show photographs of the DT5 test specimen. Figure 3. (a) shows the pipe at the beginning of the test. Strain gages on the crown of the pipe and string pots along the eastern and western springlines of the pipe can be seen in the photo. Figure 3. (b) shows the leaking that occurred after approximately 0.3 in. (7.6 mm) of crack opening. The leaking was initiated when the debonding front propagated to the south end of the pipe, breaking the end seal and causing water to flow longitudinally between the pipe and lining into the gap at the center of the specimen.

Figure 3.20. shows both the internal pipe pressure and crack opening measured during the test plotted with respect to time. The test was paused from approximately 14 minutes to 20 minutes, during which time the pressure decreased to zero and the crack opening remained constant. At all other times, the pipe pressure was maintained at approximately 80 psi (551 kPa).

The gap opening was caused by displacement of the south pipe section relative to the lining. Thus, the gap opening is equivalent to the axial displacement of the south pipe. Figure 3.21. shows the axial force versus crack opening during debonding of the DI pipe from the Aqua-Pipe lining.

Table 3.6. Instrumentation List for DT5

Location	Instrument Description	Local Instrument Name
36 in. South of Centerline	Crown, Axial Strain	-36C
	Crown, Circumferential Strain	-36CC
24 in. South of Centerline	Crown, Axial Strain	-24C
14 in. South of Centerline	Crown, Axial Strain	-14C
10 in. South of Centerline	Crown, Axial Strain	-10C
6 in. South of Centerline	Crown, Axial Strain	-6C
	Invert, Axial Strain	-6I
2 in. South of Centerline	Crown, Axial Strain	-2C
	Crown, Circumferential Strain	-2CC
	Invert, Axial Strain	-2I
2 in. North of Centerline	Crown, Axial Strain	2C
	Crown, Circumferential Strain	2CC
	Invert, Axial Strain	2I
6 in. North of Centerline	Crown, Axial Strain	6C
	Invert, Axial Strain	6I
10 in. North of Centerline	Crown, Axial Strain	10C
14 in. North of Centerline	Crown, Axial Strain	14C
24 in. North of Centerline	Crown, Axial Strain	24C
36 in. North of Centerline	Convert, Axial Strain	36C
	Crown, Circumferential Strain	36CC
Centerline	Horizontal String Pot	HSP_East
		HSP_West
Restraining Collars, North of Centerline		N_Slip
Restraining Collars, South of Centerline		S_Slip
End Cap	Pressure Transducer	Pressure_End_cap
Deck		Pressure_Deck
Actuator, South of Centerline	Actuator Displacement	Act-Disp

At 0.35 in. (9 mm) of crack opening and an axial force of 15.1 kips (67 kN), the pipe debonded to the south, causing a significant drop in axial force to 6 kips (26.6 kN).

The debonded length versus crack opening was evaluated using strain gage data, as explained for DT2. The relatively low sampling rate (2 Hz) for this test makes it more difficult to interpret the data, so there is greater variability relative to the 50 Hz sampling rate used in DT2 (see Figure 3.11) when plotting debonded length versus crack opening.

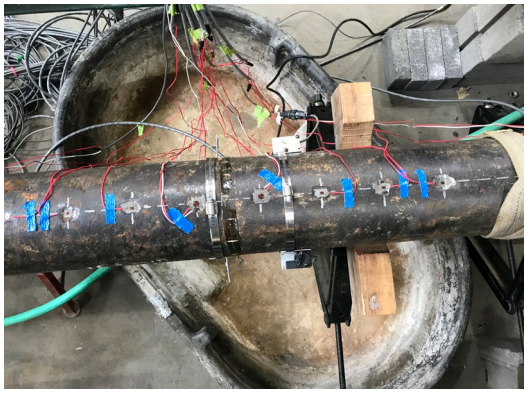

(a) View of Specimen in Load Frame before Test Initiation

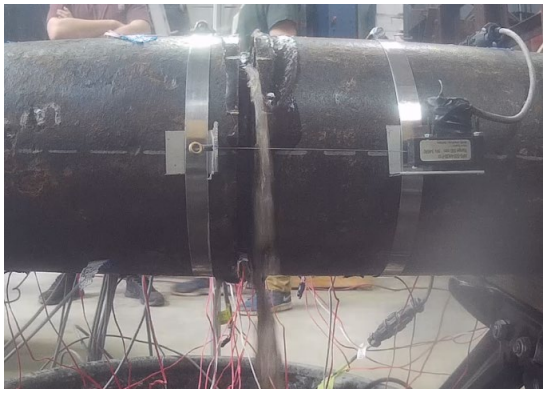

(b) View of Specimen Leaking after 0.3 in. (8 mm) of Crack Opening

Figure 3.19. Photos of the Test Specimen before and during the First Stage of DT5

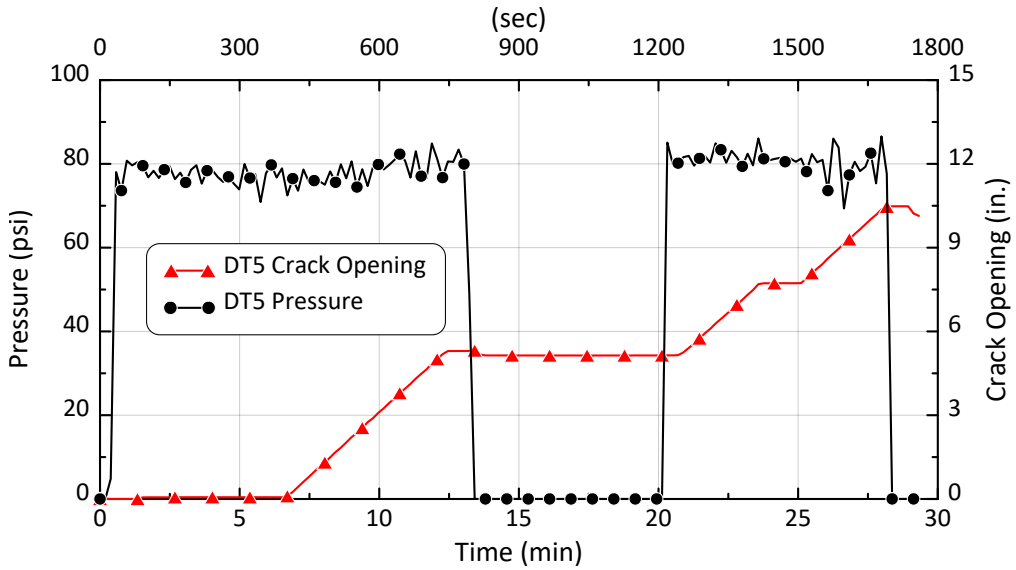

Figure 3.20. Pressure versus Time During the First Stage of DT5

Figure 3.21. shows the debonded length estimated from the strain gage data plotted with respect to crack opening. The crack opening at the sudden drop in axial force in Figure 3.21 was correlated with the maximum debonding length of the pipe equal to 51 in. (1295 mm) and plotted in Figure 3.22. The data shows that the debonding front moved rapidly through the pipe at a crack opening of approximately 0.35 in. (8 mm).

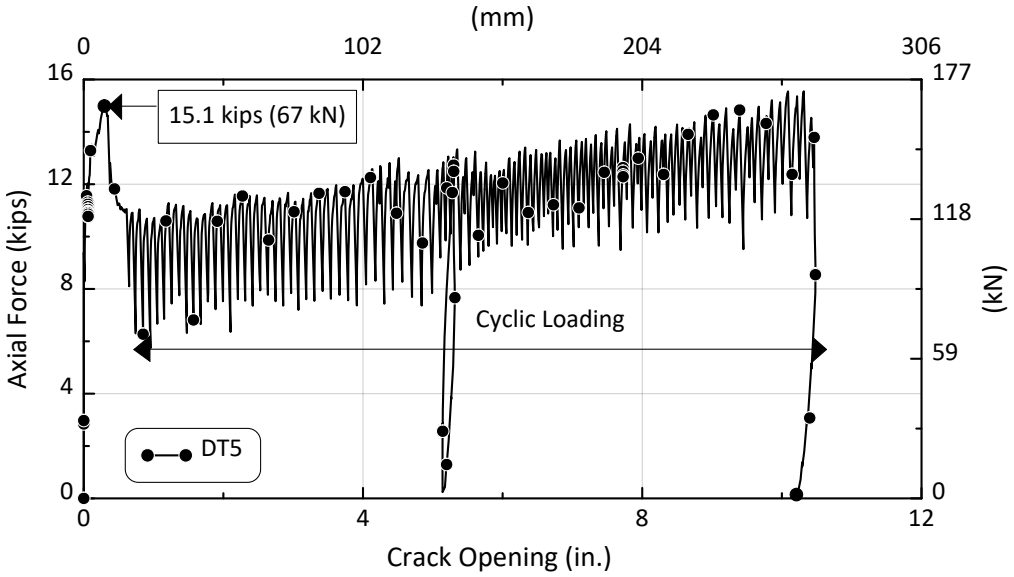

Figure 3.21. Axial Force versus Crack Opening
During the First Stage of DT5

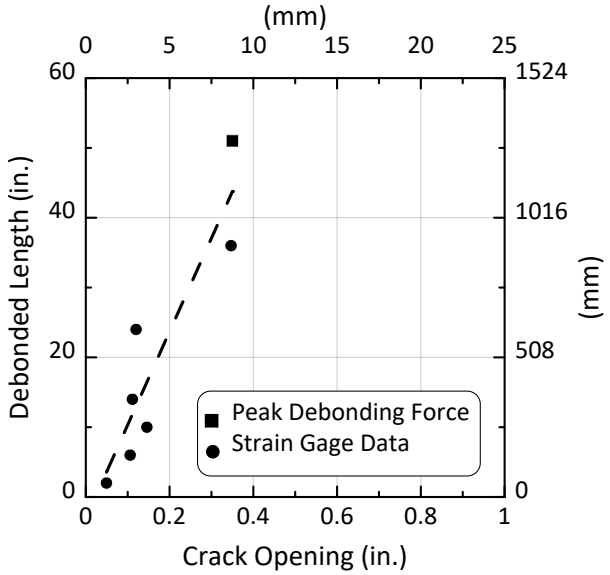

Figure 3.22. Debonding Front versus Crack Opening for DT5 Specimen

At approximately 11 in. (279 mm) of crack opening and an axial force of 15.1 kips (67 kN), the test was stopped due to significant leaking. The pipe specimen was moved to the large load frame,

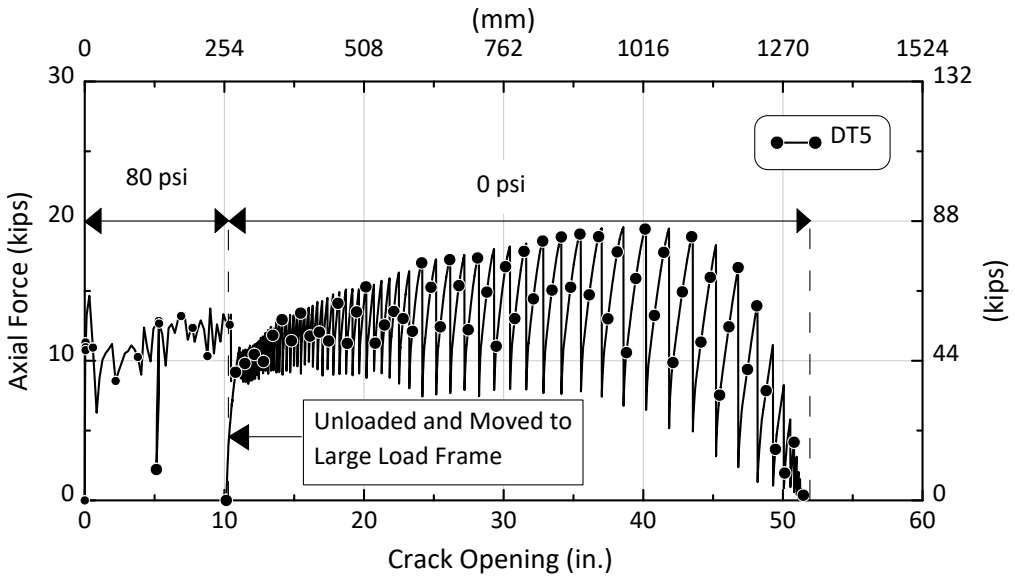

Figure 3.23. Axial Force versus Crack Opening for DT5 Specimen

and oriented so that the debonded section was located north of the gap. The pipe was then pulled from the lining in a northward direction under no internal pressure.

Figure 3.23. shows the axial force versus crack opening throughout the entire test. The crack opening was measured using actuator displacement. After the sudden drop in axial force at 0.35 in. (9 mm) of crack opening, the force increased steadily to 13 kips (58 kN) at about 5 in. (127 mm) of crack opening. The test was interrupted at 11 in. (279 mm) of crack opening and the specimen was removed to the small load frame.

After the test resumed in the large load frame, the axial force quickly increased to 10 kips (44 kN) and continued to increase to a maximum of 19.5 kips (87 kN) at 40 in. (1016 mm) of crack opening. This increase in axial force was accompanied by cyclic loading generated as the north section of the pipe was pulled along the lining. These cycles of axial force are shown in the force versus crack opening plot. The greatest difference between maximum and minimum cyclic load occurred when a maximum force of 13.1 kips (58 kN) was measured at 40 in. (1016 mm) of gap opening.

Figure 3.24. shows the average outside lining diameter plotted with respect to distance along the lining. The diameter was measured from the center of the specimen at zero to near the end of the lining at 48 in. (1219 mm). As the pipe was pulled along the lining, the smaller end of the pipe

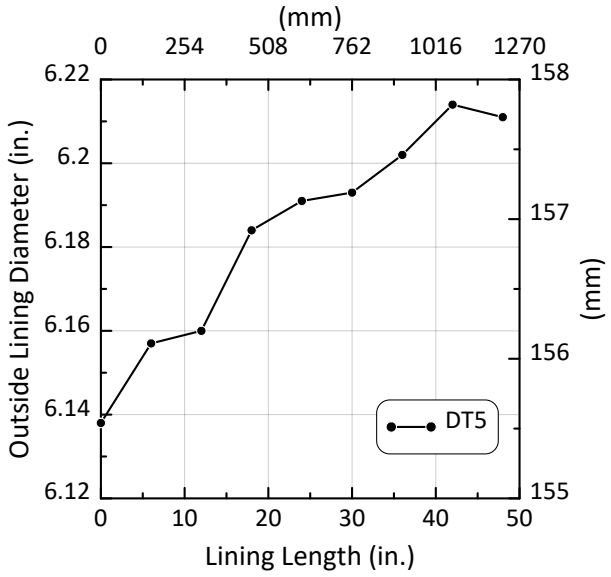

Figure 3.24. Average Outer Lining Diameter along the South Section of the DT5 Specimen

was pulled across a lining diameter that increased until a maximum distance of 42 in. (1067 mm). Pulling a smaller diameter pipe along an increasingly larger diameter lining generated an axial load that peaked at the location of the maximum lining diameter. After a crack opening of 42 in. (1067 mm), the lining diameter decreased, corresponding to rapidly decreasing axial force.

As discussed for DT2 and DT4, as the smaller diameter pipe was pulled across an increasingly larger diameter lining, the axial load increased. As explained for DT4, increased axial load was accompanied by a load-induced reduction in lining diameter that caused the lining to lurch forward, triggering a reduction in load and the beginning of another load cycle. Similar to DT4, there was an audible pop or boom during each load cycle during DT5.

3.1.6. DT6

As indicated in Table 3.1, DT6 was performed with an 8.5-ft (2.6 m)-long specimen in the small load frame. It was tested with 80 psi (551 kPa) internal pressure at a sampling rate of 25 Hz. Table 3.7 provides a list of the instrumentation used in DT6. The instrumentation for DT6 involved strain gages applied at 6 different locations both south and north of the crack at the center of the test pipe. Longitudinal strain gages at the crown and invert were established at two locations at 2 in. (51 mm) and 6 in. (152 mm) south and north of the gap. Circumferential strain gages at the crown were

Table 3.7. Instrumentation List for DT6

Location	Instrument Description	Local Instrument Name
36 in. South of Centerline	Crown, Axial Strain	-36C
	Crown, Circumferential Strain	-36CC
24 in. South of Centerline	Crown, Axial Strain	-24C
14 in. South of Centerline	Crown, Axial Strain	-14C
10 in. South of Centerline	Crown, Axial Strain	-10C
6 in. South of Centerline	Crown, Axial Strain	-6C
	Invert, Axial Strain	-6I
2 in. South of Centerline	Crown, Axial Strain	-2C
	Crown, Circumferential Strain	-2CC
	Invert, Axial Strain	-2I
2 in. North of Centerline	Crown, Axial Strain	2C
	Crown, Circumferential Strain	2CC
	Invert, Axial Strain	2I
6 in. North of Centerline	Crown, Axial Strain	6C
	Invert, Axial Strain	6I
10 in. North of Centerline	Crown, Axial Strain	10C
14 in. North of Centerline	Crown, Axial Strain	14C
24 in. North of Centerline	Crown, Axial Strain	24C
36 in. North of Centerline	Convert, Axial Strain	36C
	Crown, Circumferential Strain	36CC
Centerline	Horizontal String Pot	HSP_East
		HSP_West
Restraining Collars, North of Centerline		N_Slip
Restraining Collars, South of Centerline		S_Slip
End Cap	Pressure Transducer	Pressure_End_cap
Deck		Pressure_Deck
Actuator, South of Centerline	Actuator Displacement	Act-Disp

positioned at 2 in. (51 mm) and 36 in. (914 mm) south and north of the center of the pipe. Only longitudinal gages at the crown were placed at the other distances. Horizontal string pots were located at four different locations to measure crack opening as well as any slip of the restraints. Pressure transducers were installed at the end cap and the source on the deck to measure the internal pressure during the test.

There was substantial leaking from the beginning of the test. The leaking caused internal pressure to drop from 80 psi (551 kPa) to approximately 20 psi (138 kPa) after roughly 17 in. (432 mm)

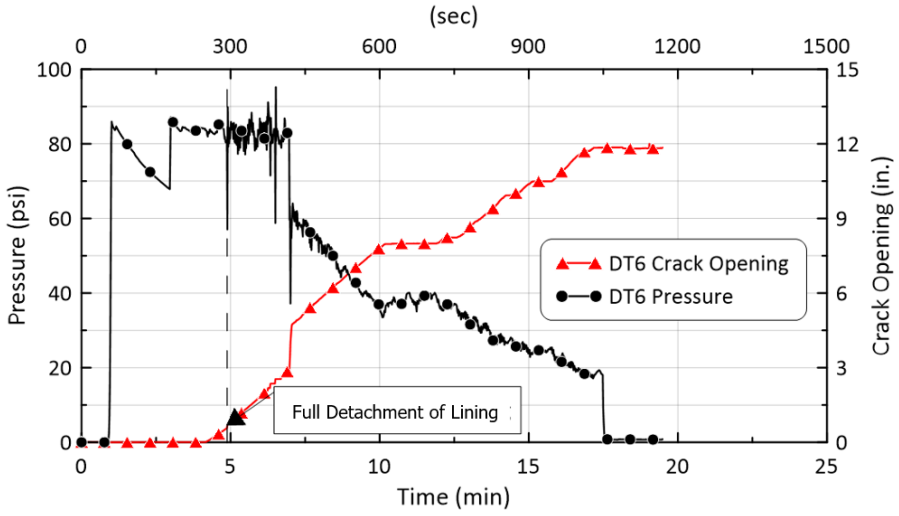

Figure 3.25. Internal Pressure versus Time for DT6 Specimen

of crack opening. The test concluded after full debonding and about 12 in. (305 mm) of pipe displacement to the south.

Figure 3.25. shows the internal pressure throughout the test superimposed on the crack opening. Virtually all gap opening was caused by displacement of the north pipe section relative to the lining. Thus, the gap opening is equivalent to axial displacement of the north pipe. The pressure was maintained at approximately 80 psi (550 kPa) until approximately 5 minutes into the test. At that time, pressure decreased due to extensive leaking. The leaking was caused by loss of seal at the end of the specimen, and continued until the test was completed at approximately 17 in. (432 mm) of crack opening.

Figure 3.26. shows the axial force versus crack opening. The maximum axial force was 14.9 kips (66 kN). The strain gage data were used to estimate how the debonded length increased with crack opening in a manner similar to that applied for DT2, DT4, and DT5. The strain gage data and pressure show full debonding along the north section of pipe at 0.6 in. (15 mm) of crack opening. As the Aqua-Pipe lining fully debonded from the DI pipe, the axial force decreased to approximately 3 kips (13 kN).

Figure 3.26. shows that, after detachment, the axial force continued to decrease with increasing crack opening. Following the procedures developed for DT2 and DT4 through DT6, the average

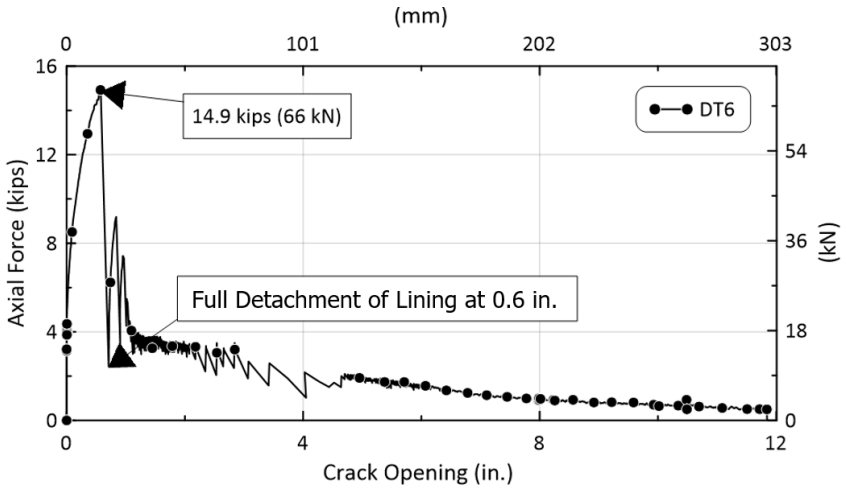

Figure 3.26. Axial Force versus Crack Opening for DT6 Specimen

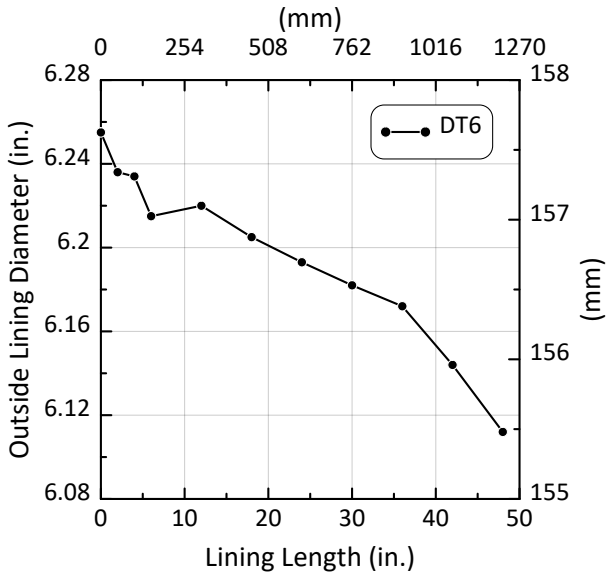

Figure 3.27. Average Outer Lining Diameter along the South Section of DT6

outside diameter of the lining was measured and plotted along the length of the lining. The diameter was measured from the center of the test specimen at zero to near the end of the lining at 48 in. (1219 mm). As can be observed in Figure 3.27., the lining diameter decreases in the direction that the north pipe section was displaced across the test specimen. Thus, a larger pipe section diameter was pulled across a progressively smaller lining diameter, resulting in decreasing axial load similar to the response of DT2.

3.1.7. DT7

As indicated in Table 3.1, DT7 was performed with a 16-ft (4.57 m)-long specimen in the large load frame. It was tested with 80 psi (550 kPa) internal pressure at a sampling rate of 50 Hz. The test included debonding from the Aqua-Pipe lining and pipe displacement along the debonded lining.

Table 3.8 provides a list of the instrumentation used in DT7. The instrumentation for DT7 involved strain gages applied at nine different locations both south and north of the crack at the center of the test pipe. Longitudinal strain gages at the crown and invert were established at every location from 2 in. (51 mm) to 36 in. (914 mm) south and north of the gap. Circumferential strain gages at the crown and invert were positioned at 4 in. (102 mm) and 24 in. (610 mm) south and north of the center of the pipe. Only longitudinal gages at the crown were placed at a distance further than 36 in. (914 mm) from the crack. Horizontal string pots were located at four different locations to measure opening of the center gap as well as any slip of the restraints. Pressure transducers were at the end cap and the source on the deck to measure the internal pressure during the test.

Figure 3.28. (a) and (b) show photographs of the DT7 test specimen. The test specimen has visible rust and pitting typical of a field specimen. Figure 3.28. (a) shows the pipe at the beginning of the test. Figure 3.28. (b) shows the specimen at the end of the test, including displacement in both the north and south directions from the initial crack location. During this test, the Aqua-Pipe lining debonded completely to the north, and then the north CI pipe was pulled over the Aqua-Pipe lining to remove it from the lining.

Figure 3.29. shows a plot of internal pipe pressure versus actuator displacement. Throughout the test, the pipe pressure was maintained with some fluctuation at 80 psi (551 kPa). This test differed from DT5 and DT6 where the pipe was pulled from the lining under diminished or near zero pressure. In DT7, axial movement of the pipe relative to the lining occurred under 80 psi (551 kPa) for the entire test.

Figure 3.30. shows the actuator displacement and crack opening versus time. They recorded similar displacements until 30 minutes into the test, at which point the string pots reached their maximum travel. During the test, most of the crack opening developed as a result of the north section of the pipe debonding from the lining. Some debonding, however, occurred in the south

Table 3.8. Instrumentation List for DT7

Location	Instrument Description	Local Instrument Name
72 in. South of Centerline	Crown, Axial Strain	-72C
60 in. South of Centerline	Crown, Axial Strain	-60C
48 in. South of Centerline	Crown, Axial Strain	-48C
36 in. South of Centerline	Crown, Axial Strain	-36C
	Invert, Axial Strain	-36I
24 in. South of Centerline	Crown, Axial Strain	-24C
	Crown, Circumferential Strain	-24CC
	Invert, Axial Strain	-24I
	Invert, Circumferential Strain	-24IC
12 in. South of Centerline	Crown, Axial Strain	-12C
	Invert, Axial Strain	-12I
8 in. South of Centerline	Crown, Axial Strain	-8C
	Invert, Axial Strain	-8I
4 in. South of Centerline	Crown, Axial Strain	-4C
	Crown, Circumferential Strain	-4CC
	Invert, Axial Strain	-4I
	Invert, Circumferential Strain	-4IC
2 in. South of Centerline	Crown, Axial Strain	-2C
	Invert, Axial Strain	-2I
2 in. North of Centerline	Crown, Axial Strain	2C
	Invert, Axial Strain	2I
4 in. North of Centerline	Crown, Axial Strain	4C
	Crown, Circumferential Strain	4CC
	Invert, Axial Strain	4I
	Invert, Circumferential Strain	4IC
8 in. North of Centerline	Crown, Axial Strain	8C
	Invert, Axial Strain	8I
12 in. North of Centerline	Crown, Axial Strain	12C
	Invert, Axial Strain	12I
24 in. North of Centerline	Crown, Axial Strain	24C
	Crown, Circumferential Strain	24CC
	Invert, Axial Strain	24I
	Invert, Circumferential Strain	24IC
36 in. North of Centerline	Crown, Axial Strain	36C
	Invert, Axial Strain	36I
48 in. North of Centerline	Crown, Axial Strain	48C
60 in. North of Centerline	Crown, Axial Strain	60C
72 in. North of Centerline	Crown, Axial Strain	72C
Centerline	Horizontal String Pot	HSP_East
		HSP_West
Restraining Collars, North of Centerline		North Slip
Location	Instrument Description	Local Instrument Name

Table 3.8. Instrumentation List for DT7

Restraining Collars, South of Centerline	Horizontal String Pot	South Slip
End Cap	Pressure Transducer	Pressure_Input
Water Hose		Pressure_Deck
Actuator, South of Centerline	Actuator Displacement	LSA1-Disp

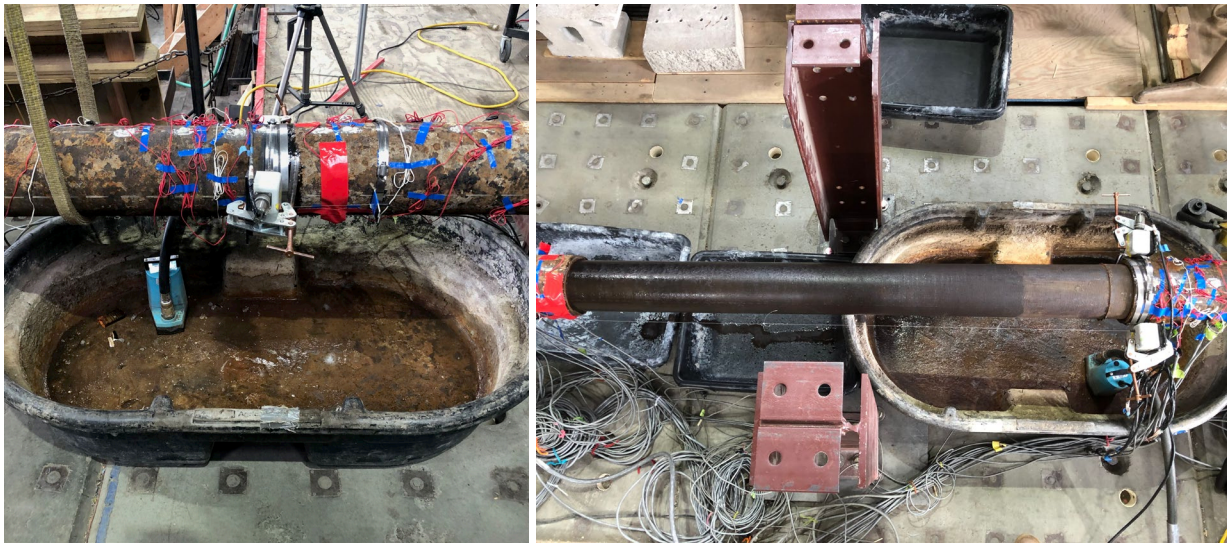

(a) Specimen in Load Frame before Test (b) Specimen at the End of Direct Tension Test

Figure 3.28. DT7 Test Specimen before and after Direct Tension Test

section of the pipe. At approximately 12 in. (305 mm) of actuator displacement, the lining included 2.7 in. (69 mm) of displacement from the south section of pipe.

Figure 3.31. shows the axial force versus actuator displacement. The north pipe section debonded from the lining. At approximately 12 in. (305 mm) of actuator displacement, the lining detached from the end of the north pipe. The force rapidly decreased to 6.5 kips (30 kN), as shown in the figure. At full debonding of the north pipe section, the north and south pipes had been pulled 9.3 in. (236 mm) and 2.7 in. (69 mm), respectively, from the lining.

Strain gage data were analyzed in a manner similar to that applied for DT2 and DT4 through DT6 to determine the location of the debonding front versus axial displacement from the north pipe section. The actual displacement of the north pipe section was determined by subtracting the south

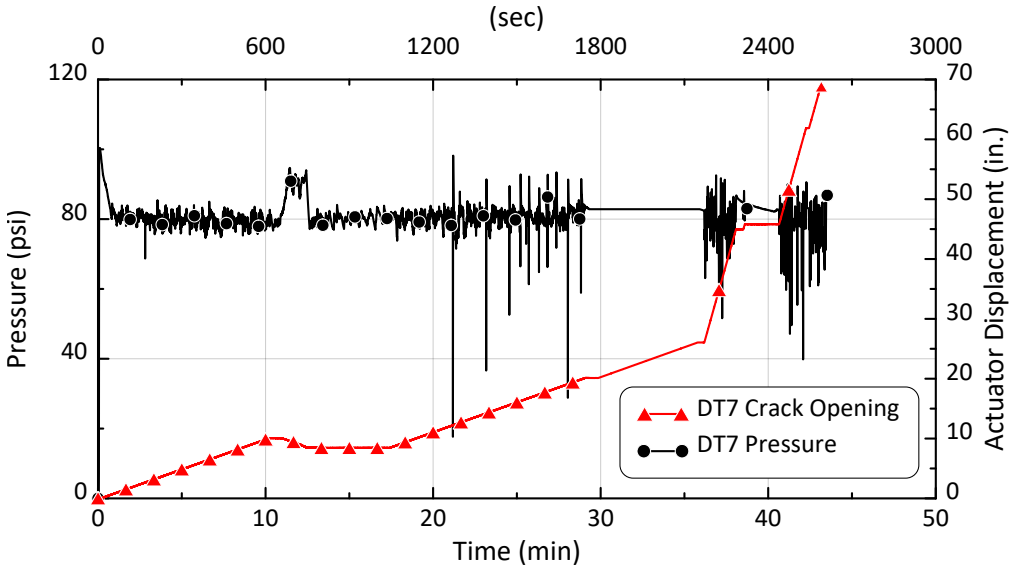

Figure 3.29. Pressure and Actuator Displacement versus Time for DT7

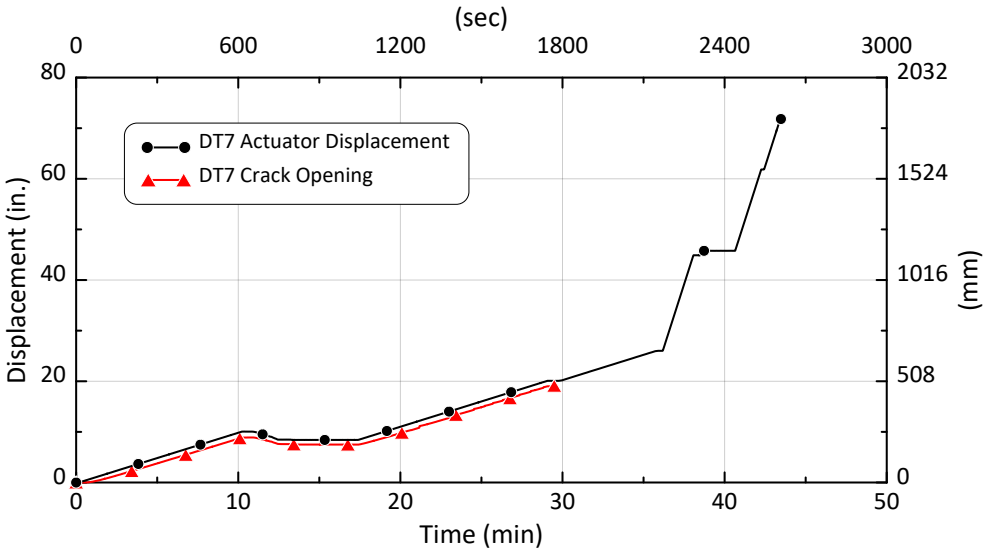

Figure 3.30. Actuator Displacement and Crack Opening versus Time for DT7

pipe section displacement from the actuator displacement. As shown in Figure 3.32., the debonding front propagated rapidly through the north section of pipe to 84 in. (2134 mm) at a north pipe displacement of 3.2 in. (81 mm). The increase in debonding length after 84 in. (2134 mm) is

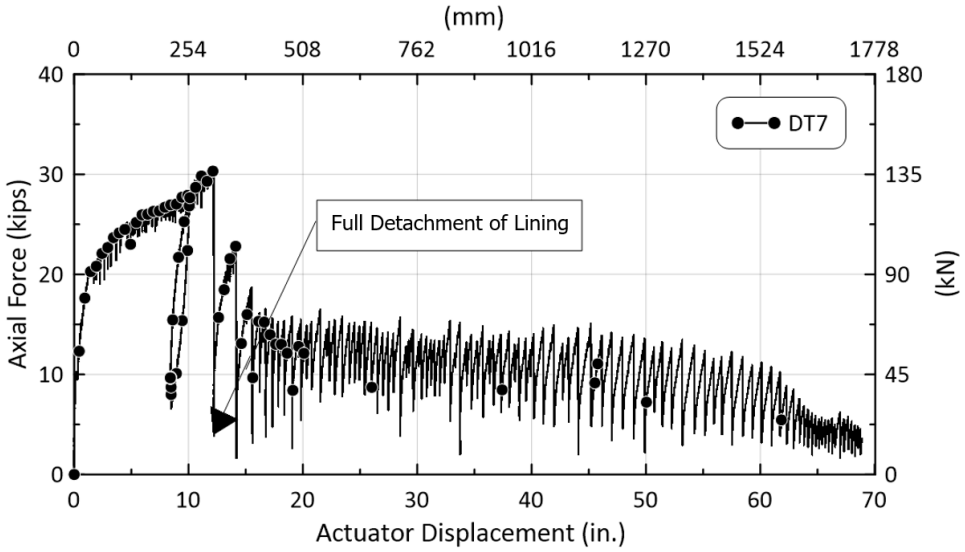

Figure 3.31. Axial Force versus Actuator Displacement for DT7

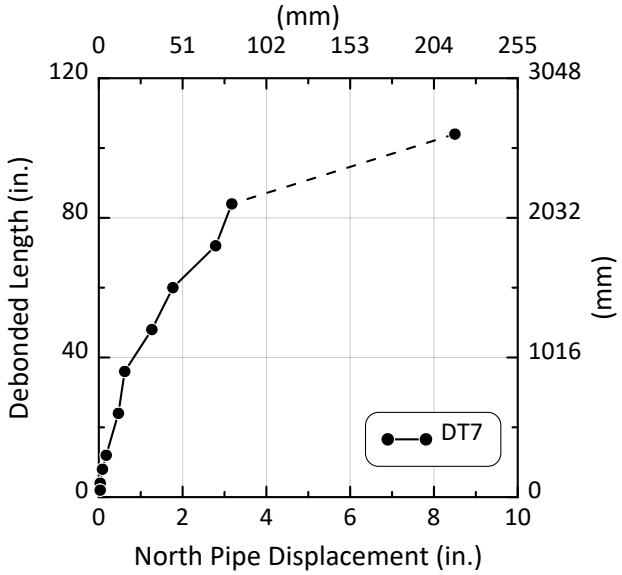

Figure 3.32. Debonding Length versus North Pipe Displacement for DT7

presented as a dashed line to indicate that there is uncertainty about the relationship between debonded length and north pipe section displacement from 84 to 104 in. (2134 to 2642 mm).

The actuator displacement was corrected to provide only the axial movement of the north pipe section after completion of debonding. Figure 3.33. is a plot of the axial force with respect to displacement of the north section of pipe after debonding occurred. After debonding there was no additional south pipe displacement and the maximum axial force remained around 14 kips (62 kN) until approximately 41 in. (1041 mm) of north pipe displacement. Then the maximum axial force decreased until a north pipe displacement of 66 in. (1676 mm).

Following the procedures developed for DT2, DT4, DT5, and DT6, the average outside diameter of the lining was measured and plotted along the length of the lining as shown in Figure 3.34. The diameter was measured from the center of the test specimen at zero to near the end of the lining at 102 in. (2591 mm). At approximately 42 in. (1067 mm) from the center, the lining diameter peaks and begins to decrease. After a pipe displacement of 42 in. (1067 mm), a larger pipe diameter section moved over a lining with progressively smaller diameters. This agrees with the decrease in axial force after 41 in. (1041 mm) of north pipe displacement seen in Figure 3.31.

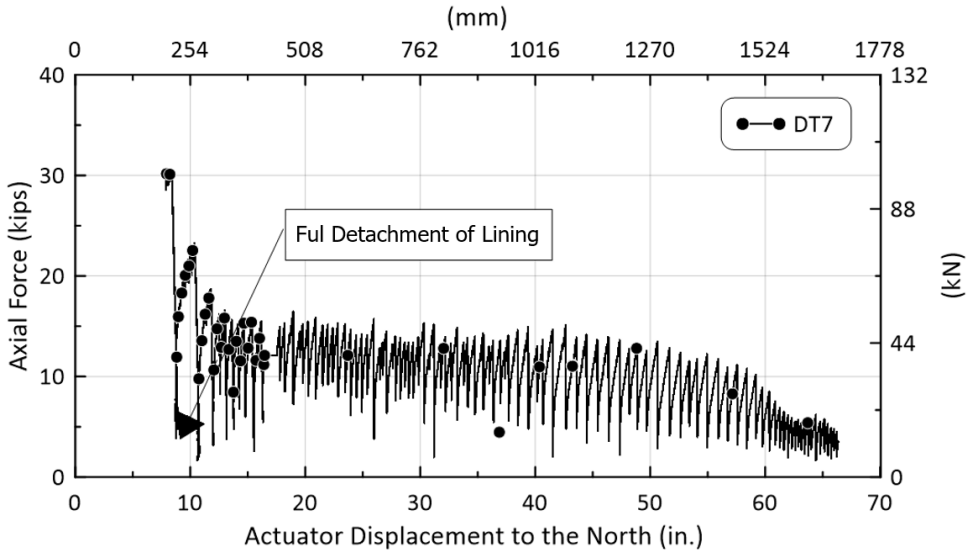

Figure 3.33. Axial Force versus North Pipe Displacement after Debonding for DT7

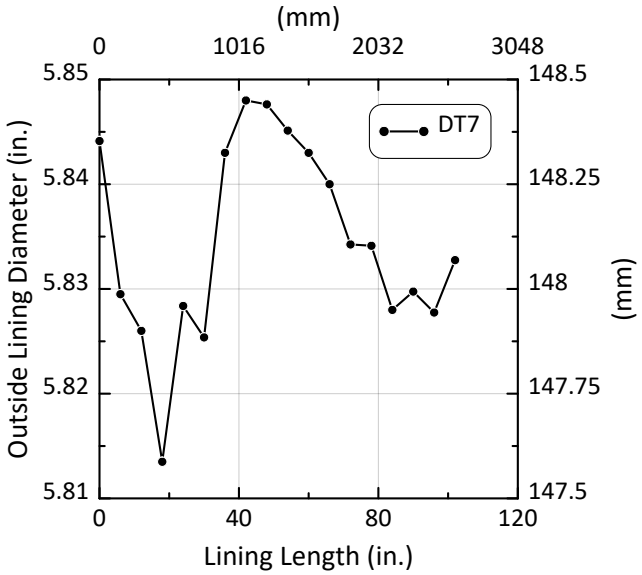

Figure 3.34. Average Diameter versus North Pipe Section Length for the DT7 Specimen

3.6 Summary

The direct tension test results allow for a comprehensive assessment of axial force versus relative displacement between the Aqua-Pipe lining and both the CI and the DI host pipes. The mobilization of axial force is affected by fracture propagation, friction between the exterior surface of the lining and interior surface of the host pipe, and geometric resistance generated by relative movement of the lining within a pipe of variable inside diameter. The tests show that the initial load response to pipeline extension is dominated by a rapid rise in axial force as debonding between the lining and host pipe occurs. Previous research (Argyrou et al., 2018) has shown that the rapid rise in initial axial force can be modeled as a Type II fracture between the lining and inside pipe surface. The direct tension test results in this study show that the debonding force is followed by both frictional and geometric interference forces.

An important finding from the direct tension tests is that substantial additional axial forces may be mobilized after debonding from geometric interference caused by lining movement through a pipe with variable internal diameter. The test results provide a first-time confirmation of this loading

mechanism. Moreover, the test results show that geometric resistance caused by variable inside pipe diameter may be the dominant and controlling failure mechanism, depending on how the internal pipe diameter varies with distance along the pipeline.

Another important finding is the debonding load required to overcome lining-pipe adhesion. The initiation of crack propagation between the lining and new, unaged DI pipe in DT1, DT2 and DT4 was approximately 28 kips (127 kN) at zero internal pressure. In contrast, the load required to debond the lining from old CI pipe removed from the field in DT5 and DT6 was approximately 15 kips (68 kN) at an internal pressure of 80 psi (551 kPa).

After debonding, the axial force related to geometric conditions may result in decreasing or increasing loads. Because the lining is cast and cured inside the host pipe, the outside diameter of the lining is the inside diameter of the pipe. As slip between the pipe and debonded lining occur, the lining will move relative to a pipe with decreasing or increasing diameter. If the lining diameter decreases in the direction of relative movement, the axial load will decrease, and geometric interference will not control failure. If the lining diameter increases in the direction of relative movement, the axial load will increase, and geometric interference may control failure.

DT2 and DT6 involve pipe movement in the direction of decreasing lining diameter, and the test results show low axial loads after debonding, followed by diminishing load with additional relative slip. In contrast, DT4, DT5, and DT7 involve pipe movement in the direction of increasing lining diameter, and the test results after debonding show increasing axial load with additional relative slip.

Figure 3.35. compares the axial force versus displacement plots of DT4, DT5, and DT7. Increasing axial loads were accompanied by tension-induced reductions in lining diameter that caused the lining to lurch forward until firm contact with the pipe was reinstated. Subsequent axial movement was accompanied by increased axial load until the next load cycle was initiated. During each load cycle, there was an audible pop or boom that accompanied the abrupt relative displacement between the lining and the pipe.

The test results show a complex interaction involving the pipe and lining geometry, friction between the lining and pipe, and internal pressure. After debonding, DT4 and DT5 were performed at zero internal pressure. The highest maximum force after debonding was recorded in DT5. A larger change in pipe and lining diameter over distance was measured in DT5 than in DT4. DT7

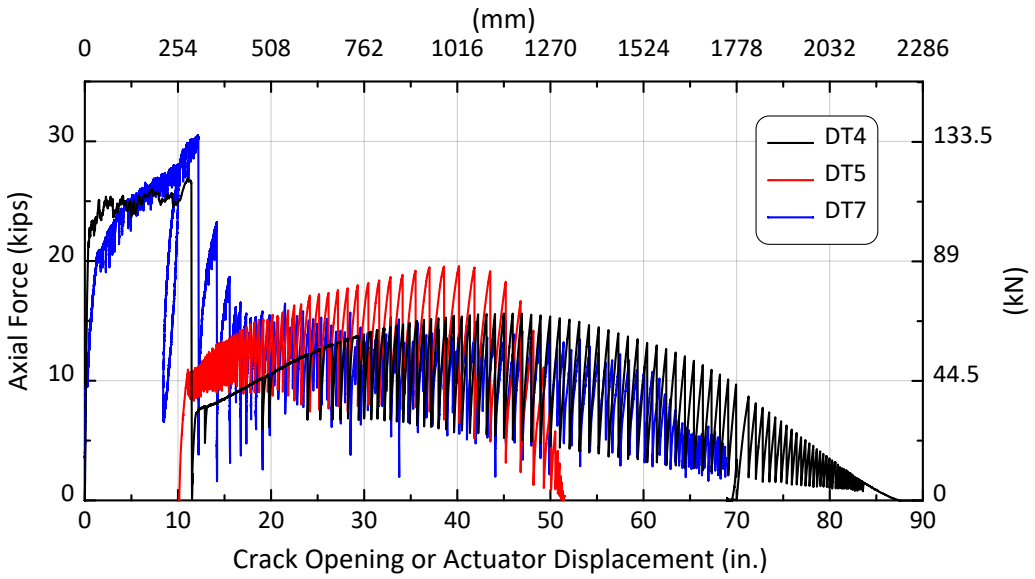

Figure 3.35. Axial Force versus Crack Opening or Actuator Displacement for DT4, DT5, and DT7

was performed with the smallest change in pipe and lining diameter over distance. Although DT7 was performed under a pressure of 80 psi (551 kPa), it nonetheless shows the lowest axial load after debonding, which is apparently related to a smaller change of diameter over distance compared with that of the DT4 and DT5 specimens.

To learn more about the relationship among axial force, internal lining pressure, and relative axial displacement, special friction tests were performed. These tests and their results are covered in the next section.

Section 4
Friction Tests

4.1. Introduction

This section summarizes the results of special tests referred to as friction tests. These tests were designed to evaluate the influence of loading rate and internal lining pressure on the axial resistance to relative movement between the host pipe and an AP1 lining. Friction tests were performed on the lining of the DT4 test specimen. The friction test specimen and test setup were configured from the DT4 specimen and modifications of the DT4 loading system.

4.2. Friction Test Setup

A plan view of the friction test setup is presented in Figure 4.1., and photographs of the setup are provided in Figure 4.2. and Figure 4.3. Two load frames, consisting of steel plates attached to steel columns bolted to concrete bearing blocks, were separated by 112.3 in. (2853 mm) center to center. The load frames supported and anchored the test pipes and Aqua-Pipe lining. Figure 4.2. shows the test setup with the north and south load frames. Due to the high cyclic loads experienced during friction tests at relatively high internal lining pressure, the north and south load frames were stiffened and strengthened by inclined chains that were tensioned to resist axial loads developed on the 24-in. (610 mm)-long section of pipe as it was pulled in a northward direction along the lining.

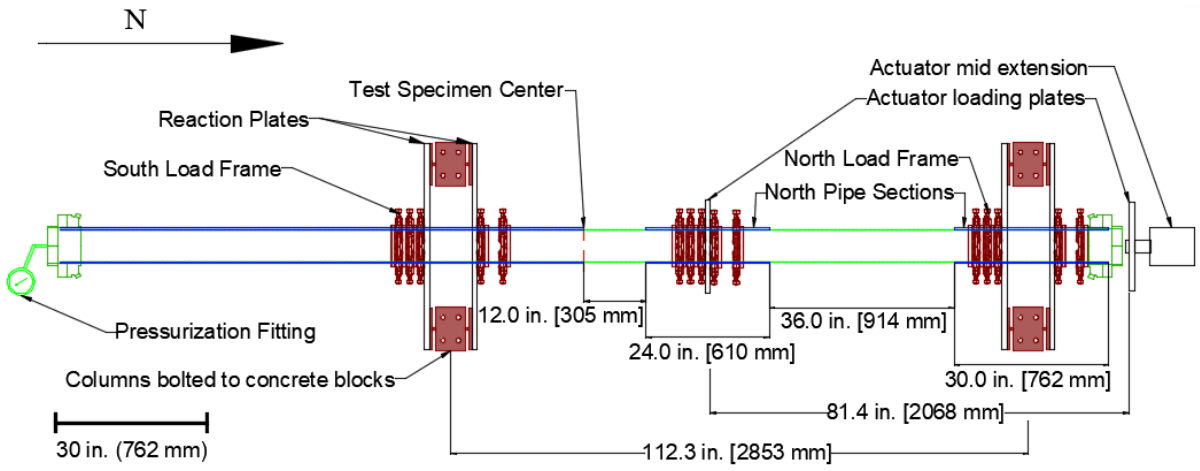

Figure 4.1. Plan View of Friction Test Setup

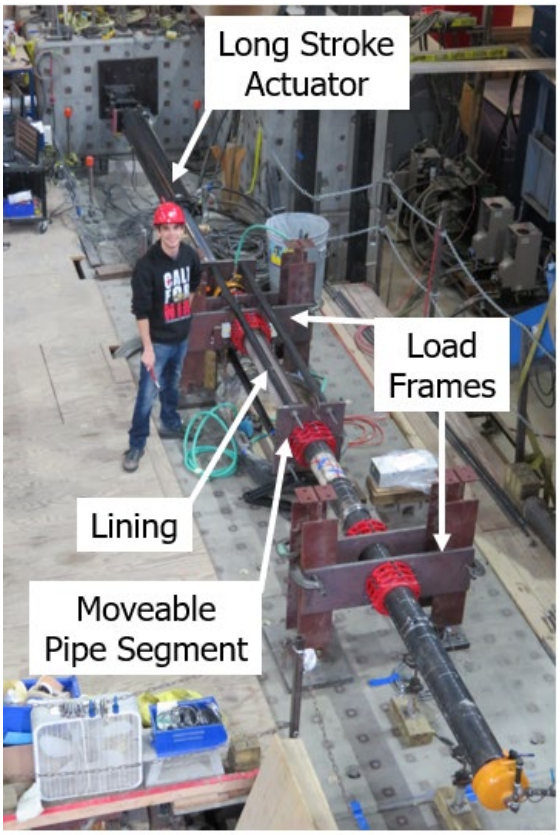

Figure 4.2. Photograph of Friction Test Setup (Facing North)

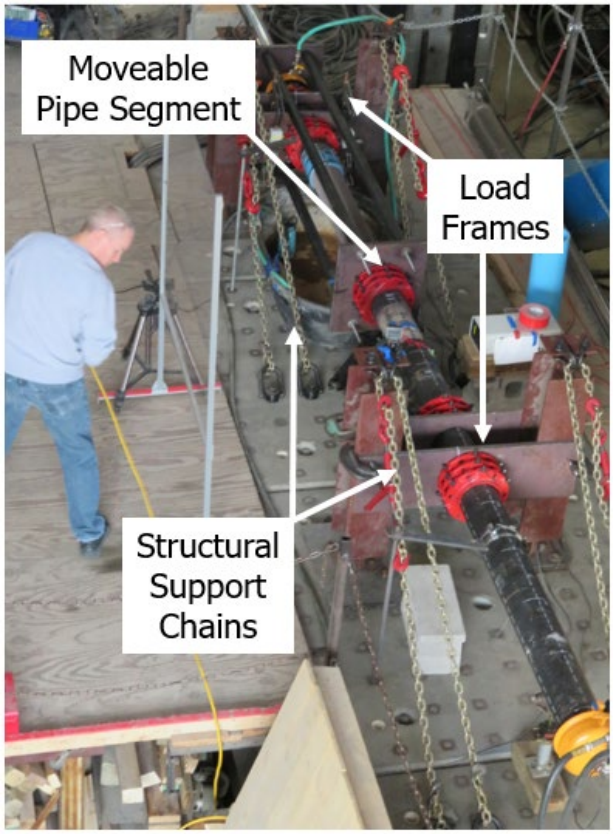

Figure 4.3. Photograph of Friction Test Setup with Structural Support Chains (Facing North)

The friction tests were performed after DT4 was completed. To set up for testing, the north section of pipe was pulled from the Aqua-Pipe lining. The 102-in. (2591 mm)-long south section of the DT4 pipe and lining was fixed to the south load frame by means of restraining collars clamped to the pipes on either side of the load frame. This arrangement is shown in the left side of Figure 4.1. The north load frame is located on the right (north) side of Figure 4.1. A 30-in. (762 mm)-long section of pipe and lining was fixed to the north load frame by restraining collars as shown in Figure 4.1. A 24-in. (610 mm)-long section of pipe was pulled from the south side of the exposed lining to the north load frame by means of steel rods connected to the restraining collars that were, in turn, attached to the mobile length of steel pipe. The steel rods were attached to the long stroke actuator on the north side of the north load frame. Although the full actuator and steel rods are not shown in Figure 4.1., they can be seen in Figure 4.2 .and Figure 4.3.

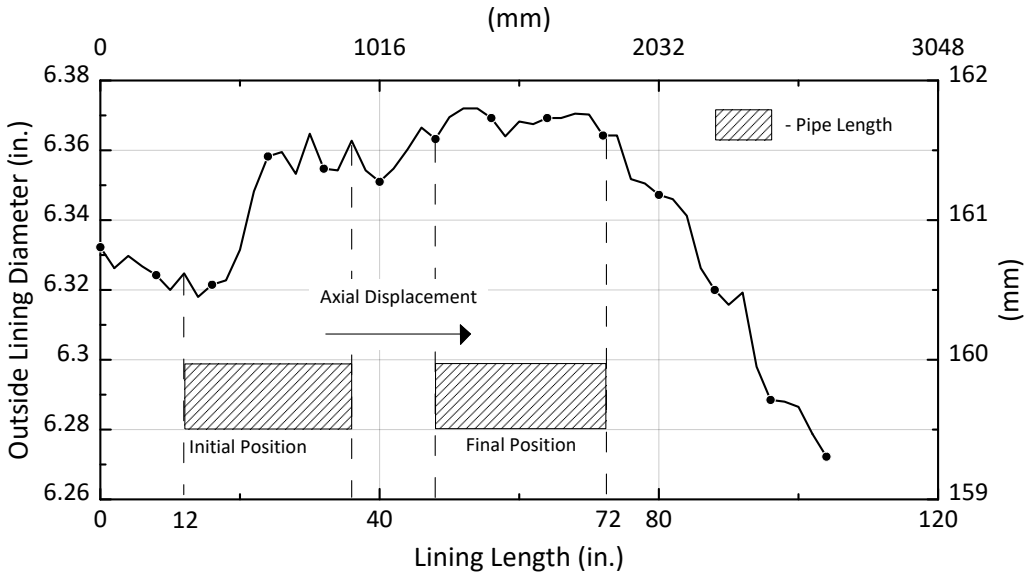

Figure 4.4. DT4 Specimen Outside Lining Diameter versus Lining Length

Each friction test was performed from an initial position where the leading side of the 24-in. (610 mm)-long section of pipe was located 36 in. (914 mm) north of the DT4 specimen center. The pipe was then pulled along the lining 36 in. (914 mm) until contact with the north section of pipe. The moveable pipe section was then reset by pushing it under zero lining pressure back to its initial position. Figure 4.4. shows the movement of the 24-in. (610 mm)-long pipe section on the plot of the DT4 lining diameter versus distance along the lining. As the pipe was pulled in the northward direction, it moved onto a lining that increased in diameter from 6.318 in. (160.5 mm) to 6.372 in. (161.9 mm) as shown in the figure.

The friction tests were performed under different loading rates corresponding to different rates of axial movement. They were also performed under different lining pressures. The pipe and lining system was sealed with end caps and pressurized through the fitting attached to the south end cap as shown in Figure 4.1.

4.3. Test Instrumentation

Axial and circumferential strain gages were located on the exterior surface of the pipe specimen at 6 in. (152 mm) from the gap at the center of the specimen. Horizontal string pots were used to measure displacement of the pipe as well as slip of the restraints. A list of the instrumentation used during the tests is presented in Table 4.1.

Table 4.1. Instrumentation List for Friction Tests

Location	Instrument Description	Local Instrument Name
6 in. North of Centerline	Crown, Axial Strain	6C
	Crown, Circumferential Strain	6CC
Actuator	Horizontal String Pot	HSP_Act_BU
Centerline		HSP_East
		HSP_West
Restraining Collars, North of Centerline	Horizontal String Pot	North Slip
Restraining Collars, South of Centerline		South Slip
End Cap	Pressure Transducer	Pres_Pipe
Deck		Press_Input
Centerline	Laser Extensometer	Laser_ext_5in
Actuator, South of Centerline	Actuator Displacement	LSA1-Disp

4.4. Effects of Repeated Loading

Figure 4.5 presents the results of two friction tests performed under zero internal lining pressure. The axial force versus pipe displacement are shown side by side for the first friction test (FT1) and a subsequent test (FT5) performed after intervening tests. The two tests were performed under identical conditions at a displacement rate of 1 in. (25 mm) per minute. Similar to the results of DT4 and DT5, during which a section of pipe was pulled along a lining of increasing diameter, the same cyclic loading phenomenon was observed with an audible pop or boom during each cycle. The loading cycles are shown in the figure.

The first test, FT1, shows a higher 20-point moving average axial force at all displacements above 10 in. (252 mm) than for the subsequent test, FT5. The FT1 axial force is on average about 25% higher than the FT5 maximum force between displacements of 15 in. (381 mm) and 30 in. (762 mm). The axial force in both specimens was approximately the same until slightly greater than 10 in. (252 mm) of axial movement was measured during the tests.

The reason for the higher force in FT1 is related to the roughness of the outside surface of the lining, which was more pronounced in the first test compared with subsequent tests.

Repeated axial displacement during each friction test resulted in a smoother lining surface with lower frictional resistance compared to the initial test. Resistance to axial movement converged after the first test to steady state, repetitive values. Additional tests run at the same pressure did not show significant differences in axial force versus actuator displacement.

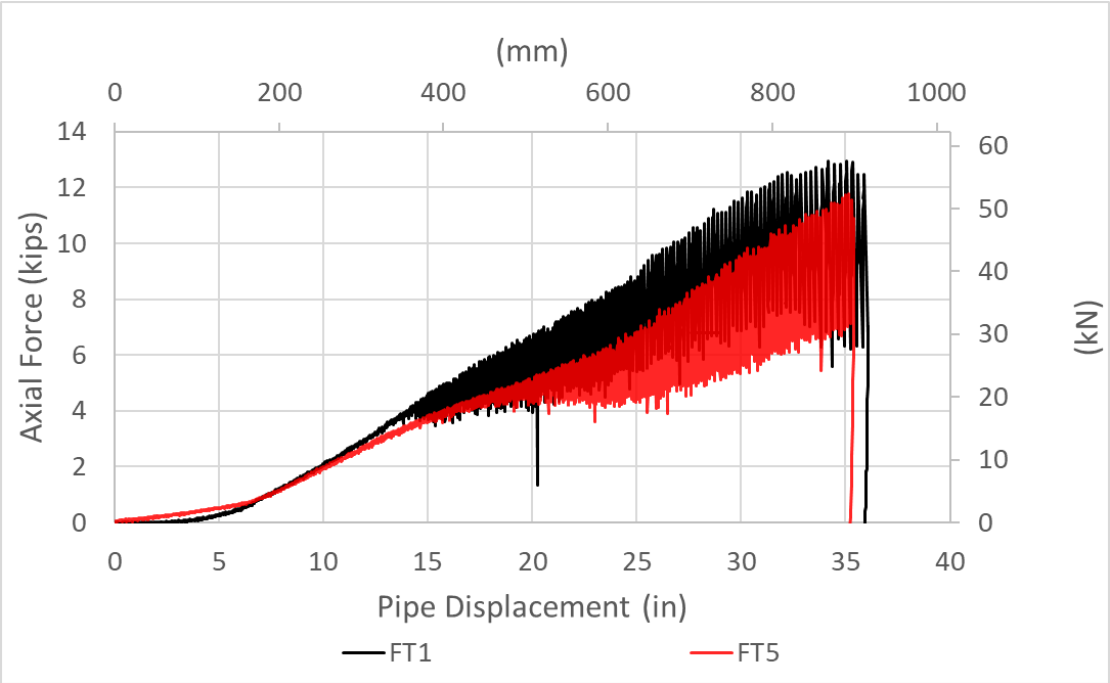

Figure 4.5. Axial Force versus Pipe Displacement for the Initial Friction Test (FT1) and a Subsequent Friction Test (FT5)

4.5 Load Rate Effects

Figure 4.6 compares the axial load versus pipe displacement plots for three friction tests at zero lining pressure and three different rates of displacements of 1 in. (25 mm) per minute, 10 in. (250 mm) per minute, and 100 in. (2500 mm) per minute. The results of the three tests are nearly identical. For each test, both the maximum force and cyclic loading range follow closely the same load versus displacement relationship.

To filter dynamic effects, the load rate database of Figure 4.6 was evaluated using ten and twenty point moving averages of the data. Figure 4.7 provides a comparison of the twenty point moving average axial force versus the pipe displacement response at zero pressure for different loading rates. The results in this figure are similar to those for the ten point moving averages.

These results show that axial load versus displacement performances is not influenced by the loading rate. The load response remains unchanged over two orders of magnitude in displacement rate. Showing the independence of load response to the rate of loading displacement eliminates an

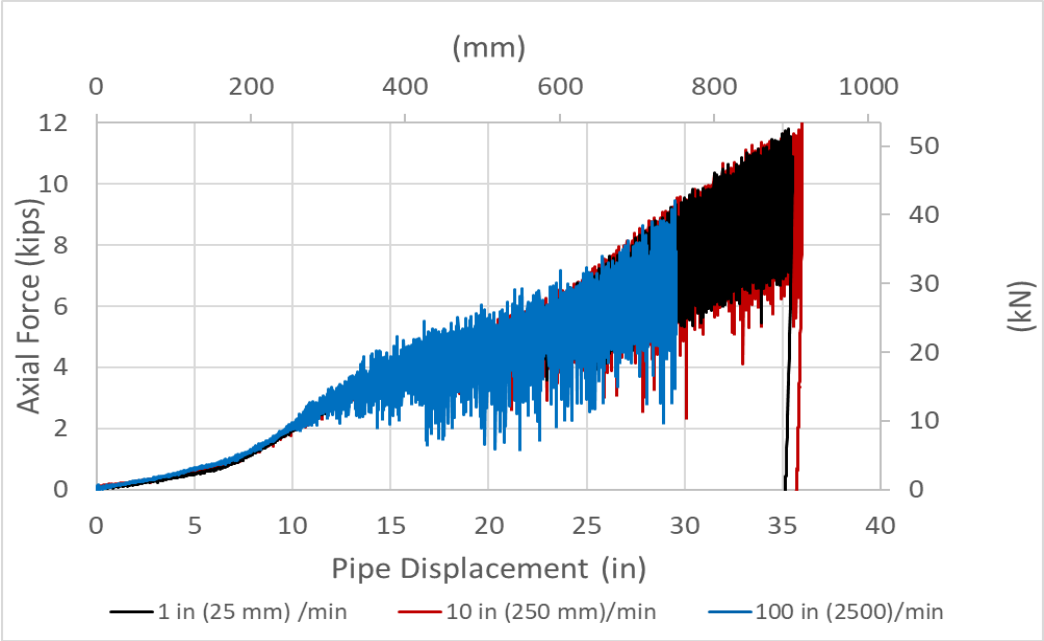

Figure 4.6. Comparison of Axial Force versus Pipe Displacement Response at Zero Pressure for Different Loading Rates

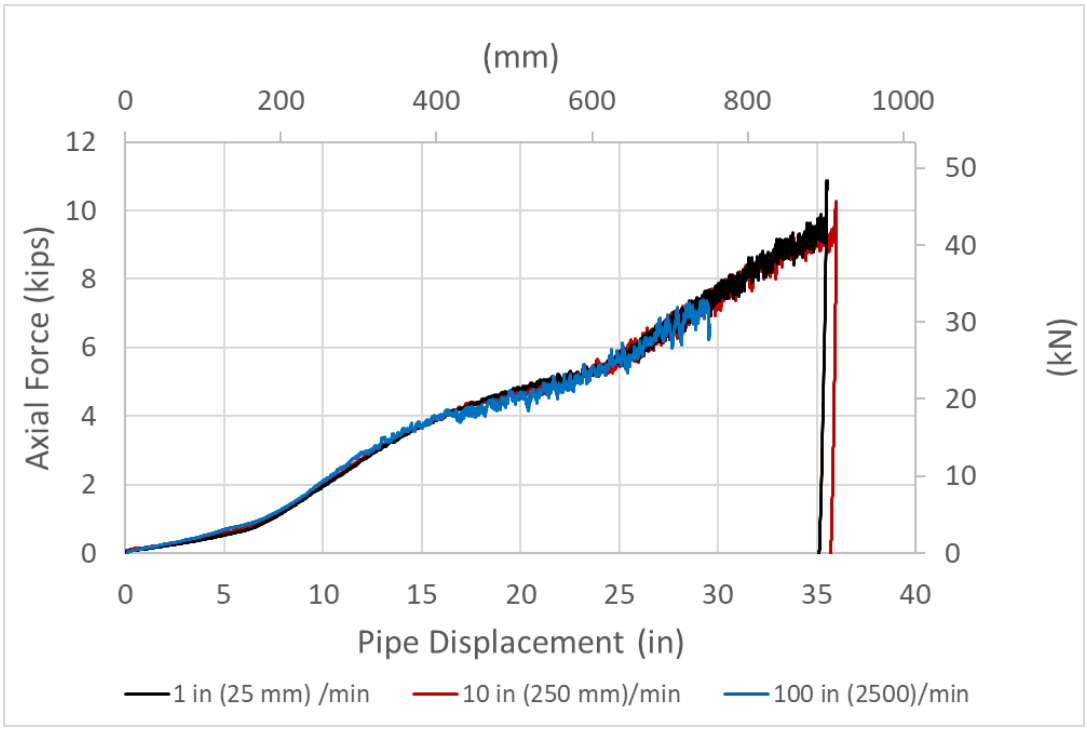

Figure 4.7 Comparison of Twenty Point Moving Average Axial Force versus Pipe Displacement Response at Zero Pressure for Different Loading Rates

an important variable, and simplifies both the experimental conditions for relevant testing as well as the characterization of ground deformation effects on cured in place pipe behavior.

4.6 Internal Pressure Effects

Figure 4.8. presents the load versus pipe displacement plots at a constant loading rate of 10 in. (250 mm) per minute for nominal lining pressures of 0 psi, 25 psi (172 kPa), 50 psi (345 kPa), and 80 psi (551 kPa). There is a marked increase in axial force with increasing internal pressure at all levels of displacement.

To explore further the relationship between axial load and lining pressure, the pressures measured in each test are plotted with respect to pipe displacement in Figure 4.9. through Figure 4.11. Because of the cyclic loading and associated rapid changes in axial movement, it was difficult to maintain constant pressure. The trend in average pressures is plotted for each test, from which the pressure at any displacement can be identified and used to evaluate the relationship between peak axial load and internal lining pressure.

Figure 4.12 shows the peak axial load at 15 in. (381 mm) and 30 in. (762 mm) of pipe displacement plotted with respect to the internal lining pressure, both of which can be taken from Figure 4.9 through Figure 4.11. Given that the friction conditions and variation in lining diameter remain unchanged, the peak axial load at a given displacement should increase in direct proportion to the internal lining pressure at the same displacement. This is indeed the case.

Figure 4.12 shows a linear relationship between axial load and lining pressure with similar slopes at two different levels of displacement. The linear regression analyses show very high levels of R^2, which provides statistical support for the linear relationships.

4.7. Summary

The friction test results further define the force versus relative displacement relationship between the Aqua-Pipe lining and the host pipe first explored through the direct tension tests. Key findings include that the frictional resistance of the lining decreased after initial loading due to decreased surface roughness through repeated axial displacement between pipe and lining. When the

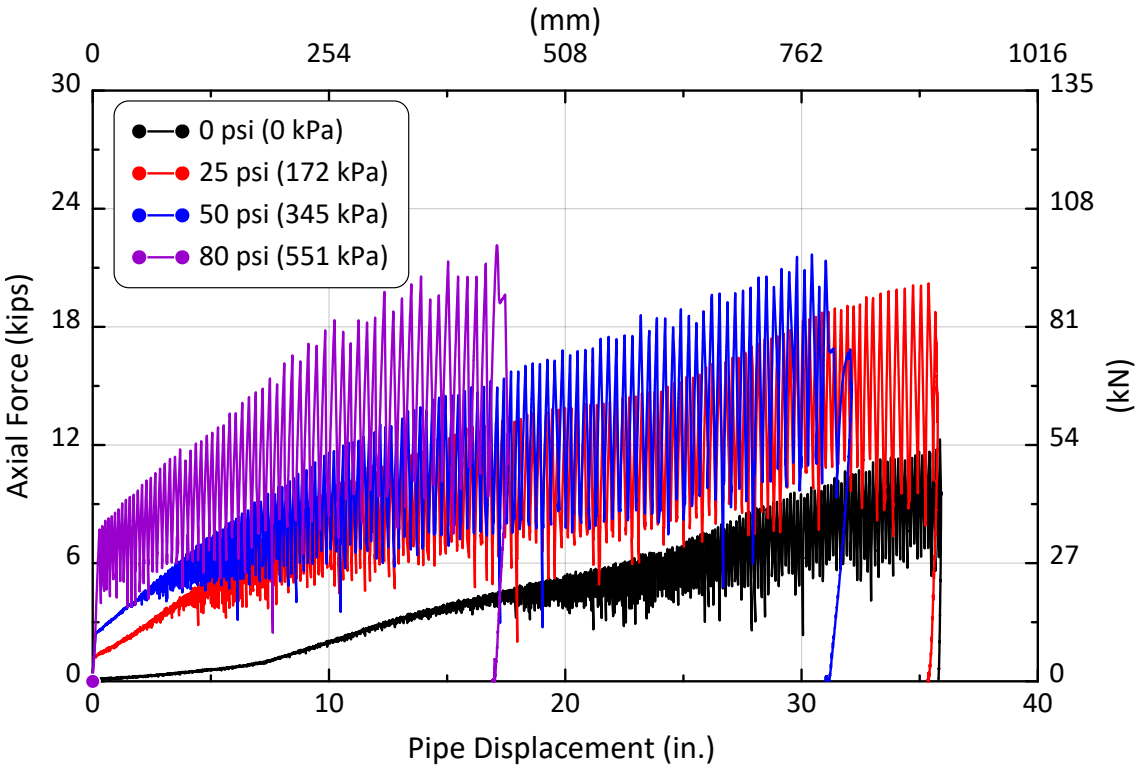

Figure 4.8. Load versus Pipe Displacement Response at Different Lining Pressures and Constant Load Rate

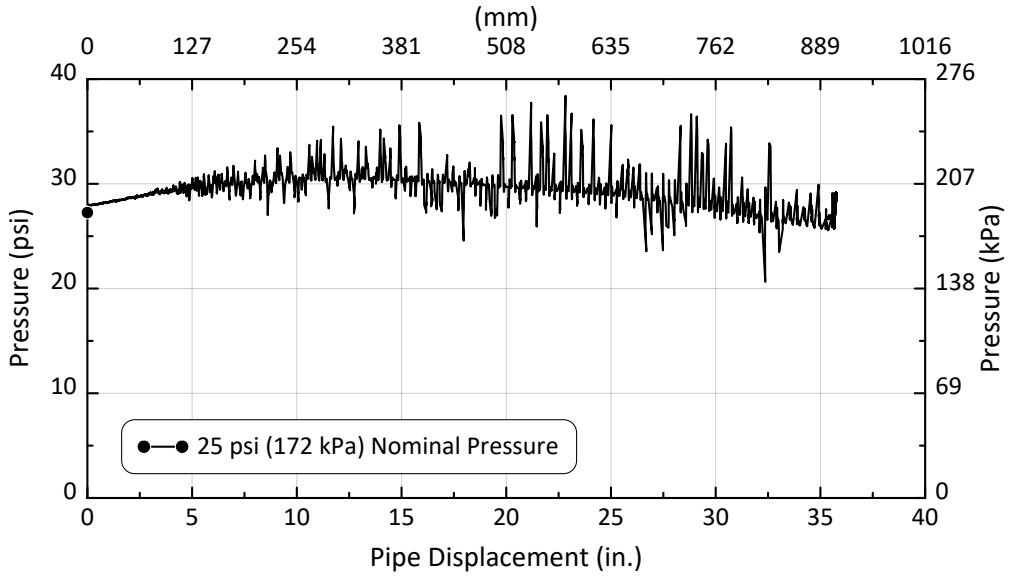

Figure 4.9. Lining Pressure versus Pipe Displacement for Nominal 25 psi (172 kPa) Pressure

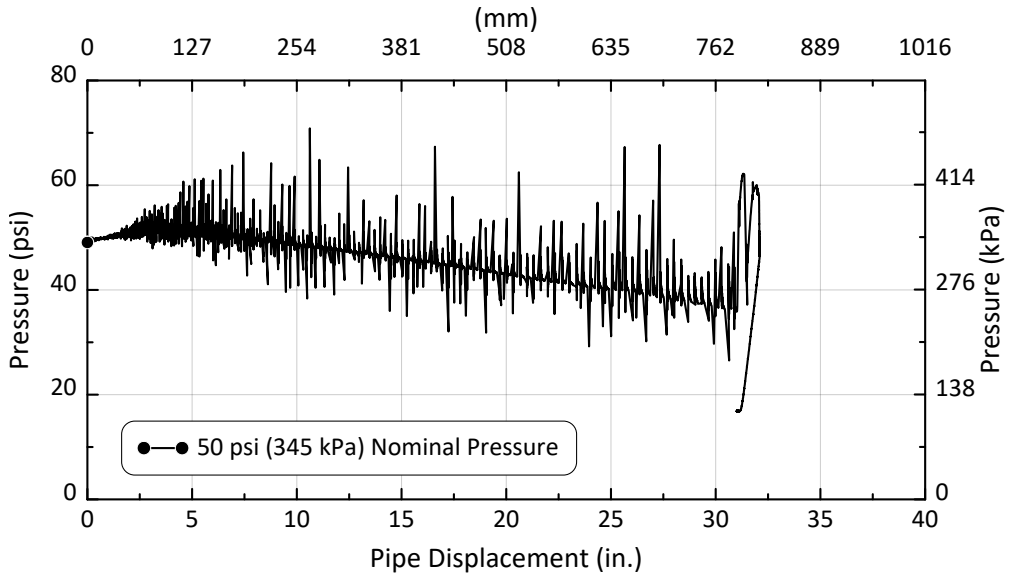

Figure 4.10. Lining Pressure versus Pipe Displacement for Nominal 50 psi (345 kPa) Pressure

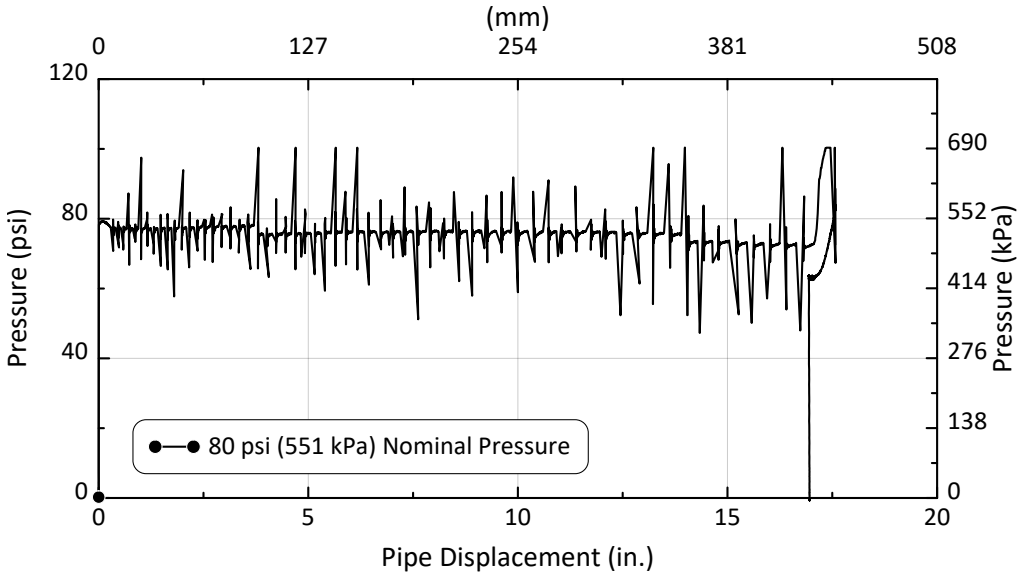

Figure 4.11. Lining Pressure versus Pipe Displacement for Nominal 80 psi (551 kPa) Pressure

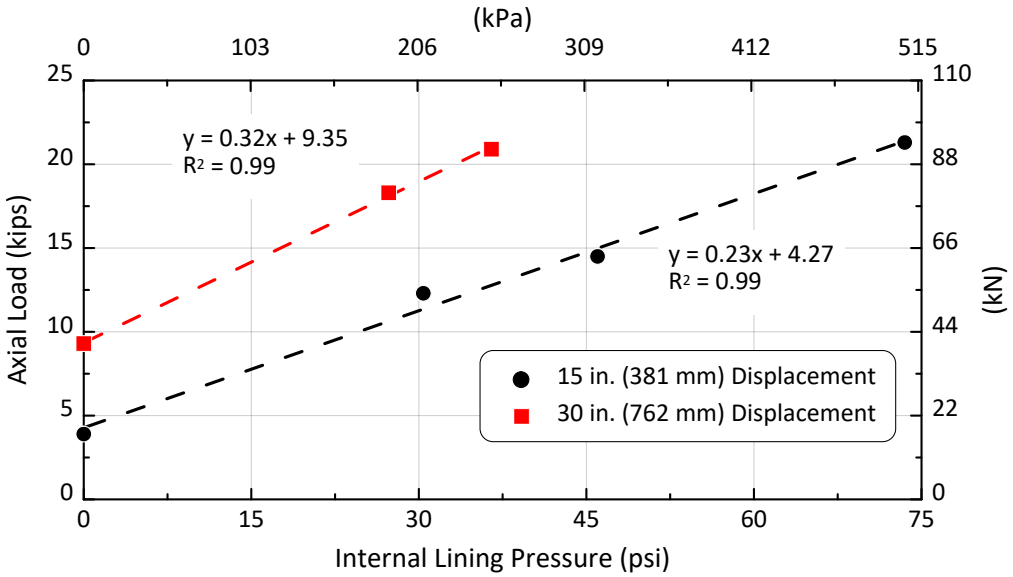

Figure 4.12. Axial Load versus Internal Lining Pressure for Different Pipe Displacements

specimen was loaded initially under zero pressure, the load response was higher due to greater surface roughness and frictional resistance. Subsequent tests exhibited a consistent, lower frictional resistance and axial load response than the first zero pressure test.

The friction tests show that the axial load response is independent of the loading rate. At varying loading rates, the axial loads experienced at each displacement were consistent in each test. The cyclic loading after debonding had a similar load range and maximum load for the tests conducted at 1 in. (25 mm)/min., 10 in. (250 mm)/min., and 100 in. (2500 mm)/min.

The most important result from the friction tests involves the influence of internal pressure on axial load response. As the internal pressure increased, the axial load for a given displacement increased linearly. Regressions of axial load versus internal pressure at the same levels of displacement show a clear linear relationship with similar slopes.

Section 5
Direct Shear Tests

5.1. Introduction

This section describes the direct shear test results for debonded AP1 lining and two variations in host pipe, involving new DI pipe and field CI pipe. As discussed under Subsection 3.3 Test Specimen Preparation, the new DI pipe had a clean interior surface with an interface between the lining and host pipe that initially was rough and irregular. In contrast, the interface between the host pipe and Aqua-Pipe lining in the CI field pipe samples was smooth, conspicuously lacking the initial roughness of the DI pipe. The CI field specimens were taken from pipe that Sanexen cleaned and installed with lining consistent with its field procedures.

The direct shear tests were performed to measure the shear forces required to slide the Aqua-Pipe lining along a debonded length of pipe under various loads normal to the sliding surface. The ratio of shear to normal force is the coefficient of friction, f, of the interface between pipe and lining. The normal force for each test was calculated from the weight applied across the curved sliding surface using the correction process explained in Appendix A.

5.2. Direct Shear Test Setup and Procedure

The direct shear tests were performed on an MTS 858 Bionix Test System. Figure 5.1 shows a schematic of the direct shear test setup including an actuator, pulley system, and test specimen. Figure 5.2 shows a photo of the setup with a weight of 25 lb (0.11 kN) applied across the sliding surface. The hydraulic actuator had a stroke of 6 in. (152 mm) and a capacity of 5.5 kips (24.5 kN). The load cell had a capacity of 2.2 kips (9.8 kN).

Pipe specimens from DT1 and DT5 were used to create test specimens for the direct shear tests. A 45-degree section of the 6 in. (152 mm) diameter lined pipe was cut as shown in Figure 5.3 (a). The section was cut so that the lining was in contact with the interior pipe surface at the location where it was cured in place during installation. The lining was then separated from the host pipe as shown in Figure 5.3 (b). The lining specimen was fixed to a wooden insert that was used to convey weights of various magnitude across the lining/pipe interface, as illustrated in Figure 5.2.

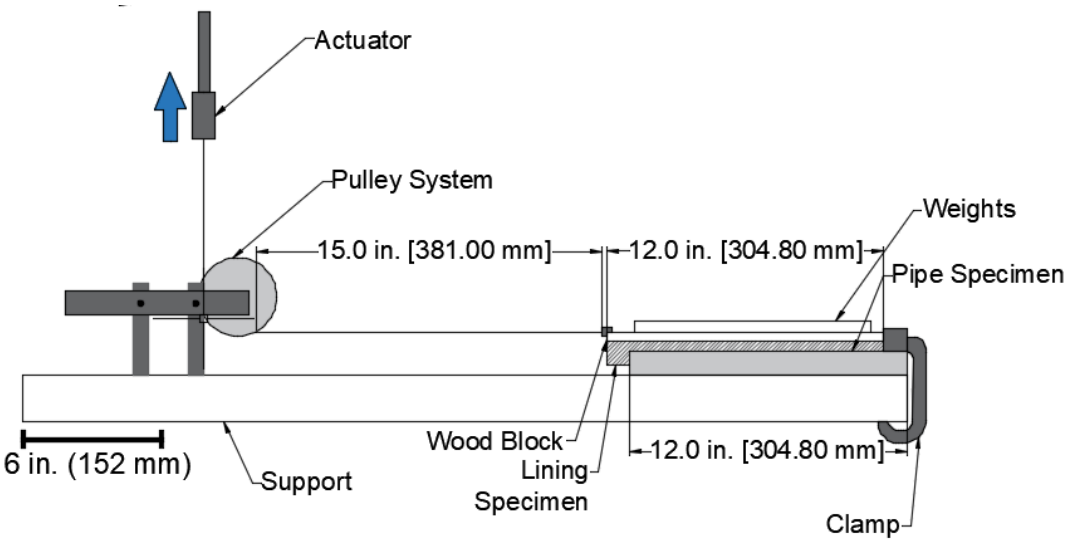

Figure 5.1. Schematic of Direct Shear Test Setup

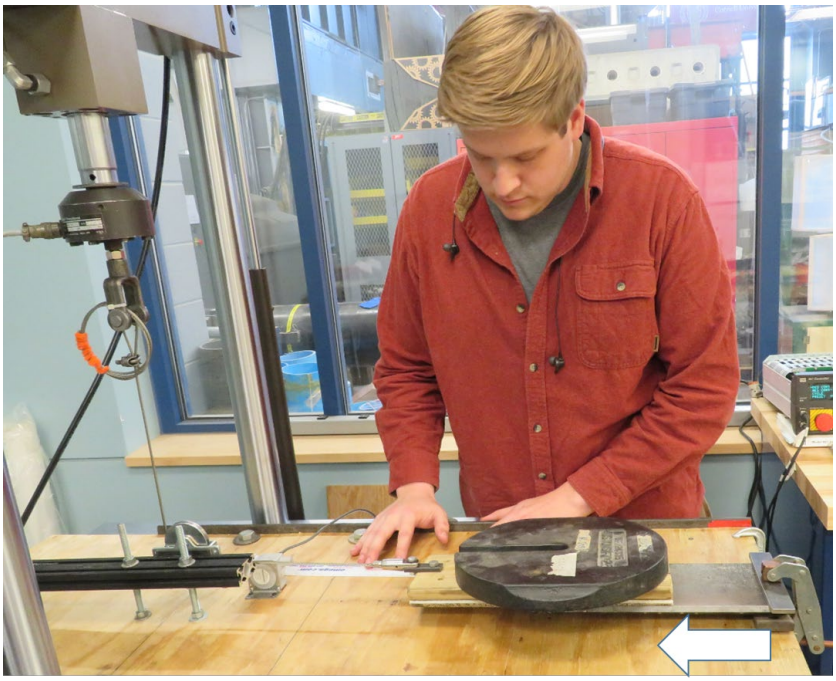

Figure 5.2. Photo of Aqua-Pipe Direct Shear Test Setup

To prepare for each test, the host pipe specimen was clamped to the table to prevent movement. The lining specimen fixed to the wooden block was attached to the pulley system and actuator. At the start of the test, the lining specimen was aligned with the clamp so that it was at its cured-in-

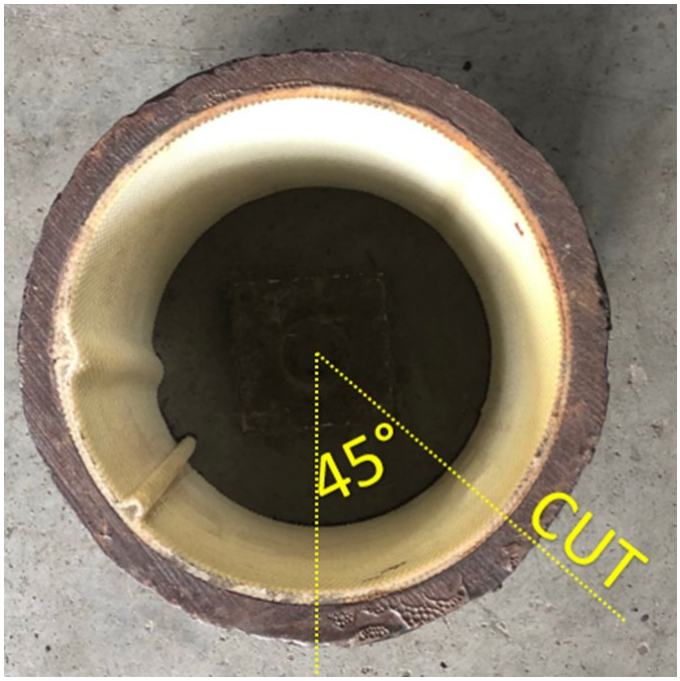

(a) Specimen before It Was Cut and the Lining and Host Pipe Separated

(b) View of Aqua-Pipe Lining and Pipe Specimen after Being Cut and Prepared

Figure 5.3. Photos of Aqua-Pipe Direct Shear Test Specimen

place location with maximum contact surface between the lining and host pipe. The lining specimen was pulled across the host pipe for a distance of 3 in. (76 mm) to 6 in. (152 mm) at a displacement rate of 10 in. (254 mm) per minute, consistent with the displacement rate used in several friction tests. This procedure was repeated for four loading conditions for both the new DI and field CI specimens.

5.3. Direct Shear Test Results

Figure 5.4 and Figure 5.5 show the shear force versus displacement for the new DI pipe and field CI pipe specimens, respectively, for weights of 50 lb (0.22 kN), 75 lb (0.33 kN), 100 lb (0.44 kN), and 200 lb (0.89 kN). The weights were converted to normal force following the procedure described in Appendix A. There was an overall downward trend in the shear force as the lining slid along the host pipe, reducing the contact between the lining and pipe surface.

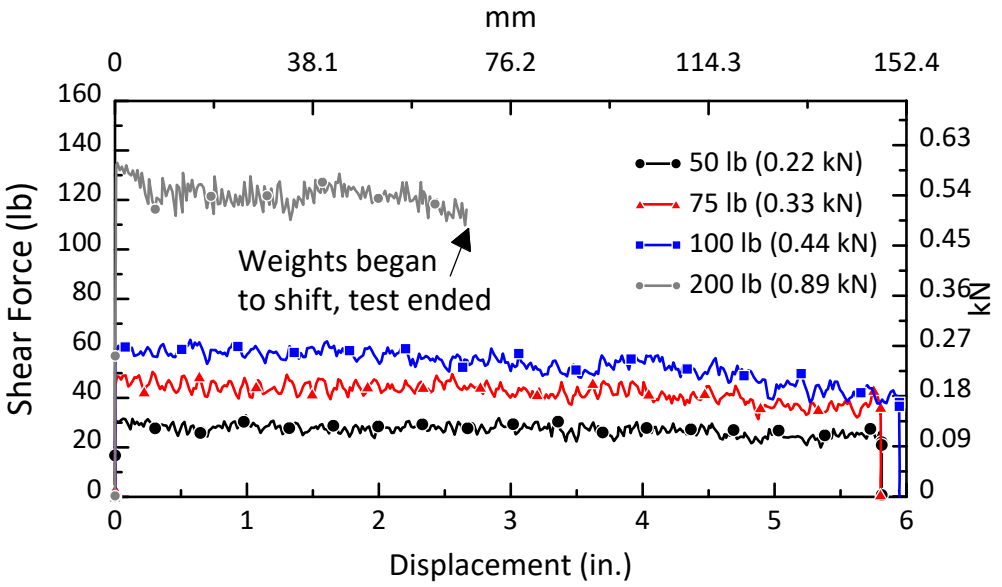

Figure 5.4. Shear Force versus Displacement for Direct Shear Tests Using New DI Pipe from DT1

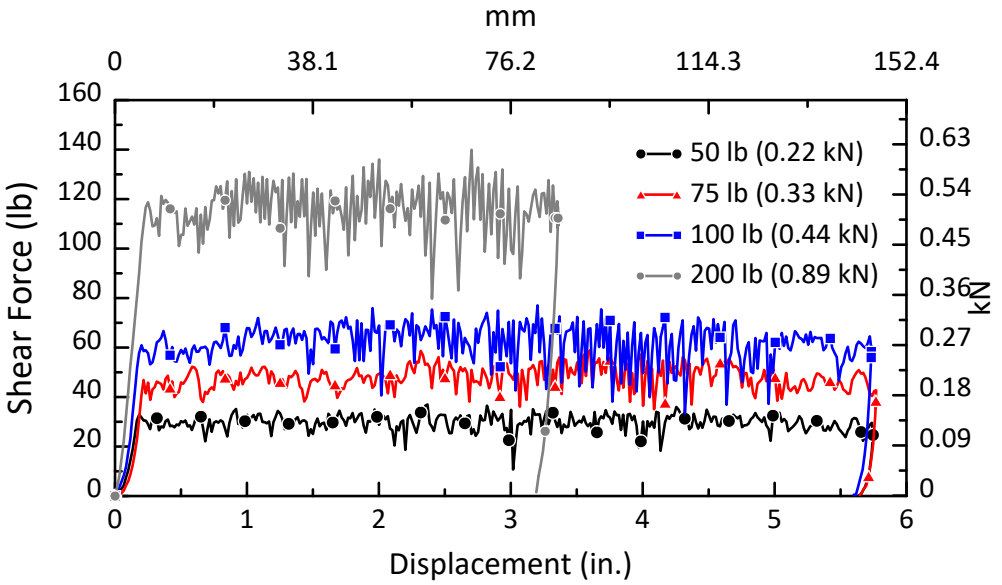

Figure 5.5. Shear Force versus Displacement for Direct Shear Tests Using Field CI Pipe from DT5

For each test, the representative shear force for each normal force was calculated for a range of 0.5 in. (13 mm) to 3 in. (76 mm) of lining displacement relative to the host pipe. The shear force was plotted with respect to lining displacement. Using linear regression, the shear force at the midpoint of displacement at 1.75 in. (44.5 mm) was selected as the representative shear force for the applied normal force.

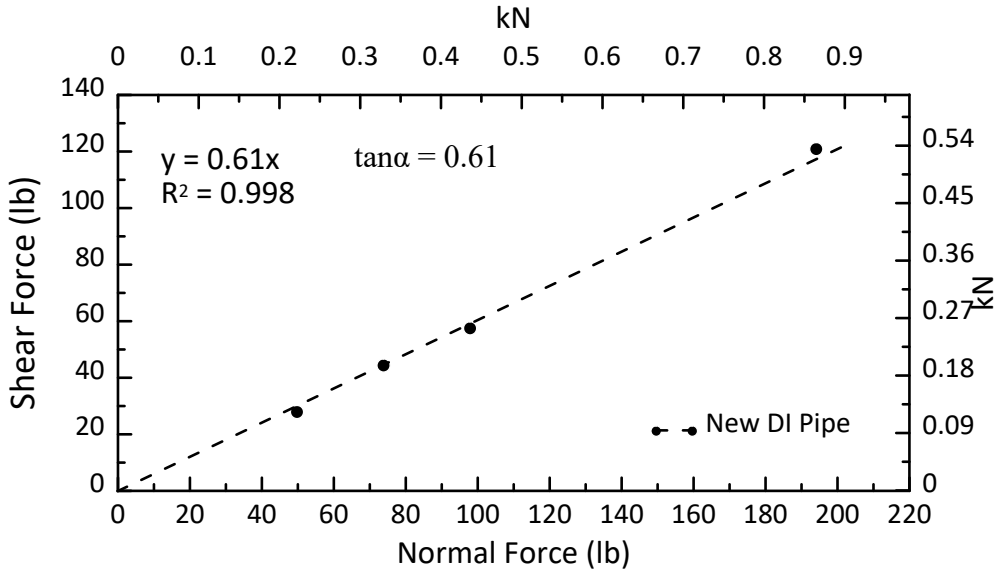

Figure 5.6. Shear Force versus Normal Force for Direct Shear Tests Using New DI Pipe from DT1

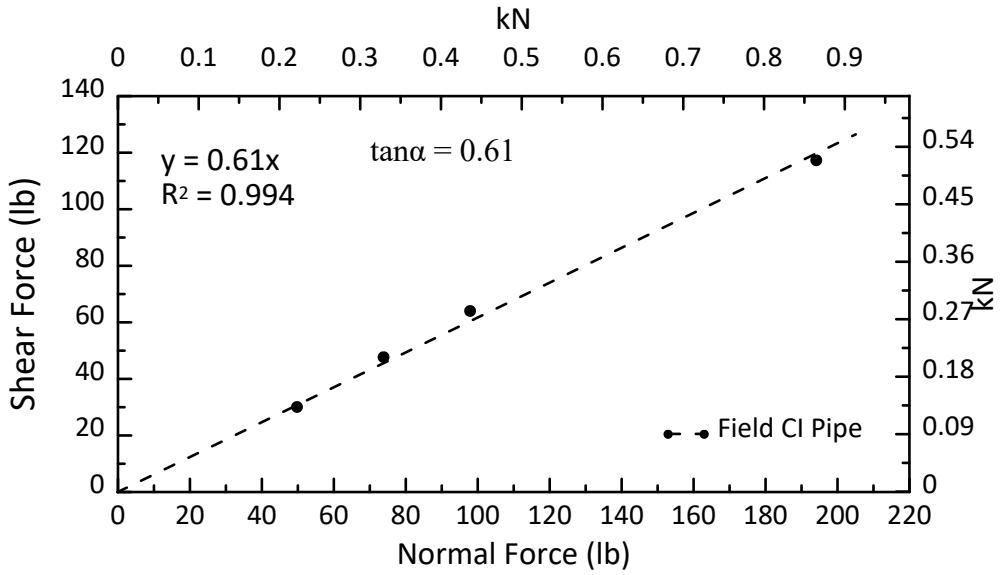

Figure 5.7. Shear Force versus Normal Force for Direct Shear Tests Using Field CI Pipe from DT5

The shear force was plotted with respect to the normal force to determine the friction coefficient for each type of surface. Figure 5.6 and Figure 5.7 show linear regressions through zero of shear force versus normal force for the new DI pipe and old CI pipe specimens, respectively. The friction coefficient is the ratio of shear force to normal force, so the slope of these plots represents the friction coefficient. The friction coefficient for the lining and both the new DI pipe and field CI pipe was 0.61. Performing the direct shear tests involved repeated displacements of the lining

along the host pipe, which promotes a smooth surface representative of field installation. The tests therefore provide the coefficient of friction that best matches field installation procedures.

To estimate the coefficient of friction representative of the initial roughness between the lining and new DI pipe, the results of FT1 and FT5 were used (see Figure 4.5). As described in Section 4 Friction Tests, these tests were performed for Aqua-Pipe lining in contact with new DI pipe. The reason for the higher axial force in FT1 is related to the increased roughness of the outside lining surface during the initial test. Both FT1 and FT5 were performed under identical conditions of zero pressure, displacement rate, displacement, and pipe/lining geometry. Assuming that the main factor contributing to the different forces was friction, one can use the ratio of the axial loads above 10 in. (252 mm) axial movement in these two tests to estimate the coefficient of friction for the FT1 lining with initially high roughness. The weighted average ratio of axial force in FT1 with respect to FT2 at identical displacements is approximately 1.25. Multiplying this ratio by $f = 0.61$ for smooth surface conditions provides an estimate of $f = 0.76$ for lining/pipe surfaces that are rough and irregular.

5.4 Summary

The results of the direct shear tests for new DI and field CI pipes show a coefficient of friction, f, of 0.61. This value represents the relatively smooth debonded lining surface conditions representative of the Sanexen cleaning and lining process for old CI water mains. It also represents the interface between the lining and new DI pipe after repeated displacements.

Using the ratio of peak axial loads in FT1 relative to FT5 one can estimate the coefficient of friction for the initially rough interface between the lining and DI pipe surface. Multiplying the weighted average ratio of 1.37 for the peak axial force in FT1 relative to FT5 at identical displacements with $f = 0.61$ for a relatively smooth lining/pipe interface results in $f = 0.76$. This coefficient of friction provides an estimate for debonded lining/pipe interfaces that are rough and irregular.

Section 6
Direct Compression Tests

6.1. Introduction

This section summarizes the results of direct compression tests, which were designed to evaluate the performance of AP1 lining in CI joints subject to compressive failure. Earthquake-induced ground deformation can impose substantial compressive movement in pipelines. Such movement will cause compressive deformation at pipeline joints. Because contact between the spigot and back of the bell tends to develop eccentric loading, compressive failure is likely to occur at the joints.

Jointed specimens of 6-in. (150 mm) CI pipe were removed from the field by the East Bay Municipal Utility District (EBMUD) and Los Angeles Department of Water and Power (LADWP) with guidance from Cornell researchers and shipped to Sanexen. The specimens were lined with Aqua-Pipe and sent to Cornell for testing. The four direct compression tests performed at Cornell are described in this section with a discussion of the test results.

6.2 Direct Compression Test Setup

A plan view of the direct compression test setup is presented in Figure 6.1. Figure 6.2 and Figure 6.4 show the test specimen, load frame, and box for encapsulating the CI joint in soil to simulate underground confinement in the field. As mentioned above, jointed pipe specimens were extracted from the field by EBMUD and LADWP crews with Cornell guidance. Figure 6.3 shows the extraction of a CI jointed pipe specimen by EBMUD personnel. Field sampling, shipping, and handling were performed with great care to avoid disturbance. Each specimen was exposed in an open trench, then removed and transported with a strongback, consisting of a stiff timber section strapped to the test specimen.

Table 6.1 provides a list of the CI pipe specimens tested with information about the test designation, utility source, age, pipe, and type of joint. All specimens measured 100 in. (254 cm) in length with a CI joint at the center of the specimen. The four direct compression tests are designated as DC1, DC2, DC3, and DC4.

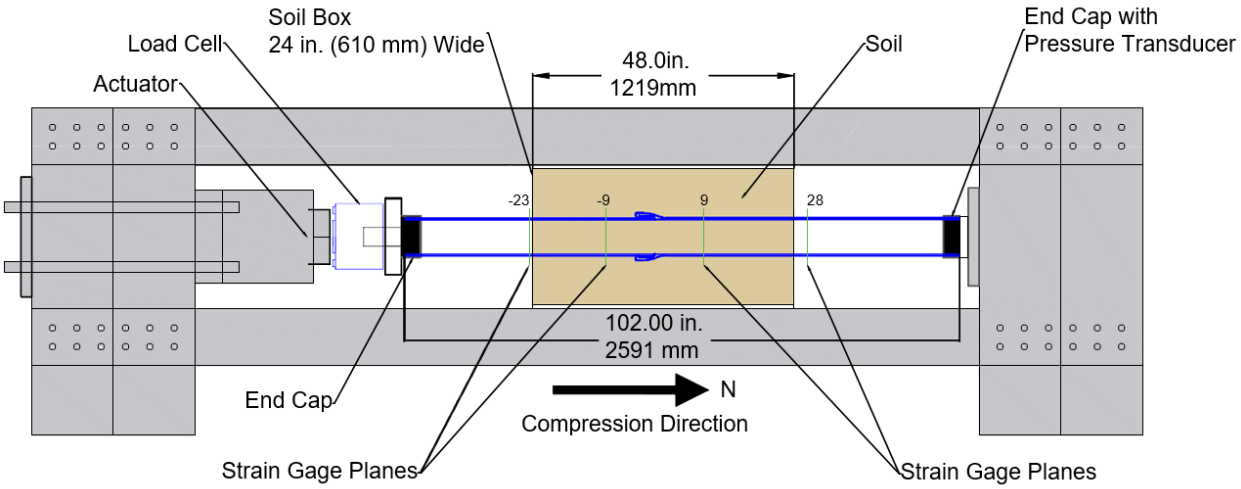

Figure 6.1. Plan View of Direct Compression Test Set Up

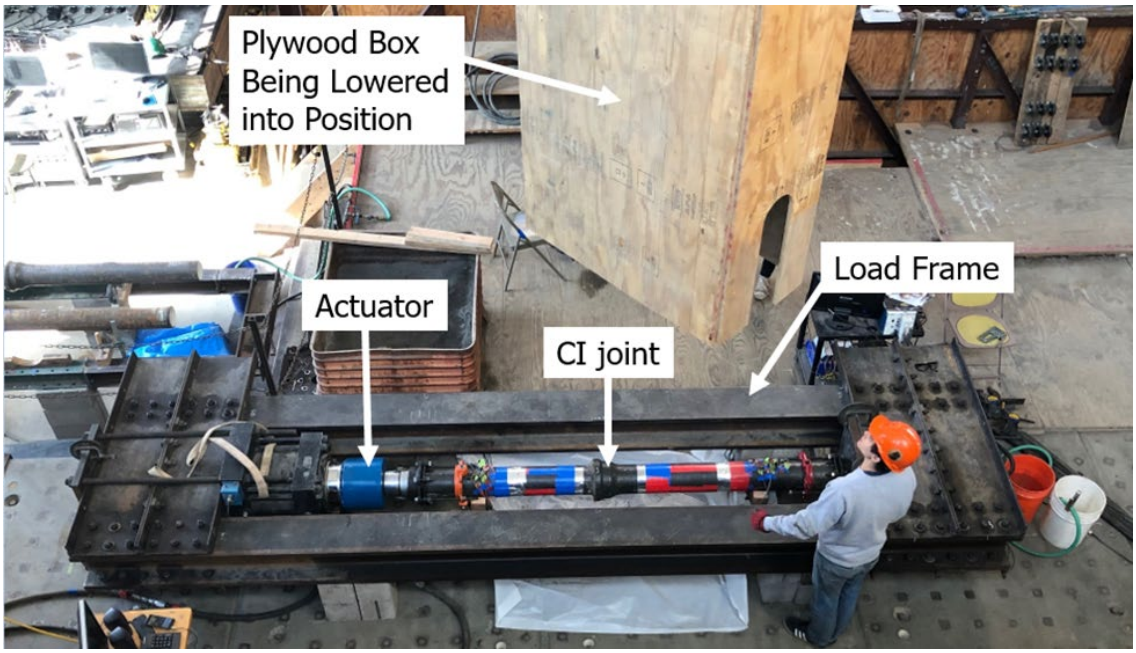

Figure 6.2. Direct Compression Jointed Pipe Specimen in Load Frame

As shown in Figure 6.1 and illustrated in Figure 6.2 and Figure 6.4, a plywood box, centered on the CI joint, was lowered onto the floor so that it encapsulated the center part of the specimen. The plywood was 0.75 in. (19 mm) thick. The exterior plan dimensions of the box were 48 in. (1219 mm) long and 24 in. (610 mm) wide. Soil was placed in the box so that there was 18 in. (457 mm) of soil beneath the invert of the pipe and 32 in. (810 mm) between the crown of the pipe and ground surface. A plastic sheet was placed between the box and floor to seal the base.

Figure 6.3. EBMUD Retrieval of a Jointed Pipe Specimen

Figure 6.4. Soil Box Used in Direct Compression Tests

Table 6.1. Characteristics of CI Test Pipe Specimens

Test	Utility Source	Installation Date	Pipe Description
DC 1 and DC 2	East Bay Municipal Utility District	1930	Cast iron main with lead caulked joints
DC 3	Los Angeles Department of Water and Power	1925	Cast iron main with cement caulked joints
DC 4	Los Angeles Department of Water and Power	1960	Cast iron main with rubber gasket and lead caulked joints

The soil was a medium dense to dense, partially saturated glacio-fluvial sand. It was placed and manually compacted with a steel tamping plate in 8-in. (200 mm) lifts to develop a direct shear friction angle (angle of shearing resistance) for the sand of approximately 40°. The water content was approximately 4%. The characteristics and properties of the sand are similar to those described in a forthcoming section of the report on the fault rupture test.

Table 6.2 provides a list of the instrumentation used in all direct compression tests. Strain gages were placed at the pipe crown, springlines, and invert at distances of 25 in. (635 mm) and 9 in. (229 mm) north and south of the middle of the test specimen. The strain gages were used to provide supplemental data about axial force, as a check on the load cell measurements, and as a backup measurement system in case there were problems with the load cell.

Longitudinal movements at select locations were measured with horizontal string pots. End caps were used in each test. A pressure transducer was used to measure the internal water pressure. A load cell measured the axial force. Axial compressive force was applied to the specimen at an initial rate of 0.1 in./min (0.25 mm/min). The sampling rate for data collection was 5 Hz.

DC1, DC2, and DC 3 were run at an initial internal water pressure on 10 psi (69 kPa). The intention was to pressurize the pipe at a low pressure to detect pressure loss and associated leakage from the lining. A low pressure was chosen due to safety concerns related to high compressive load and brittle failure of the CI pipe. All specimens that experienced CI pipe failure were pressurized after

Table 6.2. Instrumentation List for Direct Compression Tests

Location	Instrument Description	Local Instrument Name
25 in. North of Centerline	Crown, Axial Strain	25CA
	Crown, Circumferential Strain	25CC
	West, Axial Strain	25WA
	East, Axial Strain	25EA
	Invert, Axial Strain	25IA
	Invert, Circumferential Strain	25IC
25 in. South of Centerline	Crown, Axial Strain	-25CA
	Crown, Circumferential Strain	-25CC
	West, Axial Strain	-25WA
	East, Axial Strain	-25EA
	Invert, Axial Strain	-25IA
	Invert, Circumferential Strain	-25IC
9 in. North of Centerline	Crown, Axial Strain	9CA
	Invert, Axial Strain	9IA
	West, Axial Strain	9WA
	East, Axial Strain	9EA
9 in. South of Centerline	Crown, Axial Strain	-9CA
	Invert, Axial Strain	-9IA
	West, Axial Strain	-9WA
	East, Axial Strain	-9EA
Actuator	Actuator Displacement	Act_Disp
	Horizontal String Pot	HSP_Act_Disp

Table 6.2. Instrumentation List for Direct Compression Tests

	Actuator Load	Act_Load
North End Cap	Pressure Transducer	Pres_Pipe
		Pres_Input
North End Cap	Horizontal String Pot	HSP_N
South End Cap	Horizontal String Pot	HSP_S

the test at 80 psi (552 kPa) to monitor for liner leakage. DC 4 was performed at an internal water pressure of 80 psi (552 kPa) for the entire test.

6.3 Experimental Results

The experimental results for DC1, DC2, DC3, and DC4 are provided in this subsection. The actuator force versus actuator displacement is plotted for each test with observations of pipe joint response at various stages of compressive loading, supplemental data plots, and photos of the pipe test specimen after compressive failure.

6.3.1. DC1

Figure 6.5 presents a plot of the actuator force (axial compressive force on pipe) versus actuator displacement (axial displacement) for the DC1 specimen provided by EBMUD. The test was performed in two load cycles. During the first load cycle there was a partial blockage in the load cell that prevented an accurate measurement of axial load. The axial displacement, however, is accurate, and shows irrecoverable deformation of approximately 0.4 in. (10 mm). This deformation is the displacement of the spigot into the bell until there was solid contact between the spigot and back of the bell.

The load cell was recalibrated and reset in the load frame, and the second load cycle was started at approximately 0.4 in. (10 mm). The second cycle load versus displacement plot is linear until a load of 400 kips (1816 kN), which is the maximum capacity of the load cell. Unloading the specimen followed a similar linear path to zero load and 0.4 in. (10 mm).

Figure 6.6 compares the axial load versus displacement measured by both the load cell and strain gages. The axial force, F_A, was evaluated from the strain gages using the relationship $F_A = \varepsilon_A EA$, for which ε_A is the measured axial strain, E is the Young's modulus of elasticity (17500 ksi) determined from tensile coupon tests performed on samples of the CI pipe, and A is the transverse cross-sectional area of the pipe (4.27 in^2). There is excellent agreement between the load versus displacement plots from the two different measurement methods.

The linear force versus displacement relationship and strain gage measurements at different locations around the pipe circumference indicate that the axial load was applied through concentric contact between the spigot and back of the bell. Under these circumstances the axial stress calculated as F_A/A can be plotted relative to the average axial strain to estimate the CI compressive stress versus strain relationship. This relationship is compared in Figure 6.7 with the stress versus strain relationship determined from tensile coupon tests on CI specimens cut from the test pipe. The initial Young's modulus for tension and compression are in close agreement. As expected, the compressive stress versus strain relationship remains linear to a much higher stress level than that in tension. The results from this test provide a rare opportunity to compare high quality test measurements for CI pipe in tension and compression. The resulting comparison is consistent with properties and performance of CI pipe summarized by Taki and O'Rourke (1983).

6.3.2. DC2

The second compression test was performed on a specimen provided by EBMUD. Figure 6.8 presents a plot of the actuator force versus displacement. At about 0.10 in. (2.5 mm) of displacement, when the spigot made firm contact with the back of the bell, there was a rapid linear rise in force versus displacement to 0.59 in. (15 mm) and a load of 252 kips (1120 kN), when the CI bell fractured.

There was an immediate drop in axial load as shown in the figure. The test was paused at 1.5 in. (38 mm) of axial displacement and then continued to a total displacement of 3.8 in. (97 mm). The displacement rate was increased from 0.1 in./min. (0.25 mm/min.) to 1.0 in./min (10 mm/min.) when the test was resumed after failure of the CI bell.

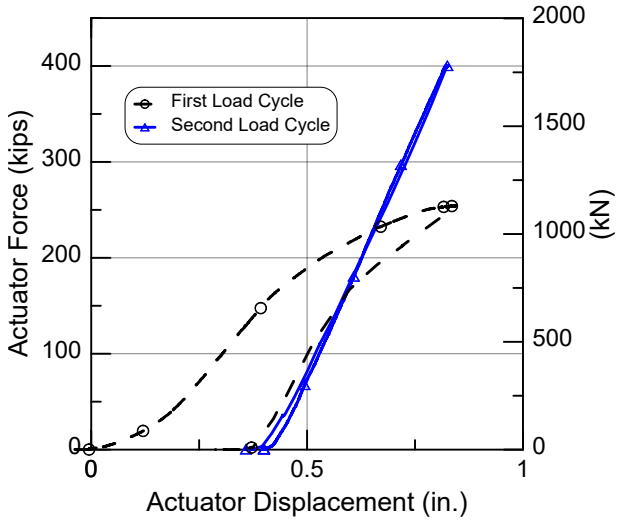

Figure 6.5. DC1 Axial Force versus Displacement

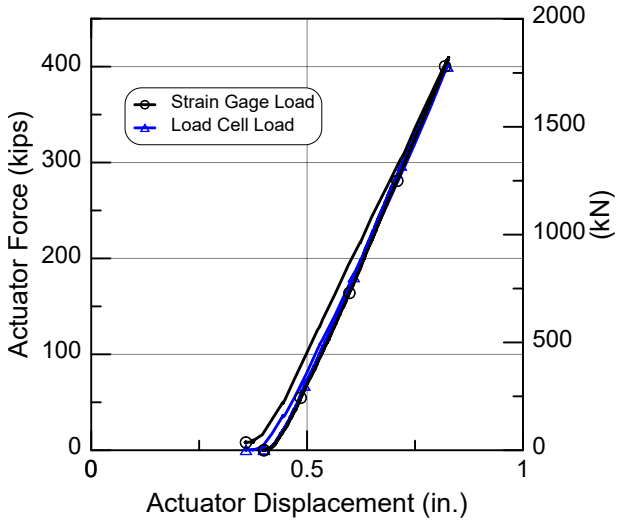

Figure 6.6. Comparison of Axial Force versus Displacement
with Load Cell and Strain Gage Measurements

Soil was excavated to expose the joint. A photo of the fractured bell is provided in Figure 6.9. Portions of the fractured bell were removed from the joint to observe the lining. A close-up photo of the deformed and wrinkled lining is presented in Figure 6.10.

The test specimen was pressurized in the condition shown in Figure 6.9 and Figure 6.10 at 80 psi (552 kPa). Drips of water were observed at two locations along the wrinkled lining. A very low leakage rate of 95 mL/min. (3.2 fl. oz./min.) was measured.

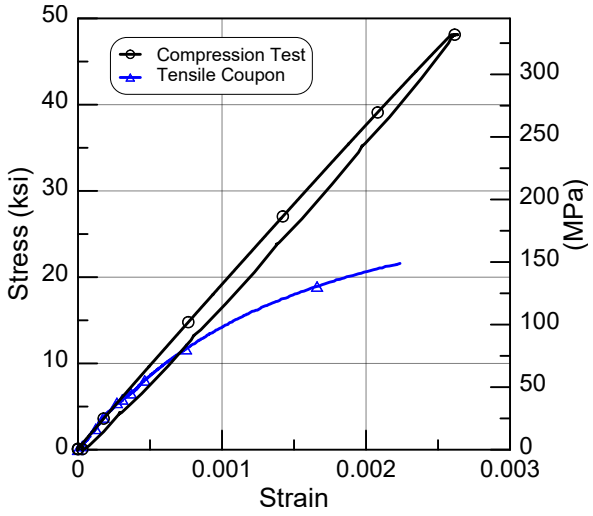

Figure 6.7. Comparison of CI Stress versus Strain Relationship from Tensile Coupon and Direct Compression Tests

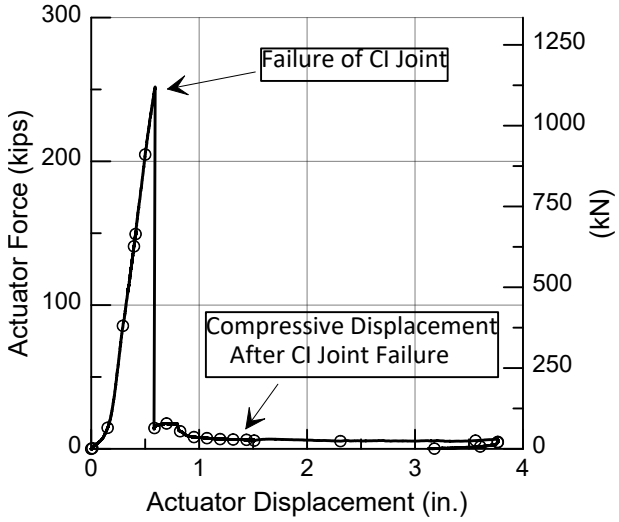

Figure 6.8. DC2 Axial Force versus Displacement Plot

6.3.3. DC3

The third compression test was performed on a test specimen provided by LADWP with a cement caulked joint. Figure 6.11 presents a plot of the actuator force versus axial displacement. There is a noticeable change in slope of the force versus displacement plot at about 0.7 in. (18 mm), when the spigot made firm contact with the back of the bell. The pipe barrel north of the joint failed at a

Figure 6.9. DC2 Fractured CI Bell

Figure 6.10. DC2 Deformed and Buckled Lining

load of 267 kips (1190 kN) and 1.20 in. (61 mm) of axial displacement. The failure occurred outside of the soil box at a location of corrosion pitting. Figure 6.12 is a photograph of the failed pipe barrel outside of the soil box. Because a cement caulked joint is much stronger and stiffer than a lead caulked joint, the failure occurred at a location of relative weakness close to, but apart from, the relatively strong cement caulked joint.

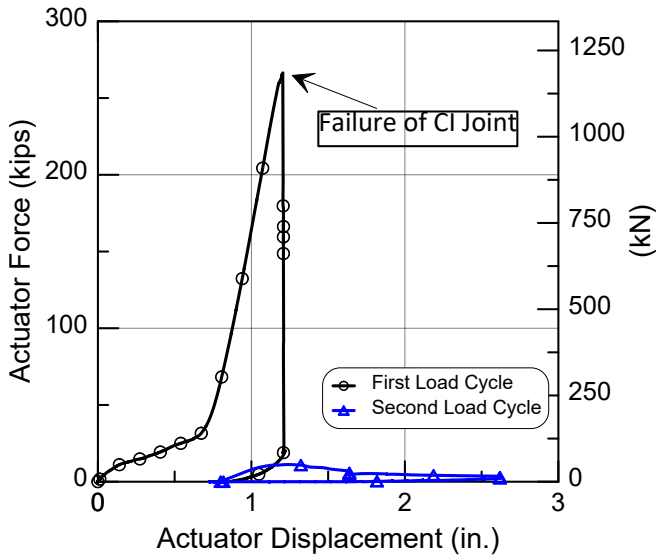

Figure 6.11. DC3 Axial Force versus Displacement Plot

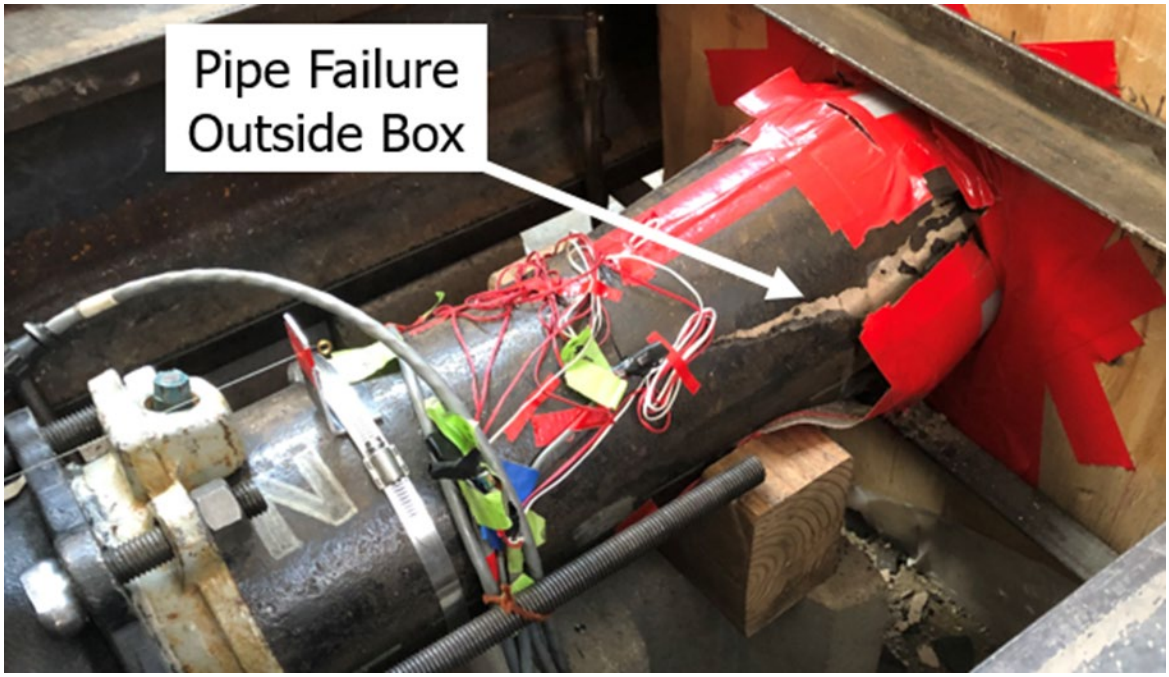

Figure 6.12. DC 3 Fractured Test Pipe Specimen

The test was paused, and the actuator was retracted, leaving a residual displacement of approximately 0.8 in. (20 mm), as shown in Figure 6.11. No leakage was detected. The pipe specimen was excavated, and the soil box was removed. The specimen was again loaded during a second load cycle with until a total axial displacement of 2.7 in. (6.86 cm). The water pressure during this second cycle was increased from 10 psi to 80 psi (69 to 552 kPa), and the displacement

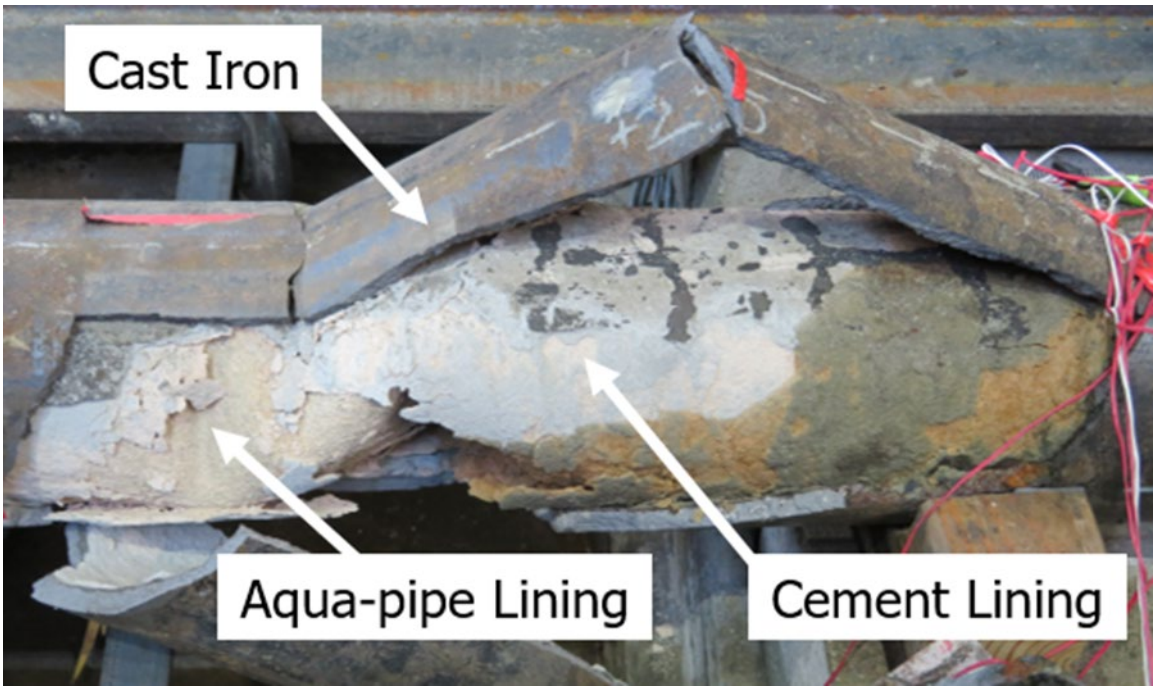

Figure 6.13. DC3 Fractured Test Pipe Specimen View of
Deformed Aqua-Pipe Lining and Cement Lining

rate was increased from 0.1 in./min. (0.25 mm/min.) to 1.0 in./min (10 mm/min.) Again, no leakage was detected. Figure 6.13 is a photograph of the fractured CI pipe barrel, underlying cement lining, and deformed Aqua-Pipe lining.

6.3.4. DC4

The fourth compression test was performed on a test specimen provided by LADWP with rubber gasket and lead caulked joint. Figure 6.14 presents a plot of the actuator force versus axial displacement. There is a noticeable change in slope of the force versus displacement plot at about 0.25 in. (6 mm), when the spigot made firm contact with the back of the bell. As depicted on the plot, the spigot slipped on the back of the bell at 1.32 in. (3.35 cm) of displacement, corresponding to an axial load of 181 kips (804 kN). After a reduction in load of approximately 40 kips (178 kN), the load increased again to a maximum 291 kips (1293 kN) at an actuator displacement of 2.22 in. (5.6 mm) when the cast iron bell fractured. The load then decreased rapidly, and remained in a range of approximately 10 to 15 kips (44.5 to 67.8 kN) until 4 in. (102 mm) of axial displacement, when the test was terminated.

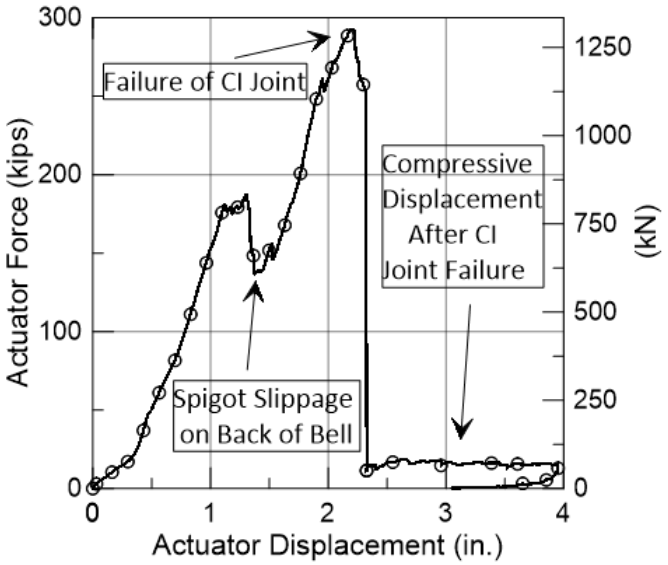

Figure 6.14. DC3 Axial Force versus Displacement Plot

Figure 6.15. DC 4 Fractured CI Bell and Deformed Aqua-Pipe Lining

As previously mentioned, DC 4 was performed continuously under 80 psi (552 kPa). At the end of the test, leakage was measured at a very low level of 10 mL/min. (0.34 fl. oz./min.). Figure 6.15 is a photograph of the failed joint and deformed lining. In the figure the broken halves of the bell

have been removed from the pipe, exposing the wrinkled lining. The broken halves of the bell, with inside surfaces in view, are positioned just below the fractured pipe and deformed lining.

6.4. Summary

Direct compression tests were performed on a variety of lined CI joint specimens retrieved from the EBMUD and LADWP water distribution systems, including lead caulked, cement caulked, and rubber gasket/lead caulked joints. The joints were confined in dense sand under burial depths and soil strength and stiffness representative of field conditions. In all test results there is a change to a steep linear slope of the axial load versus displacement plot at a displacement between 0.10 in. (2.5 mm) to 0.7 in. (18 mm), representing the displacement at which firm contact between the spigot and back of the bell is established. Bell failure occurred in CI pipe specimens with lead caulked and rubber gasket/lead caulked joints at a load of 252 kips (1120 kN) and 291 kips (1290 kN), respectively, corresponding to an axial displacement of 0.59 in. (15 mm) and 2.22 in. (56 mm), respectively. The cement caulked joint did not fail, but the pipe barrel failed at 267 kips (1190 kN). One of the specimens with a lead caulked joint was able to sustain an axial load of 400 kips (1815 kN) without failure.

In all failed CI pipe specimens, the lining was able to accommodate substantial deformation and wrinkling. No leakage was observed in the failed cement caulked joint specimen at 80 psi (552 kPa) water pressure. Very low leakage at the same pressure in the form of dripping water of 10 mL/min. (0.34 fl. oz./min.) and 95 mL/min. (3.2 fl. oz./min.) was measured for failed CI joints that sustained a total compressive deformation of 4.0 in. (102 mm) and 3.8 in. (97 mm), respectively.

Section 7
Four-Point Bending Tests

7.1. Introduction

This section presents the results of three four-point bending tests for sections of nominal 6-in. (150-mm) DI pipe lined with both AP1 and AP2. The purpose of the tests was to develop moment vs. rotation relationships for these types of joints. The tests, with experiments to characterize the direct compression and tension capacity of lined pipelines, are used with the results of a large-scale split basin test to evaluate the performance of the pipelines lined with AP1 and AP2 under severe earthquake-induced ground deformation. The work was undertaken in the Cornell Large Scale Lifelines Testing Facility, which is part of the Bovay Laboratory Complex at Cornell University.

7.2 Lined Pipeline Specimens

This section summarizes the results of four-point bending tests on the specimens listed in Table 7.1. One test was performed on a CI specimen installed in 1960 by LADWP, which is described in greater detail in Section 6.2 in conjunction with Table 6.1. The LADWP pipeline was shipped to Sanexen and lined with AP1 by them. Another test was performed on a new McWane DI pipeline joint that was aged by Sanexen with acetic acid as described in Section 9 to obtain a pipeline with an interior surface representative of CI and DI pipelines in the field. It was lined with AP1. A third test was performed on a DI pipeline installed in the Montreal area in 1974 and lined in place with AP2 by Sanexen. All pipelines were lined according to the field procedures used by Sanexen. Mechanical joint end caps with Megalug restraints were used on the ends of the test specimens to allow for water pressurization. A nominal internal pressure of 80 psi (550 kPa) was used throughout the bending tests.

7.3 Calculation Approach

The length of the test specimens between the outer supports was l_t =12 ft (3.66 m). The pipe weight was 15 lb/ft (2.63 kN/m) and the water weight was 16.2 lb/ft (2.84 kN/m.) The combined distributed weight of the pipe and water inside the pipe was w = 31.2 lb/ft (5.46 kN/m.)

Table 7.1. Summary of Four Point Bending Test Specimens

Test	Source	Installation Date	Pipe Description
AP1 LADWP	Los Angeles Department of Water and Power	1960	Cast iron main with rubber gasket and lead caulked joints
AP1 DI Joint	Sanexen	New	Ductile iron pipeline cementless and aged with acetic acid
AP2 DI Joint	City of Dollard-des-Ormeaux (DDO), Quebec, Canada	1974	Ductile iron pipeline in ground since 1974

Using a simply-supported beam approach, the maximum moment at the pipe centerline was:

$$M_{distrib} = \frac{w\, l_t^2}{8} \tag{7.1}$$

in which w is the uniform load due to pipe and water, and l_t is the total pipe length between the outer supports.

The three equal distances between the load and support points each were 48 in. (1.22 m). The additional moment applied to the central portion of the specimen, $M_{central}$, was calculated as

$$M_{central} = \frac{P\, l_t}{6} \tag{7.2}$$

in which P is the the applied load due to the weight of the spreader beam [W = 216 lb (0.96 kN)] plus the load applied by the hydraulic actuator, P, in the load frame, and l_t is the total pipe length between the outer supports.

The moment due to the pipe, water, and spreader beam weights are included in the moment vs. rotation calculations. The method for rotation uses the horizontal string pots (HSPs) at the top and bottom of the bell and the vertical separation distance to calculate the joint rotation, θ, as

$$\theta \text{ (degrees)} = \tan^{-1}\left[\frac{(\text{invert disp.} - \text{crown disp.})}{\text{distance between centers of HSPs} = 8.9 \text{ in.}}\frac{180^\circ}{\pi}\right] \tag{7.3}$$

7.4. Test Procedures

The pipe for the bending test was installed in the loading frame, leveled, and all instrumentation and data acquisitions systems were checked. The test was then performed as follows:

1) Fill the pipe with water, pressurize, and bleed the system to extend fully the bell/spigot connection. An internal pressure of 80 psi (550 kPa) generated approximately 2000 lb (8.8 kN) of axial force, which was sufficient to expand the joint.
2) Remove the temporary supports.
3) Lower the spreader beam onto the pipe.
4) Apply hydraulic force to develop moment and rotation at the joint.

The rate of loading for each test was 0.5 in./min. (12.5 mm/min.) The data sampling rate was 5 Hz. Each test was conducted until the test pipeline failed or became unstable with respect to further loading. Observations of the pipeline structural response and leakage were made throughout the test.

7.5. Test Results for AP1 LADWP

7.5.1. Test Setup for AP1 LADWP

The test results for AP1 LADWP are presented under the 7.5 heading. As indicated in Table 7.1, this specimen is composed of CI pipes and an intervening joint installed by LADWP in 1960, all lined with AP1. The joint was sealed with a rubber gasket and lead caulking. The average water pressure sustained during this test was 78.3 psi (540 kPa).

A schematic for the instrumentation used in the test is shown in Figure 7.1 The vertical load was applied to the pipeline by a 200-kip (4.45 kN) actuator through a 200-kip (4.45 kN) load cell. Vertical displacements were measured through string pots positioned horizontally along the pipeline. The vertical string pots (VSPs) were established both north (+) and south (-) of the center joint. The locations of the string pots with respect to the center are shown according to distance in in. (25.4 mm) in the figure.

Figure 7.2 presents a photograph of the test set-up depicted in Figure 7.1. The photo was taken just before load was applied through the spreader. The pipeline is still in a horizontal position. The test

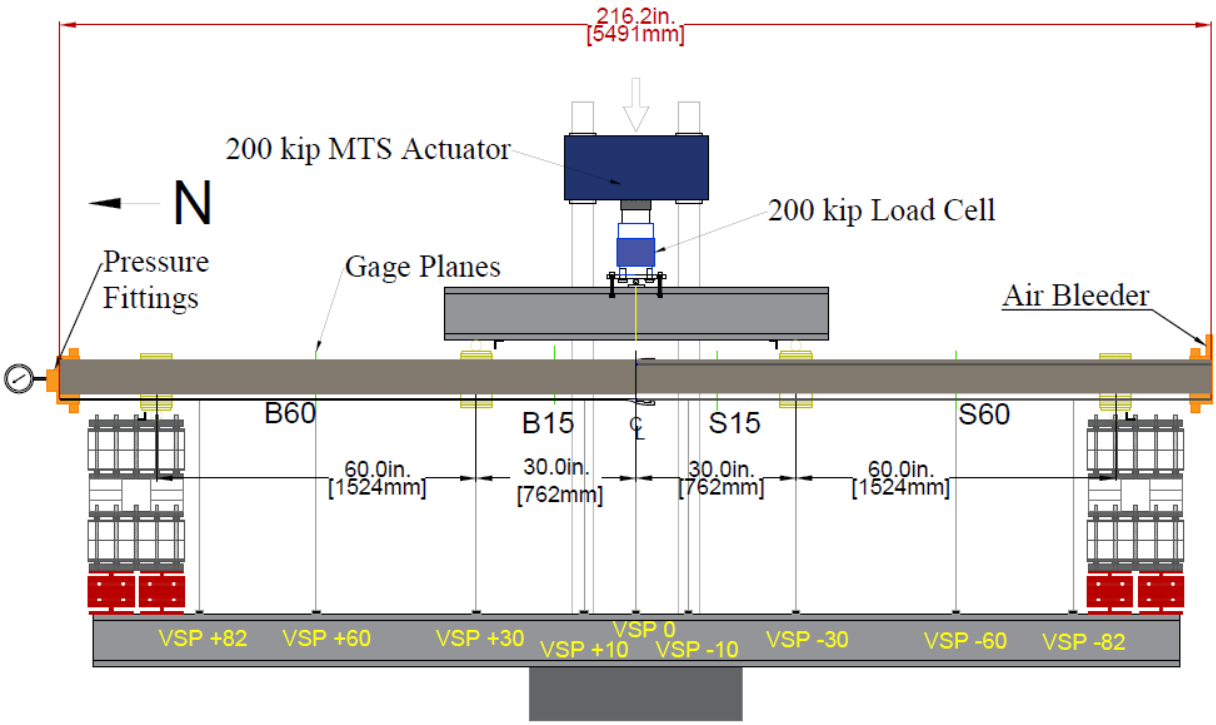

Figure 7.1. Schematic of Instrumentation for AP1 LADWP Bending Test

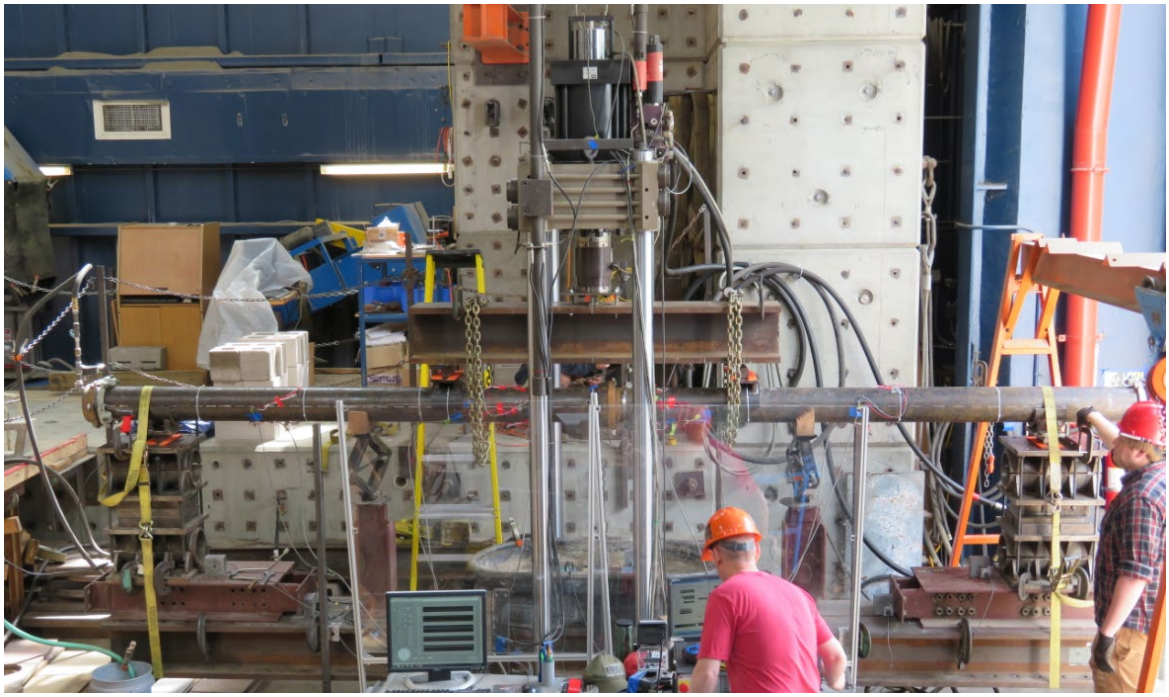

Figure 7.2. Photo of Bending Specimen

pipeline, MTS actuator, load cell, load spreader beam, load contacts and supports can be seen clearly in the figure, which is representative of all tests.

Table 7.2 lists the location, instrument type, and number for the AP1 LADWP Bending Test. The instrumentation consisted of string potentiometers (string pots) to measure horizontal displacements at the crown and invert of the pipe bell, which in turn were used to measure the bell and spigot rotation (see Equation 9.3). These horizontal string pots are referred to as HSPs. Vertical displacements along the length of the specimen were measured using seven vertical string pots (VSPs). The VSPs were employed to determine the vertical deformation of the test specimen and to calculate the vertical movements at various locations along the pipeline. Strain gages were installed to measure axial and bending strains in the DI pipe.

7.5.2. String Pot Measurements for AP1 LADWP

Figure 7.3 presents the VSP measurements along the test pipeline. The spigot and bell side VSP measurements indicate that there is good agreement between vertical movement measurements at equal distances from the center point of the test. The continuous progression of these displacements is a further indication that the assumption of rigid body motion can be used to evaluate rotations. Such estimates of rotation are close to the rotation from the HSPs provided by Equation 7.3.

7.5.3. Moment vs Rotation Relationship for AP1 LADWP

Figure 7.4 presents the moment vs rotation relationship for AP1 LADWP. The maximum moment of nearly 200 (kip-in.) (22610 kN-mm) occurred at approximately 8°of rotation when the CI joint fractured at its crown. The actuator travel was re-set and the vertical loading commenced again at about 8° rotation. The test was taken to a total of 15° rotation when it was terminated due to concerns for personnel safety. No leakage or significant reduction in average water pressure of 78.3 psi (540 kPa) were observed.

Figure 7.5 provides a photo of the failed CI pipe joint. The fracture at the top, or crown, of the bell can be seen clearly. As stated previously, the bell fracture did not coincide with leakage or loss of water pressure. Although the pipeline failed at the joint, the lining did not fail, but continued to hold full internal pressure.

Table 7.2. Instrumentation for the AP1 LADWP Bending Test

Instrumentation List for AP1 LADWP		
Location	Instrument Description	Local Instrument Name
MTS Four Post Load Frame	MTS-200K_Disp	MTS-200K_Disp
MTS Four Post Load Frame	MTS-200K_Load	MTS-200K_Load
Wall Pressure	Pressure	Pressure
Pipe Pressure at North End	Pressure Pipe	Pressure Pipe
Centerline, Crown	Horizontal String Potentiometer	HSP_C
Centerline, Invert	Horizontal String Potentiometer	HSP_I
MTS Four Post Load Frame	Vertical String Potentiometer	Crosshead Disp
Centerline	Vertical String Potentiometer	VSP0
10 in North of Centerline	Vertical String Potentiometer	VSP10
30 in North of Centerline	Vertical String Potentiometer	VSP30
60 in North of Centerline	Vertical String Potentiometer	VSP60
82 in North of Centerline	Vertical String Potentiometer	VSP82
10 in South of Centerline	Vertical String Potentiometer	VSP-10
30 in South of Centerline	Vertical String Potentiometer	VSP-30
60 in South of Centerline	Vertical String Potentiometer	VSP-60
82 in South of Centerline	Vertical String Potentiometer	VSP-82
60 in North of Centerline	Crown, Axial Strain	B60CA
	Crown, Circumferential Strain	B60CC
	Invert, Axial Strain	B60IA
	Invert, Circumferential Strain	B60IC
15 in North of Centerline	Invert, Axial Strain	B15IA
	Invert, Circumferential Strain	B15IC
	East, Axial Strain	B15EA
	West, Axial Strain	B15WA
	Crown, Axial Strain	B15CA
	Crown, Circumferential Strain	B15CC
15 in South of Centerline	Crown, Axial Strain	S15CA
	Crown, Circumferential Strain	S15CC
	Invert, Axial Strain	S15IA
	Invert, Circumferential Strain	S15IC
	East, Axial Strain	S15EA
	West, Axial Strain	S15WA
60 in South of Centerline	Crown, Axial Strain	S60CA
	Crown, Circumferential Strain	S60CC
	Invert, Axial Strain	S60IA
	Invert, Circumferential Strain	S60IC

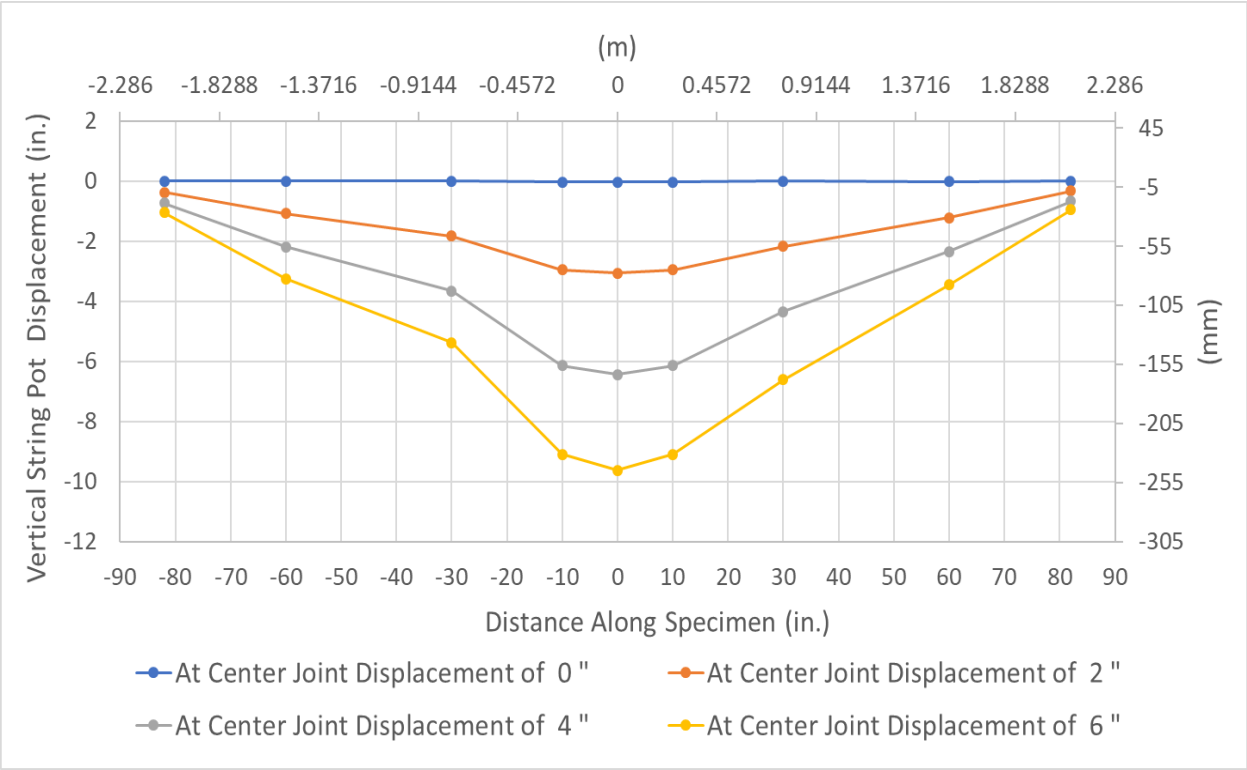

Figure 7.3. Vertical Displacements for AP1 LADWP with Various Center Joint Movements

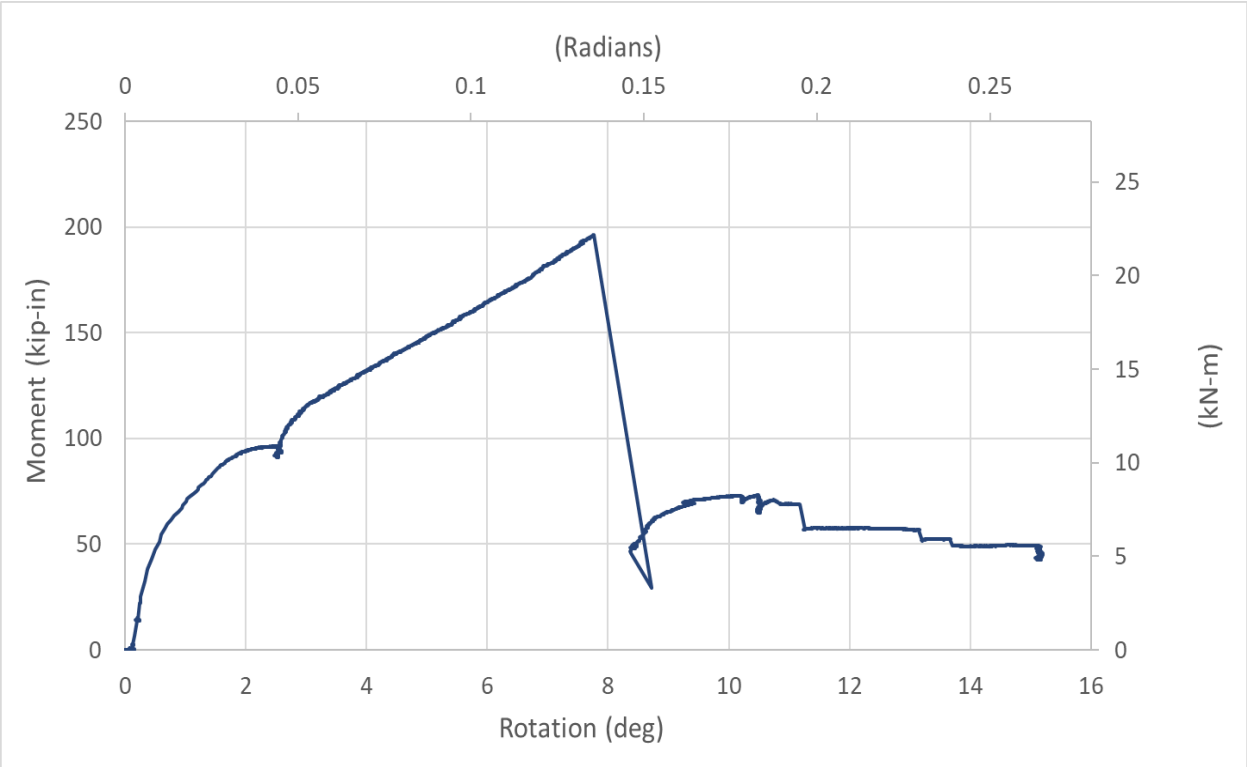

Figure 7.4. Moment versus Rotation Relationship for AP1 LADWP

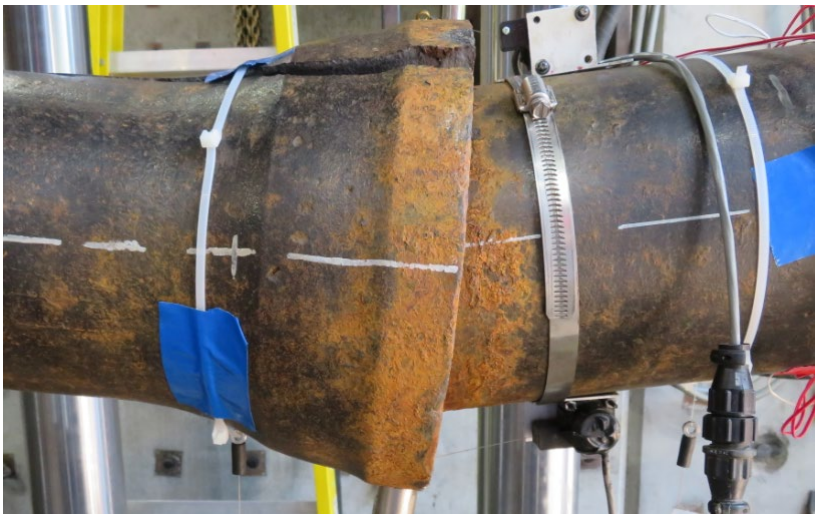

Figure 7.5. Photo of CI Bell Fracture at Crown

Figures 7.6 a, b, c, and d show photos of the initial position of the test specimen as well as its position at intermediate displacements and the final displacement at which there was rotation of 15°. This sequence of photos shows graphically the ability of a CI pipeline lined with AP1 to accommodate vertical displacements and joint rotations without leakage or failure. The maximum rotation of 15° is shown in Figure 7.6 d.

7.6. Test Results for AP1 DI Joint

7.6.1. Test Setup for AP1 DI Joint

The test results for AP1 DI Joint are presented under the 7.6 heading. As indicated in Table 7.1, this specimen is composed of a new cementless, McWane DI pipeline and joint, aged with acetic acid, and lined with an AP1 lining. The average water pressure sustained during this test was 80.9 psi (558 kPa).

A schematic for the instrumentation used in the test is the same as shown in Figure 7.1, and the equipment is the same as described above under 7.5.1. Figure 7.2 presents a photograph that is representative of the test set-up. The description, location, and instruments with abbreviations are identical to those listed in Table 7.2

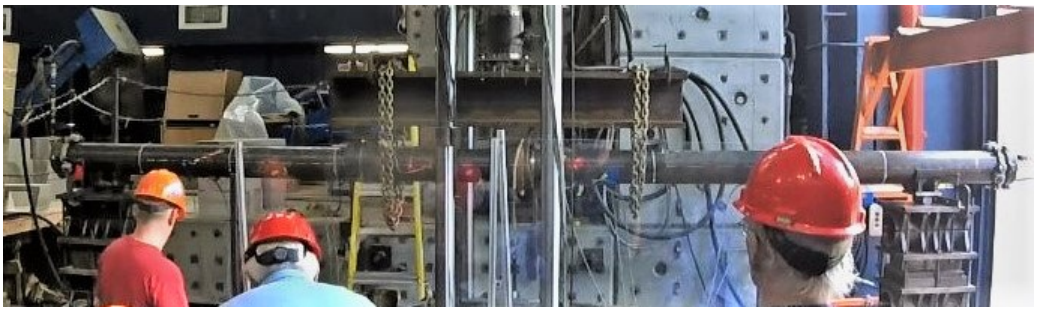

a) Initial Position

b) Approximately 5° Rotation

c) Approximately 10° Rotation

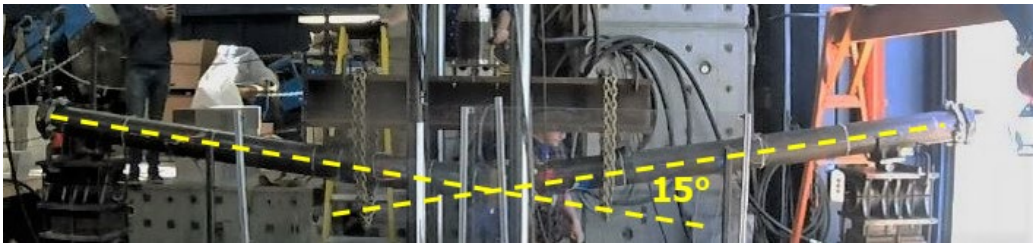

d) 15° Rotation

Figure 7.6. AP1 LADWP at Four Levels of Rotation, or Deflection

7.6.2. String Pot Measurements for AP1 DI Joint

Figure 7.3 presents the VSP measurements along the test pipeline. Again, the spigot and bell side VSP measurements indicate that there is good agreement between vertical movement measurements at equal distances from the center point of the test. The displacement pattern shows

that rigid body motion can be used to estimate rotations, which are close to the rotation from the HSPs provided by Equation 7.3.

7.6.3. Moment vs Rotation Relationship for AP1 DI Joint

Figure 7.8 presents the moment vs rotation relationship for AP1 DI Joint. A moment of nearly 200 (kip-in.) (22610 kN-mm) occurred at approximately 18°of rotation, after which the actuator travel was re-set and the vertical loading re-started. The maximum moment of approximately 275 (kip-in.) (31090 kN-mm) occurred at approximately 25.6° of total rotation, when the test was terminated due to concerns for personnel safety. No leakage or significant reduction in the average water pressure 80.9 psi (558 kPa) were observed.

Figure 7.9 provides a photo of the DI pipe joint. Neither the pipeline nor joint failed. There was no failure of the lining, which continued to hold full internal pressure.

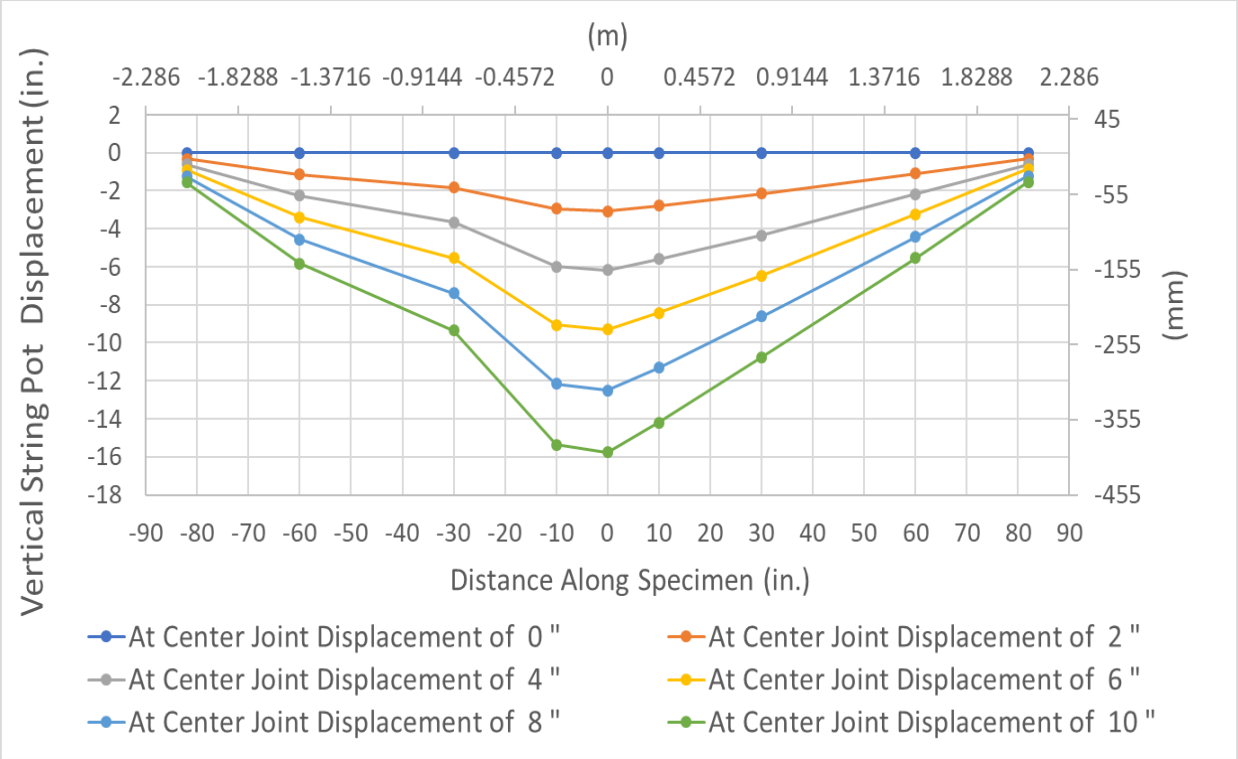

Figure 7.7. Vertical Displacements for AP1 DI Joint with Various Center Joint Movements

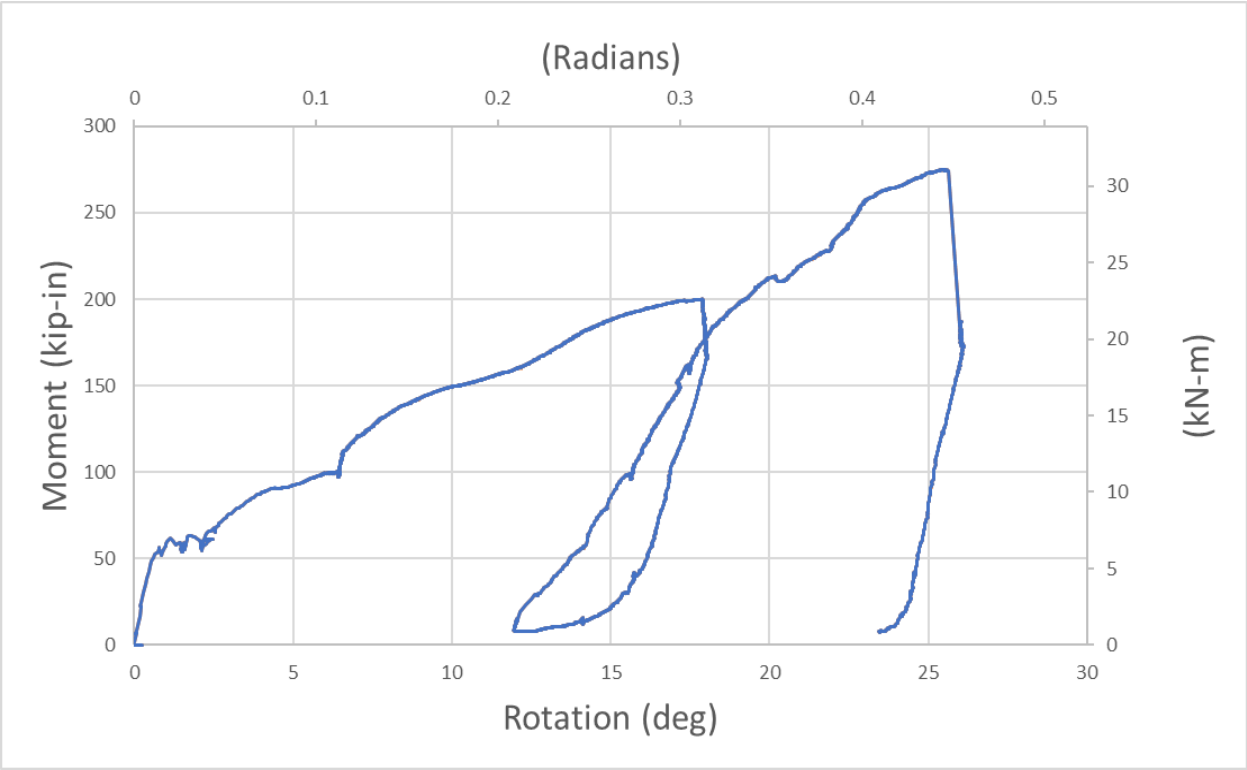

Figure 7.8. Moment vs Rotation Relationship for AP1 DI Joint

Figure 7.9. Maximum DI Joint Rotation

Figures 7.10 a, b, c, and d show photos of the initial position of the test specimen as well as its position at intermediate displacements and the final displacement at which there was rotation of 25.6°. This sequence of photos shows graphically the ability of a DI pipeline lined with AP1 to accommodate vertical displacements and joint rotations without leakage or failure. The maximum rotation of 25.6° is shown in Figure 7.6 d.

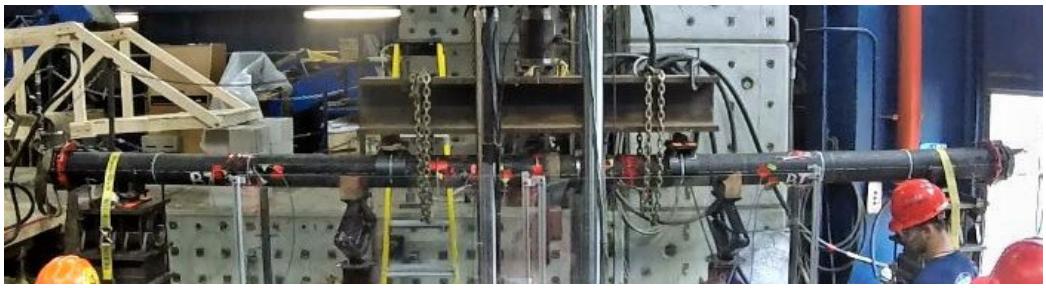

a) Initial Position

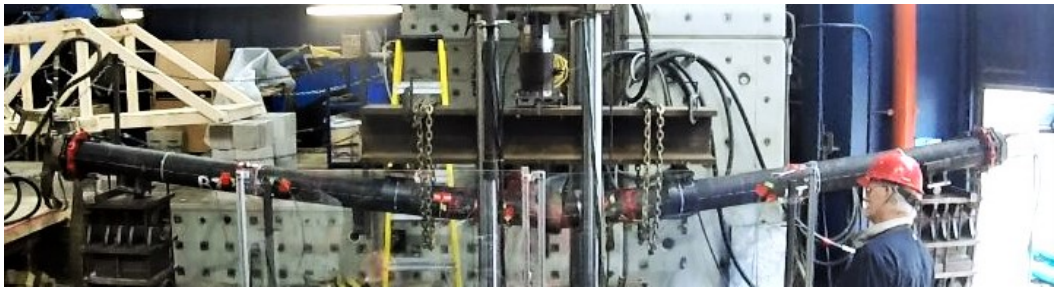

b) Approximately 8° Rotation

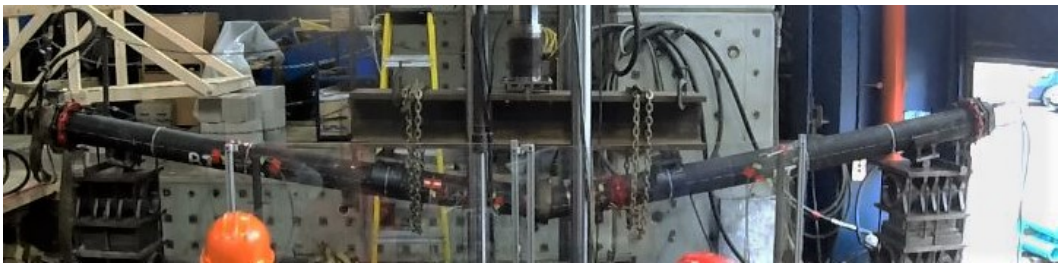

c) Approximately 16° Rotation

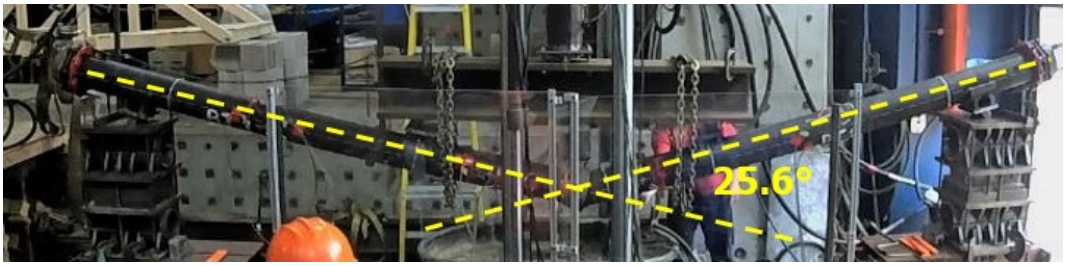

d) 25.6° Rotation

Figure 7.10. AP1 DI Joint at Four Levels of Rotation, or Deflection

7.7. Test Results for AP2 DI Joint

7.7.1. Test Setup for AP2 DI Joint

The test results for AP2 DI Joint are presented under the 7.7 heading. As indicated in Table 7.1, this specimen is composed of CI pipes and an intervening joint installed in 1974, all lined with AP2. The average water pressure sustained during this test was 82.7 psi (570 kPa).

A schematic for the instrumentation used in the test is identical to Figure 7.1. The equipment is the same as described above under 7.5.1. Figure 7.2 presents a photograph that is representative of the test set-up. The description, location, and instruments with abbreviations are provided in Table 7.3, which is similar to Table 7.2 with the exception that the invert and crown axial strain gages were not provided in AP2 DI Joint. In addition, the center VSP was moved slightly to obtain better vertical displacement of the joint.

7.7.2. String Pot Measurements for AP2 DI Joint

Figure 7.11 presents the VSP measurements along the test pipeline. Again, the spigot and bell side VSP measurements indicate that there is good agreement between vertical movement measurements at equal distances from the center point of the test. The displacement pattern shows that rigid body motion can be used to estimate rotations, which are close to the rotation from the HSPs provided by Equation 7.3.

7.7.3. Moment versus Rotation Relationship for AP2 DI Joint

Figure 7.12 presents the moment vs rotation relationship for AP2 DI Joint. Three cycles of moment and rotation were undertaken as shown by the loops in the figure. A moment of nearly 320 (kip-in.) (36180 kN-mm) occurred at approximately 12°of rotation, after which the actuator travel was re-set and the vertical loading re-started. Then a moment of about 350 (kip-in.) (39570 kN-mm) was applied to approximately 18° of rotation, after which the actuator travel was again re-set and the vertical loading re-started. The maximum moment of approximately 375 (kip-in.) (42390 kN-mm) occurred at approximately 22.4° of total rotation, when the pipe barrel fractured. The test then was terminated due to concerns for personnel safety. No leakage or significant reduction in the water pressure of 82.7 psi (570 kPa) were observed.

Figure 7.13 a) presents a photo of the DI pipe joint where failure occurred by fracturing through corrosion pits on the pipe barrel north of the joint. Figure 7.13 b) presents a photo of the DI pipe

Table 7.3. Instrumentation for the AP2 DI Joint Bending Test

Instrumentation List for AP2 DI Joint		
Location	Instrument Description	Local Instrument Name
MTS Four Post Load Frame	MTS-200K_Disp	MTS-200K_Disp
MTS Four Post Load Frame	MTS-200K_Load	MTS-200K_Load
Wall Pressure	Pressure	Pressure
Pipe Pressure at North End	Pressure Pipe	Pressure Pipe
Centerline, Crown	Horizontal String Potentiometer	HSP_C
Centerline, Invert	Horizontal String Potentiometer	HSP_I
MTS Four Post Load Frame	Vertical String Potentiometer	Crosshead Disp.
Centerline	Vertical String Potentiometer	VSP0
10 in North of Centerline	Vertical String Potentiometer	VSP10
30 in North of Centerline	Vertical String Potentiometer	VSP30
60 in North of Centerline	Vertical String Potentiometer	VSP60
82 in North of Centerline	Vertical String Potentiometer	VSP82
10 in South of Centerline	Vertical String Potentiometer	VSP-10
30 in South of Centerline	Vertical String Potentiometer	VSP-30
60 in South of Centerline	Vertical String Potentiometer	VSP-60
82 in South of Centerline	Vertical String Potentiometer	VSP-82
60 in North of Centerline	Crown, Axial Strain	B60CA
	Crown, Circumferential Strain	B60CC
	Invert, Axial Strain	B60IA
	Invert, Circumferential Strain	B60IC
15 in North of Centerline	Invert, Axial Strain	B15IA
	Invert, Circumferential Strain	B15IC
	East, Axial Strain	B15EA
	West, Axial Strain	B15WA
	Crown, Axial Strain	B15CA
	Crown, Circumferential Strain	B15CC
15 in South of Centerline	Crown, Axial Strain	S15CA
	Crown, Circumferential Strain	S15CC
	Invert, Axial Strain	S15IA
	Invert, Circumferential Strain	S15IC
	East, Axial Strain	S15EA
	West, Axial Strain	S15WA
60 in South of Centerline	Crown, Axial Strain	S60CA
	Crown, Circumferential Strain	S60CC
	Invert, Axial Strain	S60IA
	Invert, Circumferential Strain	S60IC

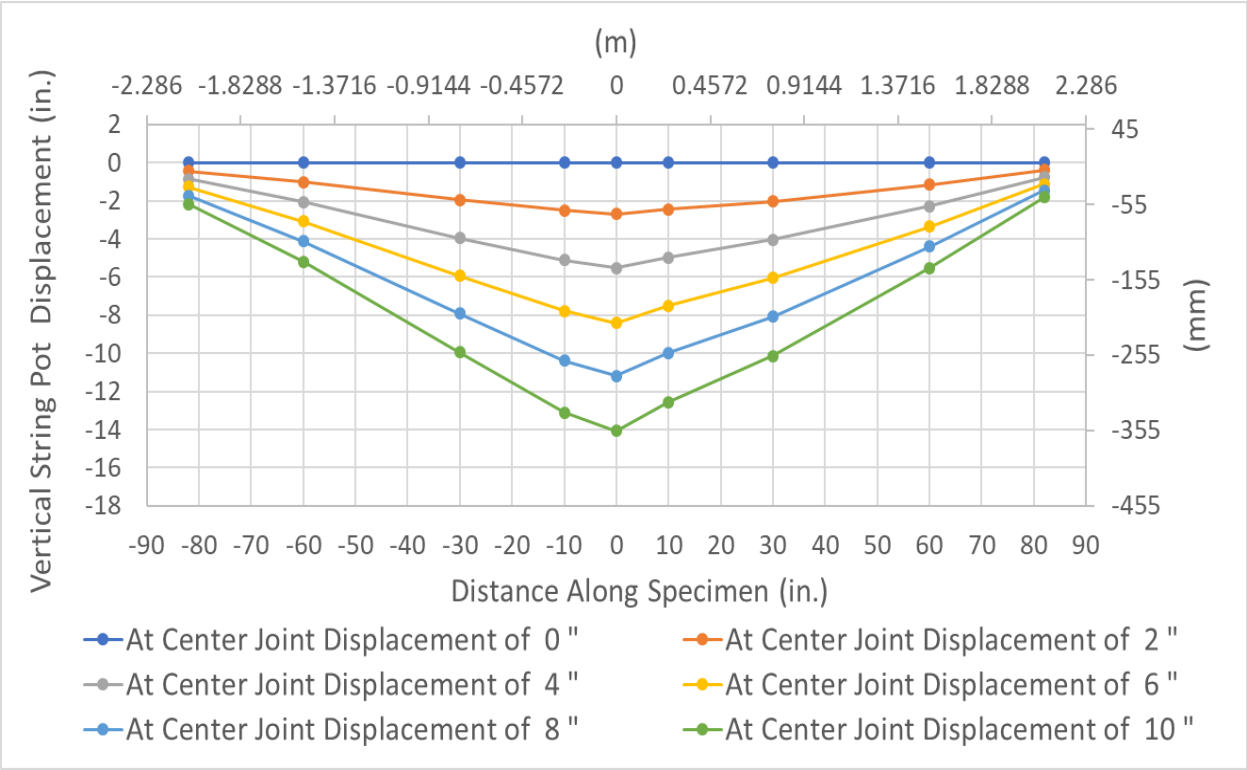

Figure 7.11. Vertical Displacements for AP2 DI Joint with Various Center Joint Movements

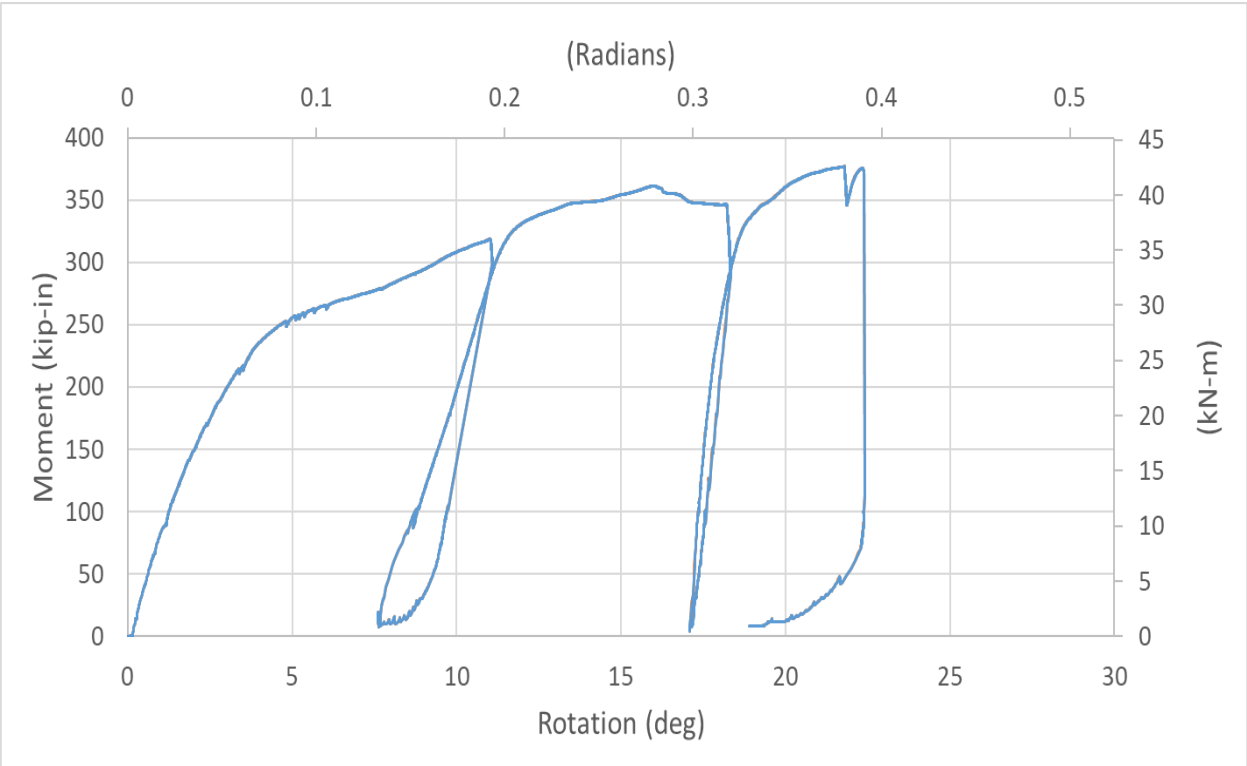

Figure 7.12. Moment versus Rotation Relationship for AP2 DI Joint

a) Corroded Pipe Barrel b) Corroded Pipe Joint

Figure 7.13. Corrosion in Test Pipeline

joint with corrosion between the centerline and invert of the joint. Upon unloading to a rotation of about 19° the pipeline started to leak by dripping at the joint under water pressure of about 82.5 psi (567 kPa).

Figures 7.14 a, b, c, and d show photos of the initial position of the test specimen as well as its position at intermediate displacements and the final displacement at which there was rotation of 22.4°. This sequence of photos shows graphically the ability of a DI pipeline lined with AP2 to accommodate vertical displacements and joint rotations without leakage or failure. The maximum rotation of 22.4° is shown in Figure 7.14 d.

7.8. Summary of Four Point Bending Tests

This section presents the results of three four-point bending tests. One test was performed on a CI specimen installed in 1960 by LADWP and lined with AP1. Another was performed on a new McWane DI pipeline joint that was aged by Sanexen with acetic acid and lined with AP1. A third was performed on a DI pipeline installed in the Montreal area in 1974 and lined in place with AP2 by Sanexen. All pipelines were lined according to the field procedures used by Sanexen. The purpose of the tests was to develop moment vs. rotation relationships for these types of joints under conditions of severe bending deformation representative of pipeline response to earthquake-induced ground movement.

The pipeline test specimens lined with AP1 and AP2 were able to sustain substantial bending deformation and joint rotation between 78.3 psi (540 kPa) and 82.7 psi (570 kPa) of water pressure.

a) Initial Position

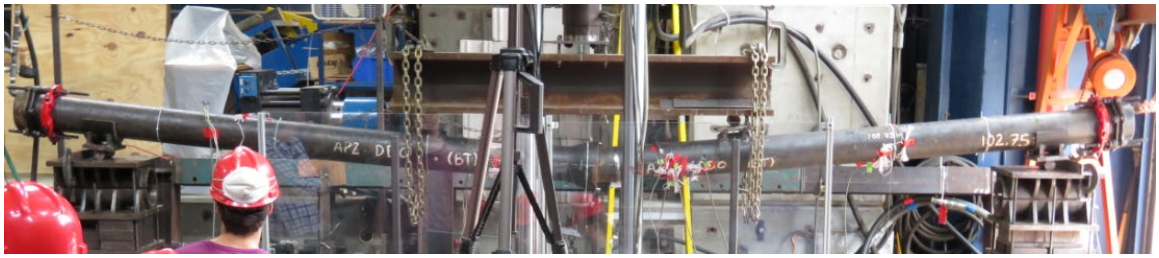

b) Approximately 7° Rotation

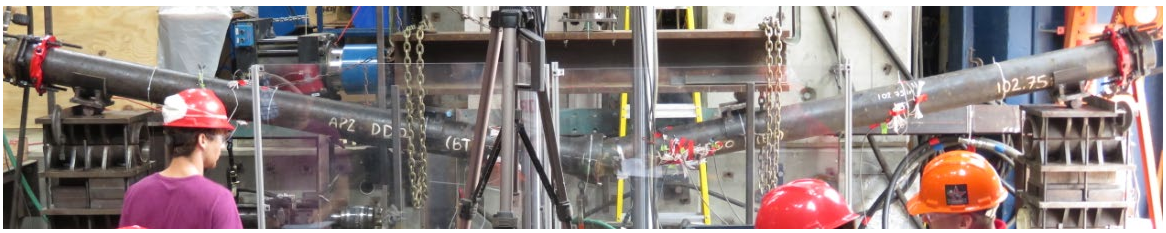

c) Approximately 14° Rotation

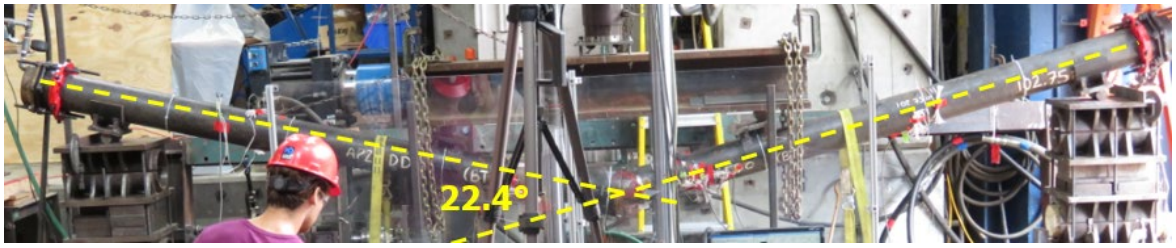

d) 22.4° Rotation

Figure 7.14. AP2 DI Joint at Four Levels of Rotation, or Deflection

Specimen AP1 LADWP broke at the bell without leakage at about 8°. This test as terminated at a rotation of 15° without leakage or loss of internal pressure. Specimen AP1 DI Joint was able to sustain 25.6° of rotation without leakage or loss of water pressure. Specimen AP2 DI Joint failed at a rotation of 22.4° at a location where corrosion pits were located in the pipe barrel. Upon unloading the pipeline started to leak by dripping from the joint at a pressure of approximately 82.5 psi (567 kPa). In each case, the lining was able to sustain locally large deformation and wrinkling without rupture and leakage.

Section 8
Additional Direct Tension Tests

8.1. Introduction

This section summarizes the results of additional direct tension tests on nominal 6 in. (152 mm) diameter pipe specimens lined with AP1 and AP2 by Sanexen in accordance with standard field procedures. The direct tension tests were performed to evaluate the debonding characteristics between the Aqua-Pipe lining and host pipe as well as determine the force versus displacement response of the lined pipe.

A summary of the full-scale direct tension tests performed as part of this investigation is provided in Table 3.1 that includes internal pressure, test pipe specimen length, sampling rate, and whether the pipe was old from the field or new and aged. As explained in Section 9, new cementless, McWane DI pipe was aged with vinegar to produce an interior surface similar to older DI and CI pipelines in the field. Four tests were performed. AP2 DT1 and AP2 DT2 were 8.5-ft (2.6 m)-long with a center crack and lined with AP2 on older CI pipelines from field installations. AP1 JDT1 and AP1 JDT2 were 8.5-ft long with a center crack and lined with AP1 on aged surfaces on new DI pipe. All tests were loaded at a displacement rate of 1 in./min (25.4 mm/min). The data sampling rate was 25 Hz.

8.2. Tension Test Setup

The plan view of the axial tension test setup and equipment for the small load frame used for these tests is provided in Figure 3.2 and photo in Figure 3.4. An actuator, load cell, and load frame were used to apply tensile load to the test specimen in each setup. Each specimen was fitted with end caps to allow for internal pressurization during loading. A photo of the test setup using the small load frame is shown in 3.2. Each test specimen consisted of two pipe sections of equal length on each side of a gap, about 0.25 in. (6 mm) wide, representing a round crack. In the small load frame setup, an actuator and load cell were installed at the south end of the load frame to apply and measure tensile force, respectively. The load cell had a capacity of 110 kips (489 kN).

Table 8.1. Summary of Direct Tension Tests

Test	Pipe Condition	Length ft (m)	Average Pressure psi (kPa)	Sampling Rate Hz
AP2 DT1	New DI Aged	8.5 (2.6)	95.2 (656)	25
AP2 DT2	New DI Aged	8.5 (2.6)	85.7 (591)	25
AP1 JDT1	Old DI From Field	8.5 (2.6)	83.4 (575)	25
AP1 JDT2	Old DI From Field	8.5 (2.6)	82.0 (565)	25

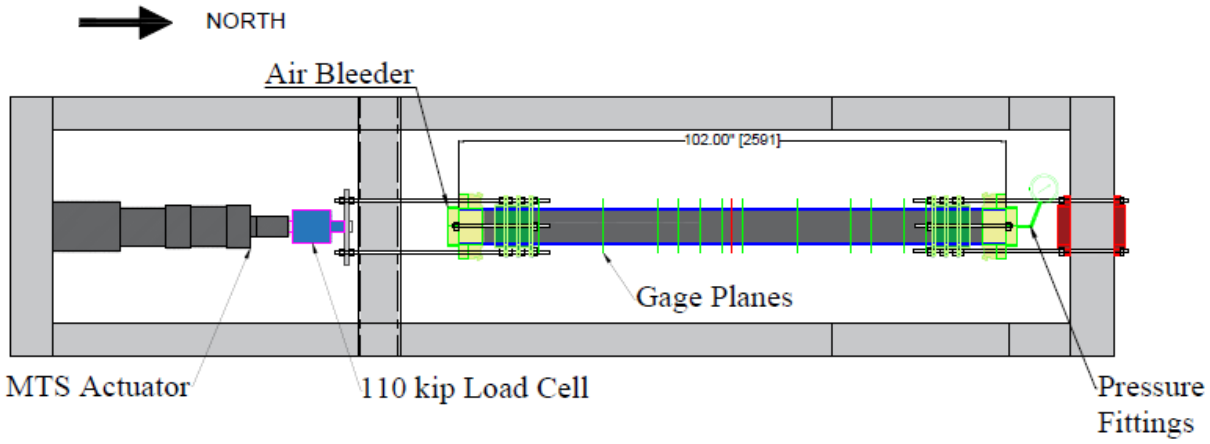

Figure 8.1. Plan View of a Direct Tension Test in the Small Load Frame

As for previous direct tension load tests, two electronic pressure transducers, located at the end cap and water source, measured internal water pressure during the test sequence when internal pressure was applied. String potentiometers (string pots) were attached to both the specimen and restraints to measure axial displacements along the specimen.

Axial strain gages were located on the exterior surface of the pipe specimen at varying distances from the gap at the center of the specimen. The gages were applied at the 12 and 6 o'clock positions around the pipe (crown and invert) for the two AP2 tests. Table 8.2 lists the instrumentation according to name, description, and location for the AP2 tests. For the AP1 tests east and west springline gages were added at the location 4 in. (102 mm) north and south of the centerline. Table 8.3 lists the instrumentation according to name, description, and location for the AP1 tests.

8.3. Test Sequence

After the specimen was instrumented and centered in the test frame, the test sequence was initiated by starting the data acquisition system and laboratory hydraulic systems. As for previous direct tension tests, the loading restraints at either end of the specimen were tightened to avoid end movement due to pressurization. The pipe was pressurized next with a nominal internal water pressure of 80 psi (551 kPa). The tests were performed under displacement control using the servo-hydraulic actuator at the end of the test frame. The actuator was located at the south end the load frame.

Both AP1 and AP2 tests involved debonding from the DI host pipe starting at the centerline and then progressing towards the north and/or south ends. As the debonding front reached each strain gage station, there was a rapid reduction in strain in the DI pipe. This strain gage response was monitored closely to locate the debonding front. As the Aqua-Pipe lining debonded in the north or south direction completely, there as a detachment force that exceeded the anchorage capacity where the lining was connected at the pipe end. Once this capacity was exceeded, the axial force diminished rapidly. Additional cyclic forces developed after the detachment force as the lining was pulled from the pipe.

8.4. Instrumentation and Experimental Results

The following subsections provide the instrumentation plan and key experimental results from the direct tension tests. The axial force versus crack opening, influence of internal pressure, geometric pipe effects, and debonding trends are described and compared in these sections.

8.4.1. AP2 DT1

As indicated in Table 3.1, DT1 was performed with a 8.5-ft (2.6 m)-long specimen in the small load frame. It was tested mostly with a water pressure of 80 psi (551 kPa). For about 20% of the test the water pressure was as high as 138 psi (950 kPa), with 95.2 psi (656 kPa) averaged throughout the test period. The data sampling rate was 25 Hz.

Table 8.2. Instrumentation List for AP2 DT1 and DT2

Location	Instrument Description	Local Instrument Name
47.5 in South of Centerline	Invert, Axial Strain	-47.5I
	Crown, Axial Strain	-47.5C
32 in South of Centerline	Invert, Axial Strain	-32I
	Crown, Axial Strain	-32C
22 in South of Centerline	Invert, Axial Strain	-22I
	Crown, Axial Strain	-22C
12 in South of Centerline	Invert, Axial Strain	-12I
	Crown, Axial Strain	-12C
2 in South of Centerline	Invert, Axial Strain	-2I
	Crown, Axial Strain	-2C
2 in North of Centerline	Invert, Axial Strain	2I
	Crown, Axial Strain	2C
12 in North of Centerline	Invert, Axial Strain	12I
	Crown, Axial Strain	12C
22 in North of Centerline	Invert, Axial Strain	22I
	Crown, Axial Strain	22C
32 in North of Centerline	Invert, Axial Strain	32I
	Crown, Axial Strain	32C
47.5 in North of Centerline	Invert, Axial Strain	47.5I
	Crown, Axial Strain	47.5C
Centerline	Horizontal String Pot	HSP_Crown
		HSP_Invert
Restraining Collars, North of Centerline		N_Slip
Restraining Collars, South of Centerline		S_Slip
Actuator, South of Centerline	Actuator Displacement	Act-Disp

Figure 8.2 shows the axial force versus gap, or crack, opening. Initially, the gripping devices slipped so there are multiple load cycles plotted at the beginning of the test. This region is labeled as regripping of test specimen. The initial gripping device was replaced, and the axial displacement was increased to approximately 10 in. (254 mm) when the test was terminated. The reductions in strain gage measurements were used to track debonding to a maximum load of about 38 kips (169 kN). The load was then cycled once to a new maximum of 40 kips (178 kN), at which point detachment occurred at an axial displacement of about 7.5 in. (190 mm). The force then decreased rapidly as the lining was pulled from the south side of the pipeline specimen.

Table 8.3. Instrumentation List for AP1 J DT1 and JDT2

Location	Instrument Description	Local Instrument Name
47 in South of Centerline	Crown, Axial Strain	-47C
	Invert, Axial Strain	-47I
32 in South of Centerline	Crown, Axial Strain	-32C
	Invert, Axial Strain	-32I
29 in South of Centerline	Crown, Axial Strain	-29C
	Invert, Axial Strain	-29I
22 in South of Centerline	Crown, Axial Strain	-22C
	Invert, Axial Strain	-22I
12 in South of Centerline	Crown, Axial Strain	-12C
	Invert, Axial Strain	-12I
4 in South of Centerline	Crown, Axial Strain	-4C
	East, Axial Strain	-4E
	Invert, Axial Strain	-4I
	West, Axial Strain	-4W
4 in North of Centerline	Crown, Axial Strain	4C
	East, Axial Strain	4E
	Invert, Axial Strain	4I
	West, Axial Strain	4W
12 in North of Centerline	Crown, Axial Strain	12C
	Invert, Axial Strain	12I
22 in North of Centerline	Crown, Axial Strain	22C
	Invert, Axial Strain	22I
29 in North of Centerline	Crown, Axial Strain	29C
	Invert, Axial Strain	29I
32 in North of Centerline	Crown, Axial Strain	32C
	Invert, Axial Strain	32I
47 in North of Centerline	Crown, Axial Strain	47C
	Invert, Axial Strain	47I
Centerline	Horizontal String Potentiometer	HSP_East
		HSP_West
Restraining Collars, North of Centerline		N_Slip
Restraining Collars, South of Centerline		S_Slip
Actuator, South of Centerline	Actuator Displacement	Act-Disp
MTS Actuator LVDT	MTS +/-3"_Disp	MTS_Disp
MTS Load Transducer	MTS-110Kip_Load Xducer	110Kip_Load
Wall Pressure	Pressure Xducer Wall	Pressure
Pipe Pressure at North End	Pressure Xducer Pipe	Pressure Pipe

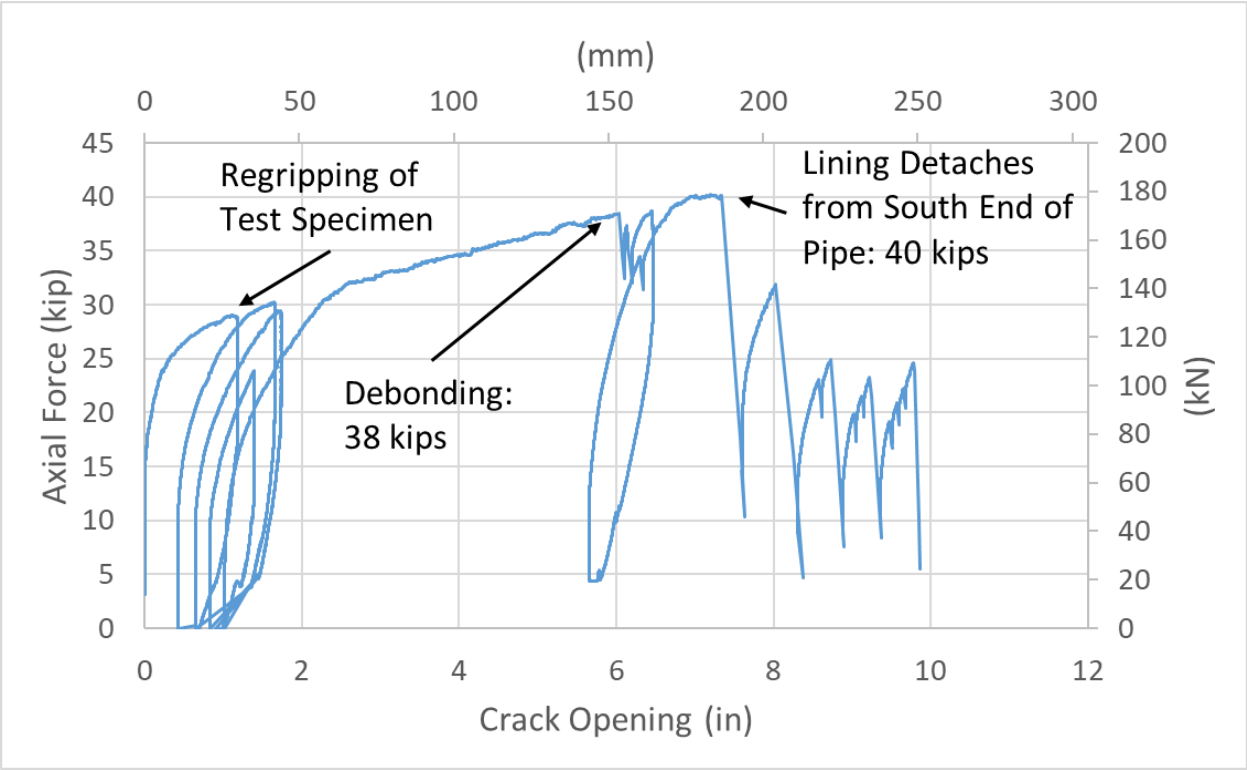

Figure 8.2. Axial Force vs Crack Opening for AP2 DT1

During the last phase of the axial force vs displacement response, increased axial load in the lining was accompanied by a load-induced reduction in lining diameter that caused the lining to lurch forward with decreasing axial load until the lining diameter increased again and came in contact with the inside pipe diameter. As described in Section 3, each axial load cycle was accompanied by a peak axial load and load-induced reduction in lining diameter as the lining lurched forward under constant pipe movement. During each cycle, there was an audible pop or boom as the lining lurched forward.

8.4.2. AP2 DT2

As indicated in Table 3.1, AP2 JDT1 was performed with a 8.5-ft (2.6 m)-long specimen in the small load frame. It was tested with an average of 85.7 psi (591 kPa) pressure at a sampling rate of 25 Hz.

Figure 8.3 shows the axial force versus gap, or crack, opening. Using the same procedures that pertain to Figure 8.2, the maximum debonding force was estimated as 23 kips (102 kN) at about 1 in. (25 mm) of axial displacement. Detachment of the lining occurred at 27 kips (119 kN) and

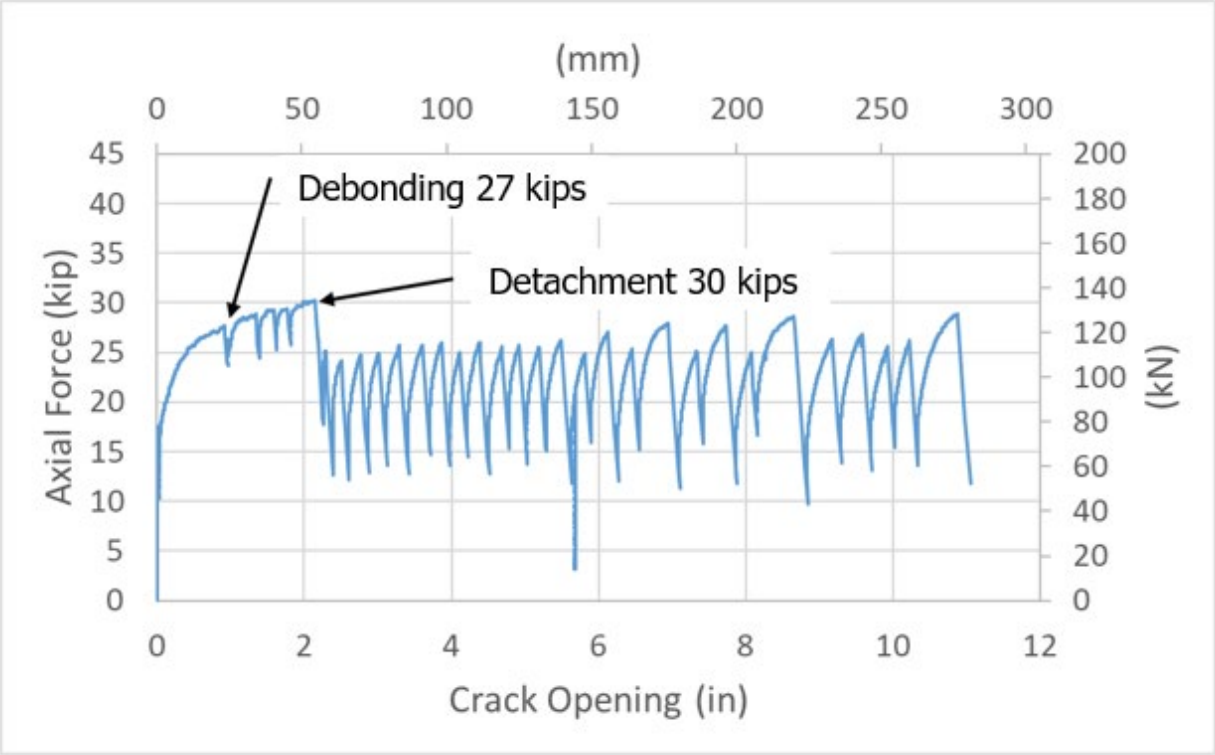

Figure 8.3. Axial Force versus Crack Opening for AP2 DT2

an axial displacement of a little more than 2 in. (51mm). There was a substantial drop in load after this, followed by cyclic forces as the lining was pulled from the south side of the pipe. The cycle forces have the same origin as explained above.

8.4.3. AP1 JDT1

As indicated in Table 3.1, AP1 JDT1 was performed with a 8.5-ft (2.6 m)-long specimen in the small load frame. It was tested with an average of 83.4 psi (575 kPa) pressure at a sampling rate of 25 Hz.

Figure 8.4 shows the axial force versus gap, or crack, opening. Using the same procedures as explained above, the maximum debonding force was estimated as 25 kips (111 kN) at about 1.5 in. (38 mm) of axial displacement. Detachment of the lining occurred at 26 kips (116 kN) and an axial displacement of about 3.5 in. (89 mm). There was a substantial drop in load after this, followed by cyclic forces as the lining was pulled from the south side of the pipe. The cycle forces have the same origin as explained above.

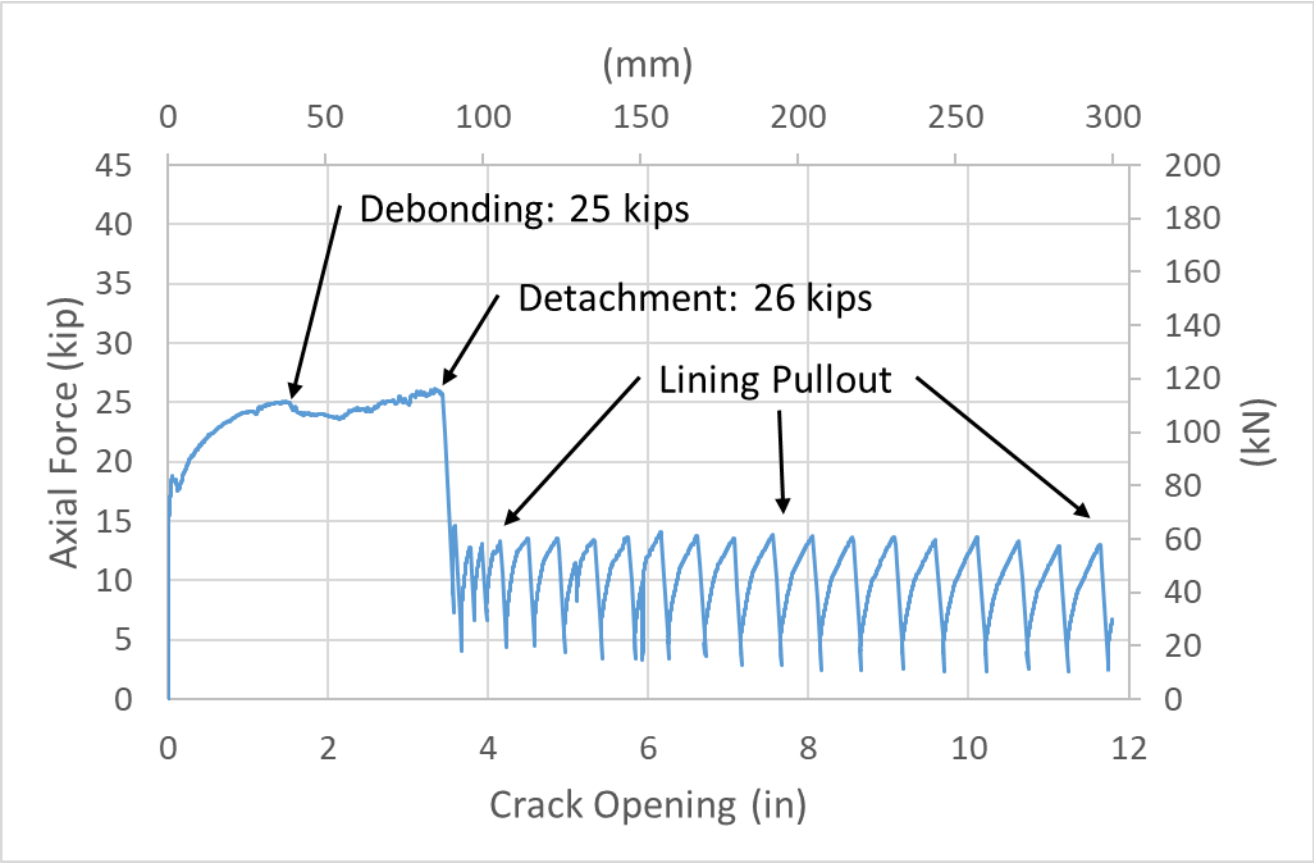

Figure 8.4. Axial Force vs Crack Opening for AP1 JDT1

8.4.4. AP1 JDT2

As indicated in Table 3.1, AP1 JDT2 was performed with a 8.5-ft (2.6 m)-long specimen in the small load frame. It was tested with an average of 82 psi (565 kPa) pressure at a sampling rate of 25 Hz.

Figure 8.5 shows the axial force versus gap, or crack, opening. Using the same procedures as explained above, the debonding was estimated at several levels of crack opening as indicated on the figure. Ultimately, debonding and detachment occurred at a load of 27 kips (119 kN) and an axial displacement of nearly 3.5 in. (89 mm). There was a substantial drop in load after this, followed by cyclic forces as the lining was pulled from the south side of the pipe. The cycle forces have the same origin as explained above, and declined steadily until the test was terminated at an axial displacement of a little over 12 in. (305 mm).

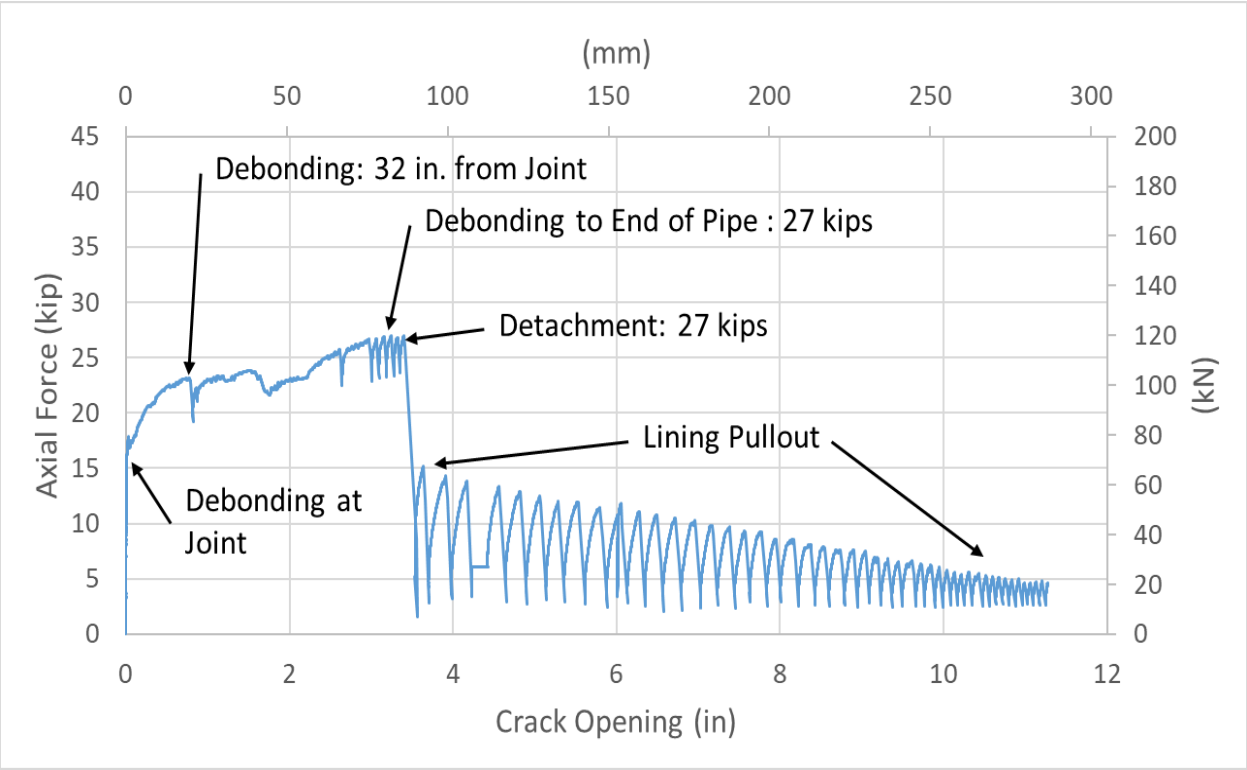

Figure 8.5. Axial Force vs Crack Opening for AP1 JDT2

8.5. Summary of Additional Direct Tension Tests

This section summarizes the results of additional direct tension tests on nominal 6 in. (152 mm) diameter pipe specimens lined with AP1 and AP2 by Sanexen in accordance with standard field procedures. The direct tension tests were performed to evaluate the debonding characteristics between the Aqua-Pipe lining and host pipe as well as determine the force versus displacement response of the lined pipe.

Four tests were performed. AP2 DT1 and AP2 DT2 were 8.5-ft (2.6 m)-long with a center crack and lined with AP2 on older CI pipelines from field installations. AP1 JDT1 and AP1 JDT2 were 8.5-ft long with a center crack and lined with AP1 on artificially aged DI interior surfaces. All tests were loaded at a displacement rate of 1 in./min (25.4 mm/min). The data sampling rate was 25 Hz. The equipment was similar to that previously used for direct tension tests.

Specimens AP1 JDT1 and AP1 JDT2 show debonding forces of 25 kips (111 kN) and 27 kips (119 kN) and detachment forces at 26 kips (116 kN) and 27 kips (119 kN). The detachment displacement is between 3.5 in. and 4.5 in. (89 and 114 mm), respectively. For Specimen AP2 DT2 the maximum debonding and detachment forces are similar at 23 kips (102 kN) and 27 kips

(119 kN) at about 1 in. (25 mm) and 2 in. (51 mm) of relative displacement, respectively. Specimen AP2 DT1 provides higher debonding and detachment forces of 38 kips (169 kN) and 40 kips (178 kN) at axial displacements of 6 in. (152 mm) and 7.5 in. (190 mm), respectively.

The tests show debonding and detachment forces well below of the axial capacity of the AP2 lining, which is about 62 kips (278 kN) for the nominal 6-in. (102 mm)- diameter pipeline. The forces are not increased by the presence of joints. All test data should a significant drop in axial load immediately after detachment, followed by cyclic forces that are generated by the lining being pulled from the test pipeline.

Section 9
Large Scale Testing of Fault Rupture Effects

9.1. Introduction

This section presents the results of the large-scale fault rupture test performed with a DI pipeline lined with Aqua-Pipe™ Generation 2 (AP2). All testing was performed in the large-scale test basin at the Cornell University Large Scale Lifelines Testing Facility. The pipeline was lined by personnel from Sanexen in the large-scale test basin according to the field procedures followed by Sanexen. The DI pipe was manufactured by McWane Ductile as a cementless pipe have a laying length of 18 ft. (5.49 m) with Tyton Joints (push-on joints), each with a depth of 3.38 in. (85.85 mm) and an elastomeric gasket. The average pipe outer diameter was 6.74 in. (171 mm). The pipe had an average wall thickness of 0.288 in. (7.32 mm) and cross-sectional area of 5.84 in^2 (3768 mm^2) as measured at different locations by laboratory personnel. Tensile coupon tests of McWane DI pipe give an average yield strength of 52.7 ksi (363 MPa) and proportional limit stress of 32.8 ksi (226Mpa). The average Young's modulus for both McWane (Pariya-Ekkasut et al. 2018) and American (Stewart et al, 2017) DI pipe is 24,200 ksi [167 GPa]. The average lining thickness was 0.192 in. (4.87 mm) and the cross-sectional area was 3.18 $in.^2$ (2052 mm^2).

The DI pipeline acts as a proxy for CI pipelines with weak pullout capacity of the joints and round crack. To match the field performance of new DI and older CI field pipelines, oxides need to be removed from the interior surface of cementless DI pipe and the pipe surface aged. As described by Sanexen (Giacometti and Jadani, 2019), the interior surface of the pipes was aged to the field condition of CI pipes by exposure to 10% acetic acid for 3 days and no additional cleaning of the pipe interior. These measures were undertaken before the pipeline was assembled and lined. As discussed in Section 2, unused AP2 lining material was taken from the northern end of the fault rupture test specimen by Sanexen personnel after lining installation. Tensile coupon specimens in the warp and weft directions were performed by CDCQ (2019).

9.2. Experimental Setup

Figure 9.1 is a plan view of the test layout, which shows the fault rupture plane and approximate locations of the four actuators generating basin movement. The pipeline consisted of five DI pipe segments with four DI joints positioned at 5 ft. (1.5 m) and 15 ft. (4.6 m) on either side of the fault. The five test pipeline segments were cut by Sanexen according to directions from Cornell to the

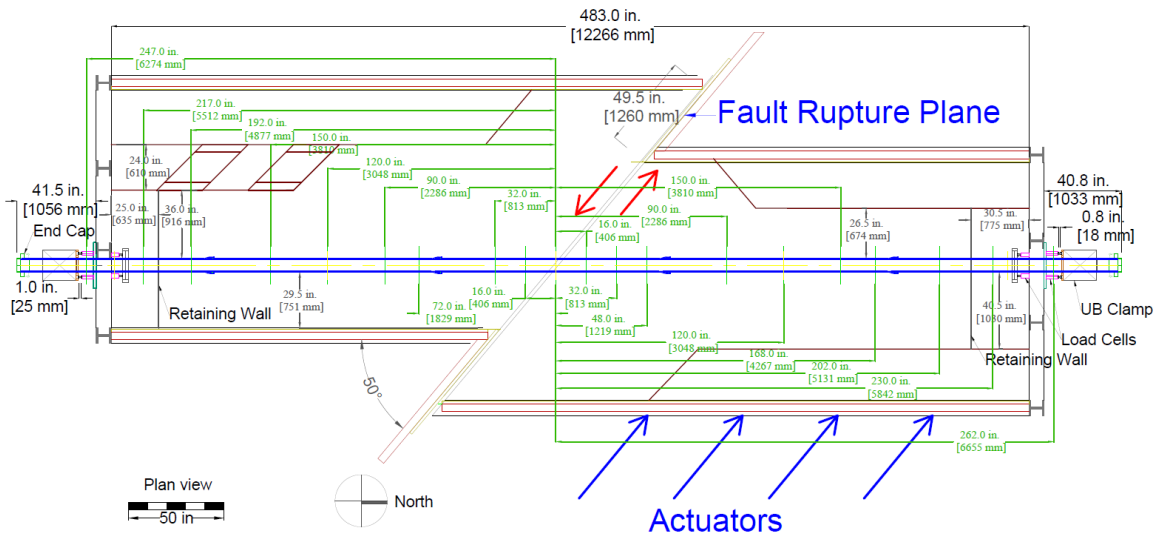

Figure 9.1. Plan View of Pipe Centered DI Pipeline with AP2 Lining in Test Basin

dimensions in the figure, lined, and then shipped to Cornell. The intersection angle between the pipe and fault was 50°.

The objective of the test was to impose abrupt ground deformation on the pipeline, which was representative of left lateral strike slip fault rupture and the most severe ground deformation that occurs along the margins of liquefaction-induced lateral spreads and landslides. The pipeline was constructed to evaluate its capacity to accommodate full-scale fault movement through the simultaneous axial pullout of the lining at four different DI joints. Measuring simultaneous performance of multiple joints allows for confirmation that the pipeline will respond to ground failure as intended, understand the complex interaction among the different joints, and determine the maximum ground deformation and axial pipeline load that can be sustained.

The pipeline was buried in the Cornell large-scale test basin in partially saturated sand that was compacted to an average, direct shear peak friction angle of $\phi' = 40^{o}$ (Jung et al., 2013 and 2016), equivalent in strength to that of a medium dense to dense granular backfill. The pipeline was assembled so that the spigot was pushed completely into the bells, which faced north. During the test, the south part of the basin remained stationary, while the north part was displaced to the northwest by large-stroke actuators to cause soil rupture and slip at the interface between the two parts of the test basin.

A 120-in. (3.05-m)-long pipe section was placed so that its center was directly over the fault, with an intersection angle of 50^{o}. Two identical 120-in.-(3.05-m)-long pipes were installed both north and south of the center pipe. The 6.16-in. (156-mm) outer-diameter pipe was placed on a bed of soil about 10 in. (254 mm) in depth. The depth of burial to top of pipe was approximately 32 in. (813 mm) resulting in 48 in. (1.22 m) of total soil depth.

The simulated fault rupture caused both tensile and bending strains in the pipeline. The length of the pipeline buried in soil, also described as "test portion," was approximately 36 ft. (11 m) long. The pipe was pressurized with water at an average 81.3 psi (561 kPa). The north (movable) portion of the test basin was connected to four MTS hydraulic actuators with load cells controlled by a MTS Flextest GT controller. All actuators were operated in synchronized displacement control.

9.2.1. Test Procedure

The general test procedure, after all instruments were installed, soil placed, and pipe filled with water, was:

a) Begin data acquisition and start the servo-controlled hydraulic system,
b) Introduce and verify internal water pressure,
c) Move the test basin at a rate of 2 in./minute (51 mm/minute) until full displacement of the actuators driving fault rupture
d) Stop basin movement but maintain hydraulic actuator pressure,
e) Verify data acquisition with a sampling rate of 10 Hz,
f) Excavate.

At a fault displacement of 48 in. (1219 mm), the internal pressure was maintained at approximately 81.3 psi (561 kPa) with no leakage in the pipeline. The test was then stopped.

9.2.2. Instrumentation

Figure 9.1, a plan view of the test layout, shows the locations of the instruments along the test pipeline. Table 9.1 provides the number of strain gage station locations with respect to the fault. The instrumentation consisted of strain gages at twenty locations (gage planes) along the pipeline, load cells at the ends of the pipeline, and string pots to measure joint displacements and rotations. Ninety-six strain gages were installed in twenty locations along the pipeline to measure strains and

Table 9.1. Strain Gage Locations and Coding for Sanexen Fault Rupture Test

Gage Station	Gages	Distance from Fault
(-247)	S247CA-Crown, Axial S247CC-Crown, Circumferential S247IA-Invert, Axial S247IC-Invert, Circumferential S247EA-East Springline, Axial S247EC-East Springline, Circumferential S247WA-West Springline, Axial S247WC-West Springline, Circumferential	(-) 247 in. (6.27 m)
(-217)	S217CA-Crown, Axial S217IA-Invert, Axial S217EA-East Springline, Axial S217WA-West Springline, Axial	(-) 217 in. (5.51 m)
(-192)	S192CA-Crown, Axial S192IA-Invert, Axial S192EA-East Springline, Axial S192WA-West Springline, Axial	(-)192 in. (4.88 m)
(-150)	S150CA-Crown, Axial S150IA-Invert, Axial S150EA-East Springline, Axial S150WA-West Springline, Axial	(-) 150 in. (3.81 m)
(-120)	S120CA-Crown, Axial S120IA-Invert, Axial S120EA-East Springline, Axial S120WA-West Springline, Axial	(-) 120 in. (3.05 m)
(-90)	S90CA-Crown, Axial S90IA-Invert, Axial S90EA-East Springline, Axial S90WA-West Springline, Axial	(-) 90 in. (2.29 m)
(-72)	S72CA-Crown, Axial S72CC-Crown, Circumferential S72IA-Invert, Axial S72IC-Invert, Circumferential S72EA-East Springline, Axial S72WA-West Springline, Axial	(-) 72 in. (1.83 m)
(-32)	S32CA-Crown, Axial S32IA-Invert, Axial S32EA-East Springline, Axial S32WA-West Springline, Axial	(-) 32 in. (0.81 m)
(-16)	S16CA-Crown, Axial S5IA-Invert, Axial S16EA-East Springline, Axial S15WA-West Springline, Axial	(-) 16 in. (0.41 m)

Table 9.1. Strain Gage Locations and Coding for Sanexen Fault Rupture Test (Continued)

0	0CA-Crown, Axial 0CC-Crown, Circumferential 0IA-Invert, Axial 0IC-Invert, Circumferential 0EA-East Springline, Axial 0EC-East Springline, Circumferential 0WA-West Springline, Axial 0WC-West Springline, Circumferential	0
(+16)	N16CA-Crown, Axial N16IA-Invert, Axial N16EA-East Springline, Axial N16WA-West Springline, Axial	(+) 16 in. (0.41 m)
(+32)	N32CA-Crown, Axial N32IA-Invert, Axial N32EA-East Springline, Axial N32WA-West Springline, Axial	(+) 32 in. (0.81 m)
(+48)	N48CA-Crown, Axial N48IA-Invert, Axial N48EA-East Springline, Axial N48WA-West Springline, Axial	(+) 48 IN (1.22 m)
(+90)	N90CA-Crown, Axial N90CC-Crown, Circumferential N90IA-Invert, Axial N90IC-Invert, Circumferential N90EA-East Springline, Axial N90WA-West Springline, Axial	(+) 90 in. (2.29 m)
(+120)	N120CA-Crown, Axial N120IA-Invert, Axial N120EA-East Springline, Axial N120WA-West Springline, Axial	(+) 120 in. (3.05 m)
(+150)	N150CA-Crown, Axial N150IA-Invert, Axial N150EA-East Springline, Axial N150WA-West Springline, Axial	(+) 150 in. (3.81 m)
(+168)	N168CA-Crown, Axial N168IA-Invert, Axial N168EA-East Springline, Axial N168WA-West Springline, Axial	(+) 168 in. (4.27 m)
(+202)	N202CA-Crown, Axial N202IA-Invert, Axial N202EA-East Springline, Axial N202WA-West Springline, Axial	(+) 202 in. (5.13 m)

Table 9.1. Strain Gage Locations and Coding for Sanexen Fault Rupture Test (Completed)

Gage Station	Gages	Distance from Fault
(+230)	N230CA-Crown, Axial N230IA-Invert, Axial N230EA-East Springline, Axial N230WA-West Springline, Axial	(+) 230 in. (5.84 m)
(+262)	N262CA-Crown, Axial N262CC-Crown, Circumferential N262IA-Invert, Axial N262IC-Invert, Circumferential N262EA-East Springline, Axial N262EC-East Springline, Circumferential N262WA-West Springline, Axial N262WC-West Springline, Circumferential	(+) 262 in. (6.66 m)

(–) = South, (+) = North

to evaluate axial forces and bending moments. Strain gages were positioned at the crown (C) and invert (I), and at the east (E) and west (W) springlines of the pipe. Strain gage locations were chosen on the basis of the expected deformed shape and axial behavior of the pipeline as determined from direct tension and four-point bending tests performed at Cornell University.

The tension on the pipeline was maintained by compression clamps on the pipe at both the north and south ends of the test basin. These clamps were developed by research personnel at the University of Buffalo (e.g., Zhong et al. 2014) and used in tests performed at Cornell University (e.g., Pariya-Ekkasut, 2018). The compression clamps were tested before the fault rupture test to confirm pullout capacities exceeding tensile rupture loads in the AP2 lining. In addition, the compression clamps were in contact with a bead that was welded to the external surface of the test pipeline at both the north and south ends of the test basin.

After the instrumentation was installed, protective metal shielding was wrapped around the joint. Figure 9.2 is a photo of the pipe joint with protective shielding. Three string pots were placed at each joint to measure the joint pullout and rotation, as well as spigot to bell face relative movement. Figure 9.3 is a photo of the wooden support behind the metal shielding that establishes the location and support for the string pots, and provides support for the shielding. The metal shielding consisted of two thin, metal sheets that could move longitudinally with respect to each other.

Figure 9.2. Joint Instrumentation Protective Shielding

Figure 9.3. Instrumentation String Pot Set Up and Wooden Support

Table 9.2 provides the locations and the labeling of the joint string pots to measure joint pullout and rotation. All string pots were set to measure 15 in. (381 mm) of joint pullout, and the shielding was set to move 16 in. (406 mm) before full longitudinal separation between the inner and outer sheets occurred. String pots were also set at the north and south ends of the test basin to measure as much as 10 in. (25 mm) of longitudinal separation between the test basin and crown of the pipeline. Linear Variable Differential Transformers (LVDTs) were established on the east and west sides to measure as much as 2 in. (51 mm) of separation between the north and south surfaces of the fault rupture plane.

Four calibrated load cells were positioned at each end of the test basin. Table 9.3 provides the locations and the labeling of the load cells. Thirty-six survey marks were scribed along the crown of the test pipeline at approximately 12-in. (305-mm) intervals. The pipeline was surveyed with a total station instrument prior to burial to determine its initial position, and again after the test, to provide a measure of global pipeline deformation.

Table 9.2. Displacement Transducer Locations and Labeling for Split-Basin Test

Location	Displacement Transducer	Type and Stroke
S Slip	S Slip – Crown	String pot + 10 in.
South Joint	S Disp C – Crown S Disp E – East Springline S Disp W – West Springline	String pot + 15 in. String pot + 15 in. String pot + 15 in.
South Middle Joint	SM Disp C – Crown SM Disp E – East Springline SM Disp W – West Springline	String pot + 15 in. String pot + 15 in. String pot + 15 in.
North Middle Joint	NM Disp C – Crown NM Disp E – East Springline NM Disp W– West Springline	String pot + 15 in. String pot + 15 in. String pot + 15 in.
North Joint	N Disp C – Crown N Disp E – East Springline N Disp W – West Springline	String pot + 15 in. String pot + 15 in. String pot + 15 in.
N Slip	N Disp – Crown	String pot + 10 in.
East Fault	East Fault	LVDT +/- 2 in.
West Fault	West Fault	LVDT +/- 2 in.

Table 9.3. Load Cell and Pressure Transducer Locations and Labeling for Split-Basin Test

Location	Force Transducer	Type

South End Outside	SEC –East, Crown
	SEI –East, Invert
	SWC –West, Crown
	SWI –West, Invert
		6” Steel, Gaged Cylinder
		6” Steel, Gaged Cylinder
		6” Steel, Gaged Cylinder
		6” Steel, Gaged Cylinder

South End Inside	SPE –East, Crown SPW –West, Invert	4” Steel, Gaged Cylinder 4” Steel, Gaged Cylinder
North End Inside	NEC – Outer, East, Crown NWI – West, Invert	4” Steel, Gaged Cylinder 4” Steel, Gaged Cylinder
North End Outside	NEC –East, Crown NEI –East, Invert NWC –West, Crown NWI–West, Invert	6” Steel, Gaged Cylinder 6” Steel, Gaged Cylinder 6” Steel, Gaged Cylinder 6” Steel, Gaged Cylinder
High Bay Wall	Wall Pressure Px309-500G5V	500 psi Pressure Transducer
South End Cap, Pipe	Pipe Pressure Px309-100G5V	100 psi Pressure Transducer

9.2.3. Soil Preparation

The soil used during the test was crushed, washed, glacio-fluvial sand obtained from RMS Gravel, Dryden, NY, consisting of particles mostly passing the ¼ in. (6.35 mm) sieve. Figure 9.4 is the grain size distribution of the RMS graded sand. Approximately 6-in. (152-mm)-thick lifts of soil were placed and compacted until there was about 32 in. (813 mm) cover of compacted sand above

the pipe crown. Every layer was compacted to the same extent and moistened with water in a similar way to achieve uniformity. Dry density measurements were taken for each layer using a Troxler Model 3440 densitometer. Moisture content measurements were obtained using both soil samples and the densitometer at the same locations.

The target value of dry density was γ_{dry} = 109 lb/ft^3 (17.1 kN/m^3), and the target value of moisture content was w = 4.0 %. Eight measurements of dry unit weight and moisture content were made for each soil lift at the different locations shown in Figure 9.5. Table 9.4 and Table 9.5 presents the measured dry soil, unit weights and moisture contents. The overall average and standard deviation of dry unit weight measurements were 108.9 lb/ft^3 (17.0 kN/m^3) and 1.5 lb/ft^3 (0.24 kN/m^3), respectively. Moisture content measurement had an average of 3.9% and standard deviation of 0.48%. As described previously, these values correspond to a direct shear peak friction angle of $\phi' = 40^o$ (Jung et al., 2013 and 2016), equivalent in strength to that of a medium dense to dense granular backfill.

9.3. Experimental Results of Split Basin Test

9.3.1. Test Basin Movements

Four actuators are connected between the movable portion of the test basin and the modular reaction wall in the laboratory. From south to north, the actuators are identified as short-stroke actuator 1 (SSA1), short-stroke actuator 2 (SSA2), long-stroke actuator 1 (LSA1), and long-stroke actuator 2 (LSA2). Each SSA actuator has a displacement range of ± 2 ft (± 0.61 m) for a total stroke of 4 ft (1.22 m) and load capacity of 100 kips (445 kN) tension and 145 kips (645 kN) compression. Each LSA actuator has a displacement range of ± 3 ft (0.91 m) for a total stroke of 6 ft (1.83 m) and load capacity of 63 kips (280 kN) tension and 110 kips (489 kN) compression.

Figure 9.6 shows the average displacement of the four actuators, which is equivalent to the fault displacement, with respect to time. The fault movement increased at a constant slope equal to the rate of imposed displacement of 2 in./min. (51 mm/min.) until a constant fault displacement of 48 in. (1.22 m) equal to the maximum stroke set for the actuators

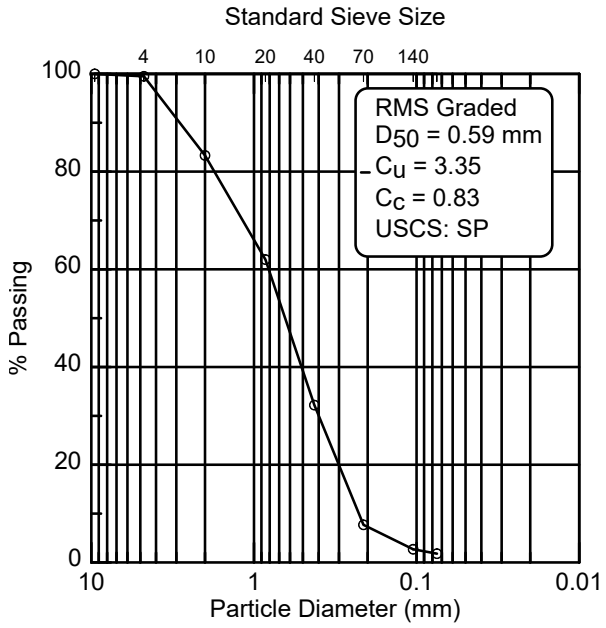

Figure 9.4. Particle Size Distribution of RMS Graded Sand

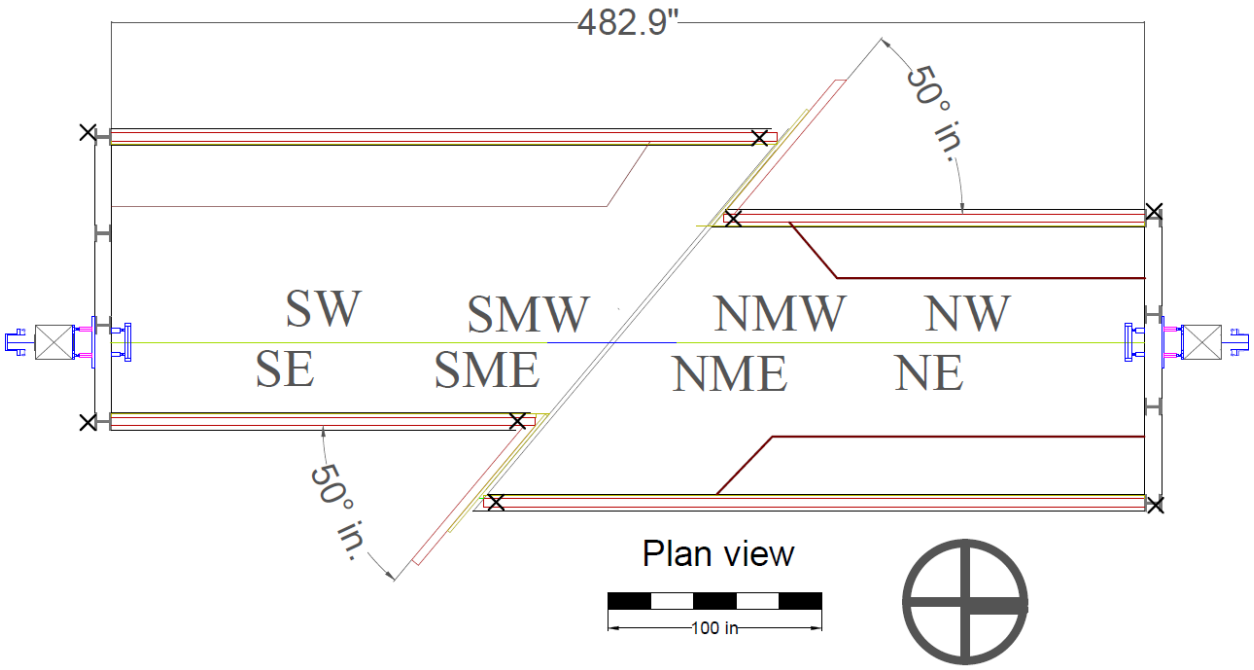

Figure 9.5. Plan View of Compaction Measurement Locations

9.3.2. Internal Water Pressure

The pipe was filled with water and pressurized to an average 81.3 psi (561 kPa). The basin movement caused the pipe to increase in overall length, causing slight fluctuations in pressure.

Table 9.4. Sanexen Split Basin Test Soil Dry Unit Weights

	Dry Unit Weights (lb/ft^3)				
Location	Lift 1	Lift 2	Lift 3	Lift 4	Lift 5
NNW	109.4	107.2	108.7	107.6	108.5
NW	110.2	108.2	107.4	109.7	112.4
SSW	107.1	109.8	107.1	105.5	108.9
SW	107.3	109.8	107.5	108.7	109.9
SE	107.2	110.0	107.5	109.3	110.3
SSE	109.4	110.7	108.4	105.5	107.8
NE	112.4	110.6	110.4	111.0	110.3
NNE	108.6	110.1	107.3	107.6	109.7
Average	108.6	109.6	108.0	108.1	109.7
Stdev	1.8	1.2	1.1	1.9	1.4
Global Average					108.9
Global Stdev					1.5

1 (lb/ft^3) = 0.1571 kN/m^3

Table 9.5. Sanexen Split Basin Test Soil Water Content Data from Moisture Tins

	Moisture Tin Water Content, w (%)				
Location	Lift 1	Lift 2	Lift 3	Lift 4	Lift 5
NNW	4.3	3.5	5.0	3.5	3.9
NW	4.6	3.1	4.1	3.8	3.6
SSW	4.0	3.1	5.3	4.7	4.2
SW	4.4	3.1	3.4	3.9	3.7
SE	3.5	3.0	3.4	4.0	3.3
SSE	4.2	2.8	4.5	4.2	4.3
NE	2.9	2.9	4.5	3.4	4.0
NNE	4.1	2.8	5.5	3.5	4.4
Average	4.0	3.0	4.5	4.2	3.9
Stdev	0.56	0.25	0.77	0.45	0.39
Global Average					3.9
Global Stdev.					0.48

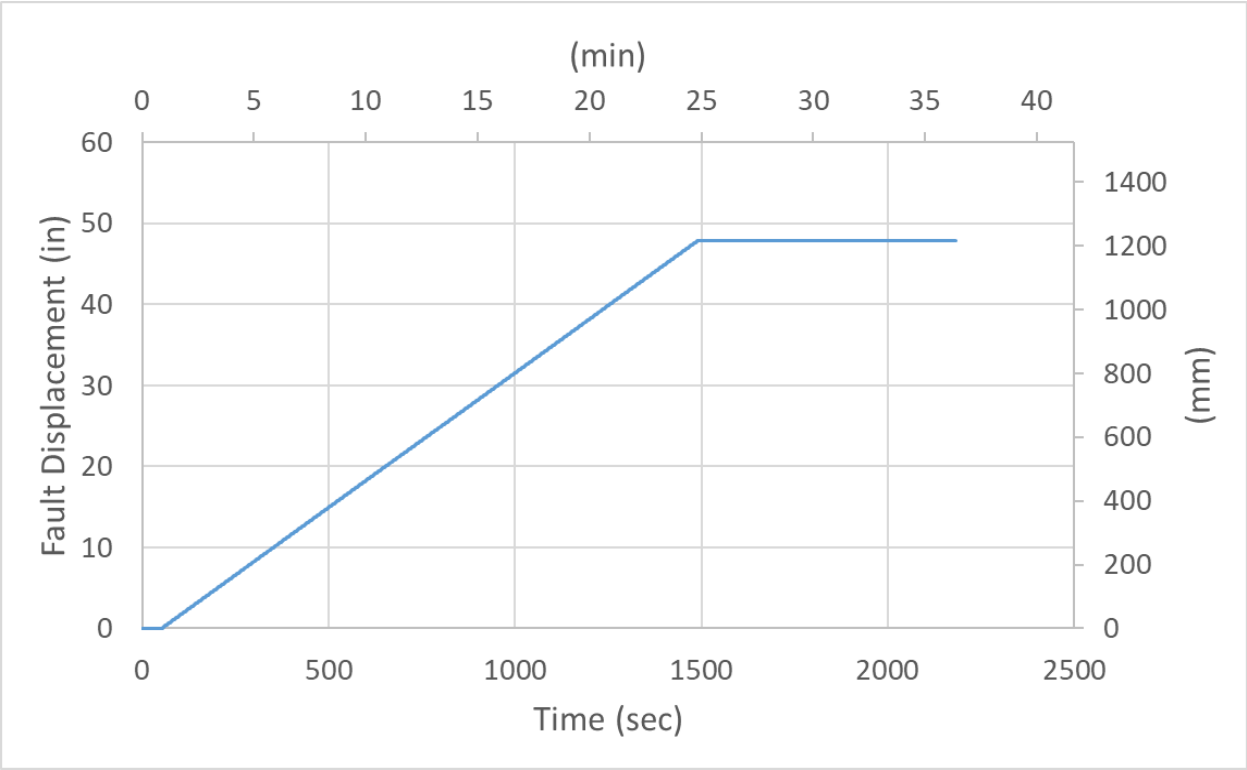

Figure 9.6. Fault Rupture Displacement versus Time

These pressure variations are shown in Figure 9.7 that displays the pipe internal pressure vs. fault displacement. When the test was stopped, water was drained from the pipe. The actuator displacement was maintained until total station positions of the excavated pipeline were surveyed.

9.3.3. Joint Pullout

The joint pullout movements were measured using string potentiometers (string pots). The string pot locations are given in Section 9.2.2 and shown in Table 9.2. Each joint had a total of three string pots, one at the crown and two at the springline locations, which are described in connection with Figure 9.2. The pullout at each joint is plotted vs the fault displacement in Figure 9.8.

The pullout begins first on the South Middle Joint. Experimental and analytical results show that pipeline pulls towards the fault. At the South Middle joint there is axial resistance to pullout of the north facing bell, so that movement initiates as the spigot moves towards the fault. The North Middle Joint moves after the South Middle Joint because more axial resistance occurs at this joint

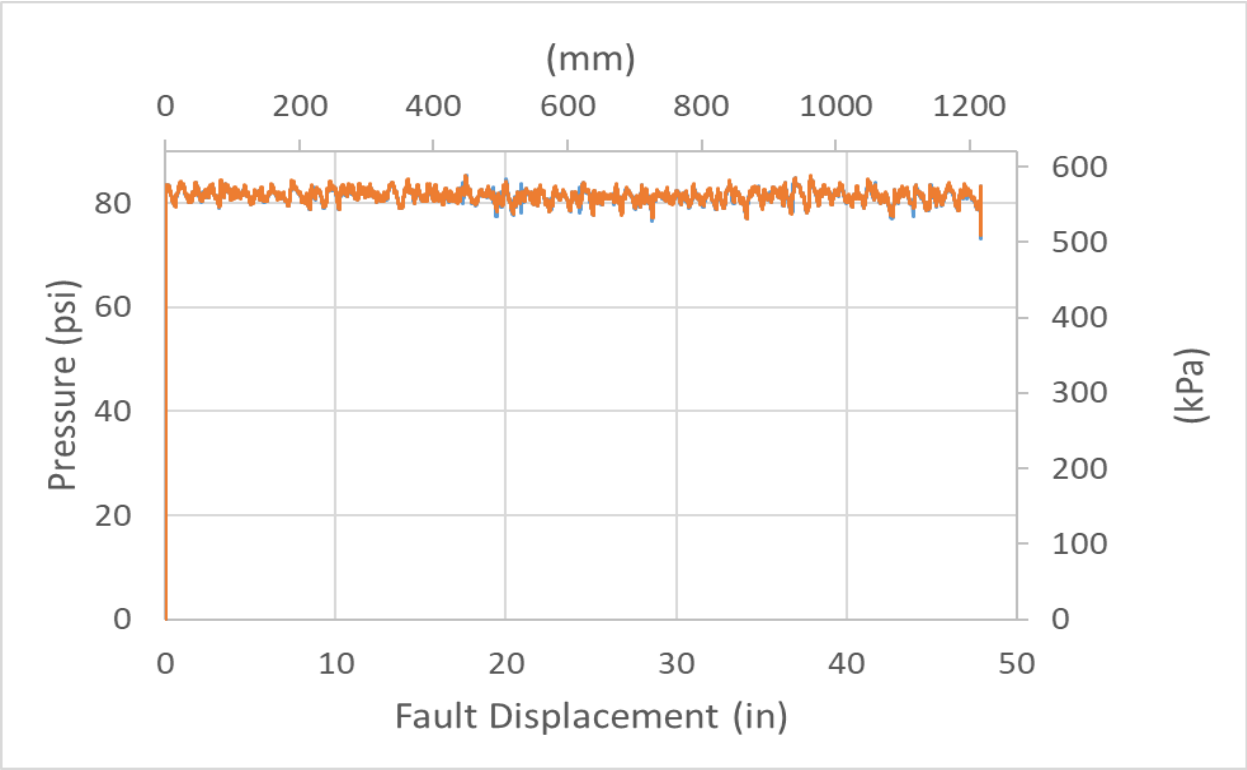

Figure 9.7. Internal Water Pressure vs. Fault Displacement

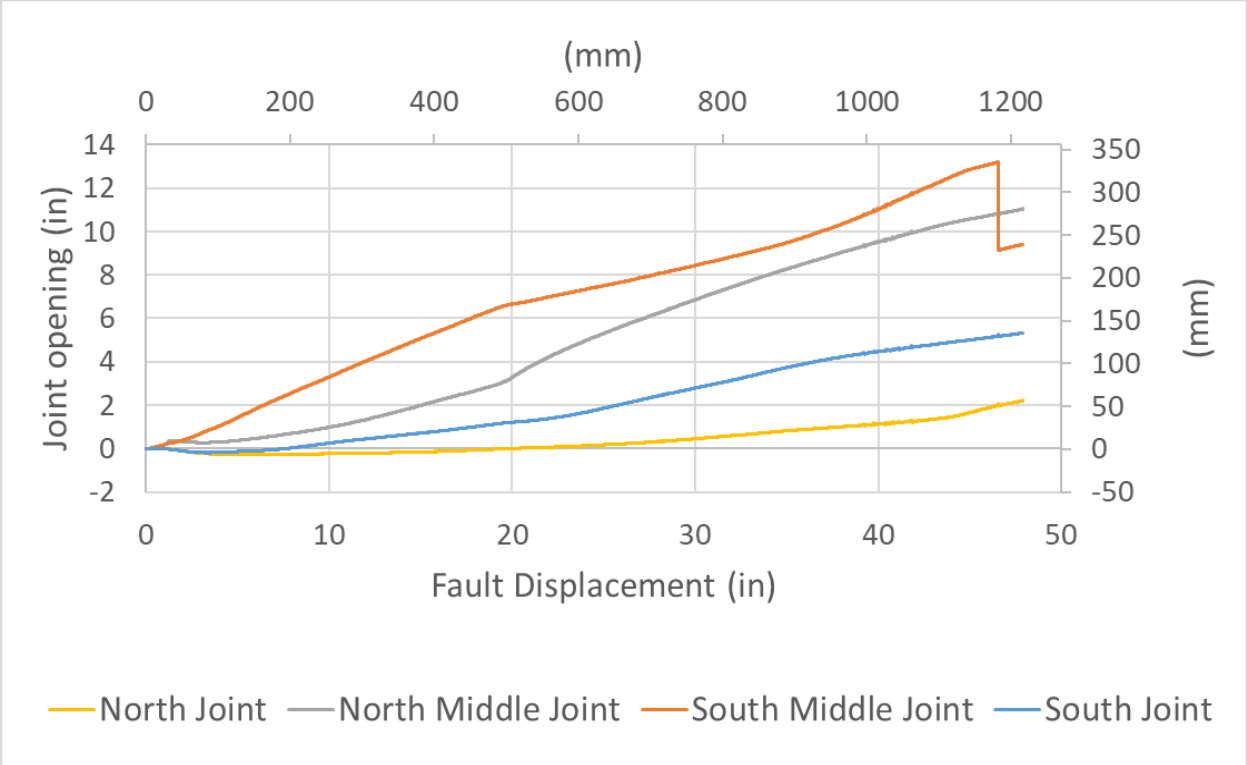

Figure 9.8. Joint Openings vs. Fault Displacement

as the curved bell moves toward the fault. Thus, the second joint to move is the North Middle Joint, followed by the South Joint and then the North Joint. This systematic response to fault displacement has been observed in other tests (e.g., Cornell University, 2015). At 47 in. (1194 mm) of fault displacement there is an abrupt decline in South Middle Joint movement, corresponding to distortion in the string pot readings. The axial movement is $d_f \cos\beta$, where d_f = 47 in. (1194 mm) of fault displacement and β = angle of pipeline/fault intersection = 50°. Thus, axial movement is (47 in.) $\cos\beta$ = (47in.) cos(50°) = 30.2 in. (762 mm). The sum of the axial displacements of all four joints at 47 in. (1194 mm) of fault displacement is nearly 29.5 in. (749 mm), which is in close agreement with the theoretical extension of the pipeline.

9.3.4. Joint Rotations (Deflections)

Joint rotations (deflections) were determined using the string pots at the springlines of each joint and using survey measurements. In this report "deflection" is used to describe the angular deflection of the pipe, consistent with industry usage.

Joint rotation is calculated from the string pot measurements at each joint as:

$$\text{Rotation}\left(\text{deg}\right) = \tan^{-1}\left(\frac{\text{East String Pot Displacement} - \text{West String Pot Displacement}}{\text{Separation Distance between the String Pots}}\frac{180}{\pi}\right) \quad (9.1)$$

The joint deflections are shown in Figure 9.9. The predominant part of the joint rotation occurs at the south and north joints closest to the fault. At about 47 in. (1194 mm) of fault displacement there is evidence of distortion in the spring pot readings for the South Middle Joint closest to the fault. The maximum rotation of the joints closest to the fault must account for an increase in pipeline length equal to the sum of the South Middle and North Middle Joints at 47 in. (1194 mm) of fault displacement. From Figure 9.8 this sum is 24 in. (610 mm). The average rotation of the joints nearest to the fault are $\alpha = \tan^{-1}[(47\text{ in.})\sin(50°)/(120 + 24)\text{in.}] = 14.0°$. The actual rotation of these joints was measured as 13.0° - 14.0°. The measured and theoretical rotations are in good agreement.

The Bovay Laboratory uses a general coordinate system established in 2012 as part of Cornell's participation in the George E. Brown, Jr. Network for Earthquake Engineering Simulation (NEES). The coordinate system was developed using a Leica Flexline TS02 reflectorless total station to

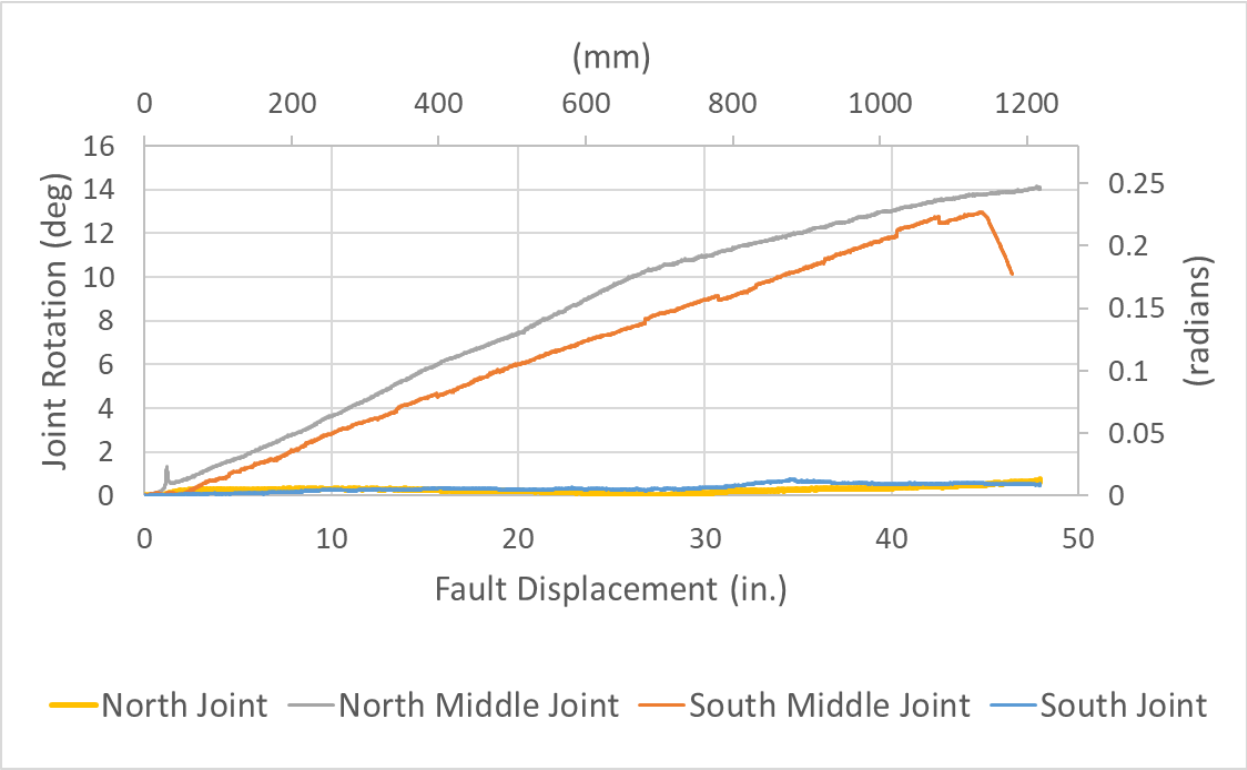

Figure 9.9. Joint Rotation versus Fault Displacement

identify baseline positions within the laboratory. When the pipeline with AP2 was placed in the basin and backfilled to approximately the springline depth, survey measurements were taken at marked locations every 12 in. (25 mm) along the pipe crown. These data provide a baseline of the initial pipe position, albeit prior to complete backfill. Following careful pipe excavation with minimal disturbance, the pipeline was re-surveyed. These data provide very close locations of the maximum pipe displacement at the maximum basin displacement.

Figures 9.10 shows, at actual scale, the Leica data for the initial and final pipeline positions. The survey data were used to estimate the overall joint rotations, or deflections, at the South and North Middle Joints of 13.8° and 12.9°, respectively. These survey measurements are very close to the maximum rotations between 13.0° and 14.0° of the South and North Middle Joints as measured by the string pots.

9.3.5. End Loads and Pipe Axial Forces

The axial tensile loads were measured with four load cells at the south end of the test basin and four load cells at the north end. The sum of the four load cells at each end of the test basin gives the total axial end load. As shown in Figure 9.1 and listed in Table 9.1, there are two strain gage

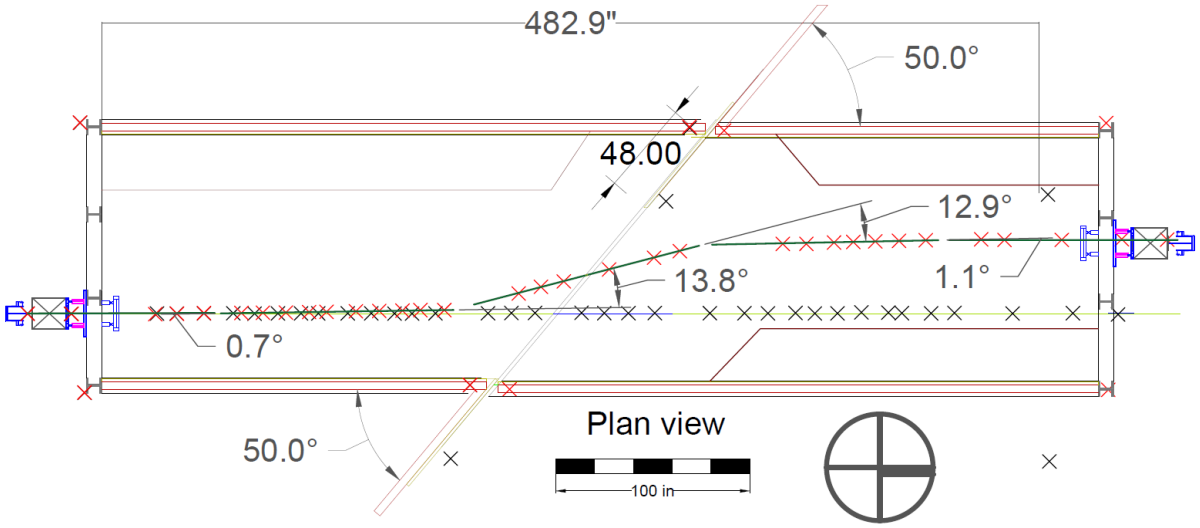

Figure 9.10. Leica Survey Showing Deformed Pipeline with AP2 Lining after Fault Rupture Test

planes outside the soil near the north end of the pipeline at Stations 230 and 262. There was no debonding of the AP2 lining at Stations 230 and 262. Thus, the combined axial load in the pipe and lining at each of those stations should be equal to the axial force as the north end of the basin as measured by the load cells.

The axial force in the DI pipe from average strain gage measurements was calculated as $F_P = \varepsilon_M A_P E_P$. As previously indicated, the pipe had an average wall thickness of 0.288 in. (7.31 mm) and a cross-sectional area of the pipe, A_P = 5.29 in^2 (3413 mm^2), with an average Young's modulus, E_P = 24,200 ksi (167 GPa). When there is no debonding, the axial forces are also carried, to a much smaller extent, by the AP2 lining. The cross-sectional area of the lining, A_L = 3.15 in.^{2} (2032 mm^2), with a Young's modulus in the longitudinal direction, E_L = 491 ksi (3.38 GPa). According to Appendix B, the combined axial force in the pipe and lining, F_{PL}, is estimated by:

$$F_{PL} = [1 + (E_L A_L)/(E_P A_P)]F_P \quad (9.2)$$

Figure 9.11 plots with respect to fault displacement the axial load from the north end load cells and the combined axial force in both the DI pipe and AP2 lining, F_{PL} (Equation 9.2), for the gage planes at 230 and 262. The loads are nearly equal at all magnitudes of fault displacement, with a maximum load of approximately 30 kips (133 kN) at 48 in. (1.22 m) of fault movement.

Figure 9.12 plots with respect to fault displacement the axial load from both the north and south end load cells. The axial load is smaller at the south end than at the north end at most of the fault displacements. The south end load is a maximum of approximately 27 kips (120 kN) at 48 in. (1.22 m) of fault movement.

The axial force measured at both the north and south ends of the basin vs fault displacement is taken as the base case. The combined pipe and lining axial force was plotted for each strain gage plane and plotted relative to the base case. In this way the axial load and fault displacement at which debonding occurred between the lining and pipe can be identified easily as the location where the axial force at the strain gage plane starts to decrease. Three planes at equal distances south and north of the fault plane are shown to illustrate the how the axial loads developed, peaked, and decreased as debonding occurred.

Figures 9.13 and 9.14 show plots of the axial forces relative to the base case for Stations -16 and 16, respectively. These stations are 16 in. (406 mm) south and north of the fault (see Figure 9.1). As previously discussed, joint pullout was initiated at the South Middle Joint closest to the fault. Debonding occurred northward from the closest south joint. At approximately 2 in. (51mm) of fault displacement there is a decrease in strain at Station -16 as shown in Figure 9.13. The difference between the base case and axial force at 2 in. (51 mm) of fault movement is approximately an additional 7 kips (31 kN) of pipe force. Under K_O conditions the axial force generated by fiction between the pipe and adjacent soil is approximately 7 kips (31 kN) from the closest end of the basin to the strain gage station.

The axial force at Station 16 in Figure 9.14 peaks at approximately 6 in. (152 mm) of fault displacement after which debonding occurs. Again the difference between the base case and maximum axial force in the pipe is approximately an additional 7 kips (31 kN). As for the south joint, the force difference at the closest north joint is equal to the axial force generated by fiction between the pipe and adjacent soil under K_O conditions. The debonding south of the Middle North Joint proceeds more slowly than its southern counterpoint as indicated by the joint axial movements summarized in Figure 9.8.

Figures 9.15 and 9.16 show plots of the axial forces relative to the base case for Stations -90 and 90, respectively. These stations are 90 in. (406 mm) south and north of the fault (see Figure 9.1). At approximately 1 in. (25 mm) of fault displacement there is a decrease in strain at Station -90 as

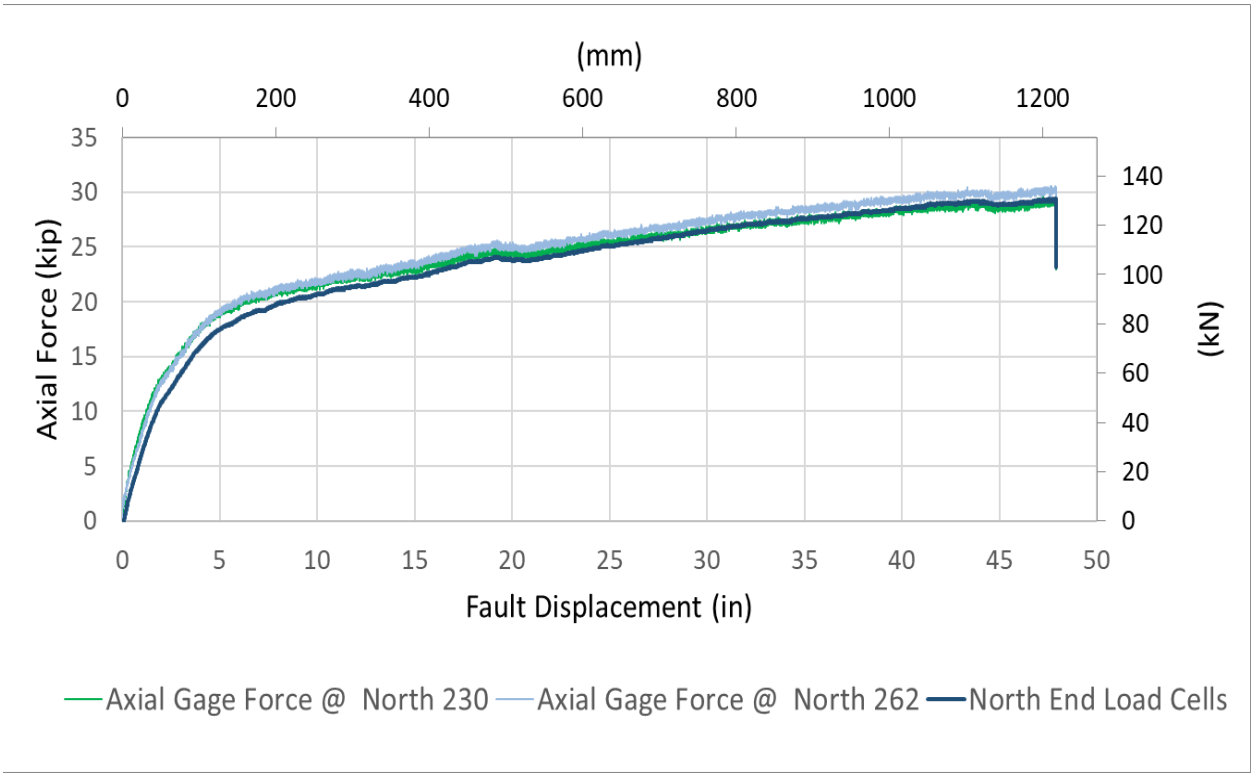

Figure 9.11. Axial Force in Both Pipe and Lining Measured by North End Load Cells and Strain Gage Planes 230 and 262.

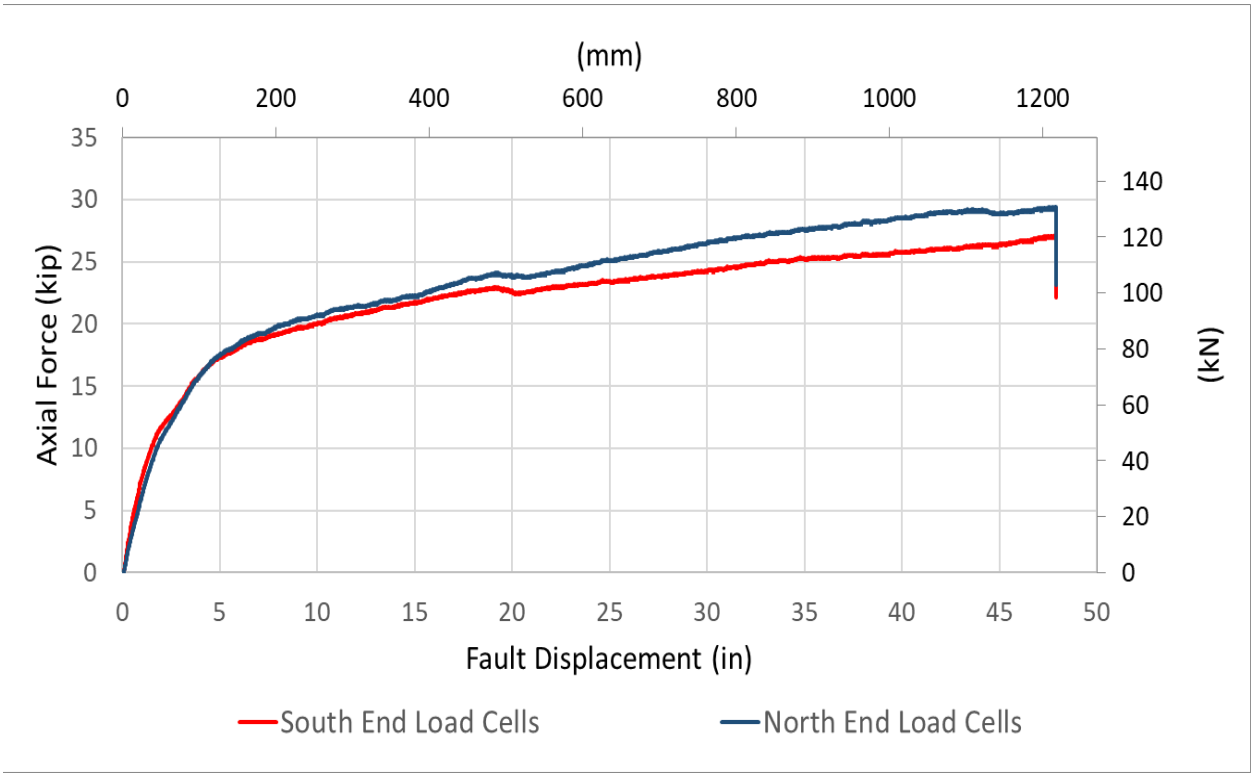

Figure 9.12. Axial Force in Both Pipe and Lining Measured by North and South End Load Cells

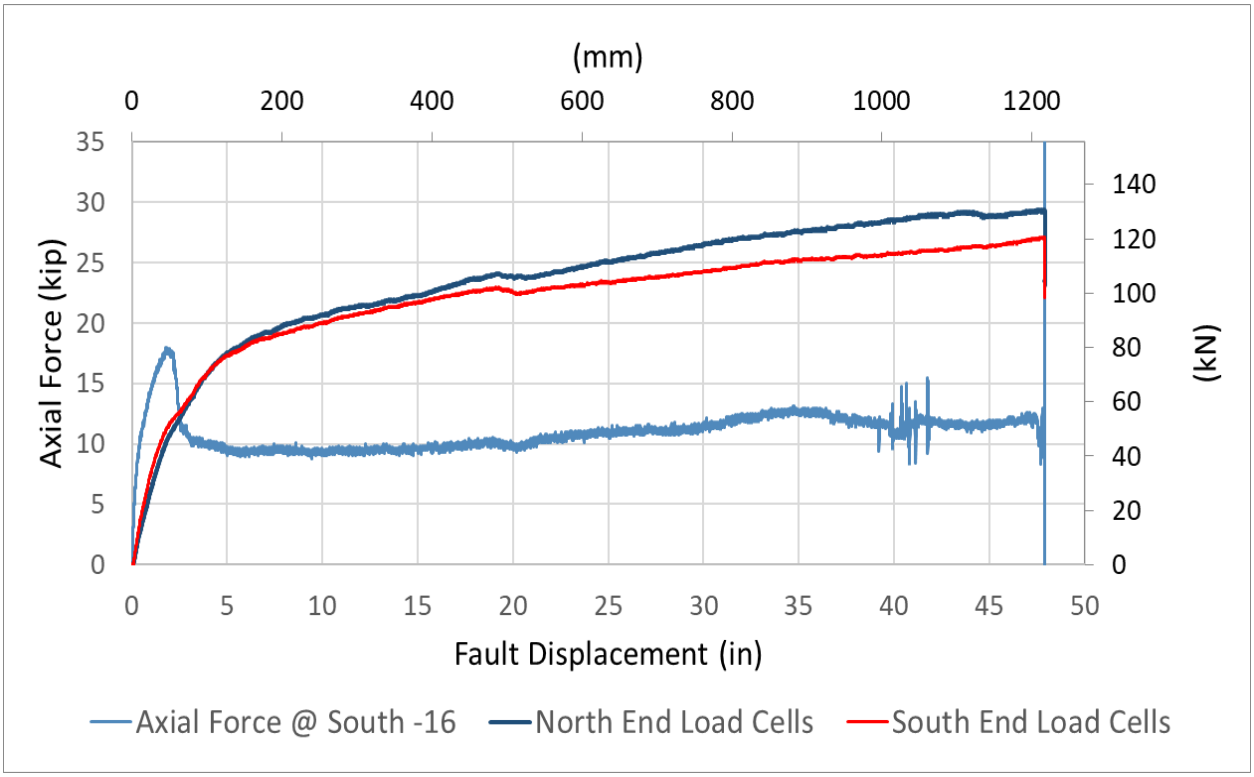

Figure 9.13. Axial Force at Station -16 Relative to the Base Case

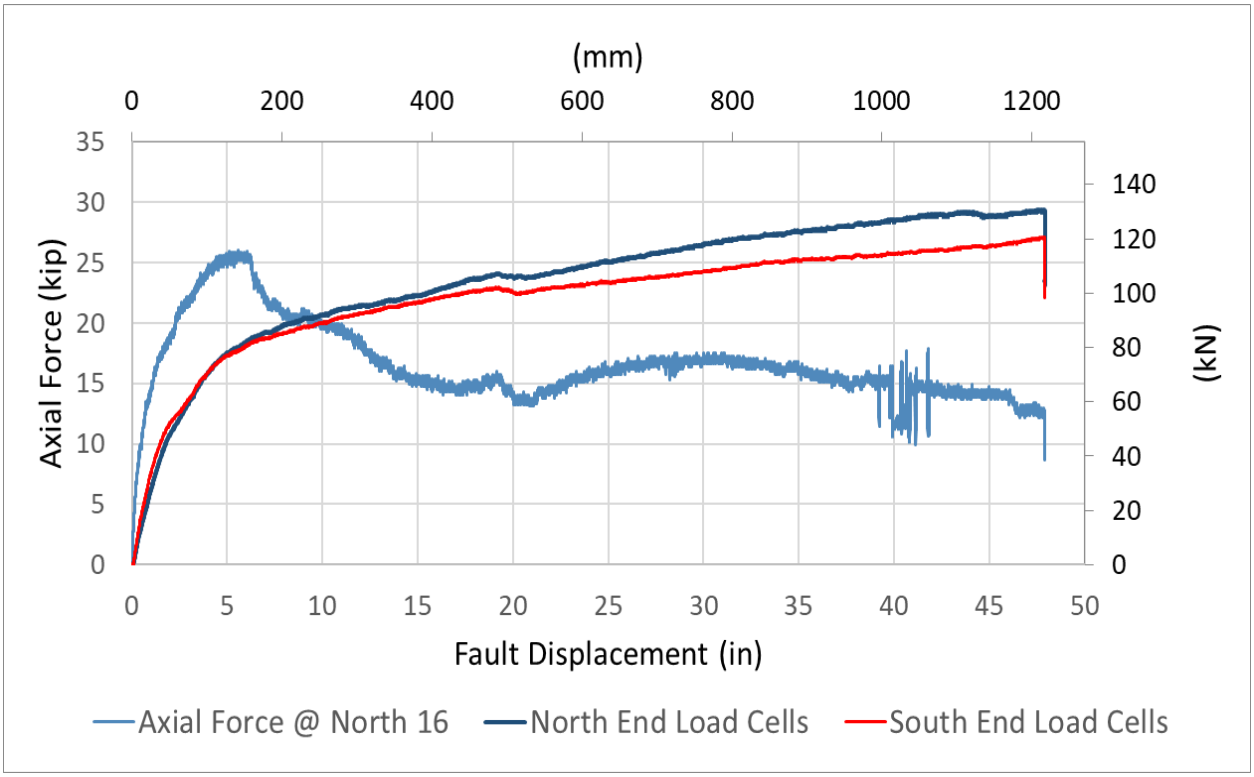

Figure 9.14. Axial Force at Station 16 Relative to the Base Case

shown in Figure 9.15. Figure 9.13 and Figure 9.14 show that debonding occurred both northward and southward from the South Middle Joint. The difference between the base case and axial force at 1 in. (25 mm) of fault movement is approximately an additional 5 kips (22 kN) of pipe force. Under K_O conditions the axial force generated by fiction between the pipe and adjacent soil is approximately 5 kips (22 kN) from the closest end of the basin to the strain gage station.

The axial force at Station 90 in Figure 9.16 peaks at approximately 4.5 in. (114 mm) of fault displacement after which debonding occurs. The difference between the base case and maximum pipe axial force is approximately an additional 2.5 kips (11 kN)). Thus, the force at the north joint closest to the fault shows the effects of friction between the pipeline and adjacent soil.

Figures 9.17 and 9.18 show plots of the axial forces relative to the base cases for Stations -150 and 150, respectively. These stations are 150 in. (406 mm) south and north of the fault (see Figure 9.1). At approximately 6 in. (152 mm) of fault displacement there is a decrease in strain at Station -150 as shown in Figure 9.17. Debonding occurred southward from the Middle South Joint. The difference between the base case and axial force at 6 in. (152 mm) of fault movement is an additional 2 kips (9 kN) of pipe force. Under K_O conditions the fictional force between the pipe and adjacent soil is about 2 kips (9 kN) from the closest end of the basin to the strain gage station.

The axial force at Station 150 in Figure 9.18 peaks at approximately 20 in. (508 mm) of fault displacement after which debonding occurs. The difference between the base case and maximum axial force in the pipe is approximately an additional 1 kip (4.45 kN). The force differential is close in magnitude to the axial force difference at Station – 150 at an equal distance south of the fault. Debonding occurs at this station at a relatively large fault movement of 20 in. (508 mm), and thus progresses more slowly in the northern part of the test pipeline.

The axial force development and debonding depicted in the preceding figures are part of a complex pattern that was studied by examining the decreases in strain gage readings as well as the axial forces relative to the base case for all stations. The general pattern (please refer to Figure 9.1) is described as follows.

Axial movement first occurred at the south joint closest to the fault, which debonded north and south past the centers of the two adjacent pipes between 2 and 3 in. (51 to 56 mm) of fault movement.

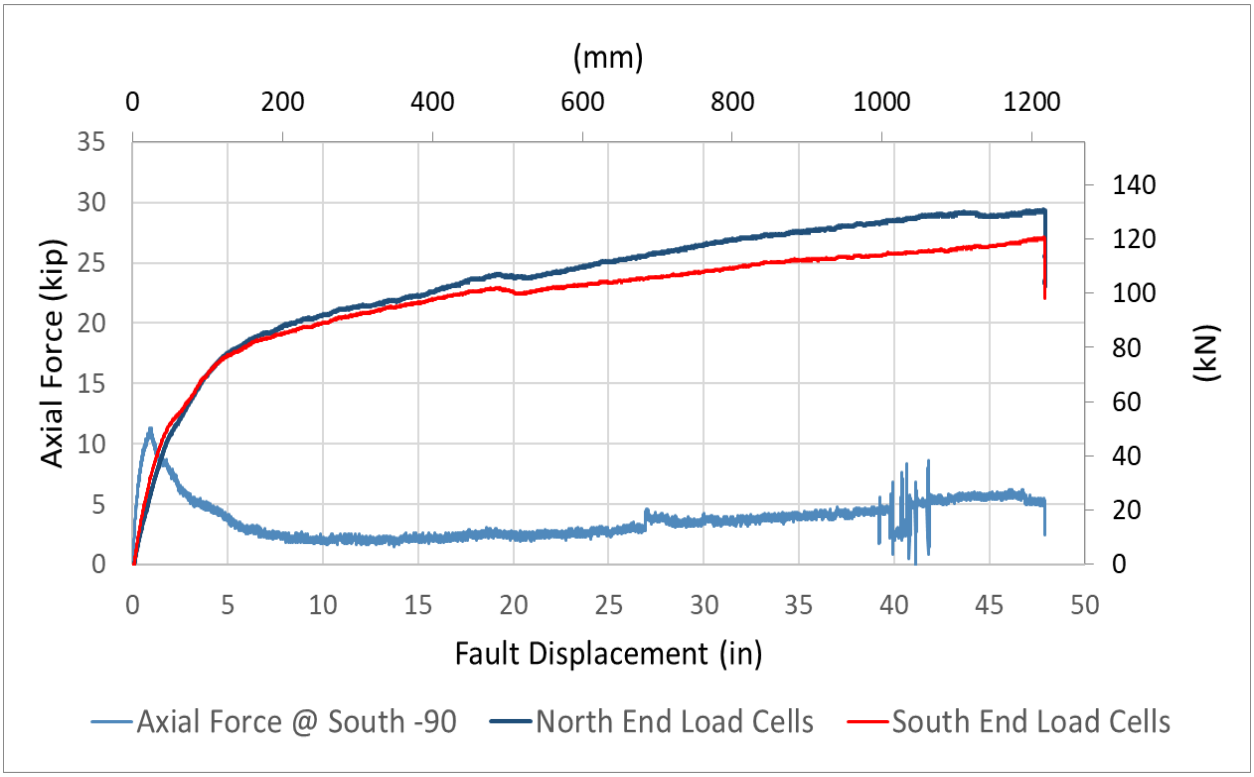

Figure 9.15. Axial Force at Station -90 Relative to the Base Case

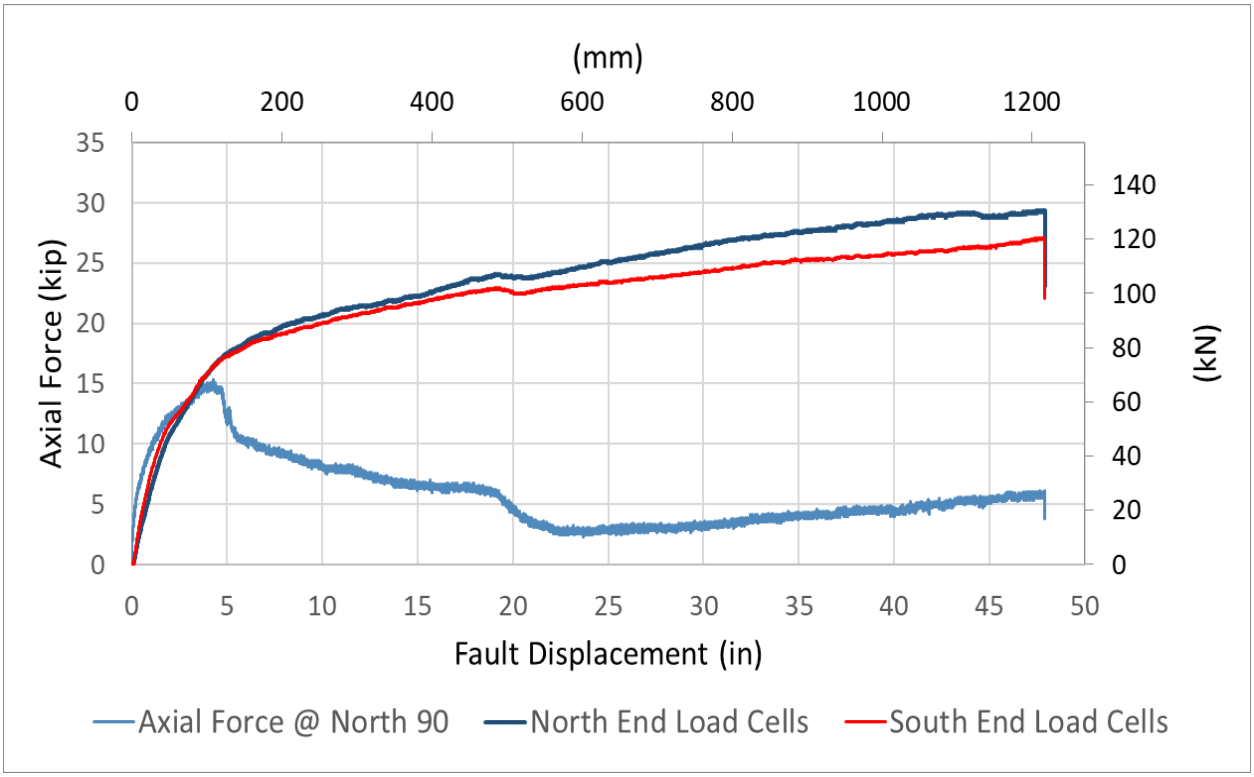

Figure 9.16. Axial Force at Station 90 Relative to the Base Case

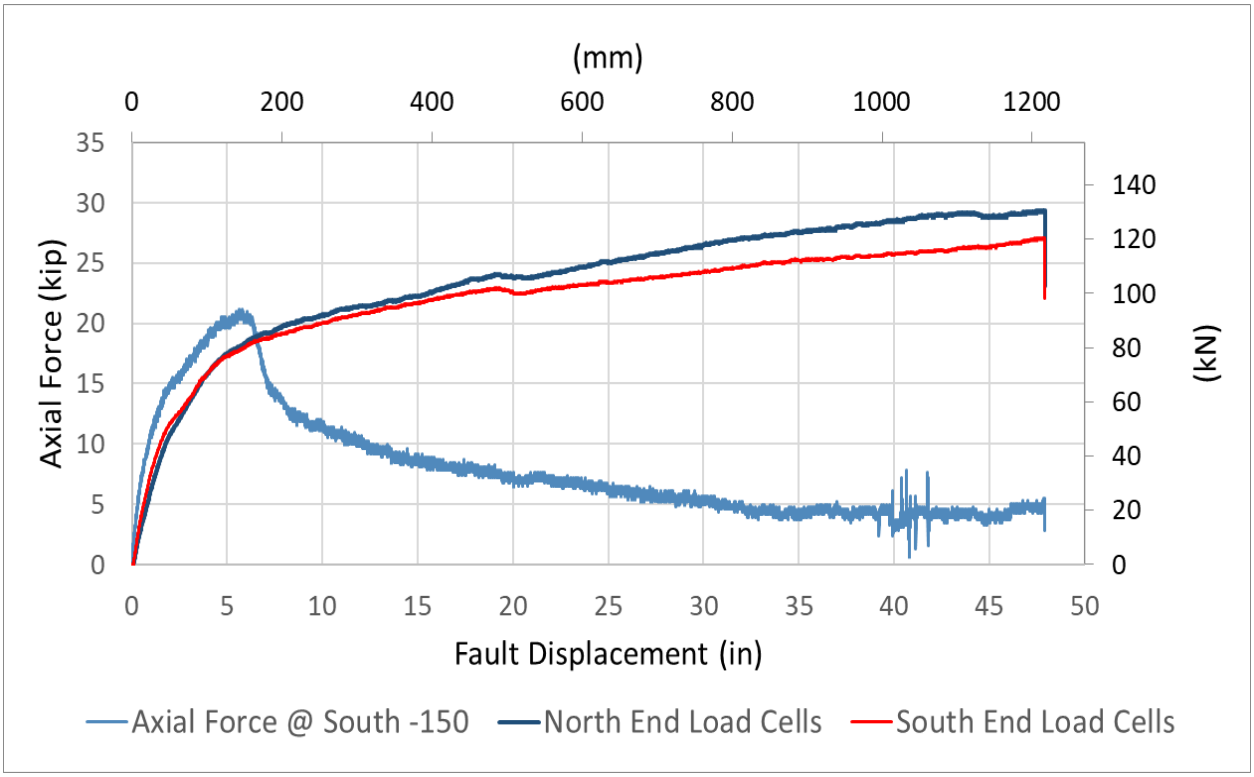

Figure 9.17. Axial Force at Station -150 Relative to the Base Case

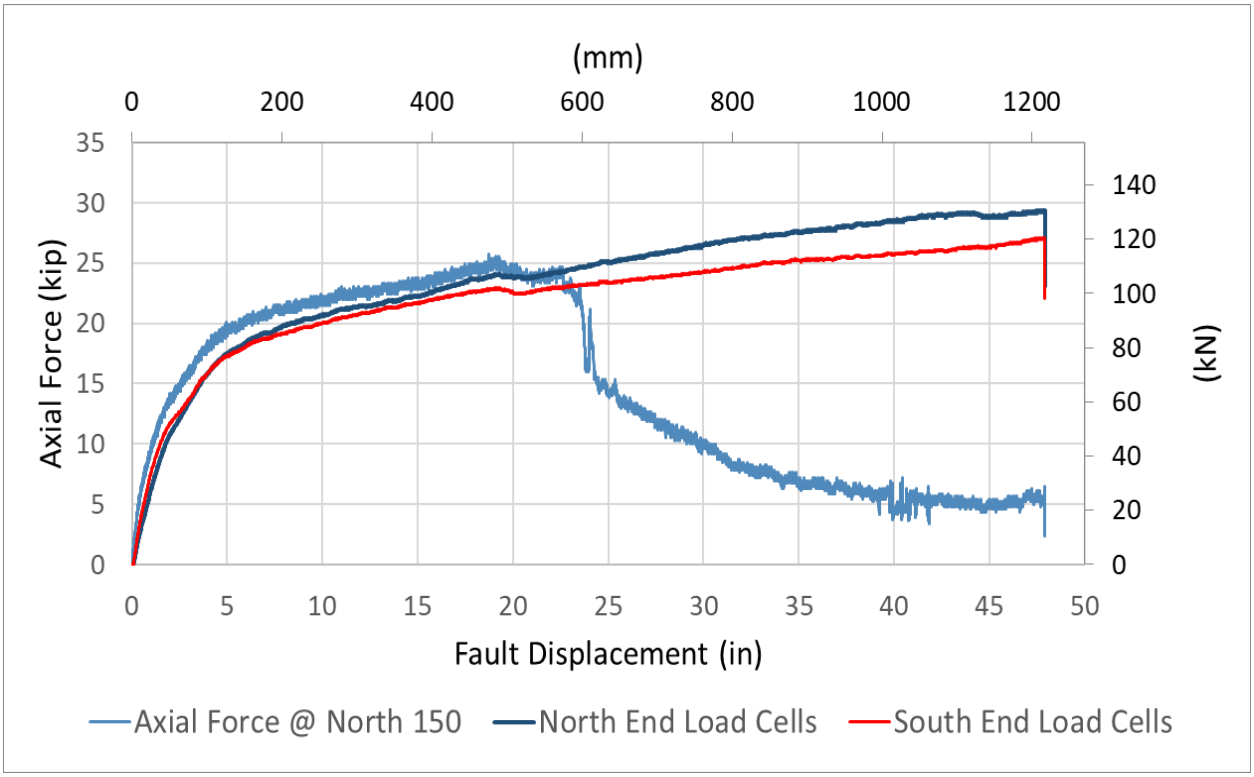

Figure 9.18. Axial Force at Station 150 Relative to the Base Case

Debonding also occurred south from the north joint closest to the fault between 2 in. (51 mm) and 6 in. (152 mm) of fault displacement. Dedonding was initiated south of both the south and north joints farthest from the fault at low levels of fault movement. Debonding continued from the closest to the farthest south joint at 6 in. (152 mm) of fault displacement. It also occurred north of the north joint closet to the fault between 4 in. (102 mm) and 22.5 in. (572 mm) of fault displacement. Debonding occurred south of the joint furthest south of the fault between 7 in. (157 mm) and 12 in. (305 mm) of fault displacement. Debonding was not observed at the south end anchorage. As previously discussed, no debonding was observed at Stations 230 and 262 as well as the north end anchorage.

9.3.6. Bending Moments

Bending moments, M, were calculated at each strain gage station along the pipeline as:

$$M = \frac{\varepsilon_{bend} EI}{c} \tag{9.3}$$

where bending strain, $\varepsilon_{bend,}$ is one half the difference between the springline strains; E is Young's modulus of the ductile iron of 24,200 ksi (169 GPa); I is moment of inertia of 30.4 in^4 (1265 cm^4); and c is distance to outer fiber of 3.37 in. (85.6 mm). Equation (9.3) was used for all gage stations except Stations -72, 0, 32, and 48. Station 0 was eliminated because of strain gage instabilities. For Station -72, only the east springline gage was used to estimate bending. For Station 32, both springline strain gages are used until 24 in. (610 mm), after which only the west gage is used to estimate the bending. For Station 48, both springline strain gages are used until 20 in. (508 mm), after which only the east gage is used to estimate bending.

Figure 9.19 presents the bending moments measured along the pipeline corresponding to fault displacements of 0, 12 in. (305 mm), 24 in. (610 mm), 36 in. (914 mm), 47 in. (1194 mm), and 48 in. (1291 mm). Also shown in the plot as full red circles are the pipeline joints. The strain gage measurements show a complex pattern in which the moments are very low or nearly zero at the joints at all levels of fault displacement. The low moments occur at these locations because the moments are resisted mostly or entirely by the AP2 lining.

At 12 in. (305 mm) of fault displacement there was little debonding in the northern portion of the test pipeline; most of the debonding was concentrated in the southern portion. Thus at 12 in. (305 mm), the maximum bending strains were measured at relatively low debonding conditions on the

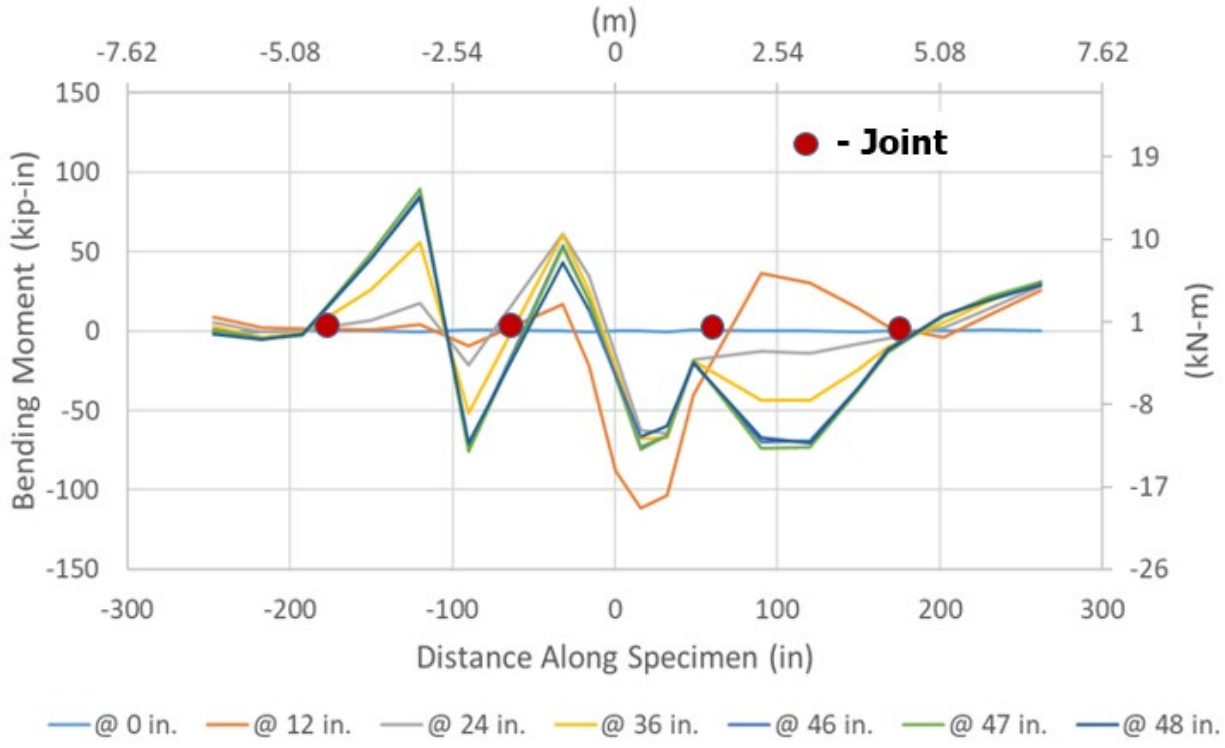

Figure 9.19. Bending Moments in Pipeline vs. Distance from Fault

northern part of the test pipeline. At higher levels of fault displacement, debonding continued in a complex pattern in which bending strains increased then decreased, resulting in the measurements shown in Figure 9.19.

9.3.7. Debonding Pattern

In Appendix C at each strain gage station there are plots of axial force given by Equation 9.2 and the axial load at that station. When plotted relative to the axial force given by Equation 9.2 for the ends of the test pipeline, the reduction in axial load at a given station is easily located. This location coincides with the fault displacement where the axial force starts to decrease because of debonding.

Figure 9.20 is a plot of the fault displacement at each station relative to the station location plotted as distance from the center of the fault plane. As indicated in Section 9.3.3 Joint Pullout, debonding began first at the South Middle Joint and progressed both north and south of that joint over the distance shown in Figure 9.20. Debonding lengths of the North Middle and South Joints could also be estimated, as shown in the figure. Because Figure 9.8 showed little or no North Joint opening at the fault displacements depicted in Figure 9.20, axial displacements of the North Joint and associated debonding lengths could not be estimated reliably. Please note that the gages at 72 in.

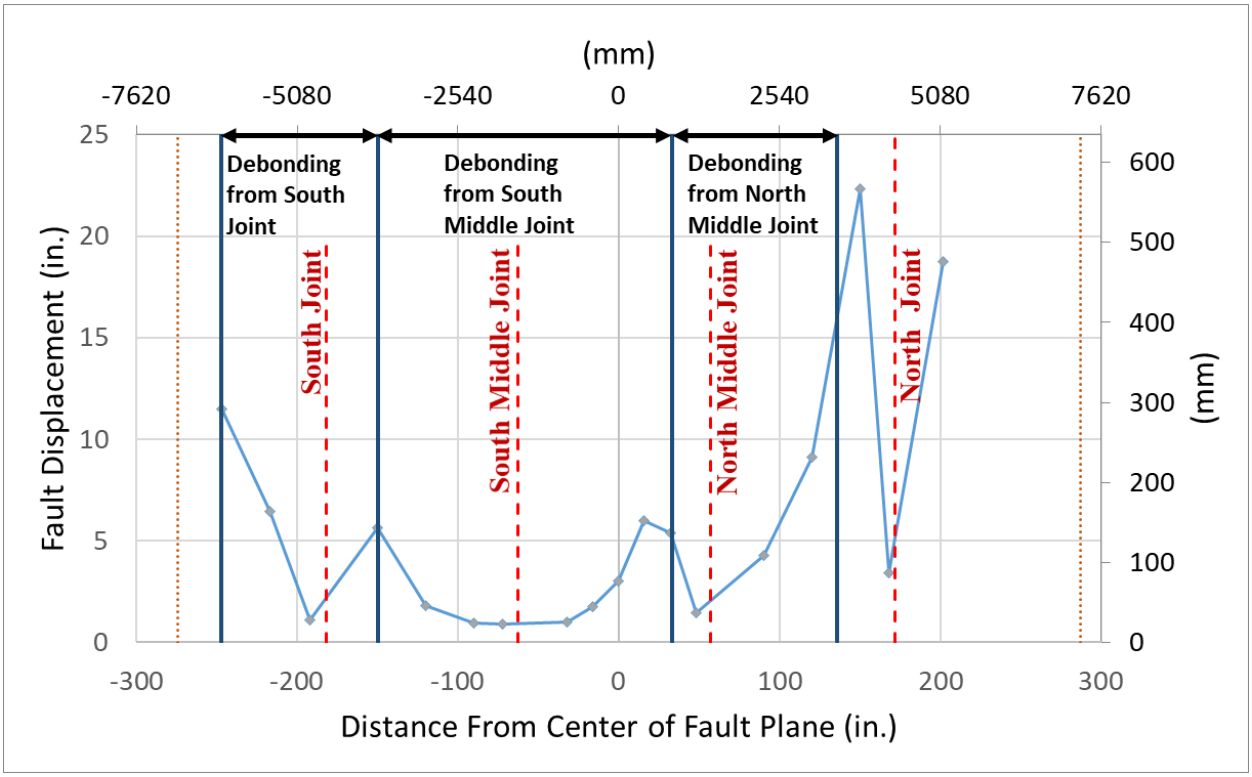

Figure 9.20. Fault Displacement at Debonding for Each Gage Station

south of the fault were not used because of instability with the gage readings. All others were used. In each instance the axial load at the ends of the debonded length were checked for equality.

From Figure 9.20 one can estimate the fault displacement at which debonding occurs at each strain gage station. From Figure 9.8 one can evaluate the axial joint movement at each fault displacement. When one uses the two figures, both the joint displacement, or opening, and the corresponding debonded length can be assessed.

For a given debonding length, L, the joint opening, δ, may be estimated for a linear elastic material by

$$\delta = (PL)/(AE) \tag{9.3}$$

in which P is the axial load, A is the cross-sectional area, and E is the elastic modulus. Rearranging the terms gives

$$L/\delta = (AE)/P \tag{9.4}$$

For AP2, E is linear to about 1% strain = 491 ksi for the warp direction. A = 3.15 in.^{2}, and E is

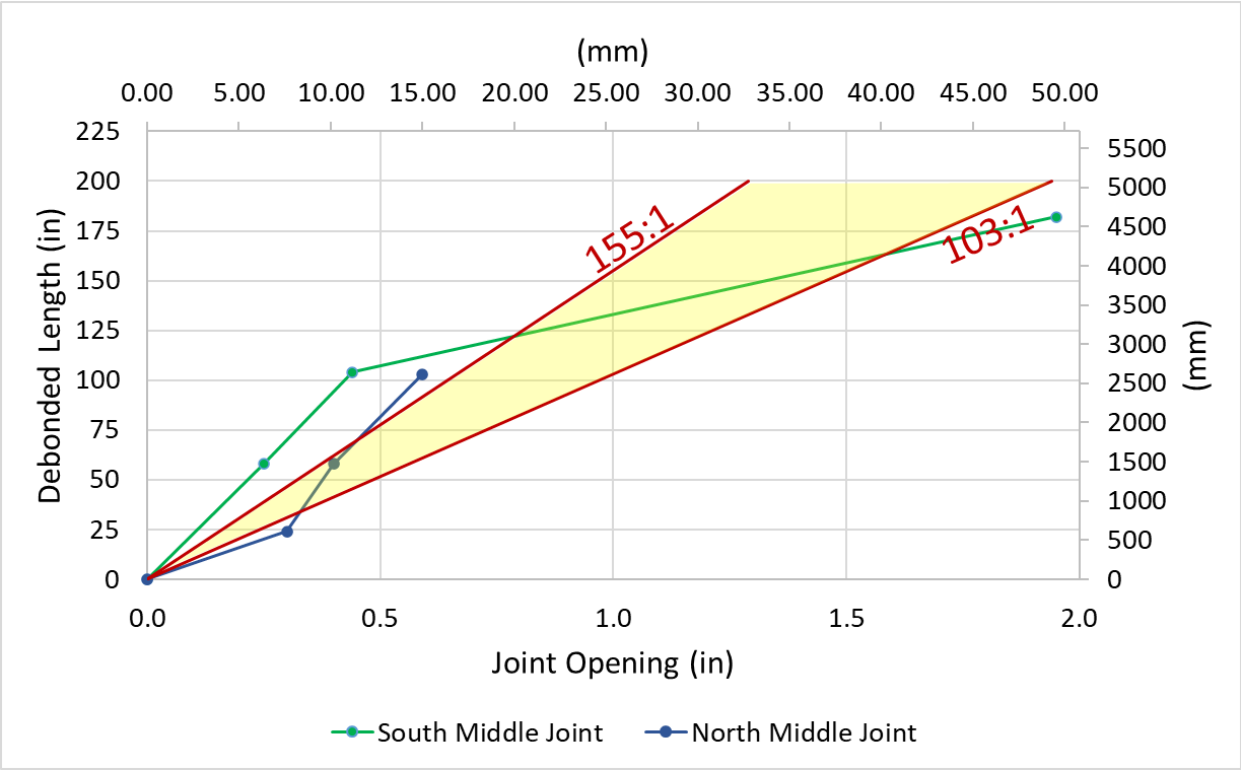

Figure 9.21. Debonded Length versus Joint Opening

constant below P = 15.5 kips. For debonding loads of P equal to 10 and 15 kips, the values of L/δ = 103 and 155, respectively. For strains ≤ 1% the elastic displacement can be calculated very closely from E in the warp direction.

Figure 9.21 shows the debonded length vs joint opening from the data for the South Middle and North Middle Joints plotted relative to L/δ for P =10 and 15 kips, both in the elastic range and representative of loads measured at debonding. The plot shows that the measured debonded length vs joint opening is consistent with elastic behavior because the data points plot within or closely to the elastic range bounded by L/δ =155:1 and 103:1 for P =10 and 15 kips, respectively. Debonding from both the South and North Middle Joints coalesced with dedonding from adjacent joints. Debonded lengths and associated joint openings are not shown for the North and South Joints because the debonding lengths of these joints were affected by anchor locations at the ends of the test pipeline.

The data shows that debonding initiated at the south joint closest to the fault and propagated both northward and southward into the adjacent pipes. There was a small amount of debonding south of the south joint farthest from the fault and south of the north joint closest to the fault during the

initial fault deformation. Debonding occurred north of the north joint closest to the fault a little before, but primarily at the same time it occurred south of the south joint farthest from the fault. Again during initial fault deformation, debonding propagated a small distance south of the north joint farthest from the fault. Debonding continued both north and south of this joint and terminated about 30 in. south of the anchor location at the north end of the basin.

The debonding shows a pattern in which joint movement and debonding started first at the South Middle Joint after which they developed almost simultaneously at the North Middle and South Joints. Apart, debonding and axial movement occurred last at the North Joint. Debonding was complete at about 22.4 in. of fault displacement, after which ground deformation was accommodated by elongation of the liner though the pipe between the anchor points at the ends of the basin. The debonding pattern was somewhat irregular, due in large part to variable debonding forces along the pipe.

Figure 9.22 shows the debonding length vs. crack, or joint, opening for three regimes of tests, pertaining to 1) fault rupture test, 2) direct tension test on pipe with 8.5-ft (2.6-m) lengths of pipe either side of the center crack: AP1-DT7, and 3) direct tension test on pipe with 4.25-ft (1.3-m) lengths of pipe either side of the center crack: AP1-DT2, AP2-DT2, and AP1-JDT2. There are equations for each regime of the form $l = mlnx + b$, where l is the debonded length, x is the crack or joint opening, and m and b are the slope and intercept of the plot, respectively. For each regime equation there is a high r^2, which means that the equations cover a large part of the variability of the data. Additional details regarding the data, equations, and meaning of the various parameters are provided in Appendix D.

The three regimes of data mean that the test affects the relationship between debonding length and crack, or joint, opening. There is a greater debonded length for a given crack opening when the direct tension specimen is twice as long (AP1-DT7 vs AP1-DT2, AP2-DT2, and AP1-JDT2). The greater debonding lengths correspond to longer specimen lengths. There is a greater crack opening that occurs as the axial force is applied to a longer debonded length.

The largest debonding length per joint opening occurs for the fault offset test. Under these conditions, debonding from the South and North Middle Joints coalesce with dedonding from adjacent joints. Especially at lower displacements, the relationship between debonded length and joint opening tends to follow linear elastic behavior, as illustrated in Figure 9.21.

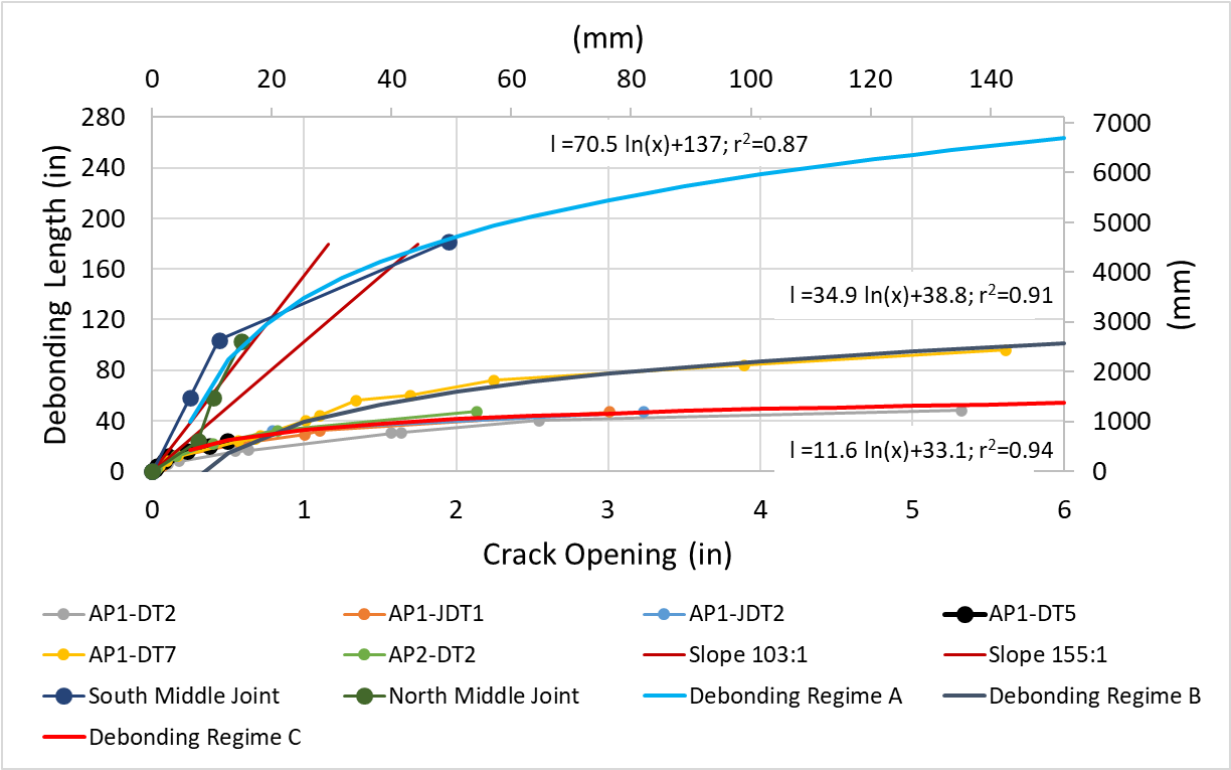

Figure 9.22. Debonded Length vs Crack/Joint Opening: Direct Tension and Fault Rupture

9.3.8. Deformed Shape and Pipe Failure

Figure 9.23 shows the maximum fault rupture of 4.00 ft. (1.22 m) or 48 in. (1,220 mm). The project consultant who operated the instrumentation, Blake Berger, is also shown in the photograph for scale. Figure 9.24 presents a photo of the pipeline upon excavation and exposure for survey measurements after the fault rupture test. The four test pipeline joints are identified in the figure. The Leica survey measurements of 13.8° and 12.9° for the South and North Middle Joints, respectively, are shown on the photo. These measurements are the same that are presented in Figure 9.10. These data provide test pipeline movements at locations very close to the maximum at the largest basin displacement. Figure 9.25, Figure 9.26, Figure 9.27, and Figure 9.28 are photos after the fault rupture test of the deformation at the North Joint, North Middle Joint, South Middle Joint, and South Joint, respectively.

Figure 9.25 shows the deformation at the North Joint primarily as pullout of the spigot from the bell of the DI pipeline. The AP2 lining is visible in the gap between the spigot and the bell, which is facing northward. Please note that the longitudinal deformation at this joint has been affected by reduction in tensile load in the lining after the water pressure was turned off, but before exposure

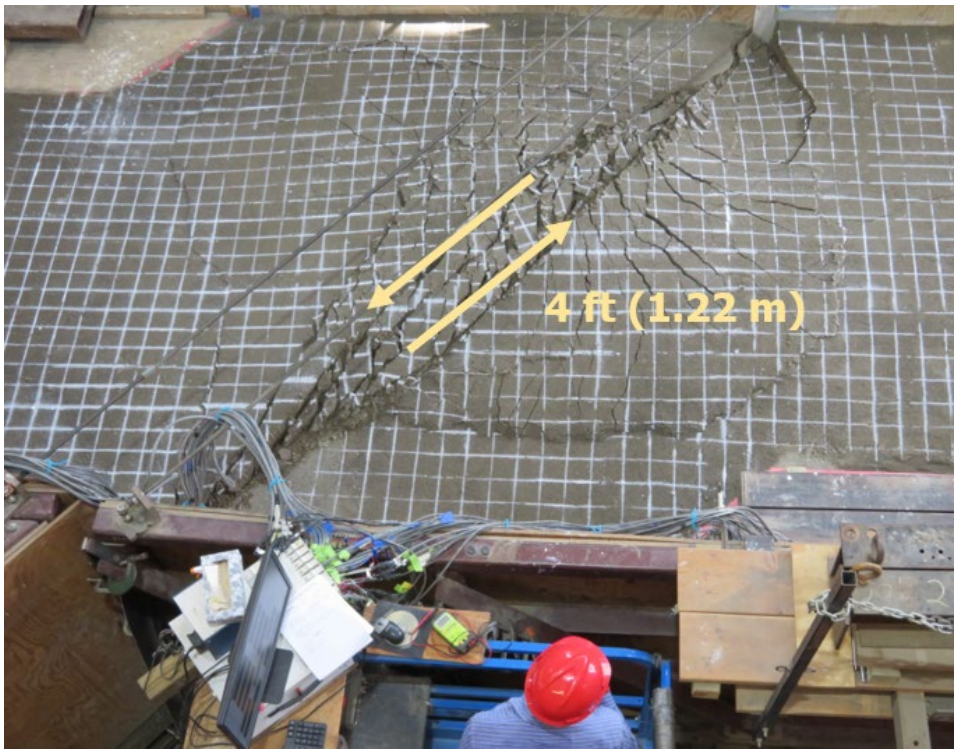

Figure 9.23. Maximum Fault Rupture

of the test pipeline for the Leica survey. Hence, the joint longitudinal deformation in the photo exceeds that shown by the measurements plotted in Figure 9.8. In contrast, the longitudinal deformation shown by the photos of the three remaining joints is consistent with the displacements shown in Figure 9.8.

Figure 9.26 shows the deformation of the North Middle Joint in the form of pullout and rotation. The metal shielding has slipped longitudinally to the north. The AP2 lining is visible in the gap between the spigot and the bell. Curvature in the lining can be seen.

Figure 9.27 shows the deformation of the South Middle Joint in the form of pullout and rotation. The metal shielding has also slipped longitudinally to the north. Curvature in the lining is visible where it is exposed between the bell face and spigot end. Approximately 10 in. (254 mm) of separation between the bell and lining can be seen. This adds to the 3.34 in. (85 mm) of spigot insertion into the bell before the fault rupture test to result in total pullout of 13.34 in. (339 mm), which is nearly equal to the maximum South Middle Joint movement plotted in Figure 9.10.

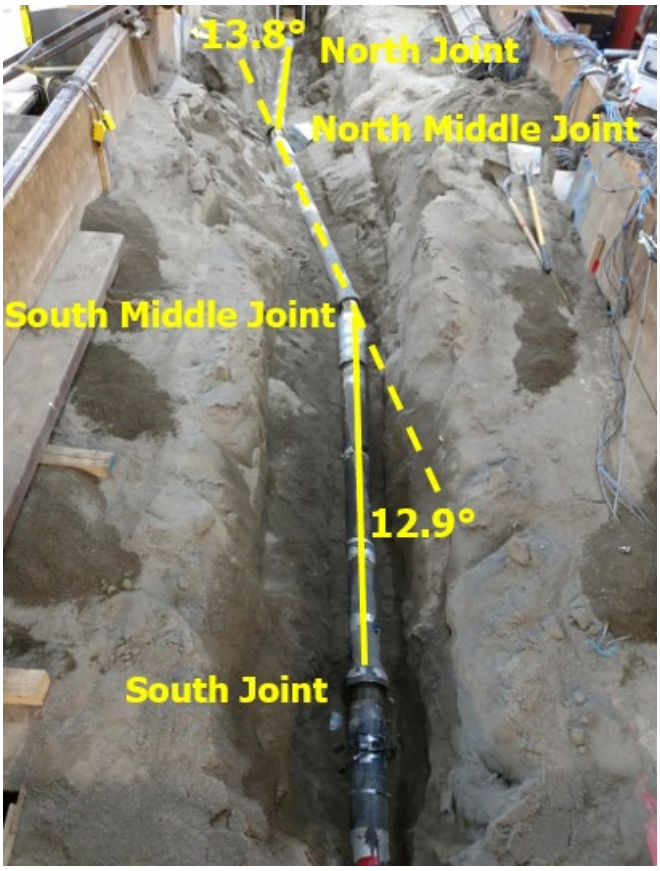

Figure 9.24. Test Pipeline Deformation after Fault Rupture Test

Figure 9.25. Deformation at North Joint

Figure 9.27 shows the deformation of the South Joint primarily in the form of pullout. The metal shielding has remained intact, and longitudinal slip between the two levels of metal shielding is about 3.75 in. (95 mm) as measured by the tape. The actual movement of the spigot with respect to the bell face cannot be ascertained in this photo.

Figure 9.26. Deformation at North Middle Joint

Figure 9.27. Deformation at South Middle Joint

Figure 9.28. Deformation at South Joint

9.4. Summary of Large-Scale Testing

An approximately 36-ft (11-m)-long in soil, five-piece section of a DI pipeline was lined with Aqua-Pipe™ Generation 2 (AP2) and tested in fault rupture at the Cornell Large-Scale Lifelines Facility. The pipeline had a total of four joints located 5 and 15 ft (1.5m and 3.6 m) north and south of the fault. The fault angle was 50º. To match the field performance of older DI and CI field pipelines the cementless pipe surface was aged by Sanexen, and the pipeline was lined according to the field procedures followed by them. The pipeline was instrumented with 96 strain gages installed at 20 locations along the pipeline to measure strains and to evaluate axial forces and bending moments. Strain gages were positioned at the crown (C), invert (I) east (E) springline, and west (W) springline of the pipe. The gage measurements were used to evaluate when debonding between the pipe and lining occurred as a function of fault displacement. There were three string pots at each joint to measure joint movements and to evaluate joint rotation. Four load cells were placed outside the test basin at each end, reacting between the test basin structural frame and pipe end restraint to measure axial force. The pipe was pressurized to an average 81.3 psi (561 kPa).

The pipeline was buried in the Cornell large-scale test basin in partially saturated sand that was compacted to have an average direct shear, peak friction angle of $\phi = 40º$, equivalent in strength to that of a medium dense to dense granular backfill. The depth of burial to top of pipe was 32 in. (813 mm). During the test, the south part of the basin remained stationary, while the north part was displaced to the north and west by large-stroke actuators to cause soil rupture and slip at the interface between the two parts of the test basin. The north section of the test basin was displaced along a 50º fault at a rate of 2 in. (51 mm) per minute. The basin was displaced until full travel of the actuators was achieved, corresponding to a fault displacement of 4 ft (1.22 m) as well as axial pipe extension of 2.57 ft (0.78 m). The lined pipeline maintained its integrity and water pressure throughout the test.

The axial forces at the south and north end of the test basin were about 27 and 30 kips (120 and 134 kN), respectively. The axial force in the pipe, as determined from the strain gage readings, was largest at approximately 16 in. (406 mm) north of the fault. The axial force was 25 kips (110 kN) at 6 in. (152 mm) of fault displacement, after which debonding between the pipe and lining diminished significantly the pipe strains and corresponding axial forces.

The DI pipeline equipped with an AP2 lining was able to accommodate significant fault movement through axial pullout and rotation of the joints. Fault rupture simulated in the large-scale test is also representative of the most severe ground deformation that occurs along the margins of liquefaction-induced lateral spreads and landslides. Pipeline extension was taken up by longitudinal movement at each of the joints. The maximum longitudinal movement was measured at approximately 14.0 in. (356 mm) at the joint closet to fault on the southern side of the fault. Pipeline lateral offset was accommodated by rotation, or deflection, of the two joints closest to the fault on the north and south sides. The maximum rotation of the north joint closest to the fault was about 14.0° as measured by the string pots and Leica total station survey. The measured and theoretical rotations are in good agreement.

9.5. Significance of Test Results

The amount of tensile strain that can be accommodated with the lined DI pipeline will depend on the spacing of the joints. The pipeline used in the large-scale split-basin test was able to accommodate a maximum of 30.85 in. (784 mm) of axial extension, corresponding to an average tensile strain of 6.3 % along the pipeline. It should be emphasized that no loss of water pressure of structural failure of the lined pipeline was sustained during the fault rupture test. Thus, the lined pipeline could have sustained more tensile strain without exceeding the pressure boundary. Such extension is large enough to accommodate the great majority (well over 99%) of liquefaction-induced lateral ground strains measured by high resolution LiDAR after each of four major earthquakes during the recent Canterbury Earthquake Sequence (CES) in Christchurch, NZ (O'Rourke, et al., 2014). These high-resolution LiDAR measurements provide a comprehensive basis for quantifying the ground strains caused by liquefaction on a regional basis. To put the CES ground strains in perspective, the levels of liquefaction-induced ground deformation measured in Christchurch exceed those documented in San Francisco during the 1989 Loma Prieta earthquake and in the San Fernando Valley during the 1994 Northridge earthquake. They are comparable to the levels of most severe liquefaction-induced ground deformation documented for the 1906 San Francisco earthquake, which caused extensive damage to the San Francisco water distribution system. The test confirms that DI and CI pipelines lined with AP2 are able to sustain large levels of ground deformation through axial displacement and deflection under full-scale conditions of abrupt ground rupture.

Section 10
Test Summary

This report presents the results of material property and full-scale testing to investigate the performance of Aqua-Pipe™. Two types of Aqua-Pipe™ lining were tested: Aqua-Pipe™ Generation 1 (AP1) and Aqua-Pipe™ Generation 2 (AP2). Aqua-Pipe™ Cured-in-Place-Pipe (CIPP) is used to rehabilitate potable water pipelines as an alternative to pipeline removal and replacement. Sanexen, which provides Aqua-Pipe™, is an environmental services contractor and consultant headquartered in Canada with a counterpart in the U.S., Sanexen Water.

The full-scale tests were designed to evaluate pipeline performance with Aqua-Pipe lining under large ground deformation that includes debonding between the lining and interior surface of CI and DI pipelines, axial force versus displacement response in tension and compression, four-point bending, and large-scale fault rupture. The relationship among lining axial force, internal pressure, and variation in pipe and lining diameter with respect to distance along the pipeline was examined.

The principal findings are summarized in this section with respect to the topics enumerated below as follows:

10.1. Tensile Coupon Test Results

Tensile coupon tests were performed on specimens of AP1 representative of longitudinal (warp) and circumferential (weft) directions of the lining. The test results show the average Young's modulus, Poisson's ratio, and ultimate tensile strength and strain in the longitudinal direction of 390 ksi (2.69 GPa), 0.23, 10.9 ksi (75.2 MPa), and 15%, respectively. The test results show the average Young's modulus, Poisson's ratio, and ultimate tensile strength and strain in the circumferential direction of 414 ksi (2.86 GPa), 0.25, 15.3 ksi (106 MPa), and 11.1%, respectively.

The test results show that, from zero to between 0.5% and 1.0% strain, the liner responds as a linear elastic solid. The Poisson's ratio is approximately 0.24 in both directions, and the difference in the Young's modulus is less than 7% lower in the warp than in the weft direction. In this range of tensile strain, the Young's modulus and Poisson's ratio are controlled principally by the epoxy. As the strain approaches and exceeds 0.5 to 1.0%, micro-fractures develop in the epoxy, and stress is transferred increasingly from the epoxy matrix to the fabric. This stress transfer results in a reduction of modulus. Moreover, the fabric stretches more in the warp direction than in the weft direction, where the strength of fibers is greater. As tensile strain exceeds approximately 5%, the

fibers stretch and tighten, leading to increased modulus in both the warp and weft directions. The stiffness and strength in the weft direction exceed those in the warp direction due to the continuous nature of fibers in this direction.

Tensile coupon tests in the warp and weft directions of AP2 were performed by CDQC. For the warp direction the average maximum tensile stress, tensile strain at maximum stress, and secant modulus at 1% tensile strain are 19.7 ksi (135.8 MPa), 22.6 %, and 491 ksi (3.38 GPa), respectively. For the weft direction the average maximum tensile stress, tensile strain at maximum stress, and secant modulus at 1% tensile strain are 10.5 ksi (72.5 MPa), 22.6 %, and 767 ksi (5.29 GPa), respectively.

Like the AP1, there is marked departure from linearity for the AP2 specimens at tensile strains between 0.5 and 1.0%. The secant modulus in both the warp and weft directions of the AP2 specimens is larger than that in the same directions at the same strains for the AP1 specimens. At 0.5% strain, the secant modulus for AP2 is about 50% and 100% greater for AP1 in the warp and weft directions, respectively.

10.2. Direct Tension Test Results

The direct tension test results allow for a comprehensive assessment of axial force versus relative displacement between the Aqua-Pipe lining and both CI and DI host pipes. The mobilization of axial force is affected by fracture propagation, friction between the exterior surface of the lining and interior surface of the host pipe, and geometric resistance generated by relative movement of the lining within a pipe of variable inside diameter. The tests show that the initial load response to pipeline extension is dominated by a rapid rise in axial force as debonding between the lining and host pipe occurs. Previous research (Argyrou et al., 2018) has shown that the rapid rise in initial axial force can be modeled as a Type II fracture between the lining and inside pipe surface. The direct tension test results in this study show that the debonding force may be accompanied by additional frictional and geometric interference forces as the debonding propagates along the pipeline.

An important finding from the direct tension tests is that substantial additional axial forces may be mobilized after debonding from geometric interference caused by lining movement through a pipe with variable internal diameter. The test results provide a first-time confirmation of this loading mechanism. Moreover, the test results show that geometric resistance caused by variable inside

pipe diameter may be the dominant and controlling failure mechanism, depending on how the internal pipe diameter varies with distance along the pipeline.

Another important finding is that is that the debonding load required to overcome lining-pipe cohesion, and therefore the initiation of crack propagation, is significantly higher in cleaned, old CI pipe than new DI pipe. The debonding force measured for new DI pipe in DT1, DT2, and DT4 was approximately 28 kips (127 kN) for zero pressure. In contrast, the debonding force measured for old CI pipe in DT5 and DT6 was approximately 15 kips (68 kN), almost 50% lower, for an internal lining pressure of 80 psi (551 kPa).

After debonding, the axial force related to geometric conditions may result in decreasing or increasing loads. Because the lining is cast and cured inside the host pipe, the outside diameter of the lining is the inside diameter of the pipe. As slip between the pipe and debonded lining occur, the pipe will move relative to a pipe with decreasing or increasing diameter. If the lining diameter decreases in the direction of relative movement, the axial load will decrease, and geometric interference will not control failure. If the lining diameter increases in the direction of relative movement, the axial load will increase, and geometric interference may control failure.

DT2 and DT6 involve pipe movement in the direction of decreasing lining diameter, and the test results show low axial loads after debonding, followed by diminishing load with additional relative slip. In contrast, DT4, DT5, and DT7 involve pipe movement in the direction of increasing lining diameter, and the test results after debonding show increasing axial load with additional relative slip.

The axial force versus displacement plots of DT4, DT5, and DT7 show similar performance as the pipe was displaced along a lining of increasing diameter. Increasing axial loads were accompanied by tension-induced reductions in lining diameter that caused the lining to lurch forward until firm contact with the pipe was reinstated. Subsequent axial movement was accompanied by increased axial load until the next load cycle was initiated. During each load cycle, there was an audible pop or boom that accompanied the abrupt relative displacement between the lining and the pipe.

The test results show a complex interaction involving the pipe and lining geometry, friction between the lining and pipe, and internal pressure. After debonding, DT4 and DT5 were performed at zero internal pressure. The highest maximum force after debonding was recorded in DT5. A larger change in pipe and lining diameter over distance was measured in DT5 than in DT4. DT7

was performed with the smallest change in pipe and lining diameter over distance. Although DT7 was performed under a pressure of 80 psi (551 kPa), it nonetheless shows the lowest axial load after debonding, which is apparently related to a smaller change of diameter over distance compared with DT4 and DT5 specimens.

10.3. Friction Test Results

The friction test results further define the force versus relative displacement relationship between the Aqua-Pipe lining and host pipe first explored through the direct tension tests. Key findings include that the frictional resistance of the lining decreased after initial loading due to decreased surface roughness through repeated axial displacement between pipe and lining. When the specimen was loaded initially under zero pressure, the load response was higher due to greater surface roughness and frictional resistance. Subsequent tests exhibited a consistent, lower frictional resistance and axial load response than the first zero pressure test.

The friction tests show that the axial load response is independent of the loading rate. At varying loading rates, the axial loads experienced at each displacement were consistent in each test. The cyclic loading after debonding had a similar load range and maximum load for the tests conducted at 1 in. (25 mm)/min., 10 in. (250 mm)/min., and 100 in. (2500 mm)/min.

The most important result from the friction tests involves the influence of internal pressure on axial load response. As the internal pressure increased, the axial load for a given displacement increased linearly. Regressions of axial load versus internal pressure at the same levels of displacement show a clear linear relationship with similar slopes.

10.4. Direct Shear Test Results

The results of the direct shear tests for new DI and field CI pipes show a coefficient of friction, f, of 0.61. This value represents the relatively smooth debonded lining surface conditions representative of the Sanexen cleaning and lining process for old CI water mains. It also represents the interface between the lining and new DI pipe after repeated displacements.

Using the ratio of peak axial loads in FT1 relative to FT5 one can estimate the coefficient of friction for the initially rough interface between the lining and DI pipe surface. Multiplying the weighted average ratio of 1.25 for the peak axial force in FT1 relative to FT5 at identical displacements with $f = 0.61$ for a relatively smooth lining/pipe interface results in $f = 0.76$. This coefficient of friction provides an estimate for debonded lining/pipe interfaces that are rough and irregular.

10.5. Direct Compression Test Results

Direct compression tests were performed on a variety of lined CI joint specimens retrieved from the EBMUD and LADWP water distribution systems, including lead caulked, cement caulked, and rubber gasket/lead caulked joints. The joints were confined in dense sand under burial depths and soil strength and stiffness representative of field conditions. In all test results there is a change to a steep linear slope of the axial load versus displacement plot at a displacement between 0.10 in. (2.5 mm) to 0.7 in. (18 mm), representing the displacement at which firm contact between the spigot and back of the bell is established. Bell failure occurred in CI pipe specimens with lead caulked and rubber gasket/lead caulked joints at a load of 252 kips (1120 kN) and 291 kips (1290 kN), respectively, corresponding to an axial displacement of 0.59 in. (15 mm) and 2.22 in. (56 mm), respectively. The cement caulked joint did not fail, but the pipe barrel failed at 267 kips (1190 kN). One of the specimens with a lead caulked joint was able to sustain an axial load of 400 kips (1815 kN) without failure.

In all failed CI pipe specimens, the lining was able to accommodate substantial deformation and wrinkling. No leakage was observed in the failed cement caulked joint specimen at 80 psi (552 kPa) water pressure. Very low leakage at the same pressure in the form of dripping water of 10 mL/min. (0.34 fl. oz./min.) and 95 mL/min. (3.2 fl. oz./min.) was measured for failed CI joints that sustained a total compressive deformation of 4.0 in. (102 mmm) and 3.8 in. (97 mm), respectively.

10.6. Four Point Bending Test Results

This section presents the results of three four-point bending tests. One test was performed on a CI specimen installed in 1960 by LADWP and lined with AP1. Another was performed on a new McWane DI pipeline joint that was aged by Sanexen with acetic acid and lined with AP1. A third was performed on a DI pipeline installed in the Montreal area in 1974 and lined in place with AP2 by Sanexen. All pipelines were lined according to the field procedures used by Sanexen. The purpose of the tests was to develop moment vs. rotation relationships for these types of joints under conditions of severe bending deformation representative of pipeline response to earthquake-induced ground movement.

The pipeline test specimens lined with AP1 and AP2 were able to sustain substantial bending deformation and joint rotation between 78.3 psi (540 kPa) and 82.7 psi (570 kPa) of water pressure.

Specimen AP1 LADWP broke at the bell without leakage at about 8°. This test as terminated at a rotation of 15° without leakage or loss of internal pressure. Specimen AP1 DI Joint was able to sustain 25.6° of rotation without leakage or loss of water pressure. Specimen AP2 DI Joint failed at a rotation of 22.4° at a location where corrosion pits were located in the pipe barrel. Upon unloading the pipeline started to leak by dripping from the joint at a pressure of approximately 82.5 psi (567 kPa). In each case, the lining was able to sustain locally large deformation and wrinkling without rupture and leakage.

10.7. Additional Direct Tension Test Results

This section summarizes the results of additional direct tension tests on nominal 6 in. (152 mm) diameter pipe specimens lined with AP1 and AP2 by Sanexen in accordance with standard field procedures. The direct tension tests were performed to evaluate the debonding characteristics between the Aqua-Pipe lining and host pipe as well as determine the force versus displacement response of the lined pipe.

Four tests were performed. AP2 DT1 and AP2 DT2 were 8.5-ft (2.6 m)-long with a center crack and lined with AP2 on older CI pipelines from field installations. AP1 JDT1 and AP1 JDT2 were 8.5-ft long with a center push-on joint, and lined with AP1 on artificially aged DI interior surfaces. All tests were loaded at a displacement rate of 1 in./min (25.4 mm/min). The data sampling rate was 25 Hz. The equipment was similar to that previously used for direct tension tests.

Specimens AP1 JDT1 and AP1 JDT2 show debonding forces of 25 kips (111 kN) and 27 kips (119 kN) and detachment forces at 26 kips (116 kN) and 27 kips (119 kN). The detachment displacement is between 3.5 in. and 4.5 in. (89 and 114 mm), respectively. For Specimen AP2 DT2 the maximum debonding and detachment forces are similar at 23 kips (102 kN) and 27 kips (119 kN) at about 1 in. (25 mm) and 2 in. (51 mm) of relative displacement, respectively. Specimen AP2 DT1 provides higher debonding and detachment forces of 38 kips (169 kN) and 40 kips (178 kN) at axial displacements of 6 in. (152 mm) and 7.5 in. (190 mm), respectively.

The tests show debonding and detachment forces well below of the axial capacity of the AP2 lining, which is about 62 kips (278 kN) for the nominal 6-in. (102 mm)- diameter pipeline. The forces are not increased by the presence of joints. All test data should a significant drop in axial load immediately after detachment, followed by cyclic forces that are generated by the lining being pulled from the test pipeline.

10.8. Large-Scale Fault Rupture Test Results

An approximately 36-ft (11-m)-long in soil, five-piece section of a DI pipeline was lined with Aqua-Pipe™ Generation 2 (AP2) and tested in fault rupture at the Cornell Large-Scale Lifelines Facility. The pipeline had a total of four joints located 5 and 15 ft (1.5m and 3.6 m) north and south of the fault. The fault angle was 50º. To match the field performance of older DI and CI field pipelines the cementless pipe surface was aged by Sanexen, and the pipeline was lined according to the field procedures followed by them. The pipeline was instrumented with 96 strain gages installed at 20 locations along the pipeline to measure strains and to evaluate axial forces and bending moments. Strain gages were positioned at the crown (C), invert (I) east (E) springline, and west (W) springline of the pipe. The gage measurements were used evaluate when debonding between the pipe and lining occurred as a function of fault displacement. There were three string pots at each joint to measure joint movements and to evaluate joint rotation. Four load cells were placed outside the test basin at each end, reacting between the test basin structural frame and pipe end restraint to measure axial force. The pipe was pressurized to an average 81.3 psi (561 kPa).

The pipeline was buried in the Cornell large-scale test basin in partially saturated sand that was compacted to have an average direct shear, peak friction angle of $\phi = 40º$, equivalent in strength to that of a medium dense to dense granular backfill. The depth of burial to top of pipe was 32 in. (813 mm). During the test, the south part of the basin remained stationary, while the north part was displaced to the north and west by large-stroke actuators to cause soil rupture and slip at the interface between the two parts of the test basin. The north section of the test basin was displaced along a 50º fault at a rate of 2 in. (51 mm) per minute. The basin was displaced until full travel of the actuators was achieved, corresponding to a fault displacement of 4 ft (1.22 m) as well as axial pipe extension of 2.57 ft (0.78 m). The lined pipeline maintained its integrity and water pressure throughout the test.

The axial forces at the south and north end of the test basin were about 27 and 30 kips (120 and 134 kN), respectively. The axial force in the pipe, as determined from the strain gage readings, was largest at approximately 16 in. (406 mm) north of the fault. The axial force was 25 kips (110 kN) at 6 in. (152 mm) of fault displacement, after which debonding between the pipe and lining diminished significantly the pipe strains and corresponding axial forces.

The DI pipeline equipped with an AP2 lining was able to accommodate significant fault movement through axial pullout and rotation of the joints. Fault rupture simulated in the large-scale test is also representative of the most severe ground deformation that occurs along the margins of liquefaction-induced lateral spreads and landslides. Pipeline extension was taken up by longitudinal movement at each of the joints. The maximum longitudinal movement was measured at approximately 14.0 in. (356 mm) at the joint closet to fault on the southern side of the fault. Pipeline lateral offset was accommodated by rotation, or deflection, of the two joints closest to the fault on the north and south sides. The maximum rotation of the north joint closest to the fault was about 14.0° as measured by the string pots and Leica total station survey. The measured and theoretical rotations are in good agreement.

10.9. Significance of Test Results

The amount of tensile strain that can be accommodated with the lined DI pipeline will depend on the spacing of the joints. The pipeline used in the large-scale split-basin test was able to accommodate a maximum of 30.85 in. (784 mm) of axial extension, corresponding to an average tensile strain of 6.3 % along the pipeline. It should be emphasized that no loss of water pressure or structural failure of the lined pipeline was sustained during the fault rupture test. Thus, the lined pipeline could have sustained more tensile strain without exceeding the pressure boundary. Such extension is large enough to accommodate the great majority (well over 99%) of liquefaction-induced lateral ground strains measured by high resolution LiDAR after each of four major earthquakes during the recent Canterbury Earthquake Sequence (CES) in Christchurch, NZ (O'Rourke, et al., 2014). These high-resolution LiDAR measurements provide a comprehensive basis for quantifying the ground strains caused by liquefaction on a regional basis. To put the CES ground strains in perspective, the levels of liquefaction-induced ground deformation measured in Christchurch exceed those documented in San Francisco during the 1989 Loma Prieta earthquake and in the San Fernando Valley during the 1994 Northridge earthquake. They are comparable to the levels of most severe liquefaction-induced ground deformation documented for the 1906 San Francisco earthquake, which caused extensive damage to the San Francisco water distribution system. The test confirms that DI and CI pipelines lined with AP2 are able to sustain large levels of ground deformation through axial displacement and deflection under full-scale conditions of abrupt ground rupture.

References

Stewart, H.E., C. Pariya-Ekkasut, B.P. Wham, T.D. O'Rourke, T.K. Bond, and C Argyrou (2017) "American Earthquake Joint System for Resistance to Earthquake-Induced Ground Deformation", report submitted to American Cast Iron Pipe Company, Birmingham, Al, School of Civil and Environmental Engineering, Cornell University, January, 2017, last accessed on Jan. 1, 2020 at https://lifelines.cee.cornell.edu/.

ASCE. (1984) "Guidelines for the Seismic Design of Oil and Gas Pipeline Systems", Committee on Gas and Liquid Fuel Lifelines, ASCE, Reston, VA.

ASTM International (2013). "Standard Test Methods for Tension Testing of Metallic Materials", *ASTM Standards*. E8/E8M - 13a, 1 – 28.

Cornell University (2015) "Hazard Resilience Testing of US Pipe Ductile Iron TR-XTREME Pipe Joints", report submitted to US Pipe, February, 2015, last accessed on Jan. 1, 2020 at https://lifelines.cee.cornell.edu/.

CDCQ (2019) "Characterization of Watermain CIPP Liners with and without Fold Cornell University Fault Rupture Test AP2", *RAP-19243-1*, report for G. Gagnon, Sanexen Services Environnementaux, Inc., Oct., 3, 2019.

Giacometti, C. and Y. Jadani (2019) "Report of Tests on Pipe Treated with Acetic Acid (Accelerated Aging)", *Project No: RD15-204-2*, Sanexen Services Environnementaux, Inc., June, 10, 2019.

International Organization of Standardization [ISO] (2006), "Earthquake- and Subsidence-Resistant Design of Ductile Iron Pipelines," ISO 16134.

Jung, J., O'Rourke, T.D., and Olson, N. A. (2013) "Lateral Soil-Pipe Interaction in Dry and Partially Saturated Sand" *Journal of Geotechnical and GeoEnvironmental Engineering*, ASCE, Vol. 139, No. 12, pp. 2028-2036.

Jung, J.K., T. D. O'Rourke, and C. Argyrou (2016) 'Multi-Directional Force-Displacement Response of Underground Pipe in Sand" *Canadian Geotechnical Journal*, Vol. 53, pp. 1763 – 1781.

O'Rourke, T.D. (1998). "An Overview of Geotechnical and Lifeline Earthquake Engineering", *Geotechnical Special Publication No. 75*, ASCE, Reston, VA, Proceedings of Geotechnical Earthquake Engineering and Soil Dynamics Conference, Seattle, WA, Aug. 1998, Vol. 2, pp.1392-1426.

O'Rourke, T.D. and J.W. Pease (1997). "Mapping Liquefiable Layer Thickness for Seismic Hazard Assessment", *Journal of Geotechnical Engineering*, ASCE, New York, NY, Vol. 123, No.1, January, pp. 46-56.

O'Rourke, T.D., A. Bonneau, J. Pease, P. Shi, and Y. Wang (2006). "Liquefaction Ground Failures in San Francisco" *Earthquake Spectra*, EERI, Oakland, CA, *Special 1906 San Francisco Earthquake* Vol. 22, No. 52, Apr., pp. 691-6112.

O'Rourke, T.D., Jeon, S-S., Toprak, S., Cubrinovski, M., Hughes, M., van Ballegooy, S., and Bouziou, D. (2014) "Earthquake Response of Underground Pipeline Networks in Christchurch, NZ", *Earthquake Spectra*, EERI, Vol. 30, No.1, pp. 183-204**.**

O'Rourke, T.D., J.K. Jung, and C. Argyrou (2016) "Underground Pipeline Response to Earthquake Induced Ground Deformation", Soil Dynamics and Earthquake Engineering, Vol. 91, 272-283.

Pariya-Ekkasut, C., B.A. Berger, H.E. Stewart, and T.D. O'Rourke (2018) "Evaluation of McWane Seismic Flex Coupling for Resistance to Earthquake-Induced Ground Deformation", report submitted to McWane Ductile, Birmingham, Al, School of Civil and Environmental Engineering, Cornell University, April, 2018, last accessed on Jan. 1, 2020 at https://lifelines.cee.cornell.edu/.

Pease, J.W. and T.D. O'Rourke (1997), "Seismic Response of Liquefaction Sites", *Journal of Geotechnical Engineering*, ASCE, New York, NY, Vol. 123, No. 1, January, pp. 37-45.

Zhong, Z., D. Bouziou, B. Wham, A. Filiatraut, A. Aref, T.D. O'Rourke, and H. Stewart (2014) "Seismic Testing of Critical Lifelines rehabilitated with Cured in Place Pipeline Lining Technology", *Journal of Earthquake Engineering*, Vol. 18, December, pp. 964-985.

Appendix A

Determination of Normal Force for Direct Shear Test

Weight applied to a circular arc sliding surface must be resolved into its component normal to the sliding surface to evaluate friction. Figure A.1 is a transverse cross-section of a symmetrical circular arc sliding surface, defined by radius, R, and the maximum angle, θ_{max}, relative to the vertical.

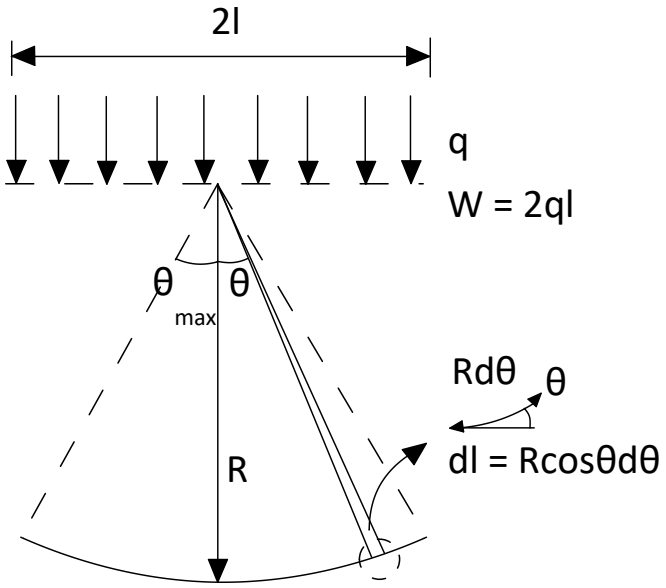

Figure A.1. Transverse Cross-section of a Uniformly Distributed Weight on a Circular Arc

The incremental weight, dW, applied to the sliding surface is

$$dW = qdl \tag{A.1}$$

in which q is the uniform vertical force per unit distance, and dl is the incremental half width over which the uniform vertical force is applied.

The incremental component of the weight normal to the sliding surface, dN, is

$$dN = dW\cos\theta = q\cos\theta dl \tag{A.2}$$

Referring to Figure A.1,

$$dl = R\cos\theta d\theta \tag{A.3}$$

Combining Eqns. A.2 and A.3 results in

$$dN = qR\cos^2\theta d\theta \tag{A.4}$$

The total force normal to the sliding surface is given by

$$N = 2\int_0^{\theta_{\max}} dN = 2qR\int_0^{\theta_{\max}} \cos^2\theta d\theta \tag{A.5}$$

that results in

$$N = 2qR\left(\frac{1}{2}\theta\right]_0^{\theta_{\max}} + \frac{1}{4}\sin(2\theta)\Big]_0^{\theta_{\max}}\Bigg) \tag{A.6}$$

For the direct shear test specimens, $\theta_{max} = \pi/8$, from which

$$N = qD\left(\frac{\pi}{16} + \frac{1}{4}\sin(\pi/4)]\right) = 0.373qD \tag{A.7}$$

Recognizing that W= qDsin(π/8) and dividing Eqn. A.7 by W results in

$$N = \left(\frac{\pi/16 + 1/4\sin[\pi/4]}{\sin[\pi/8]}\right)W = 0.974W \tag{A.8}$$

When evaluating the coefficient of friction, f, from the direct shear test measurements, Eqn. A.8 allows one to calculate the force normal to the sliding surface. The normal for the direct shear test described in this report is converted from the weight as N = 0.974 W.

Appendix B

Axial Load in Pipe and Lining

A lined pipeline, which has not debonded, carries axial load, or force, in both the pipe and lining. Equilibrium requires that the axial force carried by the pipe and lining, F_{PL}, is

$$F_{PL} = F_P + F_L \tag{B.1}$$

in which F_P and F_L are the axial forces in the pipe and lining, respectively.

Compatibility requires that the axial strain, ε, is

$$\varepsilon = \varepsilon_P = \varepsilon_L \tag{B.2}$$

in which ε_P and ε_L are the axial strains in the pipe and lining, respectively.

Combining Equations B.1 and B.2 and recognizing that the force divided by the Young's modulus and cross-sectional area is the axial strain results in

$$\varepsilon = F_P/(A_P E_P) = F_P/(A_L E_L) \tag{B.3}$$

Combining Equations B.1 and B.3 gives

$$F_{PL} = \varepsilon(A_P E_P + A_L E_L) \tag{B.4}$$

The pipe axial force is

$$F_P = \varepsilon\, A_P E_P \tag{B.5}$$

and Equation B.4 is divided by Equation B.5 is

$$F_{PL} = F_P\,[1 + (A_L E_L)/(A_P E_P)] \tag{B.6}$$

Equation B.6 gives the combined axial force in the pipe and lining in terms of the pipe axial force.

During the fault rupture test, the pipe was initially pressurized with water under axial constraint, and the strain gage readings were taken. This initial loading represents the zero condition. It was subtracted from all subsequent measurements as fault rupture was imposed. Thus, the strain gage readings are incremental to the initial conditions, and the above equations provide an appropriate estimate of the axial loads caused by the fault rupture.

The pipe had an average wall thickness of 0.288 in. (7.32 mm) and a cross-sectional area of 5.84 in^2 (3768 mm^2) as measured by laboratory personnel. The average Young's modulus for both

McWane (Pariya-Ekkasut et al. 2018) and American (Stewart et al, 2017) DI pipe is 24,200 ksi (167 GPa).

The modulus of the AP2 lining in the axial (warp) and circumferential (weft) directions are nonlinear and given in Section 2. The average lining thickness as measured by lab personnel is 0.192 in. (4.88 mm) and the cross-sectional area is 3.18 in.^{2} (2032 mm^2). The initial modulus of the AP2 lining in the axial (warp) direction is 491 ksi (3.38 GPa). Before debonding, the axial modulus is constrained to the initial linear range because of the equal and relatively small lining and pipe strains.

Appendix C

Axial Force and Fault Displacement

This appendix summarizes the axial force versus fault displacement data for each strain gage location. At each strain gage station there are plots of axial force given by Equation 9.2 for both ends of the test basin and the axial load at that station. When plotted relative to the axial force given by Equation 9.2 for both the north and south ends of the test pipeline, the reduction in axial load at a given station is easily located. This value coincides with the fault displacement at which the axial force starts to decrease because of debonding.

Plotting the axial force for the ends of the test basin is more accurate according to Equation 9.2 because it accounts for the combined axial force in both the pipe and lining. Nevertheless, this combined force (depending on properties such as the areas and moduli of the DI pipe and AP2 lining) is only 1-2% higher that the axial force in the pipe. The derivation for Equation 9.2 is provided in Appendix B.

Figure C.1 (identical to Figure 9.1) is a plan view of the test layout that shows the fault rupture plane and approximate locations of the four actuators generating basin movement. The strain gage stations are numbered according to distance north (+) and south (-) of the fault plane in inches. As listed in Table 9.1, the Strain Gage Stations are (-247), (-217), (-192), (-150), (-120), (-90), (-72), (-32), (-16), (0), (+16), (+32), (+48), (+90), (+120), (+150), (+168), (+202), (+230), and (+262), which coincide with Figures C.2 through C.21, respectively.

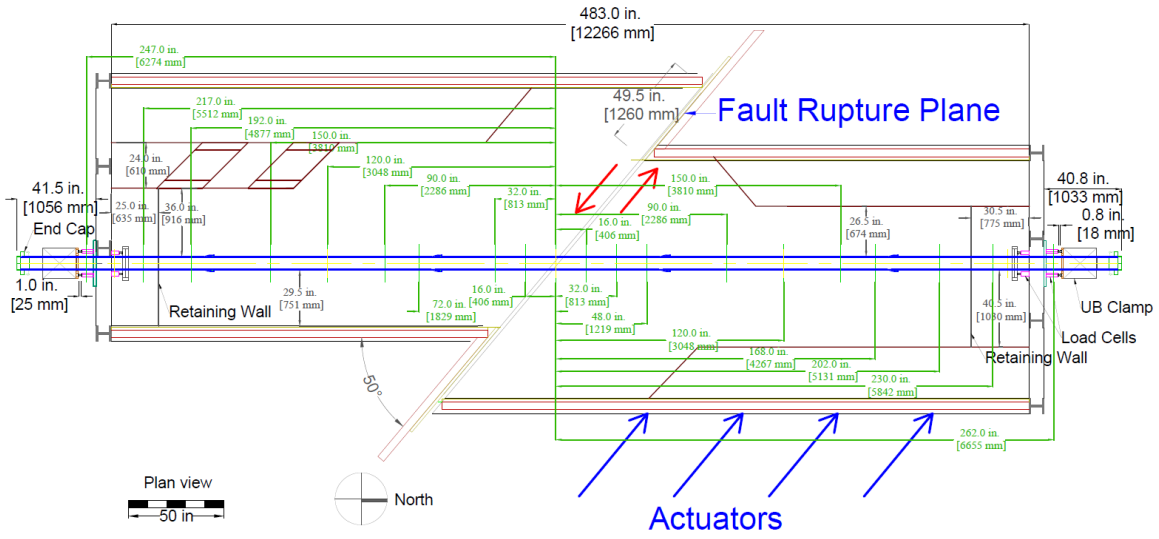

Figure C.1. Plan View of Test Pipeline with AP2 Lining an Gage Station Locations

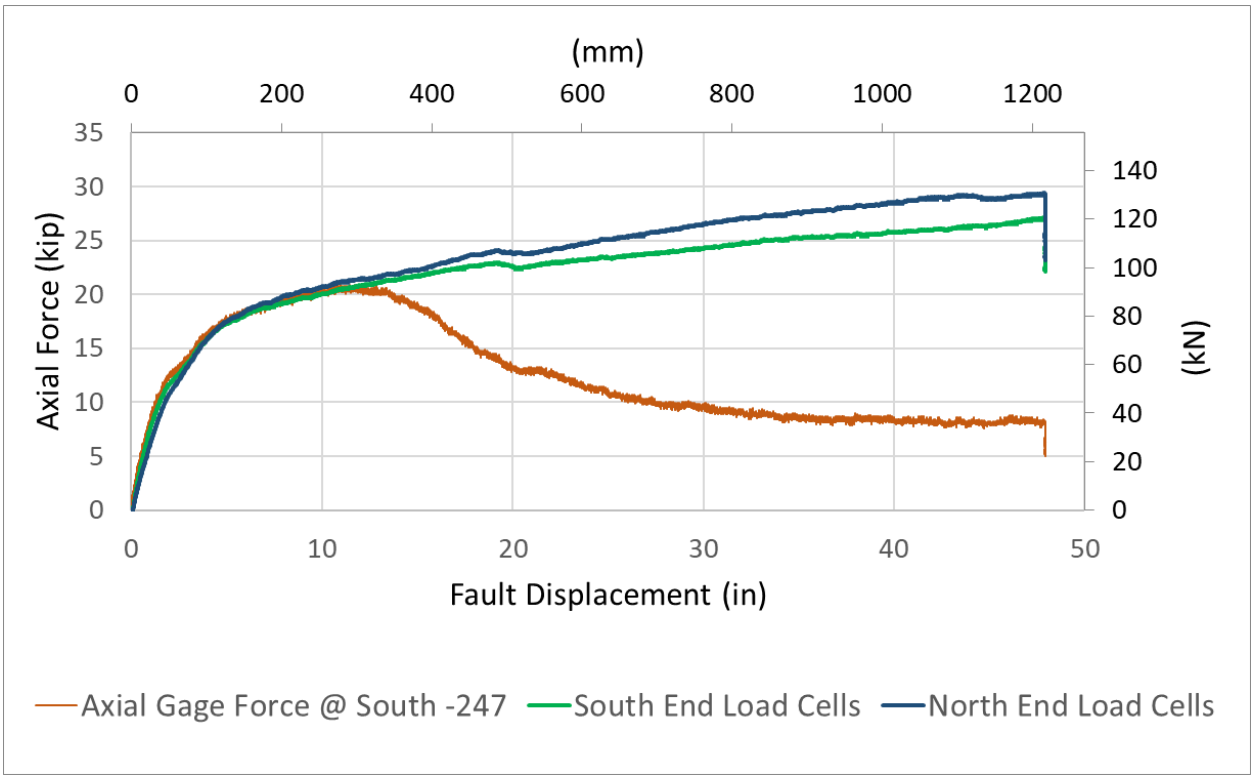

Figure C.2. Axial Force versus Fault Displacement for Strain Gage Station -247

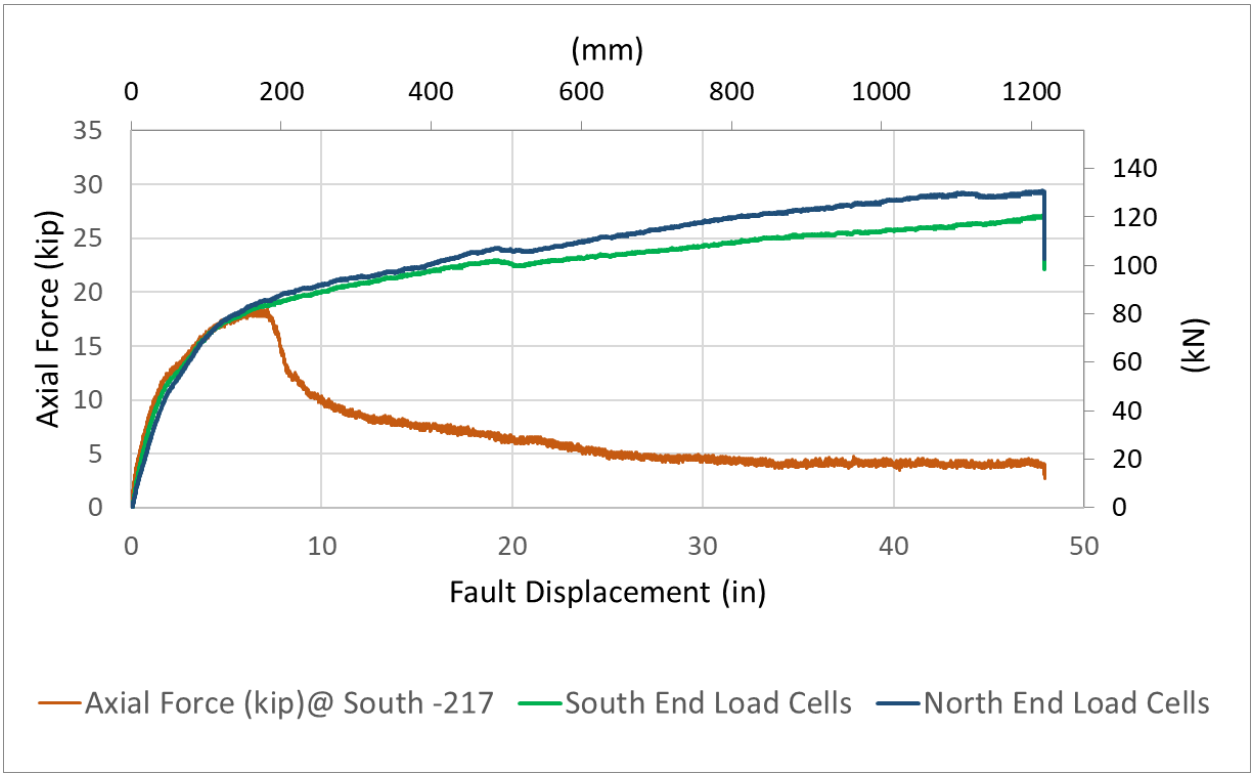

Figure C.3. Axial Force versus Fault Displacement for Strain Gage Station -217

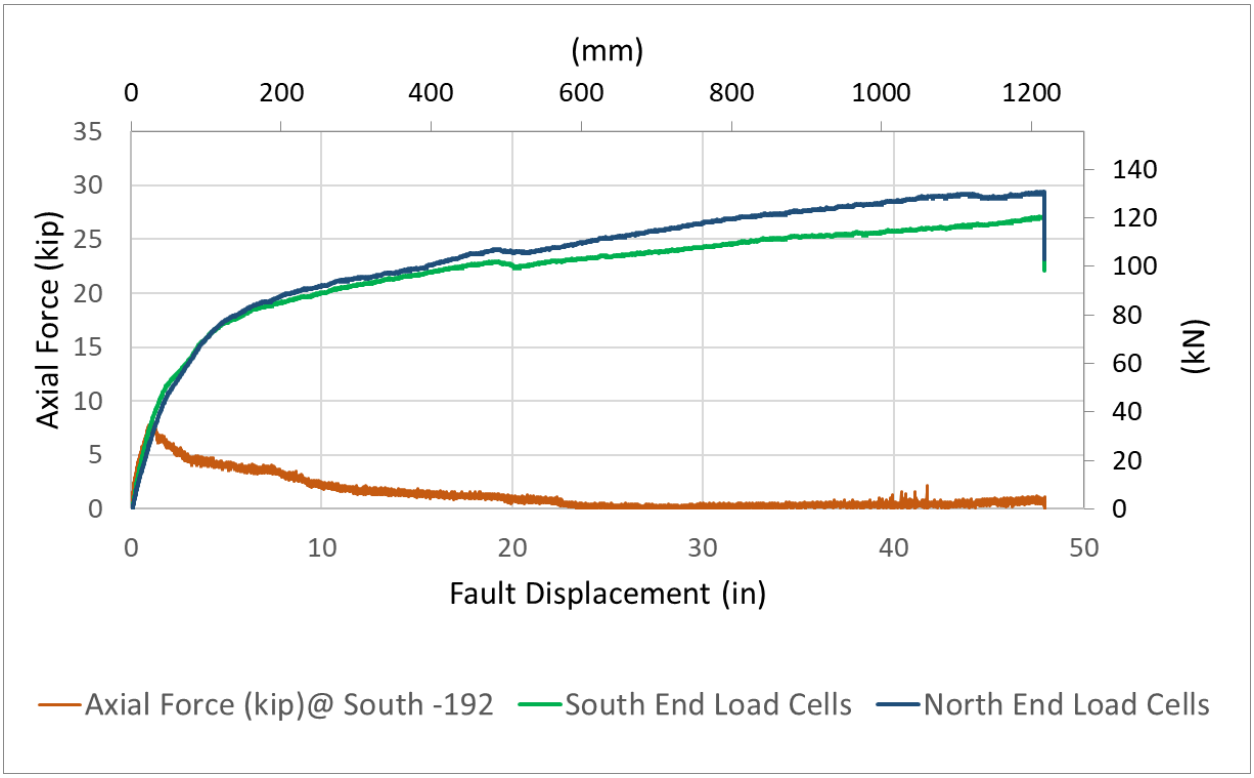

Figure C.4. Axial Force versus Fault Displacement for Strain Gage Station -192

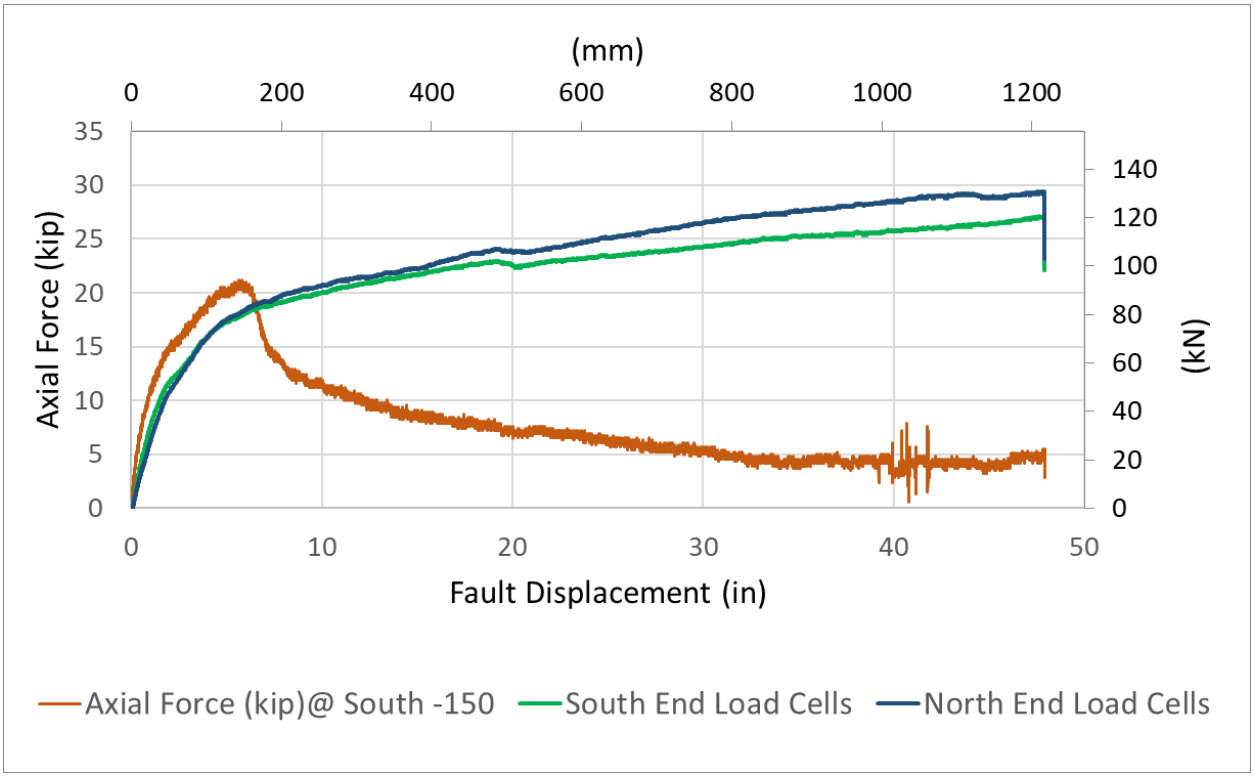

Figure C.5. Axial Force versus Fault Displacement for Strain Gage Station -150

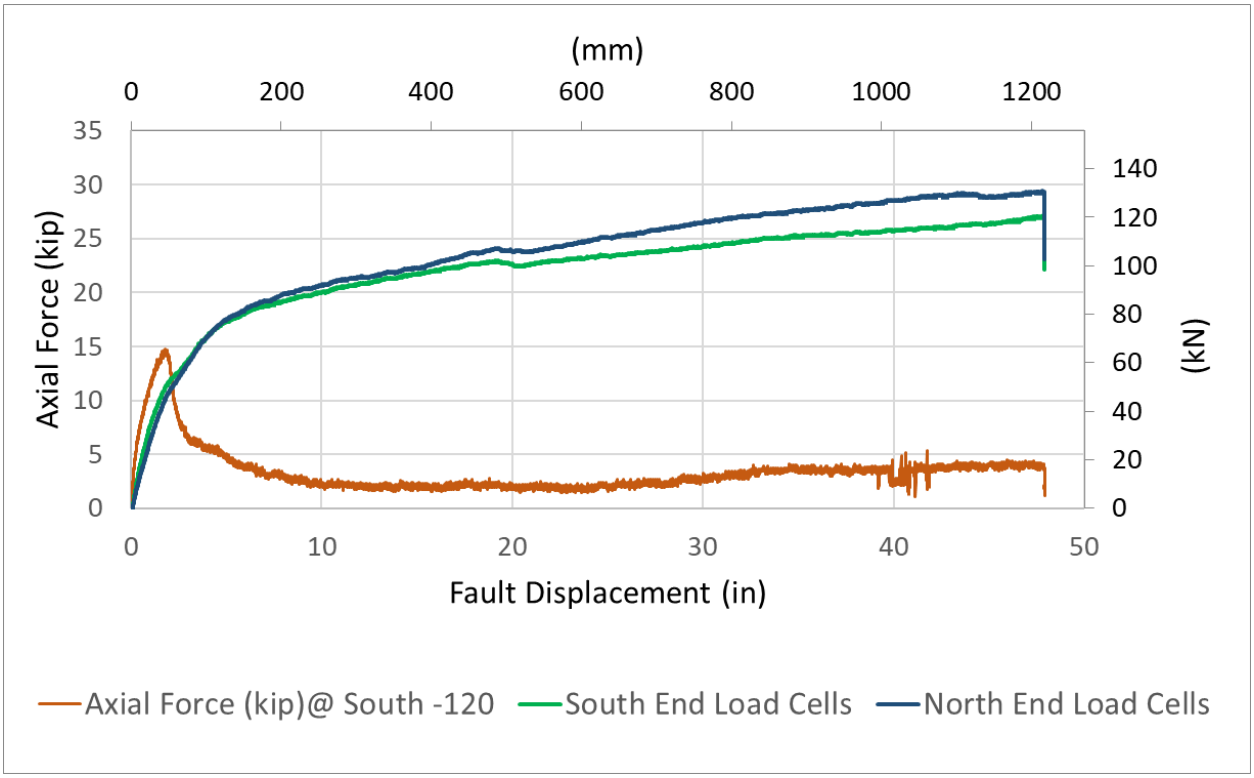

Figure C.6. Axial Force versus Fault Displacement for Strain Gage Station -120

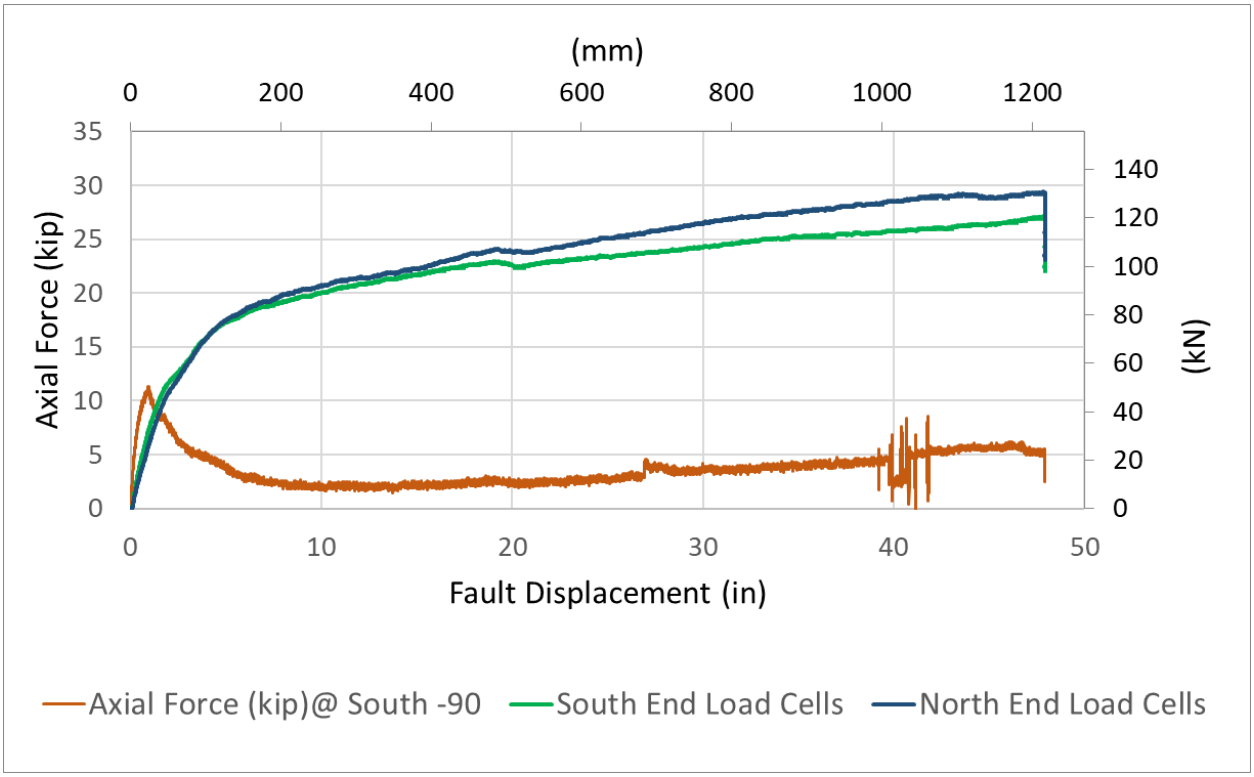

Figure C.7. Axial Force versus Fault Displacement for Strain Gage Station -90

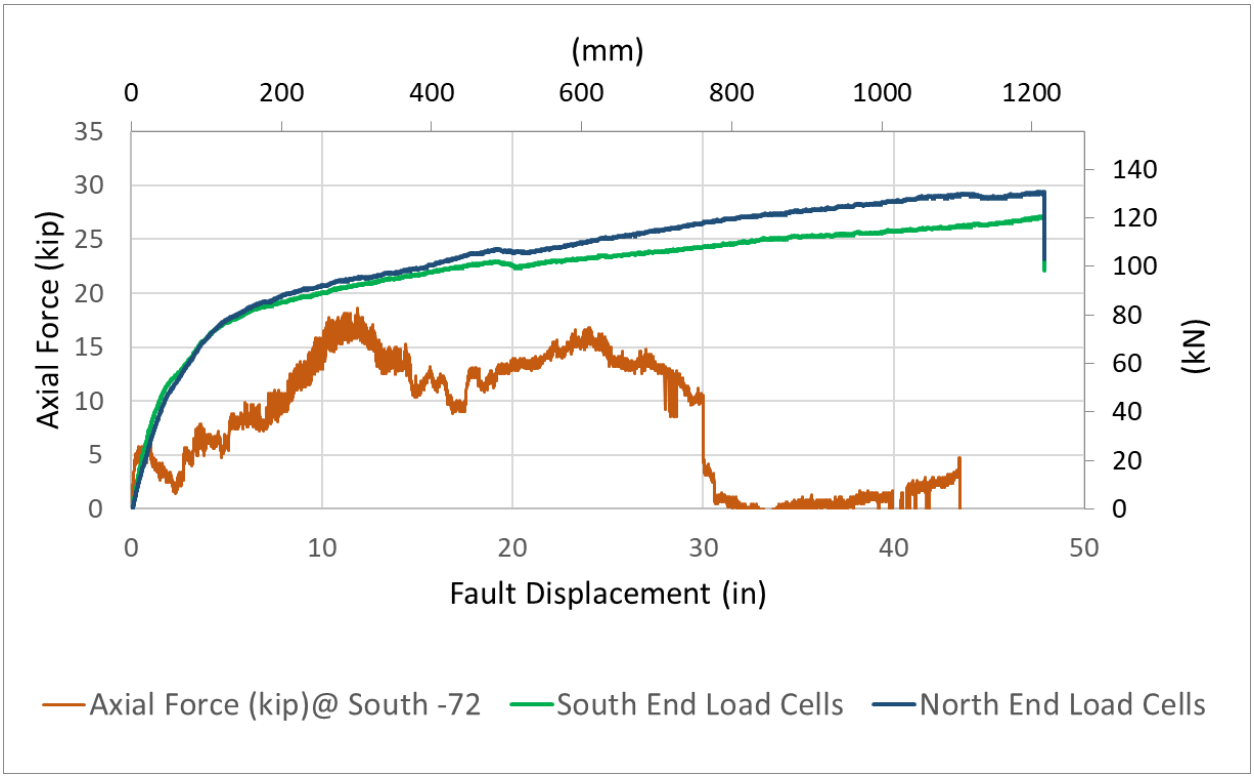

Figure C.8. Axial Force versus Fault Displacement for Strain Gage Station -72

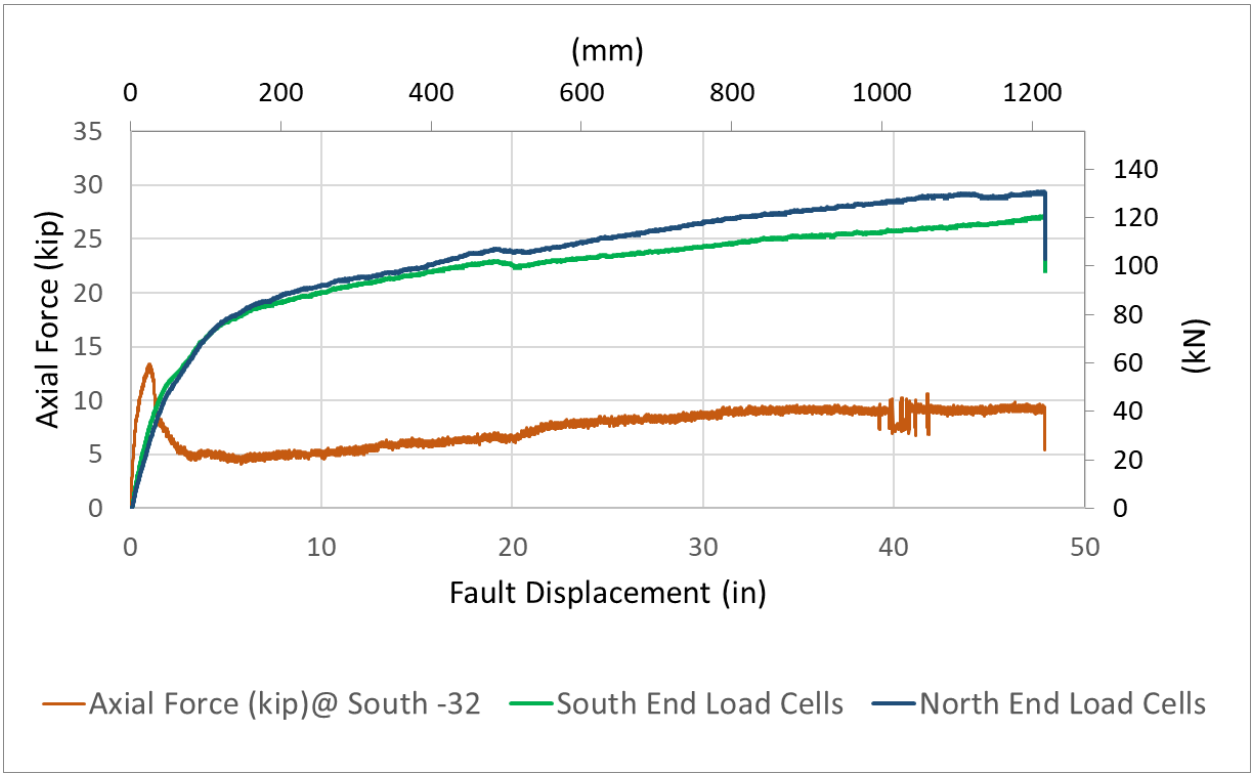

Figure C.9. Axial Force versus Fault Displacement for Strain Gage Station -32

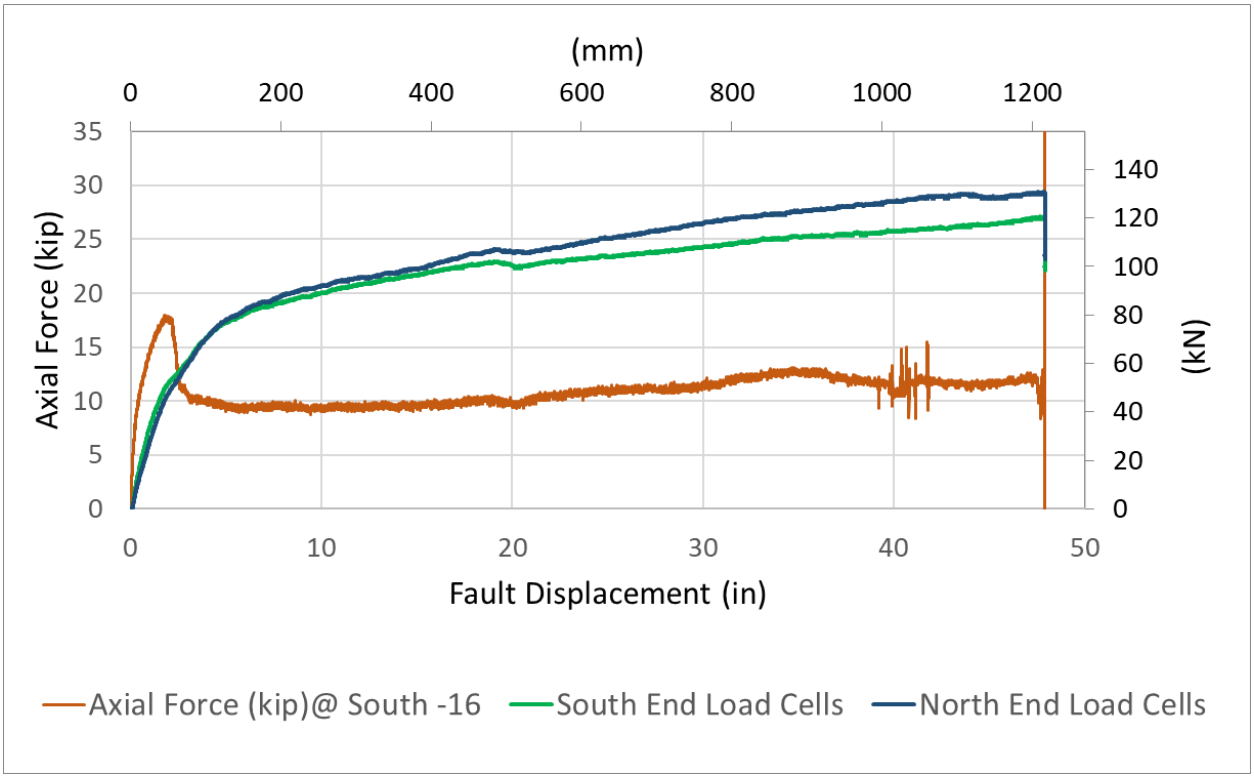

Figure C.10. Axial Force versus Fault Displacement for Strain Gage Station -16

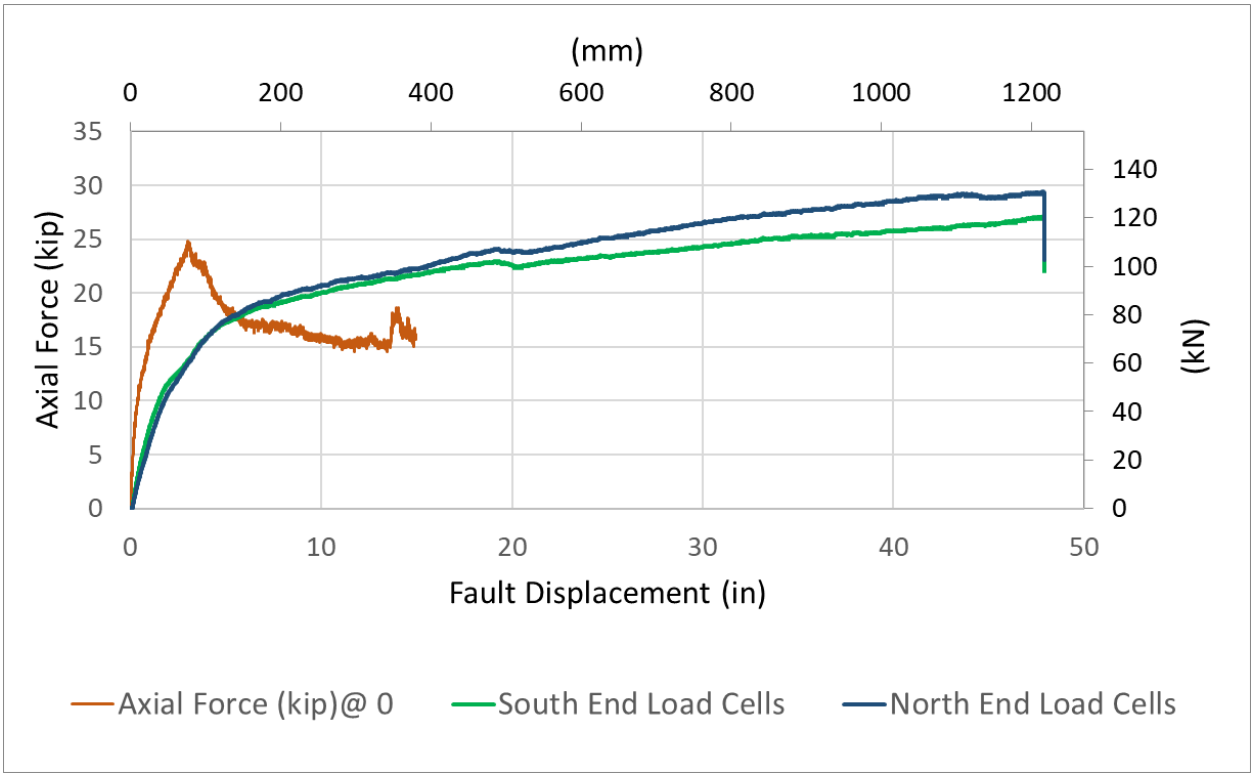

Figure C.11. Axial Force versus Fault Displacement for Strain Gage Station 0

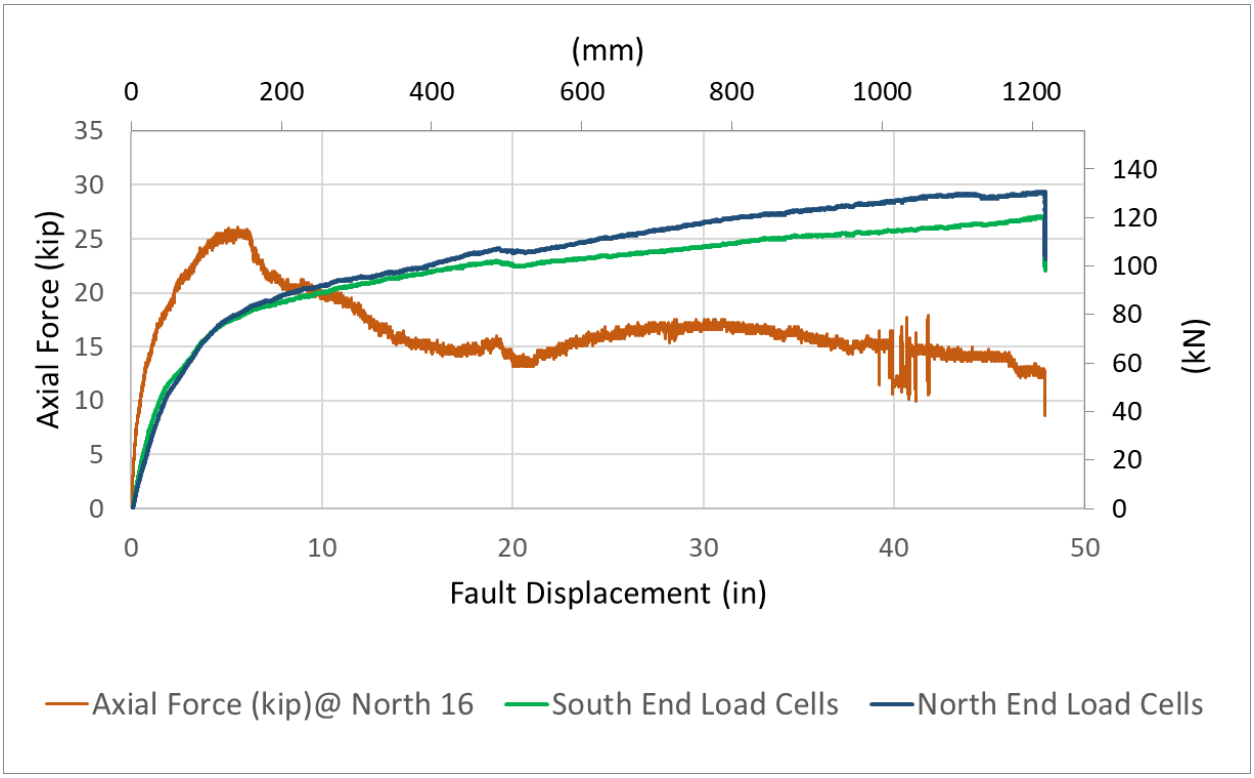

Figure C.12. Axial Force versus Fault Displacement for Strain Gage Station 16

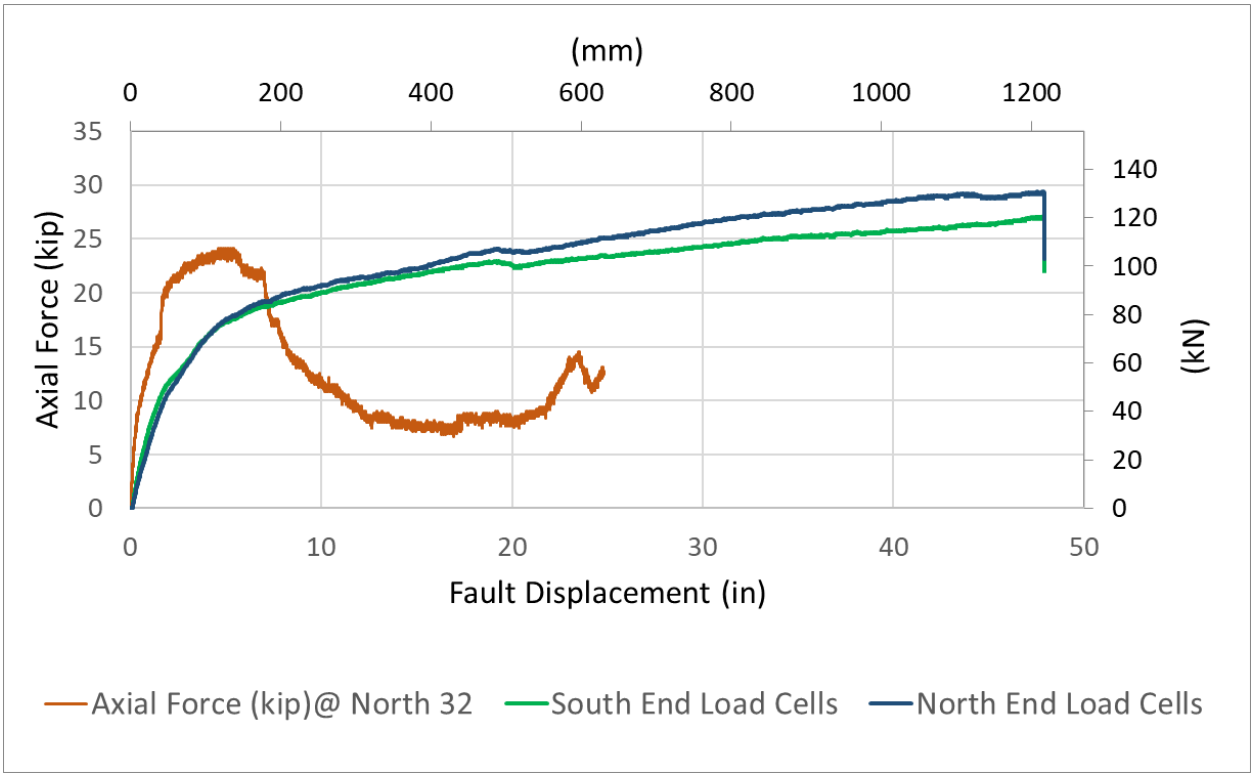

Figure C.13. Axial Force versus Fault Displacement for Strain Gage Station 32

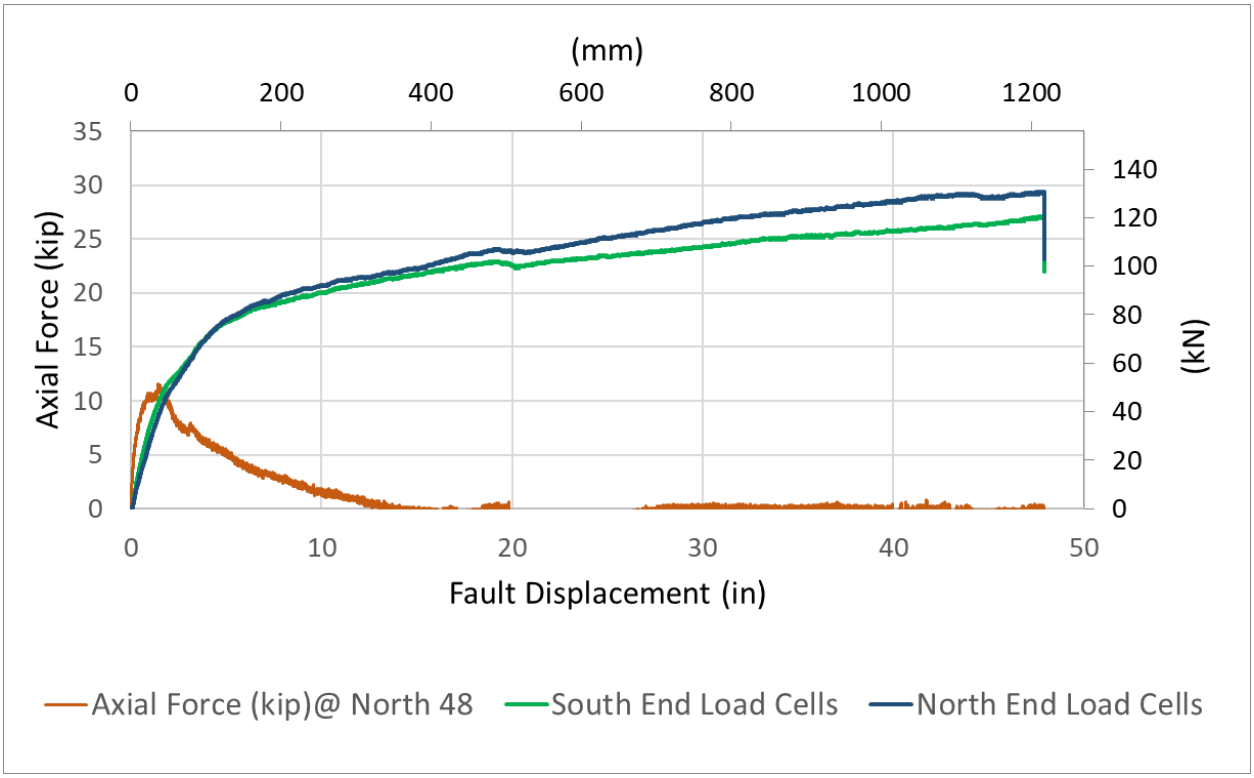

Figure C.14. Axial Force versus Fault Displacement for Strain Gage Station 48

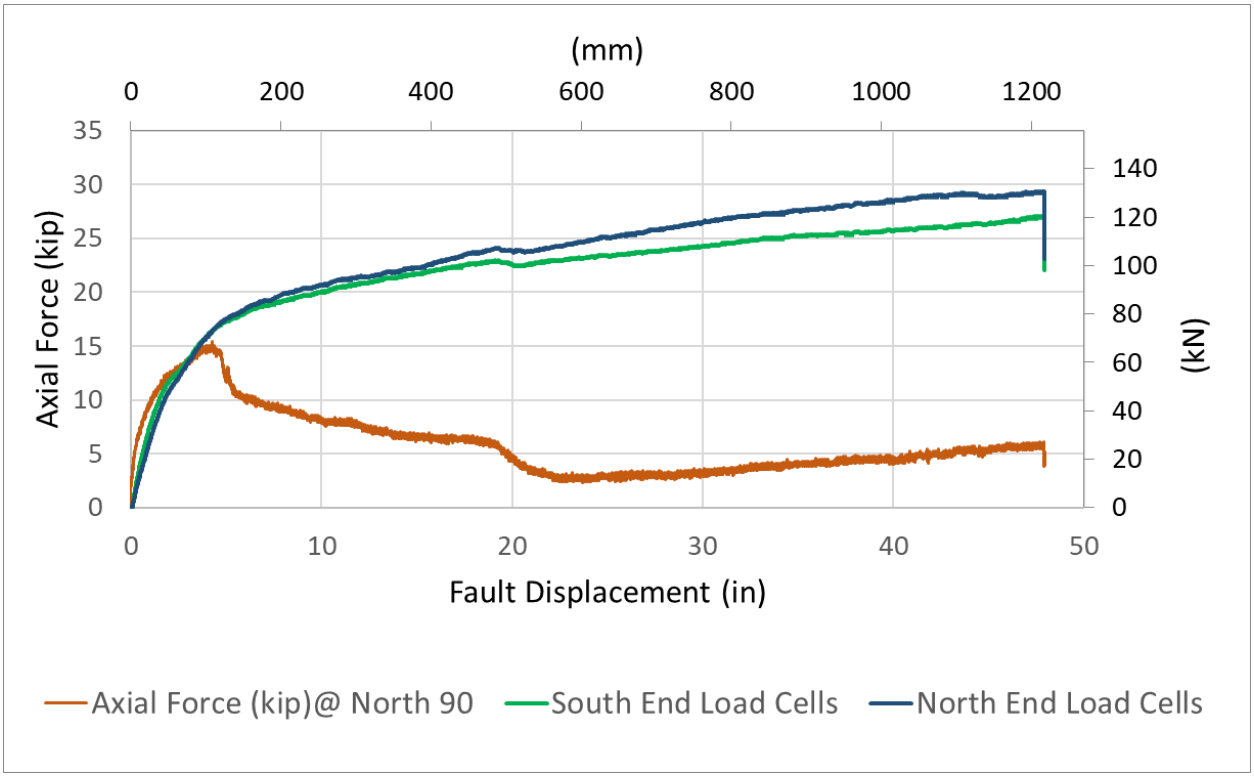

Figure C.15. Axial Force versus Fault Displacement for Strain Gage Station 90

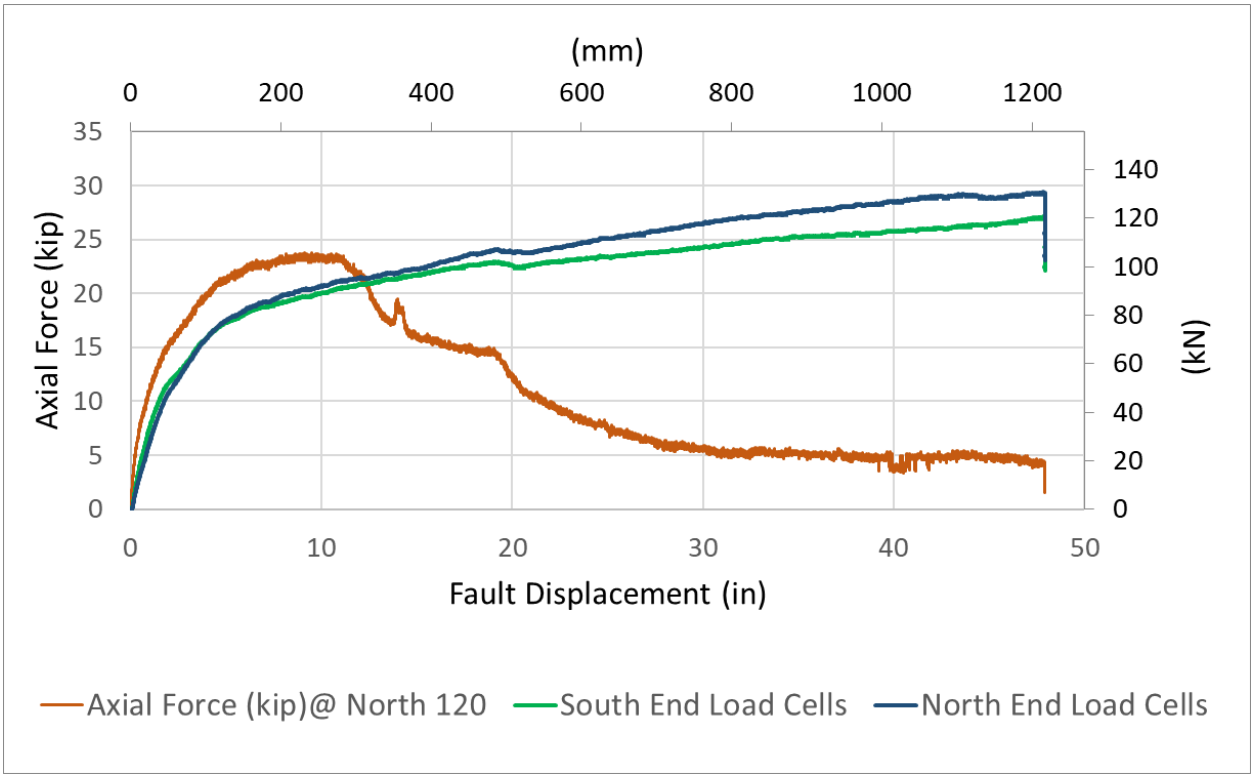

Figure C.16. Axial Force versus Fault Displacement for Strain Gage Station 120

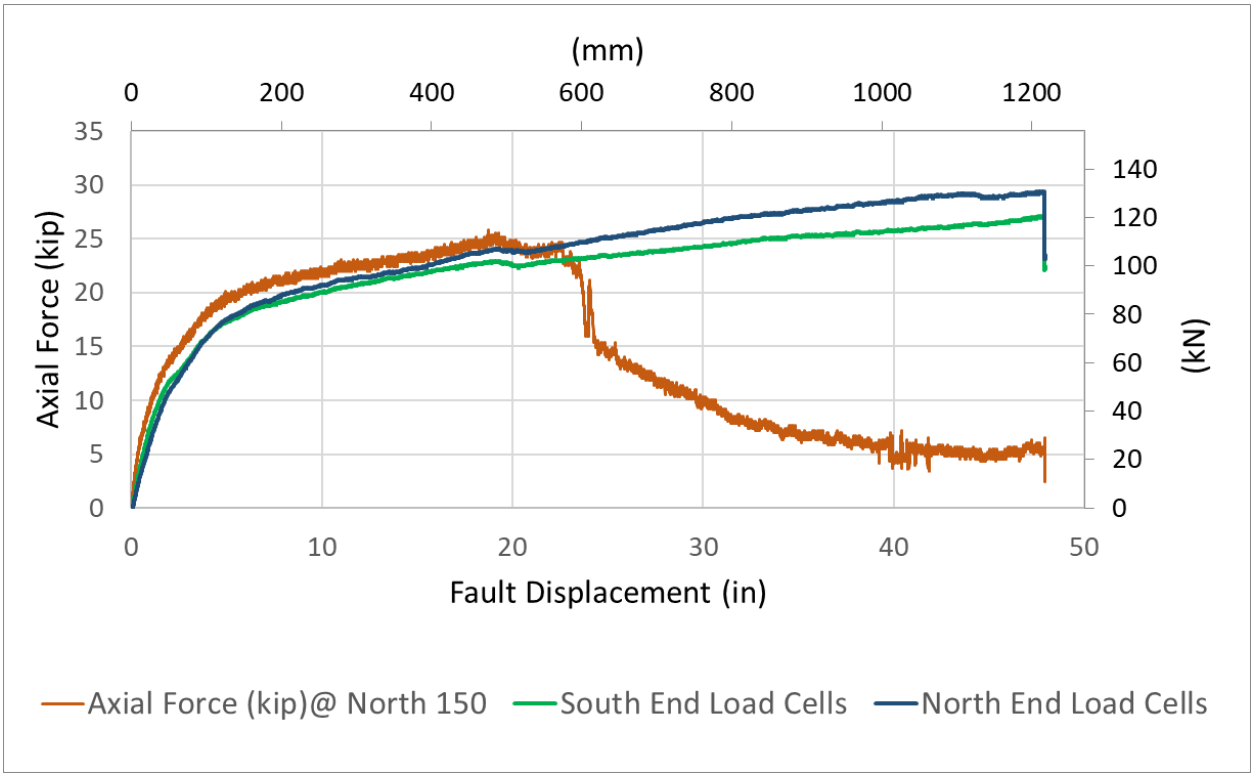

Figure C.17. Axial Force versus Fault Displacement for Strain Gage Station 150

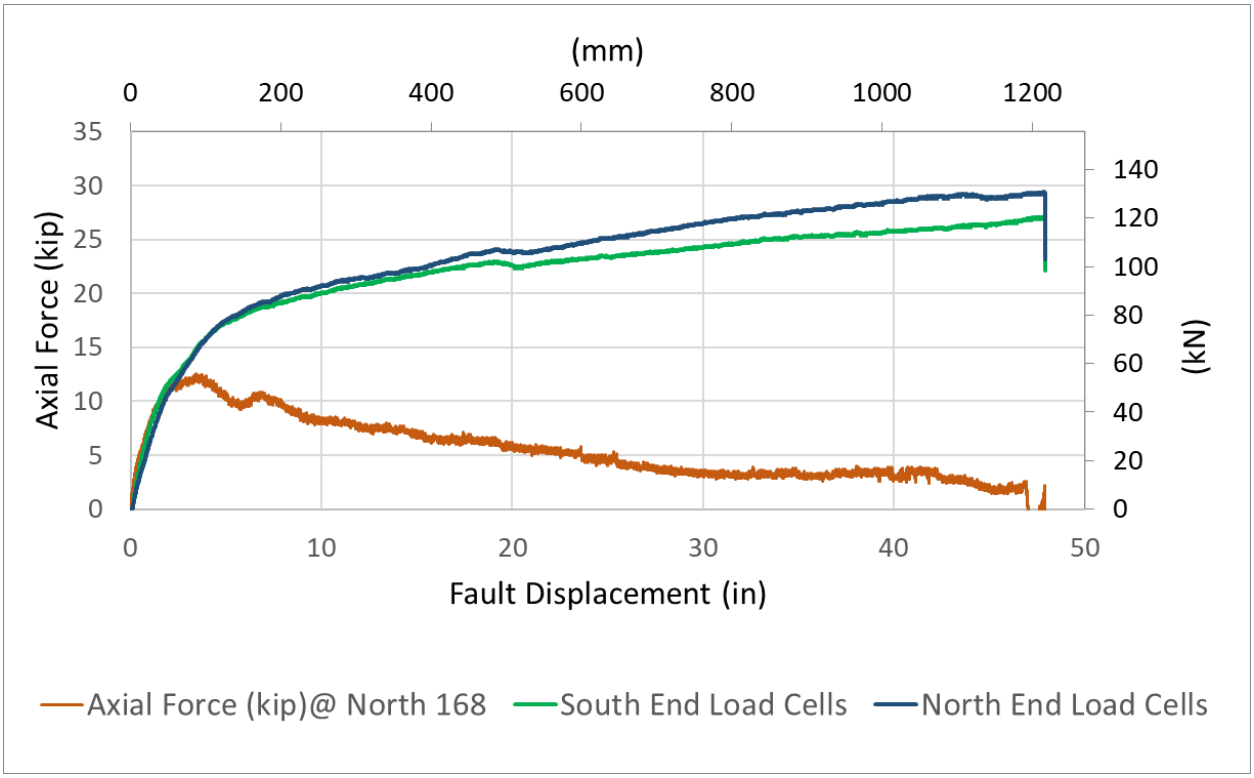

Figure C.18. Axial Force versus Fault Displacement for Strain Gage Station 168

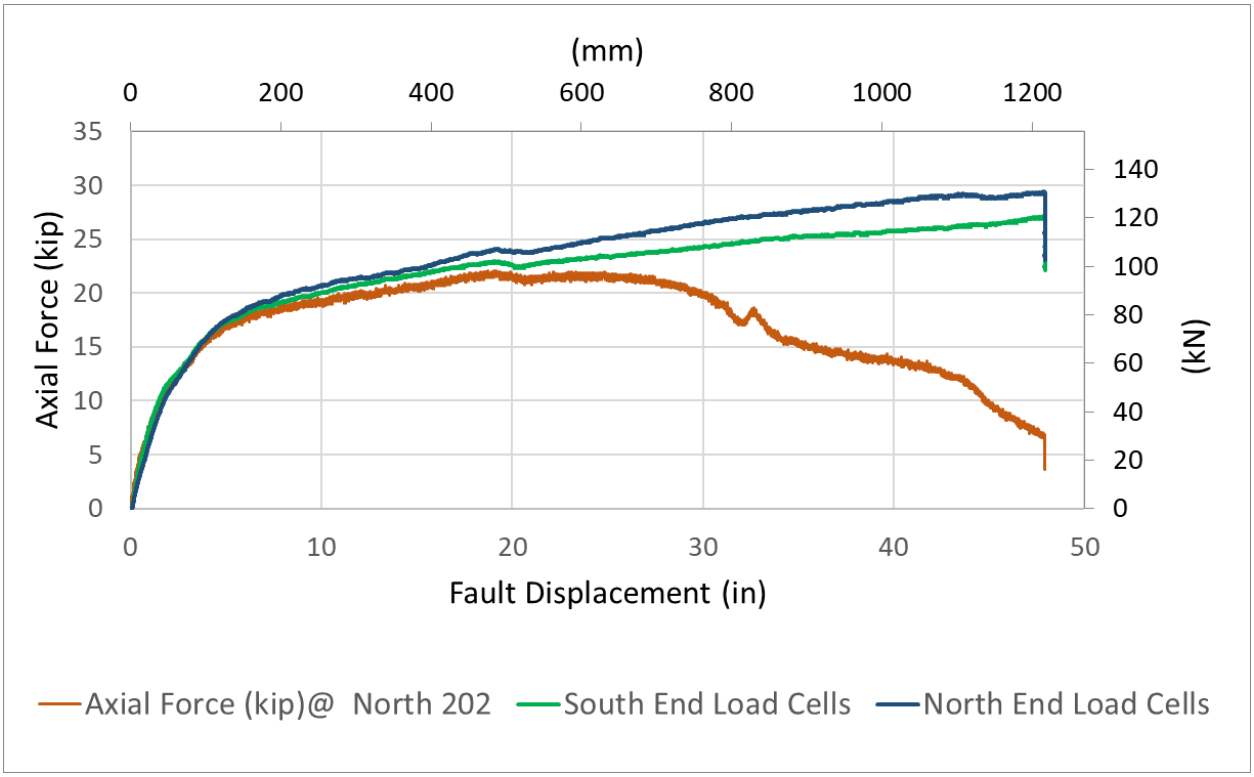

Figure C.19. Axial Force versus Fault Displacement for Strain Gage Station 202

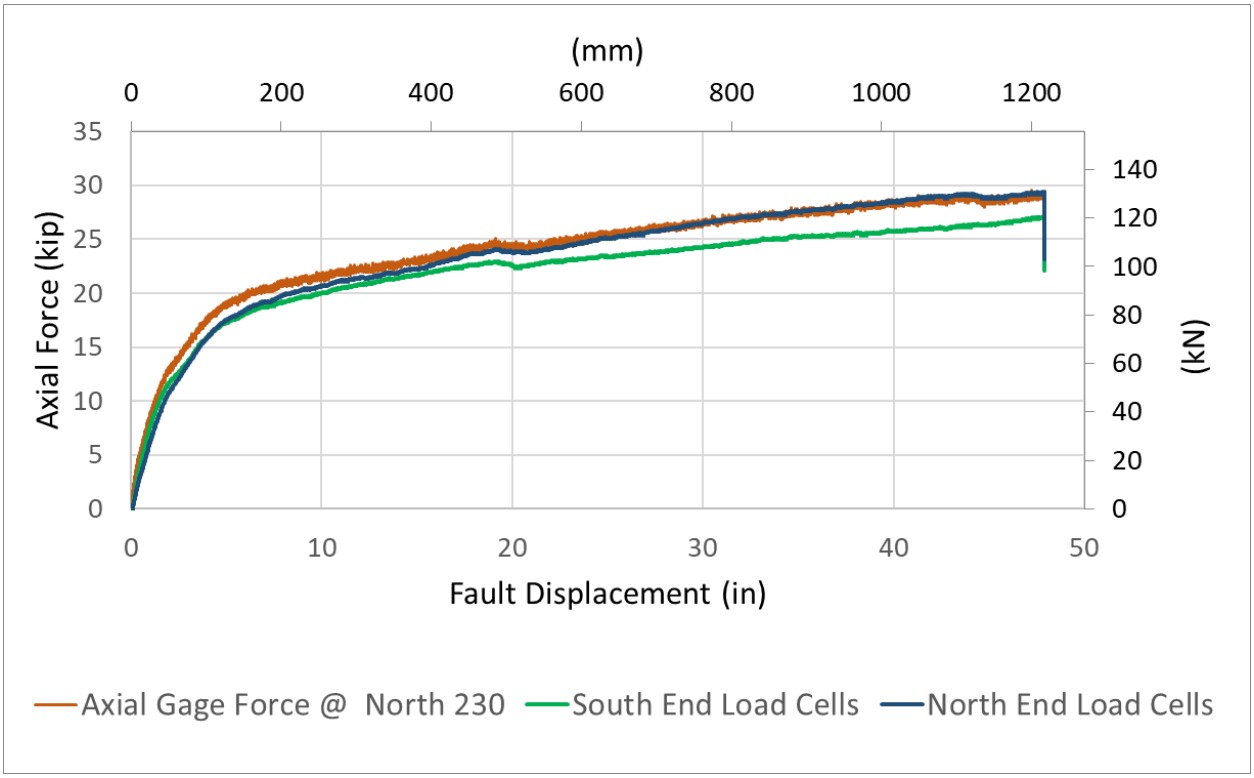

Figure C.20. Axial Force versus Fault Displacement for Strain Gage Station 230

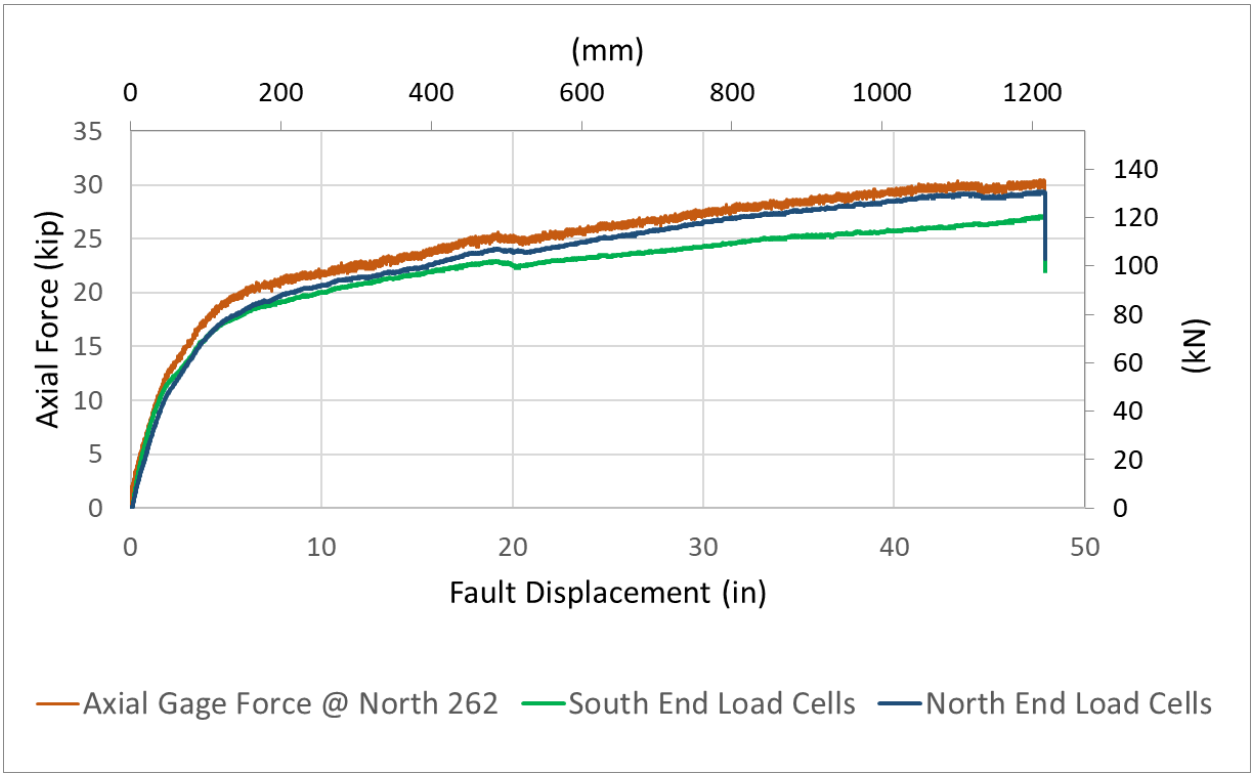

Figure C.21. Axial Force versus Fault Displacement for Strain Gage Station 262

Appendix D

Debonding Length vs Crack or Joint Opening

The debonding length vs. crack, or joint, opening was evaluated for three regimes of tests. These regimes included the 1) fault rupture test, 2) direct tension test on pipe with 8.5-ft (2.6-m) lengths of pipe either side of the center crack: AP1-DT7, and 3) direct tension test on pipe with 4.25-ft (1.3-m) lengths of pipe either side of the center crack: AP1-DT2, AP2-DT2, and AP1-JDT2.

An equation was used to characterize each regime, with the general form

$$l = m\ln(x) + b \tag{D.1}$$

in which l is the debonded length, x is the crack or joint opening, and m and b are the slope and intercept of the plot, respectively.

For each of the regimes above, the l and ln(x) data were plotted and fitted with a linear regression. The linear regression equation for each regime is provided in Table D.1. The coefficient of determination, r^2, for each equation is also provided. For each regime equation there is a high r^2, which means that the linear regression accounts for the variability of a fraction of the data given by r^2. As listed in the table, r^2 varies from 0.87 to 0.94.

The physical meaning of b is the debonded length at 1 in. of crack or joint opening. The slope, m, has a more abstract meaning as the change in debonded length per change in the natural log of the crack or joint opening in inches.

The logarithmic series expansion is given by

$$\ln(x) = 2\left(\left[\frac{x-1}{x+1}\right] + \frac{1}{3}\left[\frac{x-1}{x+1}\right]^3 + \frac{1}{5}\left[\frac{x-1}{x+1}\right]^5 + \frac{1}{7}\left[\frac{x-1}{x+1}\right]^7 + \ldots\right) \tag{D.2}$$

When the expansion involves four terms, as given in Eqn D.2, the error difference between the expansion and ln(x) is generally close to 1%.

Using the four terms of Eqn D.2, a unique value of ln(x) occurs as x goes to infinity in which ln(x) = 3.35. This value in the three equations in Table D.1, allows l to be calculated for each regime. Using the unique value of [1/2]ln(x) as x goes to infinity also results in a unique combination of l and x for each of the three regimes, such that (187.0 in., 2.0 in.), (78.0 in., 3.1 in.), and (36.0 in., 1.3 in.) apply for the fault rupture test and direct tension tests with 8.5-ft (2.3-m) and 4.25-ft (1.3-

Table D.1 Summary of Testing Regime Equations

Description	Equation[1]	Coef. of Determination, r^2
Fault Rupture Test	$l = 70.5 \ln(x) + 137$	0.87
Direct Tension Test: 8.5-ft (2.3-m) pipe lengths	$l = 34.9 \ln(x) + 39$	0.91
Direct Tension Test: 4.25-ft (1.3-m) pipe lengths	$l = 11.6 \ln(x) + 31$	0.94

1. Equations expressed in inches

m) pipe lengths adjacent to the crack opening, respectively. The regimes are characterized by decreasing l/x ratios as one goes from fault rupture to direct tension tests and diminishing pipe lengths.